Door-To-Door Air Transportation

Final Report

Group 4

July 3, 2018
Version 2.0

TU Delft

Door-To-Door Air Transportation

Final Report

by

Group 4

July 3, 2018

This version 2.0 implements the feedback received for the draft version of the Final Report and the main changes are discussed here. Figures are made more readable. Rephrasing the conclusion. Minor spelling mistakes are corrected.

Student :	Chiara Ardemani	4429575
	Peter Blom	4475011
	Natalia Elias Ortega	4468821
	Ide Govers	4461258
	Ubeydullah Kaya	4171829
	Johannes Jacob Knobbout	4303385
	Ruben Michaux	4208692
	Jur Mijjer	4459210
	Marcel Munster	4467949
	Renko Siebols	4464389
Project duration:	April 23, 2018 – July 6, 2018	
Tutor:	Dr. ir. J. van Campen,	TU Delft, supervisor
Coaches:	Q. Deng,	TU Delft
	S. Li,	TU Delft

TU Delft

Preface

For this project, a group of ten students of the faculty of Aerospace Engineering at Delft University of Technology was asked to make a design in the field of air travel for the Design Synthesis Exercise during the academic year 2017-2018.

This is the final report of DSE Team 4, commissioned by TU Delft, aiming to come up with a design solution to reduce pre-flight and post-flight waiting time within Europe. This report provides information for readers that are interested in the feasibility of such a system and the possible design options.

We would like to thank the tutor and coaches for their support and feedback during the process of writing this baseline report and special acknowledgements goes out to dr. ir. Julien van Campen for making this subject for our DSE available.

Group 4
Delft, July 3, 2018
Faculty of Aerospace Engineering

Executive Overview

Imagine being able to travel door-to-door from Amsterdam to Milan within four hours. USTI ("Unpiloted Sustainable Transport Initiative") picks the passenger up at any desired pick-up location and flies to the airport, where highly time-efficient security screening and baggage drop-off takes place in a private luxurious lounge. At the arrival airport, USTI picks up the passenger and their luggage, and flies towards their final destination. This overview presents the objectives of USTI, as well as an economic analysis and the current design.

Project Objectives

The objective of USTI is to reduce the average door-to-door travel time within Europe to four hours. Two main factors contribute to the need for a system like USTI:

- The current modes of transport to and from the airport induce significant waiting times if transfers are necessary (public transport), or are highly dependent on traffic conditions for their time efficiency (car/taxi).
- Increasing demand in air travel has put a strain on airport logistics, resulting in long waiting times for baggage drop-off and security screening.

Therefore, the envisioned design for USTI consists of two major components: (1) a set of autonomously flying and/or driving pods that can pick up and drop off on demand and (2) improved time efficiency in airport operations. In addition to a reduction in travel time, the sustainability of USTI is a major design pillar. Every aspect of the design is aimed to contribute to the Sustainable Development Goals set by the UN.

The current design nearly meets the project objective. The reduction to four hours can not always be guaranteed, even though the door-to-door time is reduced significantly. Most time is saved in travelling to and from the airport. More time can be saved by further optimising airport operations.

Economic Analysis

The Design Company of USTI will sell the product to an external Operating Company after production. For this reason, a marketing strategy is developed that considers all phases of the life cycle of the service.

Market Analysis

An extensive market analysis is performed to analyse the possible market. Feedback from the industry results in the following conclusions:

- **Potential Customers**: USTI would work optimally if the design is focused on business travellers, as they value time over money.
- **Implementation**: Due to the focus on business travellers, USTI would be implemented at airports around the largest business cities. Therefore, USTI is designed for implementation at airports with more than 10 million passengers per year.
- **Available Market Size**: If 3 % of business travellers would use such a system and a penetration rate of 30 % can be achieved, the available market volume in Europe is 11,841 pods. This market volume is used to assess the feasibility of implementing the system. Possible expansions to North America and Asia are not yet considered.

Project Outline

An outline is made for the development period and roll-out of USTI. The intention is to start operations within 10 years from the start of development. The full outline can be seen in Figure 1 and consist of the following phases:

- **Initial Design Phase (2018-2020)** The conceptual design of the system and experimental certifications to assess feasibility. Expected development cost for this phase: €42.5 million.
- **Second Design and Testing Phase (2020-2024)** Further design and testing of prototypes. Expected development cost for this phase: €74 million.
- **Final Design Phase (2024-2026)** Certification and final adjustments on design. Expected development cost: €39 million.
- **Pre-Operations Phase (2026-2028)** Start of production, building of facilities for operations. There are no development cost for the design company in this phase. Production cost per pod: €111,792.

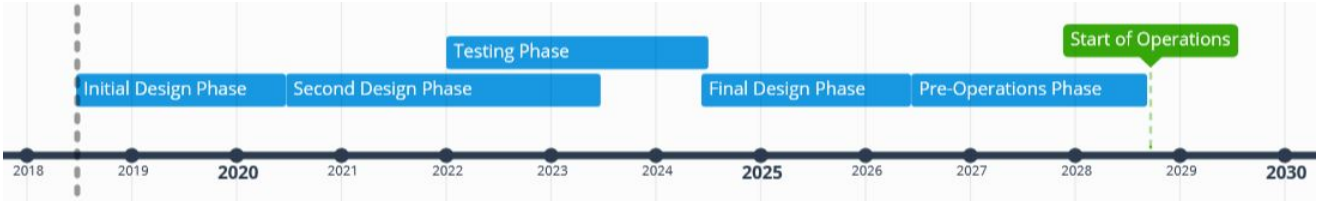

Figure 1: Project Outline Until Start of Operations

Business Plan for Design Company

The business plan for the Design Company is based on the intentions to break even in 2035, seven years after the start of operations. It is assumed that the complete available market volume for Europe of 11,841 pods is produced and delivered in ten years. This leads to a selling price per pod of €197,767. An average interest rate of 3 % is used in this calculation, based on an expected mix between bank loans and angel investors. If lower interest rates can be negotiated, or more angel investors are attracted, the price per pod can be reduced.

Based on the current price of the pod, a gross Return-on-Investment of 69.4 % is found. From this, interest and rent still has to be paid. When these are taken into account, an overall Return-on-Investment of 15 % is expected.

Business Plan for Operating Company

The business plan for the Operating Company consists of determining the price per kilometre for a trip, based on an average pod use of 2500 hours per year. The price is based on three factors:

- **Direct Operating Cost** Costs directly related to the operations of the pod. Major contributors include fuel cost and maintenance cost. Cost per kilometre: €0.38.
- **Indirect Operating Cost** Costs indirectly related to the operations of the pod. Major contributors are contractor costs and passenger handling cost. Cost per kilometre: €0.14.
- **Depreciation Cost** The cost of leasing the pod for a period of ten years from a leasing company that buys the pod from the Design Company. Cost per kilometre: €0.075.

The cost per kilometre totals €0.59. For the price per kilometre a price an operational profit of 100 % is applied. Taking into account the fact that the passenger might have to be picked up with an empty pod, this leads to a passenger price per kilometre of €2.39. This is comparable to an average taxi ride.

Pod Design

The current design solution for the pod can be seen in Figure 2 and its main specifications can be seen in Table 1. The design consists of the following main features:

- An autonomously flying and driving pod with a total range of 300 km at a cruise speed of 200 km/h.
- Enough space for two passengers and their luggage
- Hybrid-electric propulsion that allows Vertical Take-Off and Landing.
- Lift is provided by wings that can swing back during during driving mode.
- Recyclable for 78 % of the weight by using materials such as aluminium and polypropylene.

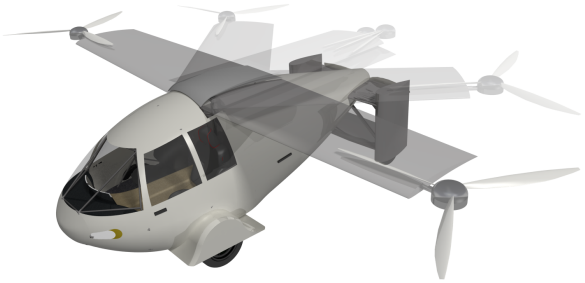

Figure 2: Current design solution for the passenger pod. The process of swinging back the wings is visualised

Maximum Take-Off Mass	794 kg
Operative Empty Mass	430 kg
Payload Mass	230 kg
Battery Mass	109 kg
Fuel Mass	25 kg
Wing Surface Area	7.00 m^2
Lift-over-Drag Ratio	9.2
Peak Power	460 kW

Table 1: Main parameters of current pod design

Propulsion System Characteristics

The hybrid-electric propulsion system consist of five electric motors and one combustion engine and is optimised for three different phases:

- **Vertical Take-Off and Landing Phase** Vertical Take-Off and Landing capabilities are provided by two electric motors mounted in the wing tips to allow pod operation within existing urban infrastructures. These engines have a peak power of 230 kW.
- **Cruise Phase** Cruise power is provided by an electric motor located in the back of the fuselage. This engine has a continuous power output of 55 kW. In this phase, the wing-mounted engines are turned off.
- **Driving Phase** Two electric motors mounted in the rear wheels of the pod provide power during the driving phase. These engines have a continuous power output of 28 kW.

Energy is provided by 109 kg of Lithium-Sulphur batteries, which is sufficient for 30 % of the total range. A combustion engine range extender is used to charge the batteries for the remainder of the range. This is a lightweight 50 kW two-cylinder gasoline engine. The total weight of the propulsion system is 229 kg including batteries and the fuel tank, and the cost is €30,000.

Structure Characteristics

The structure of the pod is a fully aluminium truss structure, which has high load-carrying capabilities at a low cost. To ensure the safety of the passengers in a crash situation, ticker aluminium trusses are used around the passenger compartment. Around the truss structure, a skin made out of polypropylene will give the pod its aerodynamic shape. This shape is based on a qualitative aerodynamic analysis to ensure low drag.

The wing is a skin-stiffened aluminium structure to cope with the high bending moments experienced during take-off. It is attached to the fuselage by two mechanical rods per half-wing. Finally, the empennage consists of two horizontal tails and two vertical tails. It is manufactured as one piece and is attached to the fuselage truss-structure by means of a snail cam locking mechanism. The two vertical tails contain the rear wheels of the pod.

The total structural weight is 101 kg and the weight of the landing gear and driving system is 90 kg combined. The cost of these structures is €3800 and €5200, respectively.

Flight Control Characteristics

The pod is able to fly and drive autonomously. Based on the input data from surrounding sensors, consisting of (heat) cameras, radar systems and environmental and positioning sensors, the attitude heading and reference systems can be determined autonomously to safely participate in traffic and safely avoid both static and moving objects. The total weight of the flight control system is 10 kg and the cost is €11,100.

Internal and Emergency Systems

The design of the interior of the pod is focused on optimal comfort for the passengers. The passengers are seated in business class seats. On a big 32" display the passengers can check their flight status. On board WiFi, power plugs, and foldable chairs allow the busy passengers to continue working during their journey to and from the airport. However, dimmable windows also allow the traveller to rest during the pod flight. A pleasant atmosphere is assured by the environmental control system. Further on-board features of the pod include a high class audio system and a drink dispenser.

Besides comfort, the safety of the passenger in case of an emergency is assured. In case a fire is automatically detected by the pod, the combustion engine is shut down and the fuel tank is isolated. Afterwards, an emergency landing is performed. Crash safety is provided by an airbag system and an emergency call is automatically sent to the emergency services and the control station.

The total weight of the internal systems is 109 kg and the cost is €45,000.

Operations Design

Currently, every passenger is suggested to arrive at the airport at least one hour and thirty minutes prior to departure. Several operational aspects of the USTI service are analysed to reduce this time interval to approximately fifteen minutes.

Booking USTI

The booking procedure is optimised for two objectives: (1) passenger comfort and (2) predictability. To ensure the former, an application is developed that enables passengers to book a pod until six hours before their flight departs. Figure 3

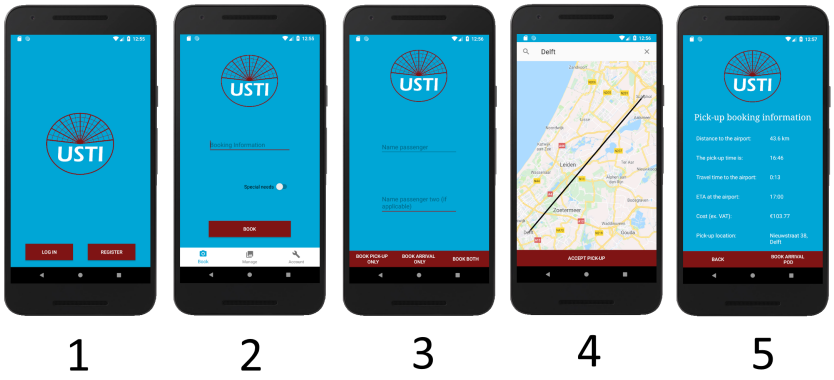

Figure 3: Application lay-out. Screen 1: Start up screen, screen 2: Flight booking information screen, screen 3: Passenger information screen, screen 4: pick-up location screen, screen 5: pick-up information

depicts what the application looks like when booking a pod.

The algorithm for assigning pods is designed to optimise the following three aspects; (1) Time efficiency; a pod can be located close to the new passenger after drop-off. (2) Range efficiency; the 300 km range for which the pod is designed is used most effectively when multiple pick-ups and drop-offs are performed without returning to the station. (3) Minimal fuel consumption; 30 % of the journey is performed with the use of the electric motor.

Airport Experience and Infrastructure

The airport experience is an important feature for USTI users. The experience at the airport should be smooth and the passengers should perceive any waiting time. Also, the design has to align with current airport infrastructure and regulations. Schiphol airport is an arbitrary example in this section.

Multiple approach routes are selected for different runway configurations at Schiphol airport to minimise interference with current regulations, which scarcely cross paths with conventional aircraft take-off and landing routes. The top of a parking garage will be dedicated for this purpose to ensure a safe landing. The pod then autonomously drives to an USTI lounge close to the departure gate. Here, not only the passenger exits the pod, but also the luggage is unloaded without inconveniencing the passenger. This process is visualised in Figure 4. In Figure 5, the internal lay-out of the USTI lounge is depicted. The lounge is situated close to the gates and shopping area to ensure passenger comfort and store revenues.

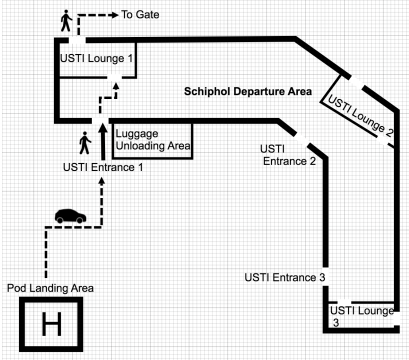

Figure 4: Schiphol arrival by pod

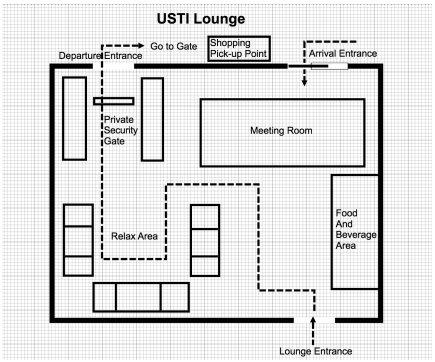

Figure 5: Top view of USTI lounge at airport

Control, Maintenance and Storage Stations

Although the designed system is autonomous, operators will have to continuously control and maintain the pods. The controllers are authorised to change the following parameters without taking full control: (1) velocity, to act when the airport is congested. (2) Route, to act in emergency situations. (3) No-go zones, to control approach routes and temporary exclusion zones. Controllers are also updated with the latest pod conditions and passenger information.

The frequency of maintenance is determined by EASA regulations. Besides pre- and post-flight checks, 100h, annual and 'C' inspections are also scheduled.

As airports facilities are already rather crowded and there is no space for the construction of new infrastructure, a new location close to the airport is chosen. The control, maintenance and storage stations are all located here, to centralise all operations.

Design Analysis

To ensure stakeholders are satisfied by the final design, the design has to be analysed to the point where compliance with the requirements can be fully tested. Before this is possible, the sustainability and risk have to be assessed.

Sustainability Analysis

Sustainability drives the design to a great extent and that is why every subsystem chapter has a section in the report dedicated about this topic. Regarding sustainability, the main objective and purpose of USTI is to design a concept that positively contributes to the Sustainable Development Goals set by the United Nations. USTI contributes positively on the goals related to clean energy, climate, infrastructure, good health and well-being but negative on reducing inequality due to target market.

As the pod has the most impact on environmental level, the *EcoDesign Strategy Wheel* tool is selected to examine this. With this wheel, scores are assigned to more specific aspects of environmental impact. The most critical aspects are revealed by assessing the initial design, which include (1) material recyclability, (2) material manufacturing ease, (3) energy efficiency and (4) emissions. During the detailed design phase, these aspects are considerably optimised, leading to the results in Figure 6.

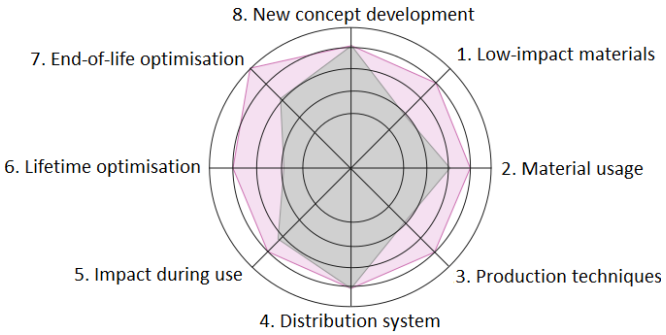

Figure 6: Comparison of the initial pod system (grey) and the finalised pod system (pink) using the EcoDesign Strategy Wheel.

Risk Assessment and Regulations

The method for risk assessment is based on a ranking system comparing both likelihood and consequence. In general, risks for the system are categorised in (1) technical risks and (2) operational risks. In the former, one of the most critical risks is sensor failure. Whereas conventional aircraft are controlled by pilots, USTIs 'eyes and ears' are its sensors. This risk can be mitigated by introducing a safe-life system of redundancy.
In the second category, the most pressing risks are being stuck in traffic in driving mode and overbooking. These are mitigated by identifying sufficient amounts of take-off and landing spots and by having a large number of pods available, respectively. Also, compliance with regulations poses a risk for the system. Current laws are not flexible towards autonomous driving, especially around airports. However, this risk is naturally mitigated as positive trends towards autonomous vehicles are becoming more and more popular

Requirement Analysis

Compliance with requirements on the system and subsystems is analysed one by one. It is found that the most driving requirements are met: an *autonomous* pod is designed that transports *two people* from door to airport to door within *four hours* up to a range of *300 km* and can be *recycled by up to 78 %* of its weight. From the 114 set requirements, 84 are fully met. Some requirements are nearly met or cannot be verified yet. Those that are not met have either been solved in a different way or have been identified as irrelevant. For example, the size requirement has not been met as USTI is bigger than a medium sized car. However, the pod will still be allowed to drive on the road, as regulations allow the current dimensions of 5.10 m x 2.06 m x 1.76 m (L x W x H).

Future Development

In the future, both the pod and the system can be further analysed and optimised. Some of the most important considerations include:

- A detailed aerodynamic analysis to allow for a more efficient design.
- Further analysis and discussion with relevant parties on the implementation of the system at the airport.
- The inclusion of multiple iterative loops to optimise the design.
- Designing a pod optimised for cargo. In the current pod, parts of the available cargo space are not used, because the maximum payload weight is already reached. Therefore, a smaller pod design would be more optimal.

Nomenclature

Symbols

α	Angle of attack	°
β	Yaw Angle	°
δ_A	Aileron deflection	-
δ_E	Elevator deflection	-
δ_R	Rudder Deflection	°
δ_R	Rudder deflection	°
$\dot{Q}_{AC}$	Required cooling load	kW
η_p	Propeller efficiency	-
η_v	Dynamic pressure efficiency	-
ρ	Density	kg/m^3
σ	Angle Between Direction of Flight and V_t	m/s
σ	Normal stress	Pa
τ_r	Rudder angle of attack effectiveness	-
τ_S	Torque experienced by the servo	Nm
A_{member}	Cross-sectional area of a truss member	m^2
AR	Aspect ratio	-
B	Boom area	m^2
b_r	Rudder span	m
b_v	Vertical tail span	m
C_Dy	Side drag coefficient	-
C_r	Rudder chord length	m
C_v	Vertical tail chord length	m
C_f	Control surface chord	m
C_{L_α}	Lift coefficient gradient	1/rad
$C_{n\beta}$	Yaw related stability derivative	
$C_{n\delta_R}$	Rudder deflection related stability Derivative	-
c_{root}	Root chord	m
$C_{y\beta}$	Yaw-related stability derivative	-
d_c	Distance center of area to CG	m
d_s	Shock absorber diameter	m
$F(t)$	Failure rate	-
h_e	Height to the glass of the cockpit	m
h_p	Height of the pod	m
I	Moment of Inertia	m^4
i	Interest rate	%
i_{gear}	Gear ratio	-
K_f	Fuselage contribution to stability derivative	-
l_c	Length of the cockpit	m
l_r	Length of the roof of the cockpit	m
l_g	Servo arm length	m
l_{tank}	Fuel tank length	m
m_e	Engine mass	kg
$M_{ac_{wf}}$	Aerodynamic moment of the wing	Nm
m_{fuel}	Fuel mass	kg
M_{hrs}	Required manufacturing labour	h
M_L	Moment created by the lift	Nm
m_{OE}	Operational empty mass	kg
$m_{structure}$	Structural mass	kg
m_{TO}	Take-off mass	kg
M_w	Moment created by the weight	Nm
n	Number of years	-
N_G	Landing gear load factor	-
n_{max}	Maximum load factor	-
n_s	Energy absorption efficiency of shock absorber	-
n_t	Energy absorption efficiency of tyre	-
NPV	Net present value	€
P^*	Power density	kW/kg
$P_{B/F}$	Maximum static load	kg
P_{peak}	Peak power	kW
P_{req}^{VTOL}	Power required for VTOL	W
P_{ss}	Steady state roll rate	m/s
PV	Present value	€
Q	Quantity of vehicles	-
r	Radius	m
$r^{fabrication}$	Fabrication rate	€/s
R_s	Reliability of the system	-
r_{back}	Fuel tank back radius	m
r_{elec}	Percentage of range performed with electricity	%
r_{front}	Fuel tank front radius	m

S	Wing surface area	m^2
S_s	Aircraft projected side area	m^2
S_v	Vertical tail surface area	m^2
S_f	Control surface surface area	m^2
S_h	Horizontal tail surface area	m^2
S_{tot}	Total top view surface area	m^2
s_t	Maximum allowable tyre deflection	m
S_w	Wetted surface area	m^2
t_p	Pull down time	s
t_D	Skin thickness	m
$T_{external}$	External temperature	°C
t_{glass}	Thickness of the glass	m
$T_{internal,0}$	Initial internal temperature	°C
$T_{surface,0}$	Initial surface temperature	°C
T_{target}	Target internal temperature	°C
t_{wall}	Thickness of the skin	m
u	Utilisation factor	-
V_i	Induced velocity by the propeller	m/s
V_s	Stall speed	m/s
V_t	Total airspeed	m/s
V_v	Vertical tail volume	m^3
V_w	Maximum crosswind speed	m/s
V_{knots}	Flight speed	kts
w_p	Width of the pod	m
W_L	Landing rate	m/s
$W_{OE_{lb}}$	Maximum take-off weight	lb
$W_{OE_{lb}}$	Operational empty mass	lb
W_{TO}	Take-off weight	N
w_t	Touchdown rate	m/s
x_{ac_h}	Distance between nose and tail	m
x_{mg}	Distance between nose and center of gravity	m
y	Distance to the neutral axis	m

Abbreviations

CG	Center of gravity m
(E)STOL	(Electric) Short Take-Off and Landing
AHRS	Attitude and Heading Reference System
ATC	Air Traffic Control
CFD	Computational Fluid Dynamics
CLP	Classification, Labelling and Packaging regulation
CO_2	Carbon Dioxide
COP	Coefficient Of Performance
CPU	Central Processing Unit
CT	Computed Tomography
CVR	Cockpit Voice Recorder
DOC	Direct Operating Cost
EASA	European Aviation Safety Agency
EUR	Euro Currency
EURO NCAP	European New Car Assessment Programme
FAA	Federal Aviation Administration
FDR	Flight Data Recorder
FEM	Finite Element Method
FM	Figure of Merritt
GPS	Global Positioning System
HVAC	Heating Ventilation and Air Conditioning
I/O	Input/Output
INS	Inertial Navigation System
IOC	Indirect Operating Cost
MTOW	Maximum Take-Off Weight
N/A	Not applicable
NO_x	Nitrogen Oxides
OEW	Operating Empty Weight
Pax	Passengers
PCU	Power Control Unit
PMT	Payment per month
PP	Polypropylene
RAIM	Receiver Autonomous Integrity Monitoring
RAMS	Reliability Availability Maintainability and Safety
REACH	Registration, Evaluation, Authorisation and Restriction of Chemicals regulation
RF	Radio Frequency
RoC	Rate of Climb
SDG	Sustainable Development Goals
TO	Take-Off
UN	United Nations
USTI	Unpiloted Sustainable Transport Initiative
UV	Ultraviolet
V&V	Verification and Validation
VFR	Visual Flight Rules
VTOL	Vertical Take-Off and Landing

Contents

1 Introduction

With the harmful effects of fossil fuels on the environment and gas prices projected to skyrocket over the coming decades, the demand for electric vehicles has soared in the past few years. Tireless work is being invested in the research and development of batteries with higher energy densities, more efficient electric motors and strong, ecologically-friendly materials. Electric vehicles, however, cannot be enjoyed while stuck in increasingly frequent traffic congestions. Roads can only be expanded with new lanes until a certain point is reached at which there is no room left. This project thus aims for the skies, both literally and figuratively, with the design of a VTOL, hybrid, autonomous pod that allows anyone to be picked up from home and to be dropped off at a location of their choosing.

The system presented in this paper will focus on transits to and from the airport and attempts to reduce the door-to-door travel time of passengers to four hours. It will pick up passengers from home, drive towards an open area, vertically take off, fly towards a hub at the airport where they will be dropped at a designated lounge to speed up the screening process, which is one of the key areas where passengers travelling by plane lose out on precious time.

This report is divided into four main sections. The first section will discuss the global picture of the project, a market analysis and the approach that is taken to ensure that the project is sustainable. The second section focuses on the design of the vehicle itself: the pod referred to as USTI (Unpiloted Sustainable Transport Initiative). The design of the operational systems surrounding USTI will be described in the third section. The last section will feature a proposal to market and produce the system, an analysis of the design process and resource allocations and presents an extensive risk assessment.

I

Preliminary Analysis

2
Global Picture

In this chapter the global picture of the project is revised. First of all, the project objectives will be discussed in section 2.1. Furthermore, the requirements and constraints of the project are stated in section 2.2. This will be followed with presenting the trade-off procedures that are used during the design phase to choose a final preliminary design, which is presented in the last section of this section.

2.1. Project Objectives

Travelling by plane is a time-consuming endeavour. In a typical door-to-door journey, presented in Figure 2.1, the passenger often wastes time waiting to continue to the next leg of their journey. Direct routes with public transportation are often unavailable, which makes waiting times inevitable. The efficiency of travelling by car or taxi greatly depends on the traffic conditions. During peak hours, especially in and around big cities, traffic is often congested. An option that evades these issues would be an interesting alternative.

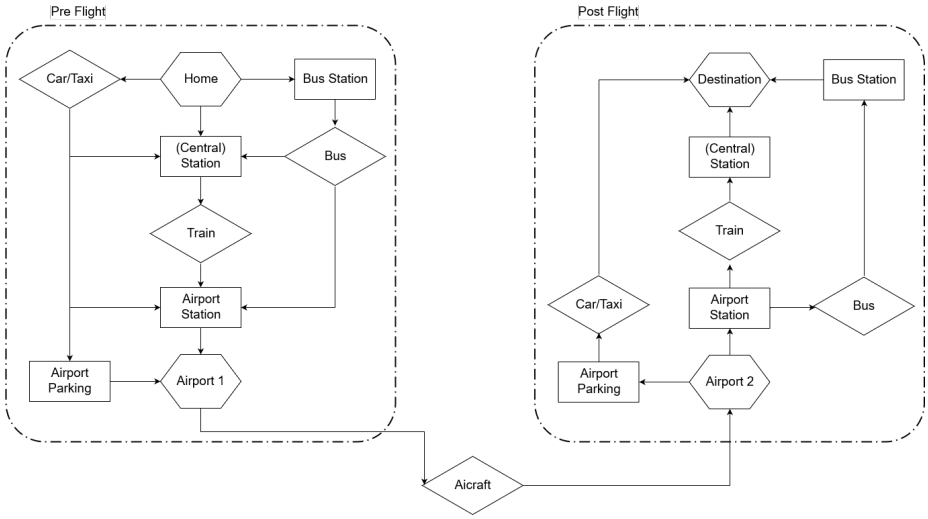

Figure 2.1: A typical door-to-door journey of an aviation user

Besides the aforementioned aspects, time is also wasted at the airport itself. The surge of air travel over the past decades has put a strain on airport logistics. Passengers are required to arrive hours in advance of their flight to drop off their checked luggage. Subsequently, passengers need to pass security checks before being allowed access to the gate. Screening is thus considered as one of the main bottlenecks in airport operations. The unpredictability of passenger arrival times frequently results in undermanned security stations, causing significant waiting times. For business people especially, for whom time efficiency is one of their highest priorities, a delayed door-to-door journey is a large source of frustration. This is even more of a problem around large business hubs such as London and Paris.

It is clear that there is a demand for a system that greatly reduces the waiting time in door-to-door journeys for business people. This also complies with the vision of the European Union, which states that in 2050, 90% of the public should be able to travel within Europe in less than 4 hours from door-to-door. Ideally, this system is autonomous to limit the operational costs for the operator to run the system.

This project aims to design and analyse the feasibility of this system. The following project objective is established:

"Impress the jury, by designing an autonomous system, which will reduce door-to-door travel time to four hours within Europe, accomplished by ten students in ten weeks."

The autonomous system envisioned in this objective consists of two major components: (1) a set of autonomously flying and/or driving pods that can pick up and drop off on demand and (2) improved time efficiency in airport operations.

The pods are able to carry two passengers with their luggage. The system is first designed for implementation within the European Union, complying with its long term vision. However, the possibility of expanding to other parts of the world is also considered. The system is expected to be operational within ten years from now.

2.2. Requirements and Constraints

Before commencing with the design of the system, it is important to establish and analyse the requirements and constraints that should be adhered to. First of all, the user requirements are listed. The main users of the system are the passengers, the airport and the operator. The user requirements can be summarised as follows:

- Passengers
  - POD-UR-PS-1: The system shall minimise waiting times.
  - POD-UR-PS-2: The system shall provide increased levels of comfort compared to current modes of transportation.
  - POD-UR-PS-3: The system shall not have a lower accessibility for disabled people compared to alternatives.
- Airport
  - POD-UR-AI-1: The system shall optimise the passenger flow in the airport.
  - POD-UR-AI-2: The system safety shall be guaranteed in all conditions.
  - POD-UR-AI-3: The system shall not cause any decrease in airport revenues.
- Operator
  - POD-UR-OP-1: The system shall make use of existing urban infrastructure.
  - POD-UR-OP-2: The system shall provide transport of passengers with minimal extra personnel cost.
  - POD-UR-OP-3: The system shall be adaptable to cargo flights.

From these user requirements, the mission requirements can be derived. These are high-level requirements that reflect the mission need, project objective and the user requirements. The focus on business travellers, for example, becomes apparent from the fact that the system should be implemented in airports with more than 10 million passengers per year. These airports are located mainly around big business hubs and are expected to benefit the most from the system.

- POD-MIS-1: The system shall be able to reduce the average door-to-door travel time within Europe to 4 hours, including all operations.
- POD-MIS-2: The system shall be able to be implemented in airports with a passenger number of 10 million per year.
- POD-MIS-3: The system shall be able to cover the range for which 90 % of the European population can access an airport which allows inter-European travelling.
- POD-MIS-4: The system shall be able to cover a circular area of radius 150 km around the selected European airports.
- POD-MIS-5: The system shall be available for people who booked the service at least one day before departure.
- POD-MIS-6: The system shall be able to operate autonomously.
- POD-MIS-7: The pod shall be able to operate with the already-existing urban infrastructures.
- POD-MIS-8: The cost of the service shall not exceed the cost of a taxi ride which travels along the same route.
- POD-MIS-9: The system shall have a unit cost of no more than 100k euro.
- POD-MIS-10: Total shopping revenues shall not be lower than current shopping revenues.
- POD-MIS-11: The system shall not negatively impact current safety levels.
- POD-MIS-12: The system shall be more sustainable than current modes of transportation.

2.3. Summary of Trade-Off

Preliminary concepts are designed that all adhere to the user and mission requirements to varying degrees. Trade-offs are performed on the pod configuration, the method of screening, and the drop-off location to choose two potential concepts of the system.

2.3.1. Initial Trade-Off

In this section, the trade-off process which lead to the selection of the two most suitable design concepts from four initial options is described.

Initial Trade-Off on Pod Configuration

The four design configurations that enter the initial trade-off for the pod configuration are:

(A) A driving pod, which, together with other pods, can create a flying central unit. This central unit has electric rotors.

(B) A driving and flying pod with rotors and hybrid propulsion.

(C) A driving and flying pod with deployable wings and electric rotors.

(D) A flying pod with fixed wings and turbojet engines.

Several trade-off criteria are devised based on the previously established requirements. The most important criteria include the possible reduction in travel time, range and the size of the pod, as it might need to be able to both drive and fly. Other criteria include the weight of the system, the operational and manufacturing cost and sustainability.

Option B and C are the most suitable in this trade-off. Option B scores high on reduction in travel time and range and it does not show any unacceptably low scores in the other criteria. Option C scores high on sustainability, operational costs and passenger comfort due to its electric rotors.

Initial Trade-Off on Screening Method

The following options are considered for the initial trade-off of the screening method:

(A) Screening outside the pod, before flight.

(B) Screening inside the pod, before flight.

(C) Screening on pod, during flight.

(D) Screening at final hub, pod is completely screened with passengers inside.

(E) Screening at final hub, outside pod.

The most important criteria in this trade-off are safety and time reduction. The other criteria are the weight increase of the pod, cost and technology-readiness level.

Option C and D are found to be the best options for the screening method. Option C scored very high on time reduction as screening is performed during flight. Option D mainly scored high because screening at the final hub does not add any weight to the pod. Furthermore, performing screening when the passengers are still in the pod is better in terms of time efficiency compared to the option in which passengers need to get out of the pod for screening.

Initial Trade-Off on Drop-Off Location

The following options are considered for the trade-off regarding the drop-off location.

(A) Drop-off at a regular gate.

(B) Drop-off at a separate gate.

(C) Drop-off at a hub and proceed to the gate with an autonomous (different) vehicle.

(D) Drop-off at a hub and proceed by walking to the gate.

(E) Land at a separate hub and proceed by driving the pod to the aircraft.

(F) Land directly at the aircraft.

The most important criterion for this trade-off is the time that can be saved. Other criteria include safety, feasibility, the need for extra infrastructure and the possible luggage flow efficiency.

Option D and E are found to be the most suitable in this trade-off. Even though option D scores relatively poor on the most important criterion, it scores well on all the others. Option E scored well on luggage flow efficiency and did not show any discrepancies in any of the other criteria.

2.3.2. Final Trade-Off

The initial trade-off results in two conceptual configurations, which are described in Table 2.1.

Table 2.1: Overview of the two design concepts as a result of the initial trade-offs

	Design concept 1	**Design concept 2**
Lifting device for cruise	Two rotors	Wing
Lifting device for take-off	Four rotors	Two tiltable rotors
Forward flight devices	Two tiltable rotors	Two tiltable rotors
Propulsion system	Hybrid	Electric
Screening procedure	On board of the pod	Upon arrival at the airport

During the midterm phase of the project, these two concepts are designed to define a clear picture of which option would be the most efficient to meet the requirements.

A trade-off procedure is then initiated to finally decide on several aspects of the final design of the vehicle. These are:

- Lift in cruise will be provided by a wing.
- VTOL is ensured by two rotors in horizontal plane, each at a tip of the wing.
- The two rotors at the tips are 90° tiltable.
- Forward flight is ensured by the two rotors at the tips of the wing, in vertical plane.
- The pod is powered by an hybrid-electric propulsion system.
- Screening will occur upon arrival at the airport, where the passengers are required to walk to their gate.

2.4. Overview of Final Concept

From the outcome of the final trade-off, the detailed design phase is initiated. This develops with the analysis of every subsystem, which will be described in Part II of this report. A render of the final design can be visualised in Figure 2.2.

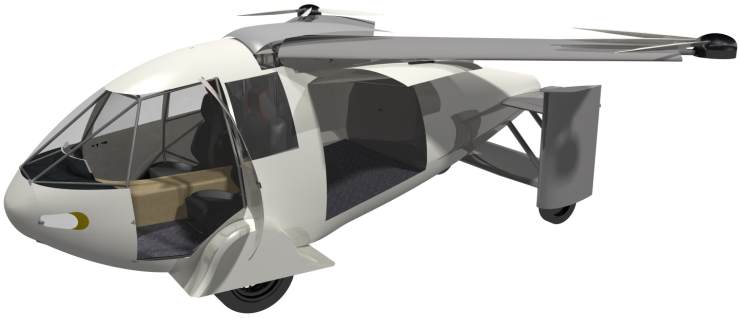

Figure 2.2: Render of the final pod design

Details of the pod in flying mode are presented in Figure 2.3 to 2.6. The pod in driving mode is presented in Figures 2.7 to 2.10

Figure 2.3: Side view of the pod in flying mode

Figure 2.4: Top view of the pod in flying mode

Figure 2.5: Front view of the pod in flying mode

Figure 2.6: Back view of the pod in flying mode

Figure 2.7: Side view of the pod in driving mode

Figure 2.8: Top view of the pod in driving mode

Figure 2.9: Front view of the pod in driving mode

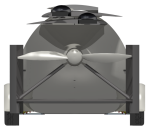

Figure 2.10: Back view of the pod in driving mode

3
Market Analysis

This chapter will present the market analysis. Firstly, the procedure will be described in section 3.1, which is followed by a summary of the preliminary market analysis. The feedback from different sources on this market analysis is presented in section 3.3. Subsequently, an update on the market analysis is given in the last section of this chapter.

3.1. Analysis of Target Market

Figure 3.1 depicts the step-by-step process to analyse the target market . The first three steps are combined in this chapter as marketing research. The subsequent marketing development phase is investigated later in the report. The confrontation phase is taken into account throughout the report, since feedback collected from experts of the aerospace industry and potential future clients is implemented in the design decisions. The last steps will be further developed in chapter 18.

Figure 3.1: Step-by-step procedure for the market analysis

Please note that the market analysis is continued in chapter 18, where a detailed cost estimation is provided, as well as a market strategy and an estimation of the upcoming revenues.

3.2. Summary of Preliminary Market Analysis

The preliminary market analysis is based on the initial requirements and assumptions for the pod design. The following parameters will be defined and/or calculated to obtain a full market overview of the system:

- Target Customers: the part of the society the company wants to sell the product to.
- Penetration Rate: the percentage of the market the company will be able to capture with respect to the total market.
- Market Volume: the number of target customers times the penetration rate.
- Market Value: the market volume times the average value of the product.

- Gross Profit Margin: the difference between cost and selling price.

The pod is designed to transport four passengers to and from the airport, in accordance with the first concepts and initial requirements. The initial calculations for the parameters are based on airport passenger data of European airports with a passenger number of 10 million per year. The results of the calculations can be found in Table 3.1. This will be iterated in the later design phase based on the feedback of external parties.

The general procedure to calculate the market value is as follows:

1. Obtain data regarding the number of passengers per year per airport from literature.[1]
2. Convert to number of passengers per day.
3. Exclude the transit passengers, because they do not need transportation to or from the airport, this is estimated to be 35 % of the total amount of passengers [2].
4. Assume that 3 % of the passengers will use the pod system.
5. Sum all the values obtained for the selected airports in Europe. The result and subsequent steps can be found in Table 3.1.
6. Determine penetration rate to determine available market volume. Since there are only very few competitors, a penetration rate of 35 % is assumed.
7. Determine the selling price of the system to obtain the market value.

Table 3.1: Preliminary market analysis

Parameter	**Value**
Total Market Volume	68,722 pods
Penetration rate	35 %
Available Market Volume	24,052 pods
Cost per pod	€100,000
Gross Profit Margin	100 %
Selling price per pod	€200,000
Available market value	€4,810 million

The possible partnerships are identified such as Schiphol Airport, Uber and Leonardo S.P.A. The initial parameters indicate that a positive business case can be established and that the design is viable. It confirms that the team can continue with the more detailed design of the system. In a later design phase, the definite selling price of the pod will be recalculated using more detailed information about the concept.

3.3. Feedback from Experts

Throughout the project, several experts in the aeronautical industry are interviewed to check the reliability of the preliminary market analysis and provide feedback regarding the design strategies of the team. Specifically, the following experts are interviewed:

- Christiaan Snabel, business developer of smart airport data at Schiphol Airport.
- Wil Ruijsbroek, co-founder of the screening technology company Stage Gate 11, which operates at Schipol Airport.
- Mattia Celli and Paolo Cerini, consultant partners collaborating with the helicopter division at Leonardo S.P.A..
- David van Proosdij, member of the engineering team of PAL-V.

Several aspects of the design of the USTI service are touched upon throughout the interview. These are listed in the following paragraphs.

Target Customer. All speakers agree on the fact that the target customer of the service shall be business travellers. They value saving time remarkably: being able to travel quickly to- and from- the airport would allow them to make their busy schedule even more productive. Moreover, as their company typically pays for the service, they do not mind spending a rather expensive price for the comfort which the service provides.

Number of Passengers. As the target customer is the business traveller, it should be noted that this typology of passengers typically travels individually or in small parties. Therefore, it is decided to design a vehicle which is able to carry two

[1] Airport Passenger Data per Year, Busiest Airports in Europe, `https://en.wikipedia.org/wiki/List_of_the_busiest_airports_in_Europe`
[2] Annual Report Schiphol, Schiphol Group, `https://www.annualreportschiphol.com/#who/travellers`

passengers.

Appeal for the Industry. It is discovered that the European market not yet ready to launch such product: the risk is that the purchase of this futuristic vehicle would be reserved to a limited amount of aerospace fanatics. However, there exists strategies which allow the product to become more appealing not only from the passenger point of view, but also from the industry perspective. Specifically, by shifting the focus on the sustainability of the vehicle, the service would become more attractive for the manufacturing and operating companies, as they would also earn a 'greener image' with respect to their competitors.

Screening Operation. Currently, screening operations are the cause of many time-delays and represent a 'bottle-neck' for the passenger flow at the airport. A convenient solution to this issue would be the addition of all screening procedures on board of the USTI vehicle. However, it is soon discovered that screening instrumentation is significantly heavy and cumbersome. Moreover, the implementation of lead plates for passenger protection would be necessary, which would increase the weight of the pod even more. Given the infeasibility of such design option, the idea of including all screening procedures on board of the pod is discarded. This means that an optimisation of the passenger flow at the airport will be necessary.

Operating Company. As design company, the team will sell the service to an operating company. A detailed estimation of the operating costs is necessary to make the product appealing to the stakeholders in charge of running the service. Three options exists which must be evaluated later in the design process:

- The service could be operated by the airports. This option is convenient as the airport staff is in charge of all the airport infrastructure. However, they do not have any information on the identity of the passengers. Therefore, it would be difficult to implement all security operations.
- The service could be operated by the airlines. This would be convenient as the airlines are in possession of identity information about the passengers and have a clear overview of all the passengers who use their service. However, door-to-door transportation is not their main focus and, in the long term, the purpose could interfere or merge with the regular flight program, undermining the foundations of the concept itself.
- The service could be operated by an external transportation company. As a regular taxi, the pod could be operated in such a way to remain external to the airport. This would be convenient as no conflict of interest would occur.

Finally, a questionnaire is proposed to future customers. It is discovered that the potential passengers are attracted by the service only if the reduction in travel time is significant and if the level of comfort in the cabin is maximum. Otherwise, the expected cost of the service is too high compared to currently existing modes of transportation, which are very convenient in terms of costs. An overview of the prices of the currently available systems of transportation is provided in Table 3.2.

Table 3.2: Results from the competitor analysis

	€/km	€/min	km/min
Taxi	2.44	3.28	1.30
Public transport	0.19	0.18	0.99
Personal transport (Diesel)	0.16	0.22	1.30
Personal transport (Euro95)	0.17	0.23	1.30
Uber	1.47	1.96	1.30

Table 3.3: Updated market analysis

Parameter	Value
Total Market Volume	33,833 pods
Penetration rate	35 %
Available Market Volume	11,841 pods
Cost per pod	€100,000
Gross Profit Margin	100 %
Selling price per pod	€200,000
Available market value	€2,250 Million

3.4. Updates on Market Analysis

Based on the feedback from external experts a more accurate market analysis is performed. The main changes in the market analysis are due to a shift in the target customers from all passengers to mainly business passengers. Business passengers amount to around 30 % of the total number of passengers at Schiphol Airport [3]. Combining this with the parameters from Table 3.1, it can be concluded that the market volume will decrease to 50 % of the initial value. The most important changes can be summarised as:

- Target customers: business travellers.
- The business passengers consist of 30 % of the airport passengers.
- The market volume is reduced to 50 % of the initial value.

The same parameters as those for the preliminary market analysis are calculated again using the updated information. The final values of the updated market analysis can be found in Table 3.3.

[3] Annual Report Schiphol, Schiphol Group, `https://www.annualreportschiphol.com/#who/travellers`

4

Sustainability Approach

Sustainability plays an extensive role in the design of the pod and the system, which is directed towards a positive impact on a social, economic and environmental level. This chapter gives an overview of the level of sustainability of the initial design, after which it elaborates on the design philosophy used throughout this report.

4.1. Sustainable Development Strategy

With respect to sustainability, the main objective and purpose of USTI is to come up with a final system that contributes to the sustainability goals set by the United Nations (UN).

In 2015, the UN approved the *2030 Agenda for Sustainable Development*,[1] which includes seventeen goals that the member states try to achieve. These goals are depicted in Figure 4.1, addressing various topics. Table 4.1 shows the impact of the pod (as described in chapter 2 and the midterm report [3]) on these goals. A plus sign (+) is noted in the table if the pod system has a positive contribution to the achievement of these goals, and a minus sign (-) represents a negative impact. Note that some goals are not directly impacted by the pod system and are thus indicated by 'not applicable'.

Figure 4.1: Sustainable Development Goals of the United Nations

Table 4.1: Impact of the pod system on the SDG's of the UN

Goal	1	2	3	4	5	6	7	8	9	10	11	12	13	14	15	16	17
Impact	n.a.	n.a.	+	n.a.	n.a.	n.a.	+	+	+	-	n.a.	+	+	n.a.	n.a.	n.a.	n.a.

The reasoning for this scoring has been described in the midterm report [3], and is briefly discussed here for the most important SDG's:

- **Health and Well-Being (3).** The well-being of passengers increases when using the pod instead of conventional modes of transport because the ride is both time-efficient and effortless for the passenger.
- **Decent Work and Economic Growth (8).** The local community benefits by an increase in job opportunities created by this innovative system.
- **Reduced Inequalities (10).** The gap between the rich and poor increases as the system is designed only for business people. The less fortunate will not benefit from the system.
- **Sustainable Cities and Communities (11).** The air quality in cities would improve when the pod's hybrid engines are used, whereas the amount of noise in the city would increase.

[1] Agenda For Sustainable Development, United Nations, `https://www.un.org/sustainabledevelopment/development-agenda/`

- **Climate Action (13).** The design has a hybrid engine, which contributes to a reduction of the emission of greenhouse gasses compared to the current standards.

Although sustainability entails social, economical and environmental aspects, the design of the detailed design phase will mostly consider the latter. From Table 4.1 it can be seen that a considerable amount of the impacted goals have environmental aspects in them. Therefore, a more detailed assessment method for the environmental footprint is used.

4.1.1. EcoDesign Strategy Wheel

The EcoDesign Strategy Wheel [10] helps to visualise the environmental impact of the design. Some of the eight indicators relate to the product component level, some to the product structure level and others to the product system level. The indicators are explained briefly below:

1. **Selection of low-impact materials.** Addresses whether the system uses lower energy content materials, recycled materials and recyclable materials.
2. **Reduction of materials usage.** This should result in a lower weight or volume for the pod.
3. **Optimisation of production techniques.** The emphasis is on fewer production steps, less production waste and alternative production techniques.
4. **Optimisation of distribution system.** Evaluates energy efficient logistics and the transport mode of the system.
5. **Reduction of impact during use.** Analysing the energy source, the energy consumption and consumables.
6. **Optimisation of initial lifetime.** The modular product structure as well as maintenance and repair are assessed with this indicator.
7. **Optimisation of end-of-life system.** Inspects the reuse of the pod and the recyclability and incineration aspects.
8. **New concept development.** The shared use of the product and integration of the system functions are addressed within this indicator.

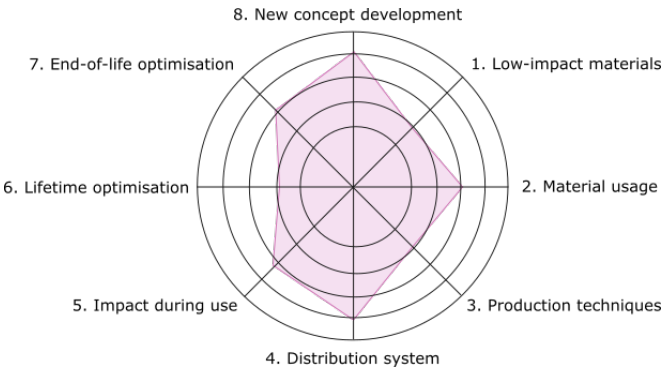

Figure 4.2: The EcoDesign Strategy Wheel for the current pod system.

The initial design scores low on the materials side, the production techniques and the optimisation of lifetime due the use of amongst others carbon fibre, as evidenced by Figure 4.2. Carbon fibre cannot be made from recycled materials, is hard to recycle, is hard to manufacture (more steps than other materials) and is also considered hard to maintain. Also, the current design scores low on the impact during use, because the selected engine and tilting rotor are not considered optimal. Besides, the pod scores relatively low on lifetime optimisation and impact during use, which is a result of having a hybrid engine with only 30% electricity. In subsection 19.2.2, another EcoDesign Strategy chart will be shown that compares the current design with the finalised design, demonstrating the progress in terms of sustainability.

4.2. Design Philosophy

All of the upcoming chapters have a section dedicated to explaining how sustainability is incorporated in that part. The team will mainly focus on improving the aspects that scored poorly regarding the UN goals and the EcoDesign Strategy Wheel. These aspects are: material manufacturing, recyclability, energy efficiency and emissions. Nevertheless, the focus will not only be limited to these aspects. A summary on sustainability is given in each chapter to ensure that the topic is addressed sufficiently. Also, data is processed here to present relevant outcomes. In these sections, only the appropriate topics on sustainability are discussed.

In chapter 19, a final analysis on sustainability is performed, collecting all the information on this topic from the various chapters. This way, a comparison between the initial and the final design is created by means of another chart created using the EcoDesign Strategy Wheel, similar to the one presented in this chapter.

II

Pod Design

5
General Design Procedure

This chapter provides a clear overview of the design procedure followed during the design of the pod. Firstly, the subsystems that are to be designed will be discussed together with their interrelations. Afterwards, a new weight estimation is performed to start the design of the subsystems with the most recent estimates.

5.1. Subsystem Design

The design process is a continuous iterative process. Multiple subsystems are being designed simultaneously at every moment. The outputs of the design process are inputs to other subsystems. The main subsystems of the pod are:

- Propulsion System
- Driving & Landing Gear
- Structure
- Flight Control Systems
- Internal Systems
- Electric Systems
- Emergency system

The interaction between the subsystems can best be visualised with Figure 5.1. The chart can be read in the same manner as an N2 chart. However, the outputs depicted are not all outputs of the subsystem, but rather represent how they interfere with other subsystems. This figure thus depicts the amount of influence some subsystems have on others. Other subsystems (e.g. Emergency Systems) do not interfere and can therefore be designed independently. To prevent inconsistencies, the weight estimation performed in this chapter will be leading for the design of the subsystems. The estimated weight will only change after all systems are designed. These subsystems are designed simultaneously due to time constraints, which means that close communication is required between every design team to create a feasible design.

Propulsion		Propeller and engine size and locations			Power required by engine	
	Driving & Landing Gear	Landing gear locations and size				
	Available gear storage	Structure	Wing folding Mechanism	Cockpit and luggage comp. dimensions		
Stability thrust requirements		Control surfaces dimensions	Flight Control Systems		Actuator required power	
		Internal systems locations and size		Internal Systems	Internal System power required	
		Battery dimensions			Electric Systems	
						Emergency Systems

Figure 5.1: Subsystem output interference chart.

5.2. Weight Estimation

In this section the iteration on both the Class I as well as the Class II weight estimation are discussed. In the detailed design, some of the subsystems are underestimated. This makes a review of the different weight estimations necessary. The estimation is based on the mission profile, which includes a range of 310 km (including contingency) and a cruise speed of 200 km/h.

5.2.1. Changes

First of all, in the initial weight estimation only a contingency factor for the range is included. However, the detailed design showed various subsystems to be heavier than originally calculated, to account for such unforeseen increases in mass, contingency factors are included in the Class I weight estimation. This contingency is set to 20% for the m_{TO}, which considerably increases the weight. The changed parameters can be found in Table 5.1. The root chord is increased to reduce wing span, which makes wing folding possible Furthermore, the concept of screening on board is considered unfeasible, as described in chapter 3. Besides, it is discovered that the mass for driving is underestimated, so the mass initially accounted for the screening is now used as additional mass of the driving system of the pod.

Table 5.1: Parameters altered from the previous weight estimation methods.

Parameter	Old value	New value
Contingency factor [−]	1.0	1.2
r_{elec} [−]	0.4	0.3
P^* [kW/kg]	1.5	0.7
η_p [−]	0.9	0.81
m_e [kg]	35	20
P_{peak}[kW]	200	440
c_{root}[m]	1.1	1.22

5.2.2. Results

The results of the weight estimations are displayed in Table 5.2. The Class II estimation is iterated three times until two consecutive results differ less than 1 %.

Table 5.2: Results of the weight estimations

	Class I	Class II	Final Class II	Relative difference
m_{TO} [kg]	881.6	819.6	782.4	11.3 %
m_{OE} [kg]	317	290	266	16.1 %
$m_{battery}$ [kg]	82.1	112.3	106.8	24.7 %
m_{fuel} [kg]	28	27.1	25.4	9.3 %
$m_{generator}$ [kg]	100.9	95.2	89.2	11.7 %
S [m^2]	7.89	7.64	7.00	11.3 %
L/D [−]	9	9.7	9.2	2.2 %

5.2.3. Verification and Validation

On both the Class I and Class II weight estimation verification and validation is performed. For the Class I weight estimation reference data from the hybrid Aeromobil 4.0[1] is used as input of the weight estimation. The outcome of the estimation matches the mass of the Aeromobil if 85 % of the energy is to be provided by fuel.

Table 5.3: Verification of the Class-I weight estimation

Parameter	USTI Estimation [kg]	Aeromobil 4.0 [kg]	Difference [%]
m_{TO}	922	960	4.0
m_{fuel}	79.7	74.97	6.7

Table 5.4: Verification of the Class-II weight estimation

Parameter	Raymer [kg]	Roskam [kg]	Difference [%]
m_{OE}	265.6	269.2	1.4

For the Class II weight estimation, conventional Raymer's equations [47] are used. The values from the Class II weight estimation differ a few percent from the Class I weight estimation and don't converge to an abnormally different value. This is a form of verification. Moreover, Raymer's equations are verified by calculating the m_{OE} with the approach as described by Jan Roskam [48]. The results of this verification are displayed in Table 5.4.

[1] Aeromobil 4.0, *date accessed: 01-06-2018*, https://www.aeromobil.com/aeromobil-4_0-stol/

6
Propulsion System

The propulsion system ensures that the pod is propelled both in driving and flying mode. First, the general lay-out of the propulsion system is presented. Then, the selection and design of the engines and propellers is explained.

6.1. Requirements and Constraints for Propulsion System

In previous design phases, the following system requirements were set that relate to the propulsion system.

- POD-SYS-F-5: The pod in flying mode shall be able to take off without a dedicated airstrip.
- POD-SYS-F-6: The pod in flying mode shall be able to land without a dedicated airstrip.
- POD-SYS-F-15: The pod in flying mode shall be able to reach a cruise speed of 200 km/h.
- POD-SYS-F-16: The pod in flying mode shall comply with CS-36 Aircraft Noise regulations.
- POD-SYS-F-17: The noise level in the pod in flying mode shall not exceed 60 dB at cruise conditions.
- POD-SYS-D-10: The pod in driving mode shall be able to accelerate from 0 to 100 km/h within ten seconds.
- POD-SYS-D-2: The pod in driving mode shall be able to travel at a maximum speed of 130 km/hrs.

Additionally, the following requirements have been added for the propulsion system:

- POD-SUB-PROP-1: The propulsion system shall provide a constant vertical rate of climb of 3 m/s.
- POD-SUB-PROP-2: The propulsion system shall provide total combined flying and driving range of 300 km.
- POD-SUB-PROP-3: The propulsion system shall provide Vertical Take-Off and Landing (VTOL) capabilities.
- POD-SUB-PROP-4: The propulsion system shall provide (Extra) Short Take-Off ((E)STOL) and Landing capabilities.
- POD-SUB-PROP-5: Propeller tip speeds shall not exceed Mach 0.8.
- POD-SUB-PROP-6: The batteries of the hybrid system shall provide enough energy to cover 30 % of the total range.

6.2. General Lay-out

A general representation of the propulsion system can be found in Figure 6.1. The single lines in the diagram represent electrical power, while the double lines represent mechanical power. The blue and red colours merely clarify the paths of the electrical power lines. The propulsion system consists of the following engines:

- Two electric motors installed at the tip of the wings to provide sufficient power for take-off in the flying phase
- One electric motor in the back of the pod to provide power during cruise in the flying phase
- Two electric in-wheel engines in the rear wheels to provide sufficient power during the driving phase
- One range extender (engine), which is a combustion engine that provides electric power to the batteries and/or engines

The propulsion system consists of the following components:

- **Battery:** The battery system will be used to store electric energy. This will be further elaborated in chapter 10.
- **Charger:** The connection between the ground power network and the battery system. This way, the battery can be charged when e.g. parked on the ground
- **Other Subsystems:** This represents the outgoing electrical power to other subsystems, these will be discussed in chapter 11.
- **PCU:** The Power Control Unit, which converts the current between AC and DC.
- **Fuel:** This is the fuel system, which will provide the required amount of fuel to the range extender engine. The size of the fuel tank is 30 L, which is determined in chapter 10.

- **Inverter:** Convert the current between AC and DC current.

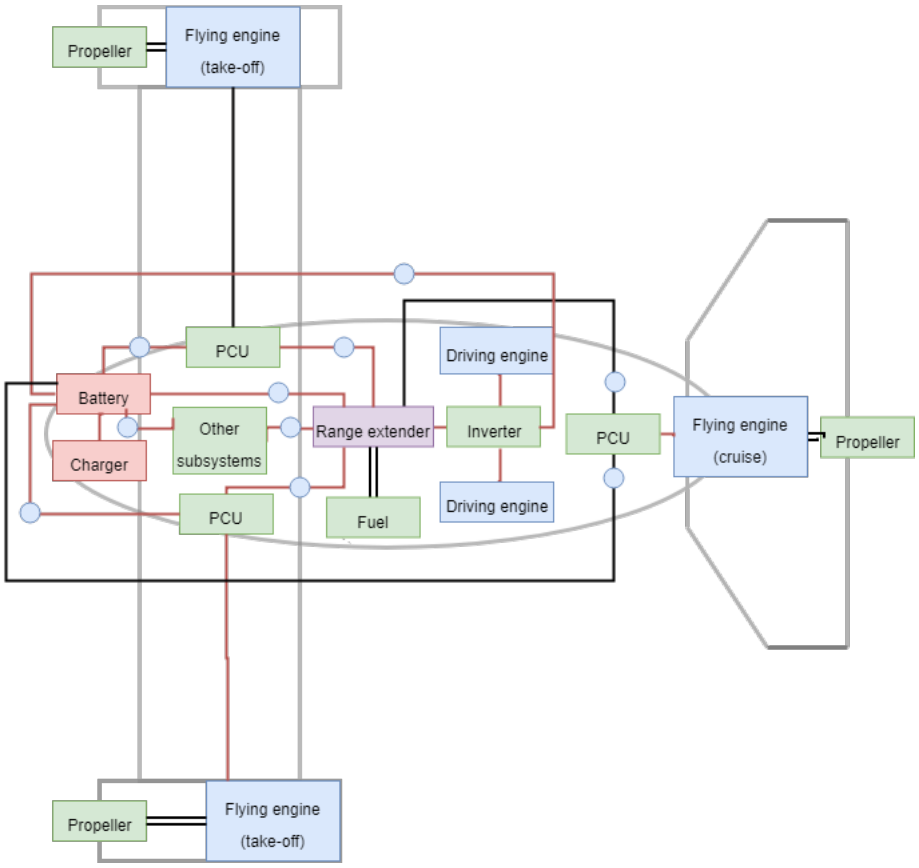

Figure 6.1: Engine System Lay-out

6.3. Engine Selection

Engine design is not in the scope of this project. Therefore, they will be bought from a third party instead, mainly due to the limited amount of resources available during the project. Specific requirements for this design will be used to select the most suitable engines.

6.3.1. Power requirements

The power requirements are calculated in the two different phases. First the VTOL phase is analysed, after which the cruise power is calculated. With this power it is possible to select the engines.

VTOL phase

During VTOL mode the thrust needs to overcome the weight as well as the drag. Aside from this, the final thrust-to-weight ratio needs to be multiplied with a factor of 1.2 to account for gust loads. This results in Equation 6.1 for the thrust-to-weight ratio equation.

$$\left(\frac{T}{W}\right) = 1.2 \cdot \left(1 + \frac{1}{\frac{W}{S}} \cdot \rho \cdot RoC^2 \cdot \frac{S_{tot}}{S_W}\right) \tag{6.1}$$

The power required can then be calculated using Equation 6.2.

$$P_{req}^{VTOL} = \frac{T \cdot V_i}{FM} \tag{6.2}$$

This results in a final value of 230 kW. A more detailed derivation can be found in the midterm report [3].

Cruise phase

During cruise the engine only needs to compensate for the drag since no further acceleration is required. Therefore the power required for the engine can be relatively easily estimated to be:

$$P_{cr} = \frac{D \cdot V_{cr}}{\eta_p} \tag{6.3}$$

This equation originates from the assumption of force equilibrium during cruise, meaning: thrust is equal to drag and weight is equal to lift. This results in a power required for the cruise phase of 52 kW. A more detailed analysis can be found in the Midterm report [3].

6.3.2. Electric Motors

Multiple motors have been selected for the different flight phases, such that the motors can run at their most efficient torque and rpm settings, resulting in smaller batteries and less fuel consumption. The propellers can be optimised for only one configuration: take-off or cruise. This increases performance compared to the situation when the same engine(s) and propellers would be used for take-off and cruise.
This design option introduces an extra engine and thus weight to the design. However, electric motors are relatively small and light-weight, which mitigates the extra weight effects of the extra engine. The installation of the engine at the wing tips will also cause a bending relief during flight, which makes it possible to design a more efficient structure.

Emrax engines will be the electric motors of choice, because they can provide engines with a high power density of 10 kW/kg.[1] This is significantly higher compared to the nearest competitors as e.g. the Siemens SP260D, which has a power density of 5.2 kW/kg [4]. Also, the company offers customisation of the engines, which might be beneficial, especially when the pod is produced on a larger scale. Furthermore, the engines have a very high efficiency of 98 %[1], which is again higher than the nearest competitors. The selected engines and propellers for each phase will be explained in more detail in the following sections.

For vertical-take-off, cruise and driving, different power requirements have been calculated. The engines are selected accordingly. An overview of the selected engines and performance for the different phases can be found in Table 6.1.[1] [2] [3]

Vertical Take-Off Phase

A total power input of 230 kW per engine is required for vertical take-off, therefore the medium voltage type Emrax 268 engine is selected, which is able to provided sufficient power during take-off. Two of these engines will be installed at the wing tips to power the propellers. Considering these engines only have to provide maximum power during a short period of time, an air cooled system was selected. This is lighter and does not significantly decrease the peak performance.

Cruise Phase

For the cruise flight, an average power of 52 kW is required, therefore the Emrax 228 is selected as the most suitable engine. Only one engine will be installed in the back of the pod. This engine will operate during a longer time in cruise and therefore proper cooling is more important for this engine design. A combined cooling system with liquid and air is selected to guarantee the highest continuous power output during the cruise phase. Also, the medium voltage version of this engine is selected to minimise the voltage differences in the system.

Driving Phase Engines

For the driving part, an input power of 38 kW is required, which is derived from the mission profile. Therefore, the smallest Emrax 188 engine is selected. This engine will be installed in-wheel to save space in the main body. The engine will be air cooled, since this is more efficient in terms of weight. Similarly to the other electric motors, the medium voltage version is selected to avoid complex and heavy conversion systems and because crucial performance parameters for this design are not changed significantly. Since the maximum driving power is lower than the cruise power in flight, the range of the driving modes exceeds the cruise range.

Table 6.1: Electric Motors Overview

Parameter Per Engine	**Vertical Take-off Phase Engine**	**Cruise Phase Engine**	**Driving Phase Engine**
Model and Type	Emrax 268	Emrax 228	Emrax 188
No. of Engines	2	1	2
Cooling type	Air Cooled	Combined (liquid+air)	Air Cooled
Continuous motor torque [Nm]	250	125	50
Maximum rotation speed [RPM]	4500 rpm (5500 rpm peak for a few seconds)	5500 (6500 rpm peak for a few seconds)	7000 (8500 peak for few seconds)
Peak motor power at max RPM (few min at cold start / few seconds at hot start) [kW]	230	100	70
Continuous motor power depends on the motor RPM [kW]	40 - 80	35 - 55	15 - 28
Weight [kg]	19.9	12.3	6.8
Diameter ø / width [mm]	268/91	228/86	188 / 77
Price [€]	4490.00	2490.00	2190.00

Mounting of the engines

The mounting of the engines to the pod is realised with brackets specifically made for the selected engines. The brackets are shown in Figure 6.2 and are manufactured by Emrax[18].

[1] Emrax 188 Technical Data *date accessed: 18-06-2018,* `http://emrax.com/wp-content/uploads/2016/12/emrax_188_technical_data.pdf`
[2] Emrax 228 Technical Data *date accessed: 18-06-2018,* `http://emrax.com/wp-content/uploads/2017/01/emrax_228_technical_data_4.5.pdf`
[3] Emrax 268 Technical Data *date accessed: 18-06-2018,* `http://emrax.com/wp-content/uploads/2017/01/emrax_268_technical_data_4.5.pdf`

Figure 6.2: Brackets to mount the engines

The engines for vertical take-off are situated at the wing tips. Therefore, an additional supporting structure is required at the wing tips to attach the brackets to. Furthermore, a nacelle is required to store the engine neatly and provide an aerodynamic shape. The engines used in cruise and for driving are stored in the fuselage and therefore do not require a nacelle.

The connection between the brackets and the pod are made from liquid filled rubber, this is often used for engine mounts to minimise vibrations and reduce the noise.[4]
The propellers will be attached to the engine using torque transmitters manufactured by Emrax [18]. Again, these torque transmitters are specifically made for these engines, allowing for a perfect fit.

6.3.3. Range Extender Engine

Next to the engines to power the pod in the flying and driving phase, the hybrid propulsion system consists of a range extender engine. The range extender consists of a combustion engine that provides mechanical power and an alternator that converts this mechanical power to electrical power. The system is able to provide electrical power to the batteries or directly to the engines. In case the batteries are empty or fail, this generator will be able to maintain cruise flight of the pod. Therefore it is designed to provide 52 kW of power. For the design of this engine, range extenders for electric vehicles of comparable power size have been studied. Looking for the engines with the highest power density, it was found that the Mahle Compact Range Extender Engine is the most suitable solution for the pod design. The specifications of the Mahle Range Extender Engine can be found in Table 6.2 [36].

Table 6.2: Mahle Range Extender Specifications

Parameter	**Value**
No. of cylinders	2 in-line, 4-stroke, gasoline
Maximum power	55 kW
Dimensions	327 x 416 x 481 mm
Engine dry weight	50 kg
Fuel consumption	240 g/kWh minimum
Price	€4,500

It should be noted that the range extender should keep the battery levels between 30 % and 80 % to minimise lifetime degradation of the battery as determined in a previous design phase. Aside from this, the battery should have enough charge left to find a safe landing spot should the range extender fail. It is assumed that the minimum of 30 % is enough.

Sustainability
The concept will use a hybrid-electric propulsion system, which is more sustainable than conventional combustion engines. By using a hybrid system, the range can be extended compared to pure electric propulsion, while at the same time the emissions of the pod can be brought to a minimum. During the selection of the different driving and flying engines, the most lightweight concepts have been chosen to decrease the weight and therefore the emissions of the vehicle. Especially the electric motors have an exceptionally high power density. Furthermore, the range extender is a very efficient combustion engine, which satisfies the strict Euro 6 emission standards. The engines are produced in Europe, so that the benefits can return to local employees.

6.4. Propeller Design

The differences between propellers for the engines ensuring vertical take-off and the engine providing cruise capabilities are notable. These two different configurations require two types of propellers, so two different designs will be presented here, each for its own application.

6.4.1. Airfoil selection

The nature of a propeller requires it to have different airfoils along the blade span (the same is true for the angle of twist of blade sections), due to the lower speeds experienced by the blade near the spinner and the higher speeds near the

[4]Engine mount: how it works, symptoms, problems, *date accessed: 18-06-2018,* https://www.samarins.com/glossary/engine-mount.html

tip. The creator of Java Prop (see also JavaFoil[5] designed airfoils specifically for propellers. These airfoils are the MH (Martin Hepperle) series, ranging from MH 126 at the root, to MH 112 at around 25 % along the blade, to MH 114 at 50 %, MH 116 at 75 %, and MH 122 at the tip. The airfoils in between are interpolated between these airfoils. Both types of propellers will use these airfoils. To account for the lower air speeds near the root of the blades versus the tip, the airfoils are positioned at an increasingly large angle towards the root of the blade.

6.4.2. Propeller geometry

The propellers for take-off are thinner (higher aspect ratio) and have a larger diameter to increase the mass air flow and lower the induced drag experienced by the blades. The tips of the blades reach 1.23 m from the centre of the spinner. This limits the propeller rpm to 2100 to prevent transonic speeds (Mach 0.8) from occurring near the blade tips. The size of the cruise blades, however, is limited by the width of the pod, so the radius of these blades is 0.8 m, but this allows for higher propeller speed: namely 2600 rpm. These two parameters, diameter and rpm, are set in this analysis, so other variables such as number of blades, chord lengths and pitch must be adjusted to find correct propeller configurations.

6.4.3. Design Process

For the design process, a program called JBlade is used.[41] JBlade is based on the open source programs XFOIL[6], XFLR[7] and QBlade[8], combining their efforts to prevent having to switch between programs, while simultaneously improving on their results by accounting for 3D flow equilibrium.[15] This program is validated in [24] by comparing the results with experimental data provided by NASA and other programs.

The program employs Blade Element Momentum (BEM) theory to determine the thrust provided and the power required by the propeller. It does so by first using XFLR to determine the lift and drag coefficients of individual airfoils. It then extrapolates these polars around the entire blade element, after which it computes the axial and tangential force coefficients of every blade element and then integrates these coefficients over the entire length of the blade to provide total thrust and torque forces. Torque forces are multiplied by the rotational speed to find power requirements. These force coefficients depend on the chord length, the angle of twist of the blade element and the total number of blades, so it is very difficult to derive a direct relation between power, thrust, chord length, pitch, and number of blades. An ideal situation would allow for the input of thrust requirements and power limits, which then outputs parameters for the blade geometry. However, this requires programming a new and advanced BEM model, which is outside the scope of this project.

Instead, a trial and error approach is used, which involves creating numerous blade geometries and testing them for thrust force, required power level and efficiency, both for take-off and cruise. Parameters such as angle of twist per blade section, or blade section chord length were repeatedly adjusted to achieve the desired results. One parameter was adjusted at a time to pinpoint the exact changes to the performance of the propeller. The weight was kept to a minimum by first adjusting the angle of twist of the blade sections, until this no longer provided any improvements, after which the chord length was adjusted and the angles were adjusted once again. However, in the case of the propellers for take-off, the thrust forces never came near the required amount of thrust, so a third blade was added to the two-blade propeller configuration. After a lot of tweaking, two blade geometries were found for the take-off engines and the cruise engine. The configurations are presented below.

6.4.4. Results

The propellers for the take-off engines look as follows:

	Take-off	**Cruise**
Radius	1.23 m	0.8 m
Root angle	30 deg	45 deg
Tip angle	2 deg	10 deg
Root chord	0.04 m	0.04 m
Tip chord	0.03 m	0.03 m
Max chord	0.09 m	0.12 m

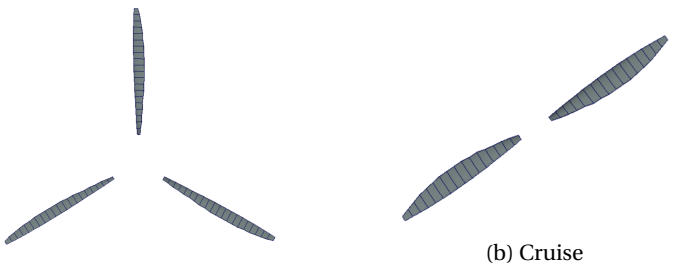

(a) Take-off (b) Cruise

Figure 6.3: The two propeller configurations for take-off and cruise conditions.

The thrust requirements for the take-off and cruise propellers are 5200 N and 800 N, respectively. These thrust levels

[5] JavaFoil, *date accessed: 24-06-2018*, https://www.mh-aerotools.de/airfoils/javafoil.htm)
[6] XFOIL, *date accessed: 24-06-2018*, http://web.mit.edu/drela/Public/web/xfoil/
[7] XFLR, *date accessed: 24-06-2018*, http://www.xflr5.com/xflr5.htm
[8] QBlade, *date accessed: 24-06-2018* http://www.q-blade.org/

are derived from the required rate of climb of 3 m/s and the cruise speed of 200 km/h (55 m/s). The thrust provided by the propellers is depicted in Figure 6.4. Although the take-off propeller produces much more thrust at a cruise speed of 55 m/s, it does so at a cost of a lot more power, a larger propeller diameter, and an extra blade. This shows why it is important to develop two separate propellers; a propeller that works effectively in one configuration might be over or under designed in another.

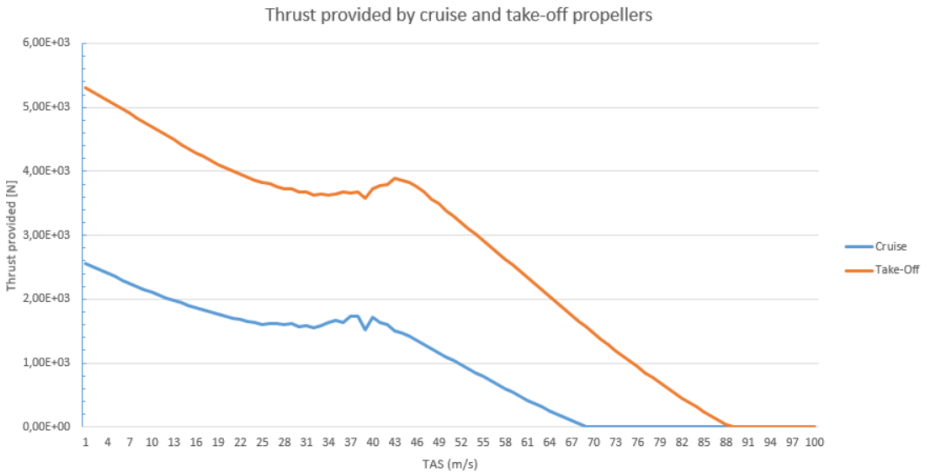

Figure 6.4: Thrust provided by propellers. Note the required thrust provided of 5200 N by the take-off propeller at 3 m/s and the 800 N provided by the cruise propeller at 55 m/s.

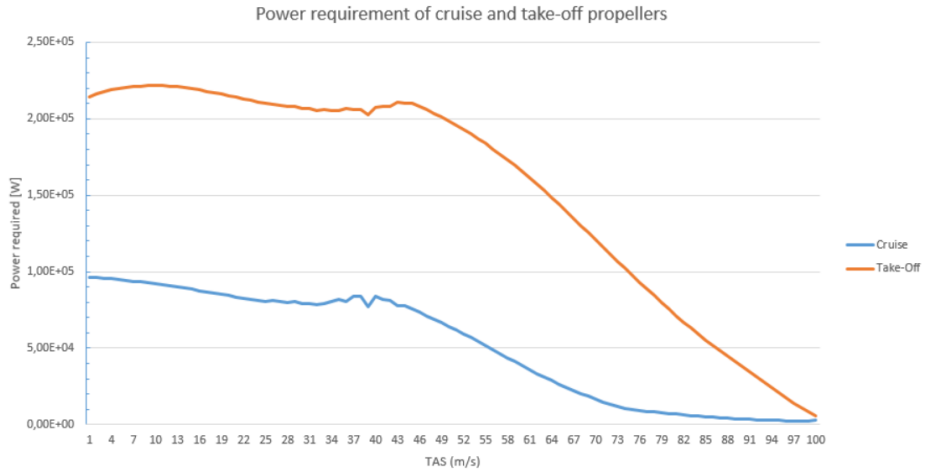

Figure 6.5: Power required by propellers. Note the required power of 225 kW at 3 m/s for the take-off propeller and the required power of 52 kW at 55 m/s for the cruise propeller.

The power required by the propellers is shown in Figure 6.5. This again shows that the power requirements for the take-off propeller are much larger than those for the cruise propeller. Using the take-off propeller in the cruise configuration would require four times the battery mass. This can be slightly accounted for by using a variable pitch propeller and by varying the rpm of the engine, but the propeller will never be optimised for both configurations.

Finally, the efficiencies of the propellers are shown in Figure 6.6. This graph stresses the fact that the propeller efficiency for take-off is extremely poor, no matter what type of propeller configuration is used. The main point illustrated by this graph is the fact that the cruise propeller has a maximum efficiency of 85 % at cruise speed.

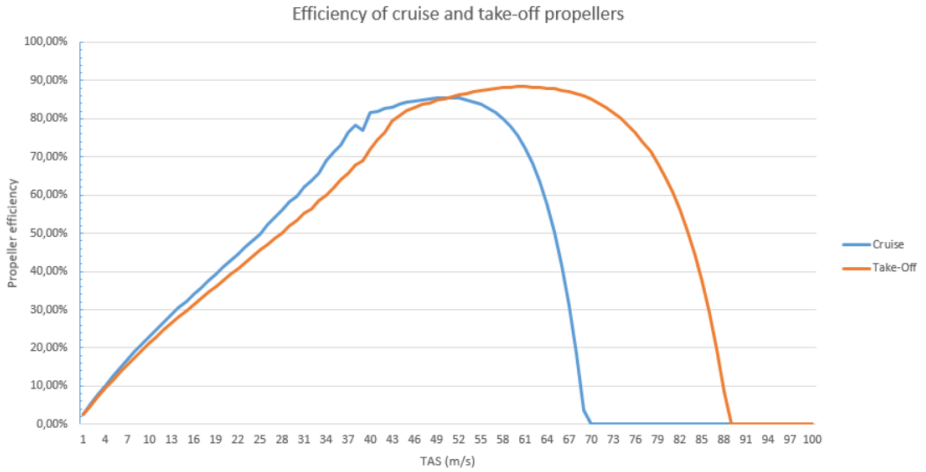

Figure 6.6: Propeller efficiencies. As expected, the take-off efficiency at 3 m/s is abysmal, but an efficiency of 85 % is achieved by the cruise propeller at 55 m/s.

6.4.5. Propeller noise

One of the requirements is the limitation of 60 dB of noise in the passenger compartment. Nowadays, many solutions are used to dampen the noise generated by the propellers. Before applying any of these measures, the sound power generated by the pod must be determined. The main source of noise will be generated by the rotating propellers, both during take-off and cruise, although that first configuration will be louder due to the higher propeller loading and the fact that two propellers are active versus one.
An analysis of the acoustic radiation of pulsating sound generated by the propeller blades, however, requires extensive numerical calculations involving an extension of the Kirchhoff equations into the field of aeroacoustics. Applications have been built around this concept, such as NASA's ASSPIN (Advanced Subsonic and Supersonic Propeller Induced Noise). This software is not readily available to students though and thus cannot be used for an estimation of propeller noise. Instead, reference data of propeller aircraft will be used to provide a preliminary estimation of the noise generated by the propellers.

The FAA provides a list of over 250 small, propeller driven certified aircraft, which includes information such as the number of engines, the number of blades per engine, m_{to} and the measured dB level per aircraft at a distance of 450 m.[9] Note that the engine is the main contributor to the noise generated by propeller aircraft, so values derived from this analysis are over-estimated and real values are likely to be higher. For the noise analysis of the cruise propeller, only single engine aircraft are included with two-bladed propellers, as the take-off propellers are shut off during cruise.

For the take-off analysis, double engine aircraft are selected with four blades per propeller. This is because of the rare occurrence of double engine aircraft with three-bladed propellers (only three were included in the list provided by the FAA). Note: these aircraft are generally much heavier than the designed pod, so the validity of extrapolating this data to the much lighter pod is questionable. The propeller loading is also much higher during this take-off manoeuvre than it is for propellers in cruise, which might also negatively affect the noise generated by the pod. Any estimation provided by this comparative analysis for the take-off propellers should therefore be considered a minimum value instead of an average.

Figure 6.7 indicates that the propeller noise in cruise configuration is around 67-68 dB. Although the cockpit does offer some insulation to this noise, the exact level of noise experienced in the cockpit is difficult to determine at this stage. Thankfully, closed-cell foam padding is cheap and lightweight, so measures taken to lower this noise will not have a large impact on the overall design and cost budget. For take-off, the noise is around 74 dB, but this is a minimum value, as stated earlier.

[9] FAA U.S. Certificated Propeller Driven Small Airplanes, *date accessed: 24-06-2018*, `https://www.faa.gov/about/office_org/headquarters_offices/apl/noise_emissions/aircraft_noise_levels/media/uscert_appendix_07.xls`

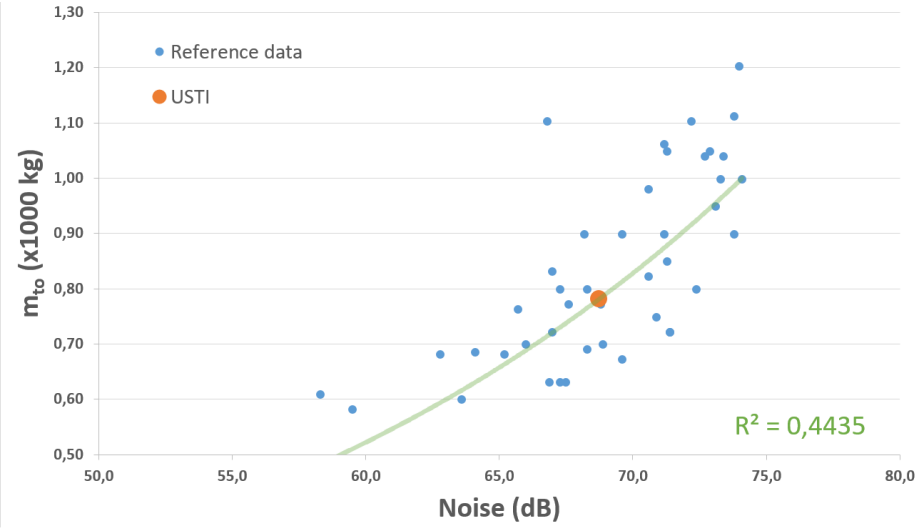

Figure 6.7: Propeller noise comparison in cruise

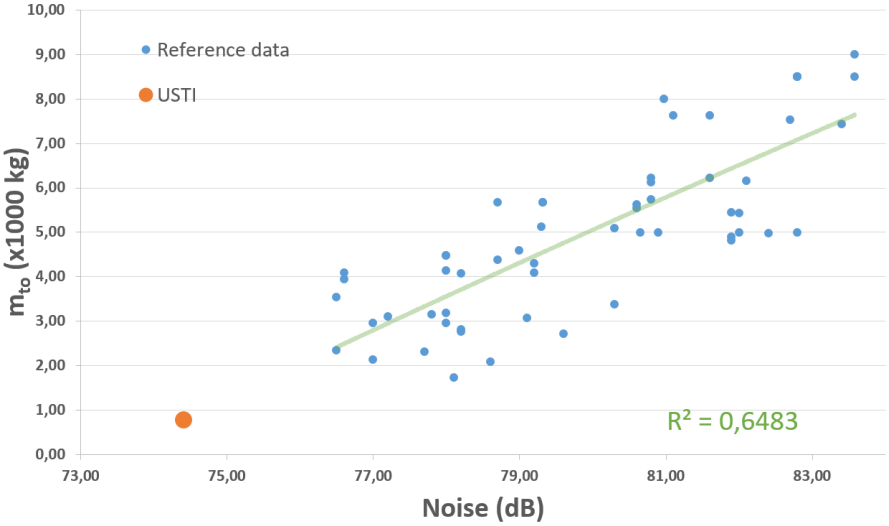

Figure 6.8: Propeller noise comparison in take-off

7

Driving & Landing Gear

This chapter covers the landing gear subsystem design process. The subsystem need to be autonomous and be able to withstand the loads. The tyres, rims and shock absorbers are sized in this chapter to achieve this requirements. Furthermore, the steering, suspension and retraction systems are designed. Finally, a cost and weight breakdown of the subsystem is created.

7.1. Requirements and Constraints for Driving and Landing Gear Design

For the design the landing gear and driving system the following requirements are specified:

- POD-SYS-D-1: The pod shall comply with current traffic regulations;
- POD-SYS-D-2: The pod in driving mode shall be able to travel at a maximum speed of 130 km/hrs
- POD-SYS-D-4: The pod shall be able to drive autonomously.
- POD-SYS-D-12: The noise inside the pod in driving mode shall not exceed 60 dB.

7.2. Autonomous Driving Hardware

The pod does not have a pilot when flying, but also not a driver when driving. The pod should therefore have the ability to travel autonomously without the need for human intervention, with various sensors that will map the environment.

The pod will use a similar technology as the autonomous cars of companies like Google, Tesla and Uber. For example, Tesla's autonomous car provides a 360 degree field of view around the car with eight cameras. It has a visible range of up to 250 m. This is accompanied by twelve sensors that detect both hard and soft objects. A forward-facing radar with improved processing capabilities provides extra data regarding the surroundings on a wavelength that can see through heavy rain, fog, dust and even the car ahead. Explaining the details of such subsystems is beyond the scope of this project, but some relevant topics regarding autonomous driving vehicles will be touched upon in the upcoming sections below.[1] An overview of the cost of the hardware for autonomous driving is given in Table 7.1.[2]

Table 7.1: The hardware cost of autonomous driving

Hardware	**Function**	**Cost [] €**
Video cameras	Read traffic lights, signs and objects	125
Radar sensors	Monitor vehicle surrounding (road, vehicles, pedestrians, etc.)	175
Lidar	Monitor vehicle surrounding (road, vehicles, pedestrians, etc.)	350
Ultrasonic sensors	Measure position of very close-by objects	20
Global positioning system	Provide positioning	350
Total cost		**1020**

7.3. Driving and Landing Gear Subsystem Design

In this section, the landing gear subsystem will be designed to account for both driving and flying.

7.3.1. Load Calculation

The maximum static and dynamic loads acting on each landing/driving gear are calculated in this section using the method given in Roskam [49]. The most critical forward and backward centre of gravity positions are considered, as well as the maximum take-off weight and assumed position of the landing gears. Furthermore, a 20 % airplane weight growth

[1] Tesla Advanced Sensor Coverage *date accessed: 1-06-2018*, https://www.tesla.com/autopilot/

[2] Turns Out the Hardware in Self-Driving Cars Is Pretty Cheap *date accessed: 5-06-2018*, https://www.wired.com/2015/04/cost-of-sensors-autonomous-cars/

is assumed to account for possible weight increases. A summary of the calculated loads is given in Table 7.2.

Table 7.2: Maximum Loads Acting in Landing Gears

Parameter	Value [kg]
P_B Maximum Static Load (Back Gear)	106.6
P_F Maximum Static Load (Front Gear)	307.9
Dynamic Load (Front Gear)	363.1

7.3.2. Tyre & Rims Selection

The maximum loads acing on the landing gears were found in the previous section and will be used in the selection of the tyres. The tyres are assumed to have a load index of 74, which is able to withstand a load of 375 kilograms per tyre, which critical loading of the structure. The selected tyre specifications can be found in Table 7.3 and 7.4. The selected tyres are developed by the company Continental and it includes a tyre pressure monitoring system. The tyres selected have a low rolling resistance, which enables fuel saving and reduction of CO2 emissions. Furthermore, the tyres also have good handling and high mileage due to a low wear rate. Finally, it includes a noise reduction technology developed by Continental, which allows for an interior vehicle noise reduction of up to 9 dB. The price of each tyre is 60 EUR [3]. Furthermore, the tyre clearance needs to be accounted for both in width and in diameter, as tyres grow in size during their service and under the influence of centrifugal forces.

Table 7.3: Front Tyre Specifications

Parameter	Tyre Type	Tyre Width	Tyre Aspect Ratio	Construction	Wheel Diameter	Max. Speed	Max. Load	Weight
Value	155/60R15(74T)	15.5	60	Radial	38.1	189.9	375	8
Unit	[-]	[cm]	[%]	[-]	[cm]	[Km/h]	[kg]	Kg

Table 7.4: Back Tyre Specifications

Parameter	Tyre Type	Tyre Width	Tyre Aspect Ratio	Construction	Wheel Diameter	Max. Speed	Max. Load	Weight
Value	3.00 - 10 M/C	7.62	100	Radial	25.4	130	243	5
Unit	[-]	[cm]	[%]	[-]	[cm]	[Km/h]	[kg]	Kg

The rims of the tyres influence the vehicle performance. The rims are made of aluminium rather than steel. This way, it will weigh less and passengers will feel fewer bumps, as the vibrations from the impact will move up through the pods suspension. A downside is its lower durability. The tyre diameter will be slightly larger than the rim, making the tyre's sidewall shorter. This way, the tyre's grip on the road and the vehicle's handling and steering response increases. The average weight of the aforementioned aluminium rim is 7.7 kg with an average cost of €100.

7.3.3. Steering & Suspension Systems

The pod will feature two-wheel drive (2WD), which means that only the two rear wheels receive power from the motors simultaneously. This approach is used in most cars as the driving force can be reliably transmitted only with 2 wheels thanks to sufficient traction on road. A 2WD layout is advantageous due to its low weight and simplicity.

Steering and Suspension systems are important to ensure correct performance when encountering bumps, turning or full braking. The steering system is necessary to ensure the wheels are pointing in the correct direction during driving mode. It is also important to have a sufficient camber, caster and toe angle. The camber angle enables better car stability by providing better contact with the ground. The caster angle provides the vehicle with straight-line stability. The toe angle affects tyre wear, straight-line stability and corner entry handling characteristics. The design of a suspension system ensures isolation of the vehicle from shocks and vibrations and ensure contact with the surface during driving mode. Furthermore, dynamic driving will be controlled by an automated driving system in all roadway conditions. The systems will be connected using a V-Link as this kind of link minimises the unsprung weight and create a reliable system, even if manufacturing is more complicated compared to other connections.[27]

[3] Continental Tires, *date accessed: 12-06-2018*,`https://www.continental-tires.com/car`

7.3.4. Shock Absorption

The landing gear needs to absorb shocks generated during vertical landing. The first step is to calculate the total maximum kinetic energy that needs to be absorbed by the landing gear. This energy is calculated by using Equation 7.1. The parameter w_t corresponds to the touchdown rate, which has a value of 3 m/s and W_L represents the landing weight. Both shock absorbers and tyres are used to absorb the calculated energy. The shock absorber is an air spring and its diameter and length can be calculated using Equation 7.2 and Equation 7.3, respectively.[49] The parameters n_s and n_t correspond to the energy absorption efficiency of shock absorbers and tyres. Furthermore, N_g is the landing gear load factor and s_t is the maximum allowable tyre deflection. All the unknown parameters have been estimated using [49] and the estimated sizing of the shock absorbers (for back and front landing gear) can be found in Table 7.5. The approximate price is 30 EUR per shock absorber.

$$E_t = \frac{0.5 \cdot W_L \cdot w_t^2}{g} \tag{7.1}$$

$$d_s = 0.041 + 0.0025 \cdot \sqrt{P_B} \tag{7.2}$$

$$S_s = \left(\frac{0.5 \cdot \frac{W_L}{g} \cdot w_t^2}{n_s \cdot P_B \cdot N_g} - \eta_t s_t\right)/\eta_s \tag{7.3}$$

Table 7.5: Shock Absorber Sizing

Parameter	Front gear	Back Gear
Shock Absorber Length [m]	0.5	0.4
Shock Absorber Diameter [m]	0.08	0.06

7.3.5. Retraction System Design

For the wheels in the back, a simple retraction system will be used where the wheels retract vertically, as can be seen in Figure 7.1. The aerodynamic drag will be lower, but a penalty must be paid in the form of weight and cost. The front wheels do not retract; they are covered by panels instead due to a lack of room underneath the pod. The spacing between the front wheels differs from the spacing between the back wheels. By doing this there will be a misalignment between the front wheels and back wheels during driving. The pod will be easier to drive and control when the wheels are not on the same lateral axis.

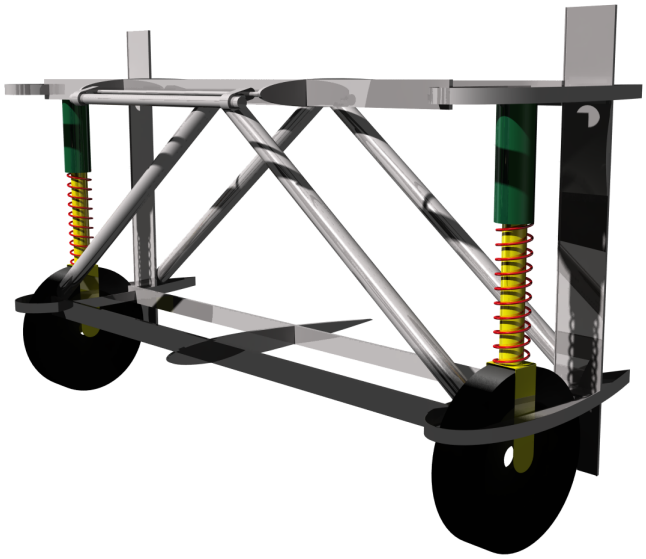

Figure 7.1: Retraction mechanism (and shock absorbers) of rear wheels.

7.4. Steering Control System

Steering a vehicle by hand means that the user plans a route by preview and adjusts the lateral deviation of the vehicle from the planned route by the steering wheel. However, for the automatic steering of autonomous vehicles, this route following is automated. The lateral deviation from the reference route is kept low by a feedback control to the steering motors.

A close-loop control system with a PID controller is used for the steering control system. The PID controller is one of the most common controllers in process control, because it is simple and highly effective for linear and time-invariant dynamic response systems [28]. The framework is shown in Figure 7.2. The letters PID stand for Proportional, Integrating and Differentiating. The control is based on the difference between the set (desired) value and measured value, which is called the error signal. The adjustment signal is determined by three separate calculations:

- P-action: Proportional means that the difference in desired value and measured value is increased by a factor Kp.
- I-action: The integrating term ensures a constant summation of the error and continues to send out a signal depending on how long an error exists between the measured and desired value. K_i is called the set-up time, i.e. the time that is necessary to get a value equal to the P-action. A small K_i gives a powerful I-action.
- D-action: The differentiating term responds to the speed of the change of the error. If the measured value changes in the direction of the desired value, then there is the risk that the measured value will overshoot. The change of this adjustment signal will then be inhibited by the D-action. When the measured value changes from the desired value, the change of the adjustment signal is accelerated with the D-action. The D-action only has an effect when the error signal changes, in other words, when the derivative of the error signal is not equal to zero. The higher K_d is, the stronger the controller responds to changes in the measured value.

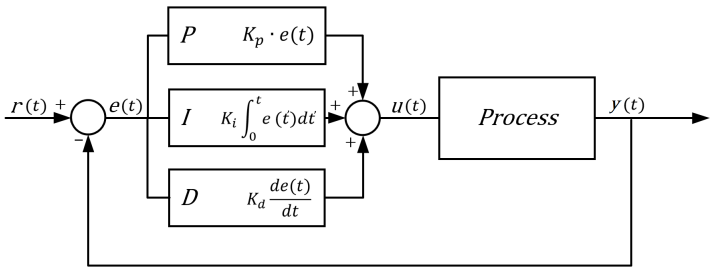

Figure 7.2: A block diagram with a PID controller in a feedback loop to illustrate the steering system

From Figure 7.2, the expression for the steering angle can be deduced, which consist of the PID-equation shown in Equation 7.4:

$$u(t) = K_p e(t) + K_i \int_0^t e(t')\,dt', + K_d \frac{de(t)}{dt} \tag{7.4}$$

The reference trajectory can be calculated from the data of sensors and cameras. For the determination of the speed during driving, it is not sufficient to use the Pitot tube due to accuracy difficulties. The tyres will have wheel speed sensors for accurate speed measurements. The speed sensor and steering angle sensor will send signal to the CPU for further processing.

7.4.1. Cost and Weight estimation

A cost and weight breakdown of the landing gear system can be seen in Table 7.6

Table 7.6: Landing gear cost & weight breakdown

Item	**Weight [kg]**	**Cost [€]**
Back tyres and wheels	25.4	300
Front tyres and wheels	31.4	340
Shock absorbers	6.8	120
Breaking system	23	64
Total	**186.8**	**3340**

7.4.2. Sustainability

Sustainability has driven the design choices in this section. The chosen brake discs are "two-piece Textar", lightweight composite brake discs developed by Textar. Each disc consists of a top hat and a friction ring, connected by rivets. The product has a low fuel consumption, so CO_2 emissions are reduced. Furthermore, it reduces the breaking noise compared to other discs. Also, the tyres selected have a low rolling resistance, which enables fuel saving and a reduction of CO_2 emissions. Finally, it includes a noise reduction technology developed by Continental, which allows for an interior vehicle noise reduction of up to 9 dB. Finally, it is found that the tyres are recyclable by approximately 80% of their weight, which is due to the full recyclability of the aluminium rims. An example of rubber recycling is pyrolysis [19]. Rubber is softened after which polymers break down in separate molecules. The rubber is theoretically fully recyclable, but in practice not all rubber is recycled.

8

Structure and Aerodynamics

This chapter describes the process of designing the structure of the pod. This can be visualised in Figure 8.1.

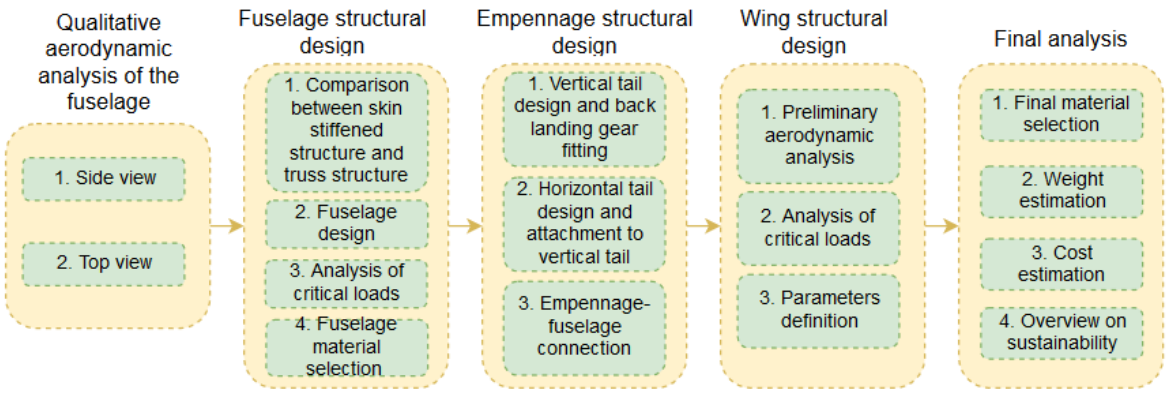

Figure 8.1: Overview on pod structural design

First of all, the most optimal aerodynamic shape of the pod is studied qualitatively. Subsequently, the structure is designed in detail. A trade-off between a truss structure and skin-stiffened structure is performed with simple calculations, after which the actual structure will be designed, considering the different load cases. After the geometry of the main body is designed, the empennage is designed followed by the wing. A final weight and cost estimation is performed at the end of the chapter.

8.1. Requirements and Constraints for Structure and Aerodynamics

In previous design phases, the requirements listed below that relate to the structural and aerodynamic design of the pod were determined. One major change is implemented in POD-SYS-OPP-1. Previously, this requirement stated that four passengers carrying luggage should fit in the vehicle. However, following the market analysis, the focus has shifted to business travellers. Therefore, this requirement is adapted such that two passengers and their luggage are now required to be fitted. No specific additional requirements are set for the detailed design phase

- POD-SYS-OPP-1: The pod shall be able to fit two people and their luggage.
- POD-SYS-OPP-5: The pod shall be able to convert between different modes of transport.
- POD-SYS-OPP-11: The pod shall be able to withstand load factors in the range of -1 to +**4.5**.
- POD-SYS-OPP-12: The pod shall be recyclable by 60 % of the pod weight.
- POD-SYS-OPP-13: The pod shall be able to withstand accelerations with a maximum of <tbd> m/s^2
- POD-SYS-OPP-14: The pod shall be able to withstand vibrations with a maximum of <tbd> Hz.
- POD-SYS-D-13: The size of the pod in driving mode shall not exceed 4.7(l)x1.7(w)x2.0(h) m.
- POD-SYS-D-14: The pod shall have a crash worthiness that would guarantee a 5 star rating from the EURO NCAP test

8.2. Preliminary Aerodynamic Analysis of Fuselage

Aerodynamic considerations regarding the main body of the pod are addressed first to select its general shape. This is done both for the lateral view and the top view of the fuselage.

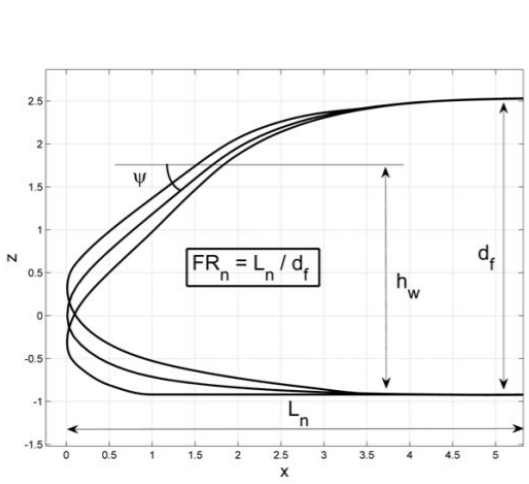

(a) Representation of the aerodynamic nose shape of the pod[42]

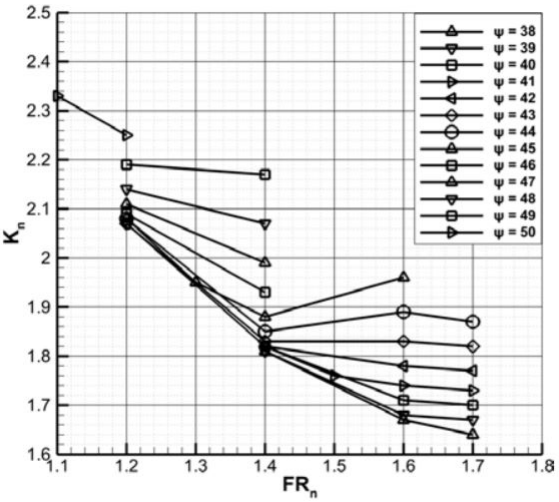

(b) Nose shape related to the parasite drag coefficient factor[42]

Figure 8.2: Nose shape analysis

8.2.1. Side View

First of all, concerning the optimal nose shape, the maximum windshield angle is taken into account. The windshield angle corresponds to the angle between the tangent line of the windshield and the horizontal line at the intersection point. It is known that a lower windshield angle with a larger nose length results in a lower drag coefficient[42]. However, the nose shape also has to be optimised to ensure that the passengers can comfortably sit in the nose. A first prediction of the shape of the nose can be seen in Figure 8.2a. This nose corresponds to a nose length of 2.1 m with a fuselage height of 1.5 m. For these dimensions, the windshield angle is optimised for angles below 43 degrees, which result in similar drag coefficients. This is shown in Figure 8.2b. The maximum angle of 43 degrees is chosen as the windshield angle to ensure sufficient cabin space in the nose.

Regarding the shape of the hind body, the length and up-sweep angle have to be considered, as presented in Figure 8.3a. Using the nose dimensions and the total pod length, the length of the hind body is estimated to be 2.6 m. Using this value with the predefined fuselage height of 1.5 m, the fineness ratio has a value of 1.73. For the fineness ratio, a lower up-sweep angle of the after body will result in a lower amount of drag[42]. This is presented in Figure 8.3b. Additionally, it is known that a negative camber of the hind body results in a lower lift as well as a lower drag for positive angles of attack, as shown in Figure 8.4 [12]. This is beneficial for the pod as lift during cruise will be provided by the wing and the pod will experience a positive angle of attack during cruise. Therefore, the most optimal hind body shape of the pod has a negative camber to lower the drag coefficient combined with an up-sweep angle that is as low as possible. To ensure an optimal design, the selected up-sweep and down-sweep angles are 16 and 12 degrees, respectively.

Verification and Validation The effectiveness of applying this method for drag reduction is validated by the reference data used. The method described by F. Nicolosi [42] and R. Wiesner & C.N. Keys [12] shows the result of this method compared to existing helicopters or aircraft. It shows an insignificant difference and thus these methods are validated.

8.2.2. Top View

The top view of the vehicle must be designed for maximum aerodynamic efficiency during horizontal flight. Specifically, the body shape must be suitable to:

1. Minimise the induced drag
2. Optimise the flow to the horizontal and vertical tail

These considerations lead to a tapered body shape that converges towards the tail.

It is known that the maximum width of the pod is 1.7 m. Several airfoil shapes are investigated by using the tool *XFOIL*. Airfoils with large thickness-to-chord ratios are preferred as they allow the airflow surrounding the main body to travel naturally towards the tail. In fact, if a thin airfoil was selected, the shape of the body would be too similar to a regular cylinder and its width would be too large towards the back of the vehicle, reducing the effectiveness of the tail. Furthermore, the airfoil has to be symmetrical.

Among the investigated airfoils are the NACA0040, NACA0036 and NACA0034. The last two digits of the airfoil code stand for the thickness to chord ratio. It is discovered that the smaller this ratio is, the further from the leading edge flow

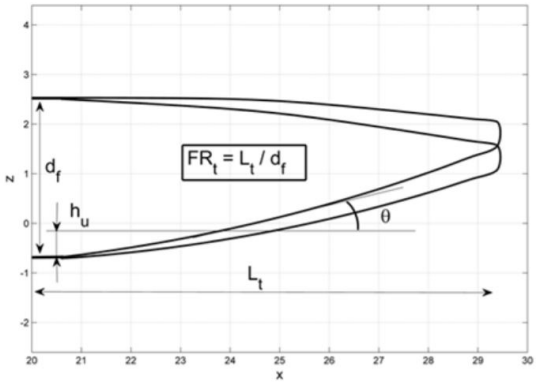

(a) Representation of the aerodynamic hind body shape of the pod[42]

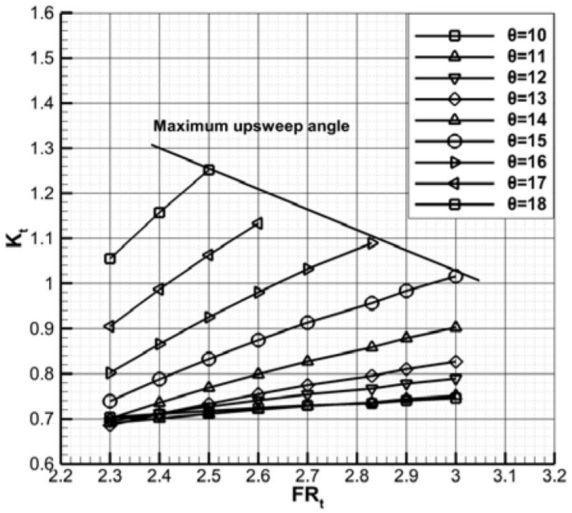

(b) Hind body shape related to the parasite drag coefficient factor[42]

Figure 8.3: A0fter body shape

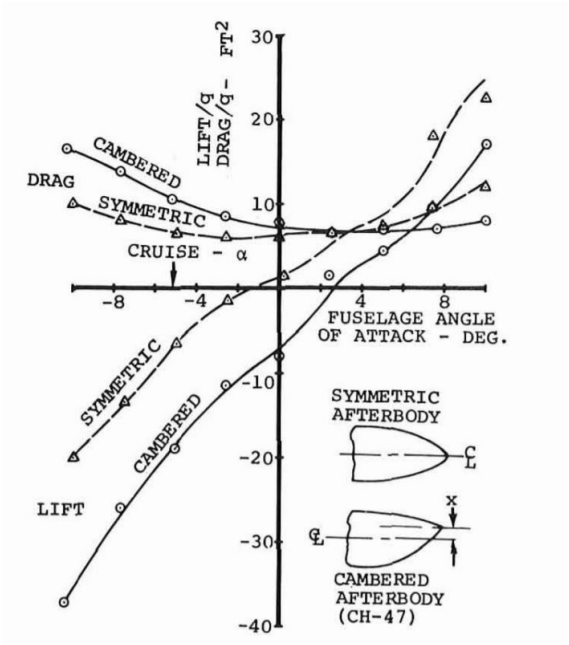

Figure 8.4: Lift and drag related to hind body shape[12]

separation occurs: in general, flow separation is detrimental as it increases the induced drag over the airfoil. However, selecting a low thickness-to-chord ratio leads to a rather reduced internal space. It is therefore decided to proceed as follows:

1. 34 % is selected as minimum thickness-to-chord ratio, which allows for a large internal space.
2. From regulations [2], the maximum width of the pod is set to 1.7 m. Therefore, given the maximum thickness-to-chord ratio of the airfoil, the length of the pod is set to 5 m.
3. The selected length does not match the requirement that the vehicle size shall not exceed the length of 4.7 m. Therefore, it is decided to 'cut' 30 cm of the airfoil chord length.
4. *XFOIL* is used to analyse where separation occurs in case of 0 *degrees* angle of attack. This occurs at 3.69 m from the nose of the vehicle, as can be visualized in Figure 8.5

Verification and Validation The effectiveness of the selected airfoil is first verified by comparing it to airfoils of different thicknesses and lengths. For example, the case of an "uncut" airfoil of length 4.7 m is tested in *XFOIL*. In this case, separation occurs at 3.47 m from the nose of the pod, meaning that the flow that reaches the tail is particularly disturbed.

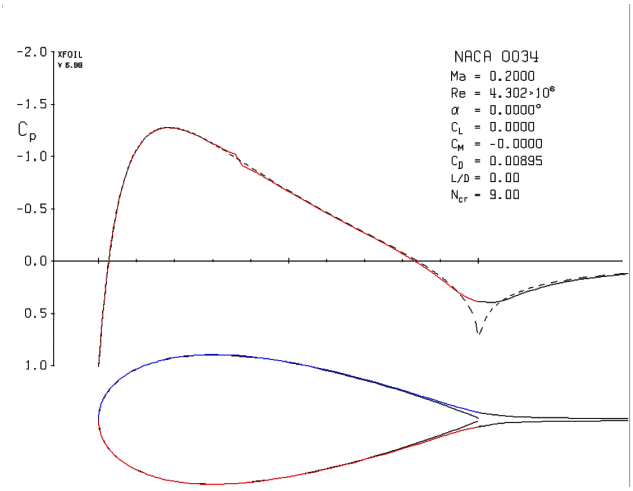

Figure 8.5: Flow separation over the fuselage, determined using XFOIL

Moreover, it must be verified that the tail size is large enough to perceive the airflow as it travels along the airfoil. In other words, the taper of the fuselage is effective. This is done by comparing the horizontal tail span to the width of the airfoil at the cut plane: this is 20 cm wide, whereas the tail span is 1.5 m. Finally, the tail chord is 0.7 m: since flow separation occurs at 3.69 m from the nose, the flow has just separated when it reattaches due to the increase in width of the airfoil in correspondence to the tail structure. For this reason, the induced drag is minimised.

In conclusion, the NACA0034 airfoil is selected to define the shape of the main body of the vehicle as seen from above.

8.3. Structural Design

In this section, the structural design of the vehicle is investigated in detail. Specifically, a detailed design procedure is provided for the fuselage, the empennage and the wing.

8.3.1. Fuselage Structure Type Comparison

In this subsection, a comparison is conducted to decide whether the main body of the pod will be constructed as a truss structure or a skin-stiffened structure.
Firstly, the Free Body Diagram and Bending Moment Diagram of a simplified version of the side view of the body are constructed. These can be visualised in Figure 8.6 and Figure 8.7. It should be noted that the values presented in the moment diagram are estimates that reflect the outcome of the preliminary weight estimations and the initial calculation of the location of the centre of gravity of the the pod. This estimation is assumed to be valid as, effectively, the preliminary weight estimation is found to be rather accurate.

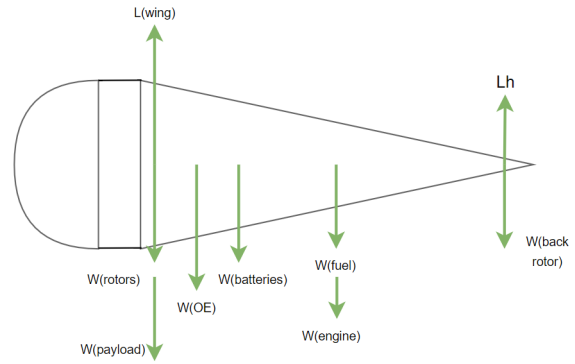

Figure 8.6: Free body diagram of the simplified vehicle, side view

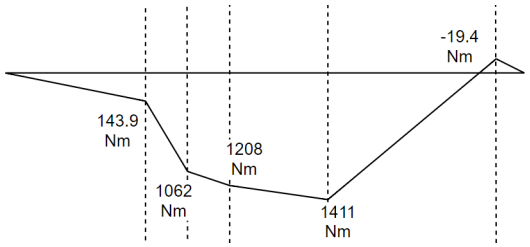

Figure 8.7: Moment diagram of the simplified beam, side view

Skin Stiffened Structure

For the sake of the comparison, a first, high level proposal of the fuselage is analysed here. The design parameters are chosen to minimise the weight of the frame and guarantee the structural integrity.

Specifically, it is assumed that the fuselage has a perfectly circular cross-section with a diameter of 1.7 m, which corresponds to the maximum allowable pod width for driving conditions. This leads to the largest inertia. The section is

stiffened by eight longerons with a cross-sectional area of 180 mm^2. The longerons' size is selected according to the components currently available on the market [1]. The entire cross-section is assumed to be made of aluminium. In fact, a metal is required as multi-directional stiffness is required and aluminium is the most efficient in terms of weight. For this reason, it is also the most widely used metal in the aerospace industry.

For this case study, the cross-section is idealised with eight equally spaced booms that represent the stringers. First, a bending analysis is performed to check whether this structure is able to withstand the stresses induced by the moments displayed in Figure 8.7. The area of each boom area and the bending stresses are computed by applying Equation 8.1 [38].

$$B_1 = \frac{t_D \cdot b}{6}\left(2 + \frac{\sigma_2}{\sigma_1}\right) + A_{stringer} \qquad \sigma_z = \frac{I_{xx}M_y - I_{xy}M_x}{I_{xx}I_{yy} - I_{xy}^2}x + \frac{I_{yy}M_x - I_{xy}M_y}{I_{xx}I_{yy} - I_{xy}^2}y \tag{8.1}$$

The bending stresses are very low, in the order of magnitude of 6 MPa. This result can be visualised in Figure 8.8.

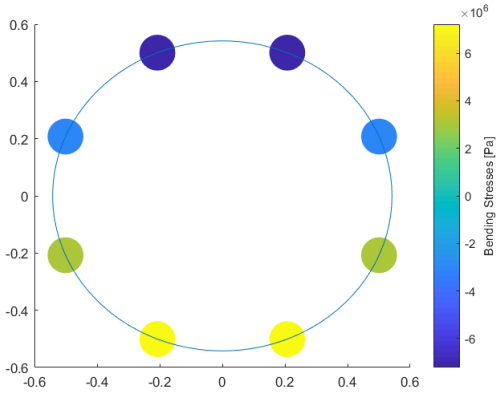

Figure 8.8: Simplified bending stresses on the idealised fuselage cross-section

The number of longerons (and consequently of booms) is reduced to six to reduce the weight of the structure. Even in this case, the aluminium structure is perfectly able to withstand the loads. The structure is in fact redundant. However, for structural integrity reasons, it is not advised to reduce the number of longerons below six, as the structure would become very flimsy. The same is true for the thickness of the skin.
An analysis of the shear stresses is then performed [38]. Specifically, it is assumed that the boom area remains constant as the cross-sectional area of the fuselage decreases. This leads to an overestimation of the shear. The maximum shear stress, in this case, is 11.3 MPa, which can be well withstood by the selected aluminium frame.

Once it is discovered that the structure is stiff enough to overcome bending and shear stresses, it is important to estimate the weight of the skin-stiffened structure to check whether it would actually be more convenient than the truss structure. Simple volumetric calculations are performed to evaluate the weight of the aluminium structure. Then, by multiplying the volume of the idealised frame by the density of aluminium, 2710 kg/m^3, the final mass is calculated. It should be noted that the mass of the nose is not added to the mass of the idealised tail cone to keep the calculations consistent to the ones performed for the truss structure.

$$m_{fus_{ss}} = 22.9\text{kg}$$

Verification and Validation The stress evaluation of the skin stiffened structure is verified by applying the bending analysis manually on the cross-section with eight booms. The results of this procedure are shown in Table 8.1.

Table 8.1: Verification overview of bending stress calculations

Maximum bending stress according to simulation [MPa]	**Maximum bending stress according to verification [MPa]**	**Offset [%]**
6.37	5.92	7.1

The difference in magnitude is due to the approximations made throughout the manual procedure. Specifically, the bending moments plugged into the manual calculations are approximated to the nearest unit, as well as the boom areas derived with Equation 8.1.

As the results are of the same order of magnitude, however, the validity of the method is confirmed.

Truss Structure

For the initial analysis of the body of the vehicle, modelled as a truss structure, only the hind body of the pod is taken into account. The hind body corresponds to 2.2 m from the nose of the pod, where the luggage compartment ends, up to the end of the pod at 4.7 m. For this analysis, the forces for every member are determined. For the truss structure, a truss joint is placed at the locations where a load is applied. The estimated truss structure in 2D is shown in Figure 8.9. For this truss structure, the shear force diagram obtained from the free body diagram, depicted in Figure 8.6, is used.

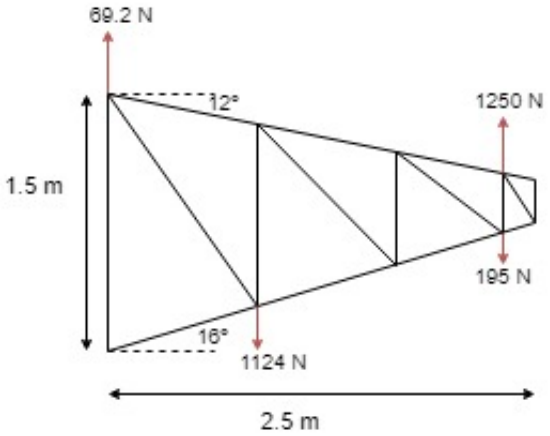

Figure 8.9: Side view of estimated 2D truss structure of the hind body

At the joint locations from the start of the hind body till the end of the hind body, the equations for force equilibrium in x and y directions are determined. Firstly, for these equations, the different angles between the horizontal and the different members are determined. Additionally, it can be predicated already that the forces in the members GI, IJ are equal to zero. Using the force equilibrium equations gives 15 equations with 15 unknowns, excluding the force equilibrium in x-direction for the H and J joint due to redundancy. Solving this gives the maximum force, which is a compression force taken by member CF.

For this initial analysis, it is assumed that the cross-section of the members in the truss structure is constant over the length of the hind body. Thus, using the maximum force, which is the compression force in member CF, gives the required thickness to sustain the loads using Equation 8.2. For this, the normal stress with a safety margin of 4.5 is taken into account, which corresponds to the compression force in member CF.

$$\sigma_{max} = \frac{F_{max}}{A_{member}} \cdot \frac{1}{SF} \tag{8.2}$$

In Equation 8.2, the unknowns are the area and thus the dimensions of the cross-sections of the members is unknown. A hollow rod will be used for the members to reduce the weight of the truss structure. The relation below can be used to compute the thickness and radius of the members:

$$A = \pi \cdot D \cdot t$$

Aluminium is selected as the truss material. A total truss mass of 0.653 kg is found. A skin mass of 3.2 kg is estimated, using the same material. The total mass for this analysis is estimated to be approximately 3.85 kg. Note that this is only a first estimation to assess whether a skin-stiffened structure or a truss structure should be used.

Verification and Validation The verification of the computed loads is done as follows. First of all, the signs of the loads the different members have to withstand is reasoned. Doing this showed no discrepancies or unexpected signs. Secondly, the force values are verified by substituting the values in the force equilibrium equations of the truss joints. This shows that these forces indeed satisfy the force equilibrium equations.

Final Selection of Fuselage Type

From the preliminary analysis on the fuselage structure, it is clear that the truss structure is much more convenient than the skin stiffened stiffened structure. This is mainly due to the fact that, in case of the truss structure, the skin, which does not have to carry any structural load, can be made of a very lightweight material.

In general, skin-stiffened structures are used in the aerospace industry when pressurisation is needed and the vehicle is subjected to very large loads. In this case, however, a skin-stiffened structure would be too expensive in terms of weight. It is therefore decided to proceed with the design of a truss structure, in line with what is done in the automotive industry.

8.3.2. Fuselage Truss Structure Design

The design of the truss structure for the fuselage is performed using the software tool *SkyCiv*. This program performs structural analyses on a user-defined combination of trusses and loads. The approach to designing the truss structure is as follows: first, an initial truss structure is generated based on the earlier defined fuselage shape. Afterwards, different load cases are specified and a structural analysis is performed on the truss-structure using *Skyciv*. Based on the results of the analysis, the truss structure is iterated until the optimal structure is found.

Working Principle of *Skyciv*

The software tool *Skyciv* solves user-defined truss structures by means of a Linear Static Analysis. In this analysis, the assumption is made that the structure's behaviour is linear and follows Hooke's Law. Therefore, plastic deformation is not considered. Next to that, the loading is assumed to be static, which means that the magnitude and direction of the applied loads do not vary over time.

These assumptions are considered to be valid for the analysis of the truss structure, as the structure will be made out of Hookean materials that show linear stress-strain behaviour. Furthermore, plastic deformation is not desired in the structure.

It should be noted that for the analysis to run, the structure should not be able to move. Therefore, supports need to be defined in the program. This does not fully resemble for instance the flying situation, in which the pod is free to move and rotate around all three axes. However, since in the cruise situation the pod is in equilibrium, it is reasoned that the defining supports, that are actually not present, will not harm the results of the analysis.

Considered Load Cases

The structure needs to be designed in such a way that it can withstand a variety of load cases. In the design process, the following load cases are considered:

- Take-Off
- Cruise
- Touchdown
- Frontal impact
- Side impact
- Hard landing

During the analysis of the load case in flying mode, it is checked whether the structure is able to withstand a load factor of 4.5, which was found to be the load factor that should be designed for in previous design procedures [3]. Every analysis is performed using maximum payload conditions, so the total passenger weight is 160 kg and the luggage weight is 70 kg. Furthermore, the fuel tank is assumed to be completely full.

In these analyses, the structural weight is assumed to be acting at the centre of gravity, whereas other components such as the motors and payload are acting at their actual location.

During take-off, it is assumed that the full lift force generated by the wings acts at the hinge location of the wing, as well as the drag force experienced by the wing. For the landing analysis, a touchdown rate of 3 m/s is analysed, and it is assumed that the pod touches down on all four wheels simultaneously.

For the front impact and side impact the regulations of the EURO NCAP are considered. These regulations state that a frontal crash into a wall with 56 km/hr and a side impact with a barrier at 50 km/hr should be withstood without excessive deformation. [1] The behaviour of the structure under these loads is further investigated in subsection 8.3.2.

Considerations for Truss Structure Design

The following factors will negatively impact the load carrying capabilities of the fuselage truss structure:

- Room for front and side windows
- Entrance to cabin and cargo compartment
- Attachment of the empennage section
- Attachment of the front suspension
- Attachment of the swinging wings
- Battery replaceability

Whereas a truss structure ideally consists of only triangles, these factors will hinder that. For instance, it is not desired to have truss members interrupt the front and side windows. Therefore, the structure might be weakened and around these locations reinforcements are necessary to ensure that all load cases are handled properly.

[1] `https://www.euroncap.com/en/vehicle-safety/the-ratings-explained/adult-occupant-protection/side-mobile-barrier/`

A visual approach is used to take these factors into account. After every iteration, it is visually analysed whether there is sufficient space and whether necessary attachments are not hindered. If this is case, the truss structure is iterated and a new structural analysis is performed to see if all load cases are still satisfied.

Material Selection for Fuselage Truss Structure

For the fuselage truss structure, multiple different materials are considered: eventually, aluminium and carbon fibre reinforced plastic are compared as most suitable materials. Carbon fibre is disregarded as connecting carbon fibre tubes is a rather difficult process. Connectors are required, which are made of either carbon fibre or aluminium. These connectors increase the weight of the truss structure significantly. Therefore, even though carbon fibre has a significantly lower density, a carbon fibre truss might not be much lighter than a full aluminium truss. The connectors also increase the manufacturing cost of the truss. Another main reason for not using carbon fibre in the truss, is that carbon fibre cannot deform plastically. Therefore, if a crack occurs, the structural integrity is greatly decreased. Finally, carbon composites can only marginally be recycled, reducing the overall sustainability of the pod.

Aluminium is chosen as the main material for the fuselage structure, because of its relative high strength, low cost and low weight. However, during the design of the truss structure, it was found that a truss completely made out of aluminium would not be sufficient to withstand the loads of a front or side impact, if the thickness of the aluminium plates is of 0.5 mm. This will be presented in subsection 8.3.2. Therefore, the choice is made to increase the thickness of the aluminium plates of the truss structure by a factor of 2.

Analysis of Critical Load Cases

The truss structure of the pod is tested under critical load cases, to check whether the safety of the passengers is protected in critical conditions. Specifically, the stiffness of the vehicle is tested in case of frontal impact, lateral impact and hard landing.

Since frontal impacts may occur in driving mode, crash-test data taken from regular cars is taken as a reference [16]. Specifically, the truss structure of the fuselage is tested in *Skyciv* with a force of 40 kN applied to the nose of the vehicle. This corresponds to the assumption that the pod hits a still wall when travelling at a velocity of 56 km/hrs, and it stops within 0.5 s.
It is first discovered that the initial structure made out of 0.5 mm thick aluminium would not provide the required safety around the passenger cabin, as it would fail under buckling. In fact, in this case the buckling factor would be 0.272. It should be noted that the structure is subjected to buckling if the buckling factor is lower than 1. It is therefore decided to reinforce the aluminium truss members located at critical locations by increasing their thickness by a factor of 2. This causes an increase in structural mass, which will be taken into account in the mass estimation procedure, presented in subsection 8.3.7. The maximum stresses of the final reinforced structure are presented in Table 8.2. The buckling factor, in this case, equals 0.81: although this value is lower than 1, buckling is not critical. The structure is in fact expected to undergo some deformation, however, the stiffness of the truss member is high enough to prevent the structure from failing.

Side impacts could also cause the structure to fail. Therefore, a check of the stresses during lateral impact must be performed. Specifically, a load of 36 kN is considered. This corresponds to a side impact at 50 km/hrs as specified by regulations[17]. The results of this analysis are presented in Table 8.2. Also, buckling is an issue in this case, as the buckling ratio is lower than 1. However, it occurs in the tail compartment, due to the long truss members located in the back section of the pod. Since the safety of the passengers is not compromised, the vehicle is still considered to be safe.

The third critical load case taken into analysis is the hard impact with the ground. Specifically, it is assumed that the fully loaded pod lands without deceleration. By assuming that the loads are equally distributed between the four wheels, it is found that each gear experiences a load of 5.25 kN. The results of the analysis are presented in Table 8.2.

In conclusion, the structure is stiff enough to withstand the stresses in every load case. The most critical loading case occurs during a lateral impact, as that is when the maximum stresses occur.

Final Fuselage Structure Design

The final truss structure side view can be found in Figure 8.10. The grey bars are made out of 0.5 mm thick aluminium, whereas the blue bars are made out of 1 mm thick aluminium. In the structure, the locations for the windows, cabin doors and passenger doors are easily visible. At the top, a straight section can be seen. This is to allow the wings to be retracted during driving mode, as explained in Figure 8.3.5.

Important to note is that this fuselage structure is only 4.0 metres long, whereas the pod will become 4.7 m in length. This is done because the tail, which will be described in detail later, will be connected to the end of the fuselage.

Table 8.2: Results of crash tests on fuselage truss structure

Frontal impact				
Load magnitude [kN]	Load location	Buckling factor [-]	Maximum compressive stress [MPa]	Maximum tensile stress [MPa]
40	Nose	0.806	220.8	124.2

Lateral impact				
Load magnitude [kN]	Load location	Buckling factor [-]	Maximum compressive stress [MPa]	Maximum tensile stress [MPa]
36	Side	0.399	308.8	250.8

Hard landing				
Load magnitude [kN]	Load location	Buckling factor [-]	Maximum compressive stress [MPa]	Maximum tensile stress [MPa]
26	Landing gear nodes	5.57	37.2	58.3

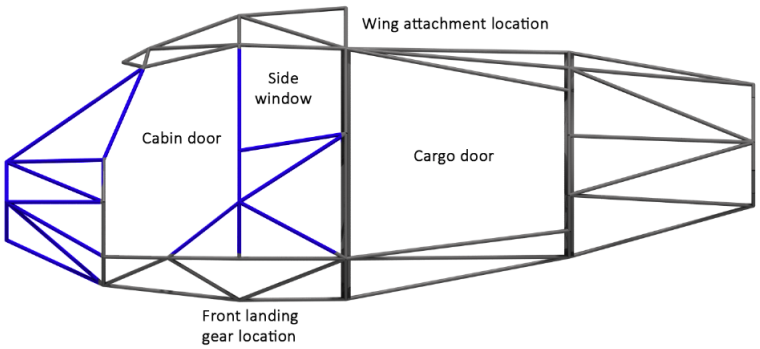

Figure 8.10: Side View of Truss Structure, a blue colour indicates a reinforced rod.

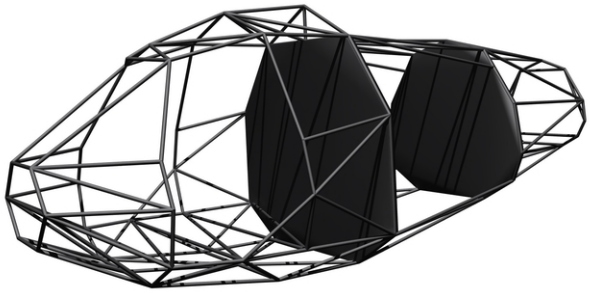

Figure 8.11: ISO View of Truss Structure

Floor Inside The Fuselage

The floor inside the fuselage not only covers the passenger compartment, but also the luggage compartment. The area required for this floor is determined using the 3D model to come up with the most accurate result as possible. The floor was then selected from an outside contractor.[2] Using the density described in the data sheet, a total mass of 10.2 m^2 was found.

8.3.3. Front Landing Gear Structure Design

The front landing gear is attached to the fuselage at the location that can be seen in Figure 8.10. Initially it was intended to design a retracting mechanism to allow for a smooth aerodynamic shape during flying. However, analysing the fuselage, it was found to be impossible to fit such a retracting mechanism.

[2] AIRFLOOR® AFR, *date accessed: 12-06-2018*, `http://www.cooperstandard.com/sites/default/files/aviationsPdfs/Datasheet_AIRFLOOR.pdf`

Therefore, a fixed landing gear is chosen. For the suspension and the attachment to the fuselage structure, a double wishbone configuration is used. This configuration can be seen in Figure 8.12. It consists of two triangles, called 'wishbones', that can move upwards and downwards. This vertical movement is then damped by the shock absorber. In Figure 8.13, this configuration is attached to the fuselage structure.

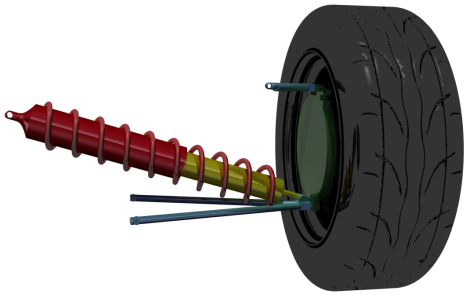

Figure 8.12: Front landing gear suspension

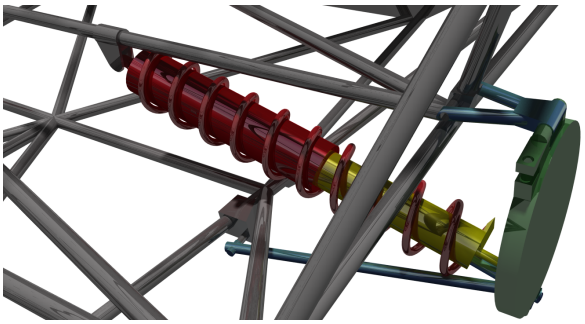

Figure 8.13: Attachment between front landing gear and fuselage

8.3.4. Aft Landing Gear and Empennage Structure Design

The tail surfaces at the back are there for stability purposes. The dimensions of the horizontal and vertical tail with control surfaces will be derived in chapter 9. As described before, two vertical tails are located at the side of the pod. They are carried by the upper one of the two horizontal tails. The design process followed is described throughout this section. First, the vertical tail structure is designed using the fact that the aft landing gear has to be housed here. Afterwards, the connections to the horizontal tails are designed.

Vertical Tail Structure Design

The structure of the vertical tail follows from the the procedure described in the midterm Report [3]. In Table 8.3, the values evaluated at this early design stage are presented. The same table lists the dimensions of the rudder, derived in chapter 9.

Table 8.3: Summary of vertical tail parameters

Vertical Tail	Value		Rudder	Value
S [m^2]	1.32		S [m^2]	0.60
c [m]	0.66		c [m]	0.30
b [m]	1		b [m]	1

A thick airfoil has to be selected to ensure that enough space is available for the 40 cm diameter landing gear. Moreover, the airfoil should be symmetric. The NACA 0030 airfoil is selected through an iterative process using different NACA airfoils. This airfoil allows the landing gear to be stored inside the tail, while leaving a margin of three centimetres to the leading edge. In Figure 8.14, the vertical tail and the dimensions of the wheel are shown.

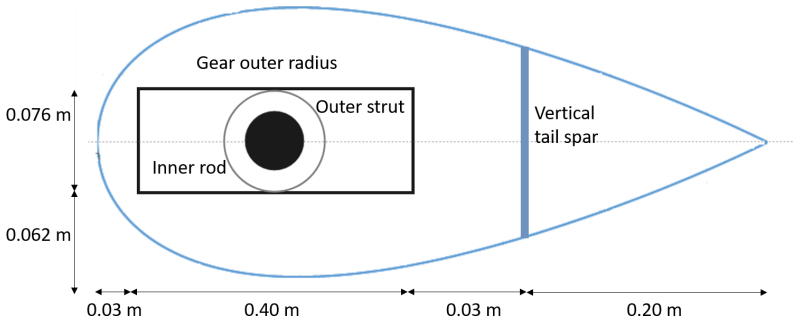

Figure 8.14: Top view of one side of the tail structure

The structure designed to retract and deploy the landing gear consists of an outer and an inner rod. The outer rod is attached to a spar in the horizontal wing. A smaller rod inside has a pin lock mechanism. The pin is removed from its lock when the landing gear is to be moved. The holes in which the pin is locked are located in the outer rod. To ensure a fail-safe system, multiple pins are used. The length of the rods is such that the entire wheel can be retracted.

In Figure 8.15, the structure inside one of the vertical tails is illustrated. At the leading edge of the rudder, a spar is placed to attach the rudder to the vertical tail. A rib is introduced at the locations where the horizontal tails are connected to the vertical tail.

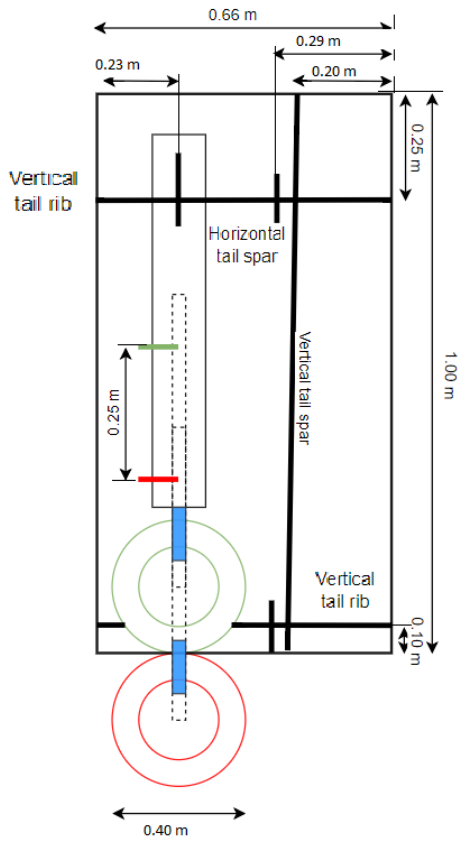

Figure 8.15: Vertical tail structure, side view

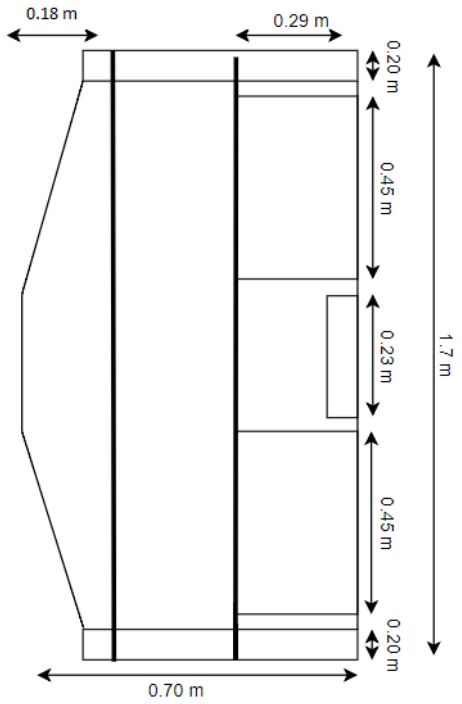

Figure 8.16: Horizontal tail structure, top view

Horizontal Tail Structure Design

The structure of the horizontal tail follows directly from the sizing procedure described in the midterm Report [3]. Here, the parameters listed in Table 8.4 have been derived. In the same table, the geometric parameters of the elevator are presented, which are determined according to the procedure described in chapter 9.

Table 8.4: Summary of horizontal tail parameters

Horizontal Tail	Value		Elevator	Value
S [m^2]	2.19		S [m^2]	0.32
c [m]	0.7		c [m]	0.28
b [m]	1.5		b [m]	0.9

As was the case for the vertical tails, a spar is located in the horizontal tail at the leading edge of the elevators. This is to enable the elevators to be attached and to provide support for the elevator actuators. Another spar is located at 0.18 m from the leading edge to carry the landing gear. The connections between the vertical and horizontal tails are made by the ribs in the horizontal and vertical tail.

To connect the empennage to the fuselage, a clicking mechanism is used. This allows for easy maintenance and a lightweight design. A rod of the main structure is clicked together with the spar of the horizontal tail. This concept is tested and used in the front wing attachment of Formula 1 cars [56]. The operation of the system can also been found in Figure 8.17.[3]

The clicking mechanism can be locked after the system is in place. This ensures that the empennage and main structure do not separate at undesired moments. When maintenance is required, the mechanism is unlocked after which the horizontal tail can be separated.

8.3.5. Wing Structure Design

The design of the wing structure is fundamental as this component is the main lifting device that is responsible for the achievement of the long-range requirement.

[3]The Snail/Drop Cam, date accessed: 25-05-2018,http://www.technologystudent.com/cams/snail1.htm

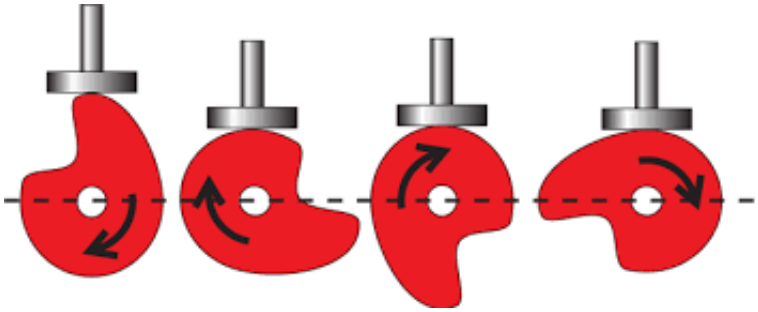

Figure 8.17: Functioning mechanism of a snail cam locking mechanism

Geometric Parameters

The general geometric parameters of the wing are summarised in Table 8.5.

Table 8.5: Wing parameters

Parameter	Value
Surface [m^2]	7.0
Span [m]	6.4
Taper ratio	0.8
Root chord [m]	1.22
Airfoil	BE50

The surface area is derived from the power requirements and wing-loading diagram generated for the vehicle [3]. The span is determined by the size requirements of the vehicle in driving mode: the length of the pod shall not exceed 4.7 m to allow the vehicle to fit in the urban traffic. It is convenient to attach the wing to the vertical plate in the fuselage ,which separates the passenger cabin from the luggage compartment, to provide structural stiffness. In fact, the highest shear loads are applied at the aerodynamic centre of the wing, which can conveniently be overcome by the vertical rib in the fuselage. Given the maximum length of the vehicle and the location of attachment, the span is calculated.

Given the limited dimensions of the pod, it is not possible to select a low taper ratio. This would cause the root chord to be too large. Therefore, a rather large taper ratio of 0.8 is selected. This leads to a root chord at the centre line of the fuselage of 1.22 m.

Finally, an airfoil is selected after determining the sizing requirements and the main aerodynamic characteristics. The Reynolds number plays a significant role in choosing an airfoil. This parameter depends mainly on the velocity and the altitude. Initially, the altitude is set to be between 0.15 and 3.0 km. A higher altitude was disregarded earlier as this introduces cabin pressurisations. This is disadvantageous as this increases the stress on the pressurised part and additional mechanisms are needed to ensure safe oxygen levels. After determining the Reynolds number, the velocity, the lift coefficient and L/D ratio from calculations and empirical relations, an airfoil is selected from existing airfoil data. A set of 1500 airfoils were downloaded beforehand and checked for a match with the characteristics of the pod, for example the$C_L - \alpha$curve. There is a certain number of airfoils that meet these requirements, such as the BE50, NACA 6409 and SD7003. The low thickness of the BE50 airfoil is particularly convenient for storing the wings in driving mode, so that one is chosen.
Having selected the airfoil, an aerodynamic analysis is performed on XFOIL. The outcome can be visualised in Figure 8.18.
This allows for an estimation of the expected drag and lift coefficient for a zero-degree angle of attack:

$$C_d = 0.0068 \qquad C_l = 0.57$$

The reader should refer to chapter 24 for further recommendations on the aerodynamic analysis of the wing.

Structural Analysis of the Wing

Generally, the wing is provided with spars to resist the bending moments, and ribs to distribute the shear stresses. An analysis of bending and shear loads must therefore be performed to check whether the addition of spars and ribs is required.

At previous stages of the design process [3], it is studied that the most critical flight phase in terms of bending stresses is take-off. In fact, during vertical flight, not only is the lift applied as a point load at the wing tip, but the drag is also particularly high, due to the large perpendicular surface area and the drag coefficient C_d, which can be approximated

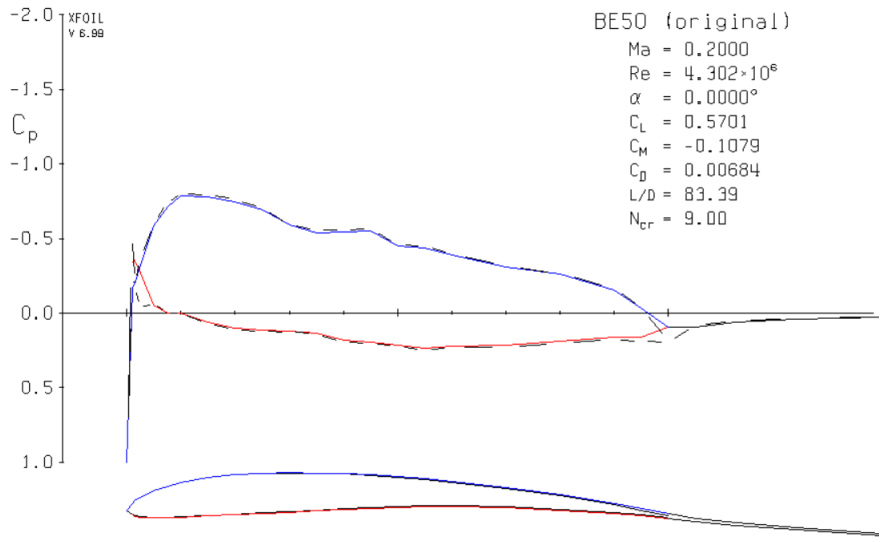

Figure 8.18: Aerodynamic analysis of the airfoil for initial drag estimation

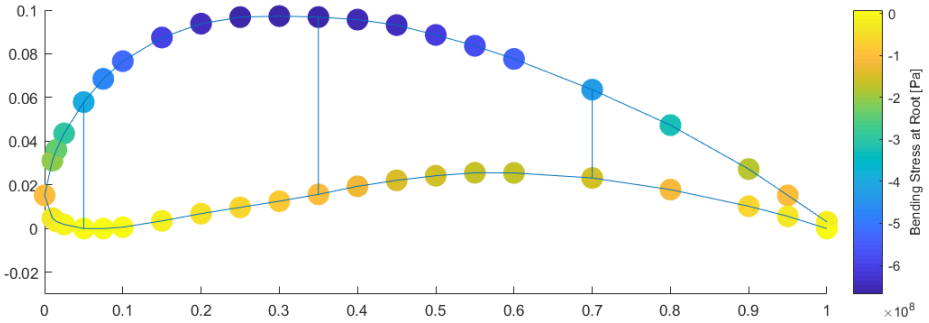

Figure 8.19: Bending stresses at the root

as:

$$2 \cdot sin^3(\alpha) = 2 \cdot sin^3\left(\frac{\pi}{2}\right) = 2 \qquad \text{for vertical manoeuvres}$$

For this reason, a bending analysis is performed for vertical take-off. As the half-wing is modelled as a simply supported beam, it is important to note that the maximum bending moment is found at the root of the wing. The wing cross-section is then idealised, keeping the following considerations in mind:

- 43 booms are distributed along the cross-section, corresponding to the coordinates of the airfoil as provided by the online database Airfoil Tools.[4]
- The back spar is located at 75 % of the chord to support the aileron. The design process of the control surfaces will be described in detail in chapter 9.
- The front spar is located at 15 % of the chord, to provide the necessary stiffness to sustain the hinge that allows for the rotation of the wing from driving to flying mode and viceversa. Details about the swinging mechanism will be presented in the next section of the report.
- A central spar is located at 45 % of the chord to provide additional bending stiffness to the wing.

According to these considerations, the bending stresses at the root of the wing are evaluated by using Equation 8.1. It should be noted that the root of the wing is not located at the centre of the fuselage: in fact, the central section of the wing is left empty during flight and is instead covered by a part of the fuselage skin. For this reason, the root chord of the wing is 1.19 m, and it is located 0.33 m away from the centre line of the main body of the vehicle.

The results of the bending analysis at the root are depicted in Figure 8.19.
The maximum bending stresses are found in the order of magnitude of 80 MPa.

Shear stresses should also be evaluated as the addition of vertical ribs might be necessary. In this case, two flight cases are analysed: cruise conditions and vertical flight. It is discovered that, also in this case, vertical take-off is the critical

[4] Airfoil Tools, date accessed: 10-05-2018, http://airfoiltools.com/

condition as the largest shear loads are applied. It should be noted that it is assumed that all loads are applied through the shear centre and therefore do not produce any torque.

An analysis of the shear stresses along the span is performed by developing a *Matlab* program that iterates at every cross-section along the span, calculates the shear loads at the specific cross-section and computes the shear flows between every boom. In general, the following conclusions are drawn:

- For each half-wing, one rib is located at the root chord to provide structural stiffness at the location of the attachment of the wing to the fuselage.
- For each half-wing, one rib is located at 1.75 m from the root to withstand the maximum shear stress of 22.7 MPa.
- For each half-wing, one rib is located at 2.2 m from the root to withstand the high shear stress of 14.2 MPa.

Finally, a summary of the wing dimensions is provided in Figure 8.20.

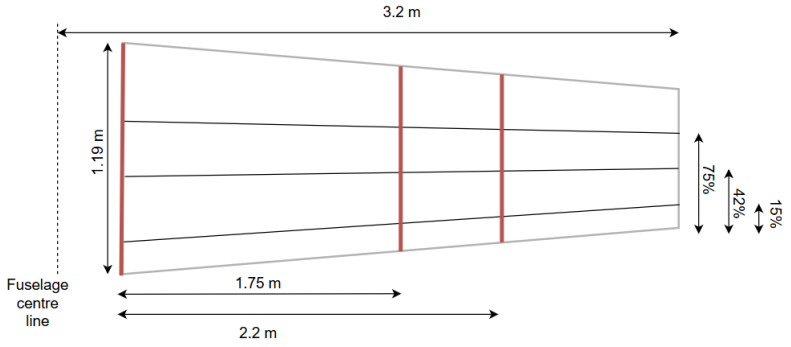

Figure 8.20: Wing spars and ribs location

Verification and Validation

The process is verified by applying the same program to a far more simplified cross-section, as unit check of the calculations. In fact, the process itself has already been verified in Figure 8.3.1. Specifically, the cross-section considered represents the multi-cell wing box of the wing: the short sides represent the two outer spars and a central member is added to simulate the presence of the central spar. The dimension of the larger side of the rectangular cross-section corresponds to the distance of the two outer spars at the root of the wing; the height of the cross-section is sized according to the thickness-to-chord ratio of the airfoil. Six booms are located at the corners of the cross-section and at the edges of the central spar.

The maximum bending stress found, in this case, is 27.6 MPa. The offset with respect to the results of the simulation is rather large. This is due to the heavy idealisation of the cross-section, which leads to an overestimation of the moment of inertia of the wing section.

Wing-Fuselage Connection and Swinging Mechanism

The connection between the wing and the fuselage is a critical part, as it needs to provide the stiffness to support all the loads applied to the wing and, at the same time, allow for the rotation of the wing structure.

In flying mode, the wing must be continuous as it is aerodynamically beneficial not to interrupt the airfoil shape. For this reason, the central part of the wing span is covered by the skin of the fuselage, which causes the flow to create a smooth profile around the vehicle. This situation is represented in Figure 8.21.

Underneath the central section of the fuselage skin, however, the pod is hollow. The two half wings are connected via a sliding mechanism which connects the back spars making the wing continuous and alleviating the bending moments at the root. The continuous spar is secured to the fuselage as shown in Figure 8.22.
A swinging mechanism has to be designed to initiate driving mode. Due to the large dimensions of the wing, the two half-wings have to overlap in driving mode. For this reason, one mechanical rod on each half-wing are installed on the vertical aluminium plate between the passenger cabin and the luggage compartment, and connected to the front spar. The mechanical rods do not only provide the strength to translate one half-wing vertically, but also rotate the wing to switch configuration. The hinge point around which each half-wing rotates is located in the front spar and directly connected to the mechanical rod. This mechanism can be visualised in Figure 8.23.

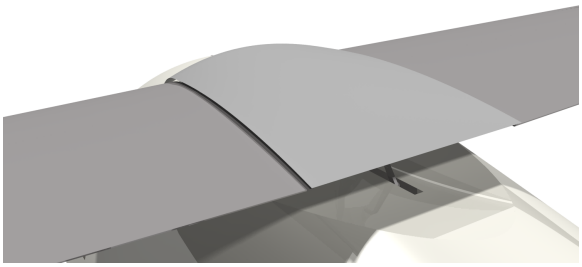

Figure 8.21: Vehicle in driving mode

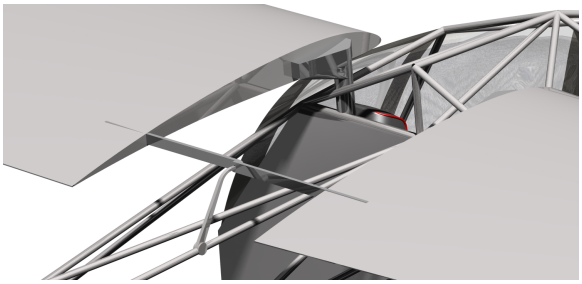

Figure 8.22: Spar sliding mechanism

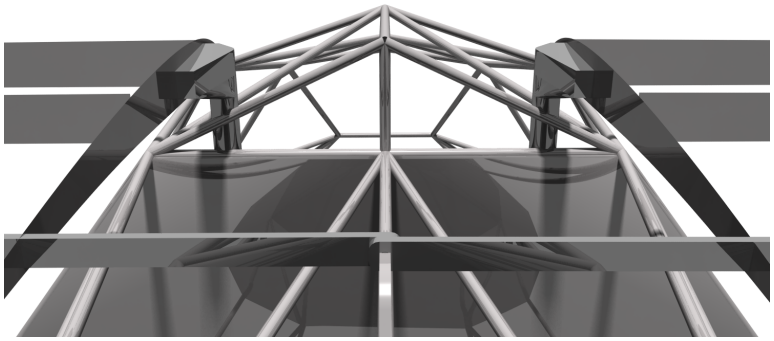

Figure 8.23: Rod mechanism for wing rotation

8.3.6. Material Selection

In this section of the report, clarifications are provided regarding the materials used for the structure of the vehicle.

Truss Structure

Firstly, aluminium is selected as the frame material for the truss structure of the fuselage. The reasons for this decisions have been described in detail in subsection 8.3.2. In terms of sustainability, the use of aluminium is convenient as it is fully recyclable. On the other hand, the recyclability of composites is very limited. Only up to 70 % [5] of the weight of these components can be re-used. Moreover, composite materials are in generally more expensive than aluminium. This is true not only in terms of material costs, but also in terms of manufacturing costs.

Skin

For the skin of the fuselage, different solutions are considered: aluminium, glass reinforced composite and polypropylene. Since the frame is designed to carry away the loads and pressurisation is not needed, it is not necessary to design a metallic skin as it would cause the weight of the structure to increase drastically. The use of composites would reduce the weight slightly, but it would also decrease the sustainability of the vehicle as it is not recyclable. It becomes evident that the use of polypropylene is very convenient, thanks to the following characteristics:

- With a density of 0.85 kg/m^3, it is lightweight.
- It is fully recyclable.
- With a price of 1.496 €/kg, it is relatively cheap.
- In the future, it will be easily manufactured in series by 3D-printing techniques.

There are some downsides to using polypropylene. The following downsides can be identified:

- Polypropylene is flammable.
- Polypropylene uses pollutant resources like oil and natural gas.
- Polypropylene is subject to UV degradation, which causes CO_2 to be released to the atmosphere. [22]
- Polypropylene is difficult to bond together, making assembly more complex.

Even though polypropylene has quite some disadvantages, some of them can be mitigated. For example, UV resistant coating can be applied to the skin to reduce degradation. In terms of the sustainability, alternative materials like metals also emit greenhouse gases in their production. For these reasons, polypropylene is selected for the skin of the fuselage.

[5] Composites World, date accessed: 5-06-2018, https://www.compositesworld.com/columns/recycled-carbon-fiber-its-time-has-come-

Empennage

Considerations for the wing are also formulated for the empennage: the internal parts are designed with aluminium. They have to be stiff, because they are responsible for the connection between all parts. Moreover, enough stiffness must be provided by the structure in correspondence to the rear landing gear location, as the loads are particularly high at that location.

The skin, however, can be manufactured from polypropylene, as high stiffness is not required and low weight is preferred. Specifically, it is very convenient to manufacture the skin of the entire empennage as one whole piece, so that no assembly weight has to be added to the weight budget.

Wing

As the wing has to be able to withstand the highest critical loads, its structure must be reliable. For this reason, a skin-stiffened frame is designed. This is made of aluminium, as it is the most convenient metal in terms of weight and cost optimisation. The reason why polypropylene cannot be applied in this case is that the skin is now expected to carry critical loads.

8.3.7. Mass and Cost estimation

An overview of all the selected materials is provided in Table 8.6. The mass estimation of the structure is then performed according to a volumetric calculation of each structural component. Then, each volume is multiplied by the respective density to obtain the mass. The results of this procedure are listed in Table 8.6

Table 8.6: Structural mass estimation

Component	**Fuselage**		**Empennage**		**Wing**
	Frame	**Skin**	**Frame**	**Skin**	
Material	Aluminium	Polypropylene	Aluminium	Polypropylene	Aluminium
Mass [kg]	16.95	9.2	4.5	2.1	17.2

From this mass estimation, a preliminary cost estimation is performed. This is done according to the procedure proposed by reference documents [51].

Specifically, for each structural component, two costs are estimated: the price of the raw material and the price of manufacturing. The raw material costs are estimated according to statistical data [6]. This means that, for each structural component, the mass is multiplied by the cost per kilogram of the raw material. This leads to the results listed in Table 8.7.

Furthermore, the manufacturing costs are computed as follows:

- For the truss structure of the fuselage, Equation 8.3 is used. This relation is derived from statistical data and it is currently used as reference in the aerospace industry [11]. This is only valid for the manufacturing of aluminium sheets. For steel sheets, a margin of 25 % is added.

$$c_{truss}^{fabrication} = 7.731 \cdot 10^{-1} \cdot L^{truss} \tag{8.3}$$

  To relate the standard manufacturing time to the actual costs, Equation 8.4 is used.

$$C_{truss} = r^{fabrication} \cdot u^{fabrication} \cdot c^{truss} \tag{8.4}$$

  Here, $u^{fabrication}$ corresponds to the utilisation factor, which is assumed to be equal to 1.45 for simplicity. $r^{fabrication}$ is the fabrication rate, which is assumed to be equal to 35 €/s [51].

- The manufacturing costs of the inner structure of the empennage and the wing are estimated in the same manner. The standard labour time of the manufacturing process of a sheet of aluminium is computed with Equation 8.5[51].

$$c_{sheet}^{fabrication} = 2.303 \cdot 10^{-3} \cdot t_{sheet} \tag{8.5}$$

  The same expression presented in Equation 8.4 is used to derive the total manufacturing cost.

- The manufacturing cost of the skin of the fuselage and the empennage is estimated with reference data.[7] The total manufacturing price is calculated by multiplying the manufacturing cost per kilogram of material times the overall amount of polypropylene.

[6] Aircraft Materials. 2001, date accessed: 12-06-2018, http://www.aircraftmaterials.com/

[7] Polypropylene Prices, Markets & Analysis, date accessed 08-06-2018, `https://www.icis.com/chemicals/polypropylene`

The total structural costs are summarised in Table 8.7.

Table 8.7: Overview of structural costs

Component	**Fuselage**		**Empennage**		**Wing**	
	Frame	**Skin**	**Frame**	**Skin**		Total
Cost- raw material [€]	17.50	13.80	5.54	5.25	269.50	€311.59
Cost- manufacturing [€]	804.00	741.50	342.7	282.80	403.20	€2573.60
					(Assembly cost)	€865.60
						€3750.79

It should be noted that in the cost estimation presented in Table 8.7, a cost of assembly is added. This is typically estimated by considering the number of rivets to be applied to the structure. In this case, however, the detail of the design process has not yet reached this level. Therefore, an indicative 30 % is added to the overall structural cost to account for assembly costs. This value is derived from statistics [51].

8.3.8. Overview on Sustainability

During the design of the structure, sustainability plays a leading role, especially during the selection of materials. The decision to have a polypropylene skin is heavily based on the fact that it is fully recyclable. Although the skin of the pod only contributes to a few percent of the total weight, the polypropylene skin does make the recyclability requirement of 60 % of the pod weight more attainable. The achievement of this requirement is further investigated in chapter 19.
However, it should be noted that when polypropylene is not properly recycled, it poses a serious risk for the environment and health. The material degrades slowly: it takes around 20 years before the material decomposed [32]. Therefore, the recycling should be done properly. Polypropylene is also compatible with the REACH requirements established by the European Chemicals Agency.[8] No additional hazards have been classified for this material.

The recyclability of the product is also improved with the use of aluminium. This metal cannot only be easily melted and reused after the vehicle is disposed, but it can also come from recycled sources. In fact, it requires up to 95 % less energy to recycle aluminium than to produce the metal from scratch.[9]. This avoids all related emissions, including greenhouse gases.

[8] REACH Requirements, European Chemical Agency. 2018, date accessed: 29-05-2018, https://echa.europa.eu/nl/substance-information/-/substanceinfo/100.117.813

[9] Aluminium for Future Generations, date accessed: 22-06-2018, http://recycling.world-aluminium.org/review/sustainability.html

9
Flight Control

This chapter considers the flight control of the pod. First the stability in each flight phase is considered followed by an explanation of how the flight control system operates to remain stable. Afterwards, the ailerons, rudder and elevator are designed based on their critical load cases.

9.1. Requirements and Constraints for Flight Control

The following requirements were set in previous design phases for the flight control:

- POD-SYS-F-1: The pod shall be able to fly autonomously.
- POD-SYS-F-2: The pod in flying mode shall be able to detect obstacles in all flight directions;
- POD-SYS-F-3: The pod in flying mode shall be able to avoid detected obstacles on its route.
- POD-SYS-F-7: The pod shall be able to abort landing if obstacles on desired landing location are detected.
- POD-SYS-F-8: The pod in flying mode shall have statically stable flight characteristics.
- POD-SYS-F-9: The pod shall perform emergency landing within 1 minute after emergency landing is requested.
- POD-SYS-F-10: The pod in flying mode shall have dynamically stable flight characteristics.
- POD-SYS-D-4: The pod shall be able to drive autonomously
- POD-SYS-D-6: The pod in driving mode shall be able to detect non-moving obstacles in all driving directions
- POD-SYS-D-7: The pod shall be able to avoid obstacles without endangering traffic.
- POD-SYS-D-8: The pod shall be able to detect moving obstacle.
- POD-SYS-SC1: The pods shall be able to communicate with an external system at all times.

Additionally, the following requirements are set for the detailed design phase. The reasoning and rationale for the requirements is explained in the sections to which the requirements belong further in this chapter.

- POD-SUB-FC-1: The pod shall have stable flight characteristics in horizontal flight.
- POD-SUB-FC-2: The pod shall have stable flight characteristics in vertical flight
- POD-SUB-FC-3: The pod shall reach a minimum pitch acceleration of 0.32 rad/s^2 in cruise conditions.
- POD-SUB-FC-4: The pod shall reach a bank angle of 30^o within 1.3 seconds from a steady bank angle.
- POD-SUB-FC-5: The pod shall land safely with a 90^o crosswind of 6.2 m/s.

9.2. Stability

The stability of an aircraft can be analysed around different axes. The most important axis for USTI is the longitudinal axis. When lateral stability is required, a difference in thrust on each side can provide stability. To have a longitudinally stable aircraft, the moments around the centre of gravity of the pod should all add up to zero. Firstly, the location of the centre of gravity is defined, after which the three flight phases (take-off, cruise, landing) are analysed.

9.2.1. Loading Diagram

The loading diagrams are created to obtain the most extreme locations of the centre of gravity. In Figure 9.1, the loading is assumed to be such that the most front components are loaded first. So first the passengers, then the fuel and finally the luggage. In Figure 9.2, the most aft components are loaded first. The order of this type of loading is fuel first, then luggage and then passengers.

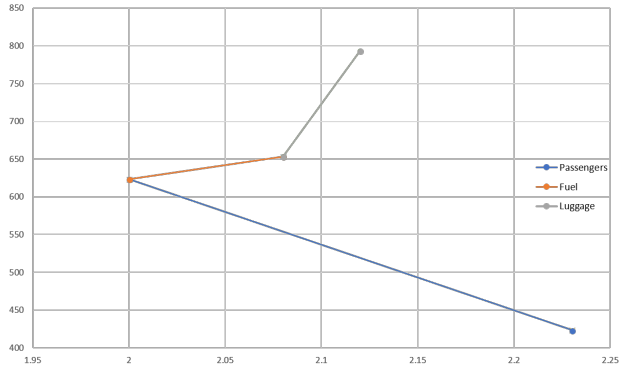

Figure 9.1: Loading diagram with front loading first

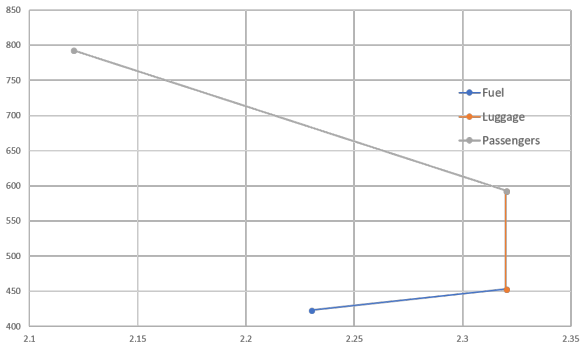

Figure 9.2: Loading diagram with back loading first

From these figures, it can be found that the most forward CG location is at 2 metres from the nose. The most aft CG location is located at 2.32 metres from the nose. This corresponds to 21 % and 52 % of the mean aerodynamic chord.

9.2.2. Take-off

During vertical take-off, the wings do not produce lift. It was found in the midterm review that the required thrust for take-off is 1.35· W_{TO} [3]. The provided thrust comes from the two rotors mounted to the side of the wing, dedicated for take-off. As these are located on the same line of action, maintaining stability is a major complication for the pod. When the thrust vector does not point through the centre of gravity, a moment is created that cannot be counteracted. There are two options to mitigate this problem: 1) the back rotor could be operative during take-off to create an additional moment, or 2) the rotor blades could pitch such that the thrust vector is always through the centre of gravity.

The first option is discarded for two reasons: the thrust required to counteract the moment in the most extreme case is close to 8 kN, whereas the back rotor is only designed for approximately 800 N as found in chapter 6. Secondly, the pod would accelerate in horizontal direction, which is not desired during a vertical take-off.

The second option is to tilt one of the rotor blades. In conventional helicopters, this is called the cyclic [14]. The lower swash plate is rotated, tilting only one of the blades. The effect this has is a change in the direction of the thrust vector, whereas tilting both blades would only increase its magnitude. A drawback of this option is the fact that the magnitude of thrust would have to increase to have the same thrust magnitude in vertical direction. This option is depicted in Figure 9.3.

When the CG is located at the most aft position, the blade is rotated over an angle α = 19 ^{o}. The total thrust has to be increased by 5.3 % to retain a vertical thrust component of 1.35·W_{to}. Due to the forward component of the thrust, the take-off will not be fully vertical. This is to be taken into consideration when taking off. Note that the rotors are located such that the centre of gravity is always aft. This way, a forward component of the thrust vector is always required. This is favourable as the passengers will always have visuals of the direction they are heading towards.

The clearance area is found by plotting the expected horizontal velocity versus the vertical speed. Two phases can be identified during the take-off phase. In Figure 9.4, the first twenty metres are travelled at an angle of 45 ^{o}. Afterwards, the horizontal velocity becomes larger than the vertical velocity, decreasing the clearance angle to 25 ^{o}. In the figure, the red triangle depicts the area in which there should be no obstacles on the ground.

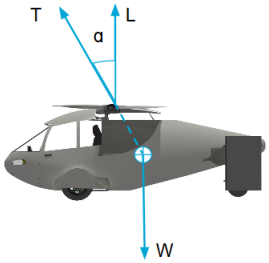

Figure 9.3: Longitudinal stability with tilting rotors

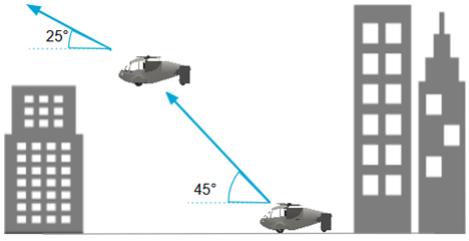

Figure 9.4: Clearance angle required for take-off

9.2.3. Cruise and Landing

When the aircraft is at cruise altitude, the main electric motors shut down and the back rotor takes over. As the thrust vector of the back rotor does not go through the centre of gravity, control surfaces are used to trim the aircraft. The flight control systems will ensure the actuation of the stabilisers. The maximum moment that has to be counteracted by the

elevators is well within their capabilities.

During approach, the back rotor stops to allow the pod to go into a gliding mode. The main rotors become active again to ensure VTOL. The lower swash plate can be rotated to change the direction of thrust backwards to reduce the forward velocity. A consequence of this type of thrust vectoring is that a moment is created. Due to the large inertia of the pod, this would not immediately impose a significant rotation [25]. An algorithm in the flight computer enables the possibility of VTOL while stability is ensured. The flight computer algorithm operates as depicted in Figure 9.5

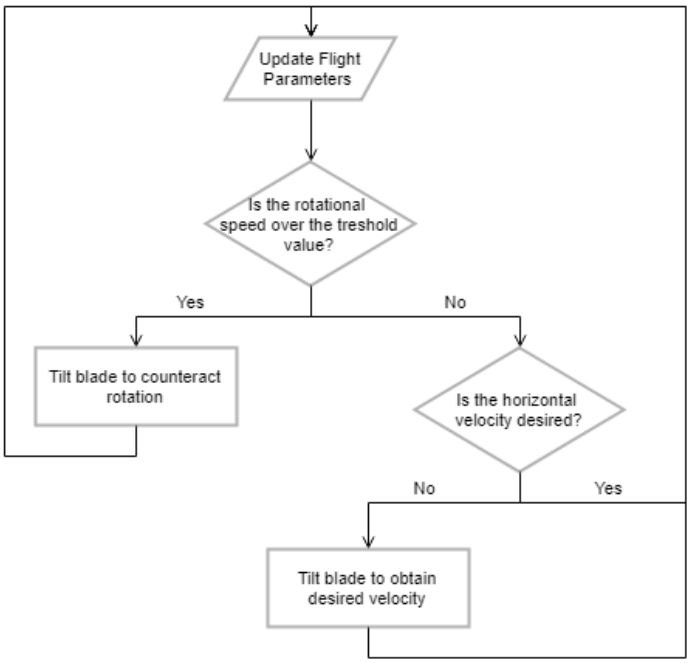

Figure 9.5: Algorithm assisting with vertical landing procedures.

9.3. Control Surface Design

In this section, the control surfaces are sized. Initially, it is decided to install three kinds of control surfaces: elevators on the horizontal stabilisers for longitudinal control, ailerons on the wing for rolling control and rudders for yawing control.

9.3.1. Elevator Design

Elevators are pitch control surfaces attached to the trailing edge of the horizontal stabiliser to provide longitudinal control. This is typically governed by a rotation about the y-axis, which can be induced by providing an incremental lift force on the horizontal tail.

In symmetric aircraft, the longitudinal control is independent of the lateral control, so the elevators can be designed separately from rudders and ailerons. A schematic representation of the elevator and all its geometric parameters is depicted in Figure 9.6.

For conventional aircraft, the design procedure that sizes the aileron is generally based on take-off pitching requirements, as the largest angular pitching acceleration is required during this phase. However, in this case, this situation never occurs, as the pod is designed to perform vertical take-off. For this reason, the cruise condition is analysed instead.

First, the angular acceleration is evaluated according to regulation requirements [6] with Equation 9.1. Here, V refers to the cruise speed of 200 km/h, whereas n_{max} is the maximum load factor as evaluated in previous steps of the design process and it is equal to 3 [3].

$$\alpha = \frac{3.9}{V} \cdot (n_{max}) \cdot (n_{max} - 1.5) \tag{9.1}$$

Given the calculated acceleration, a reference S_e/S_h ratio is selected according to statistical data [52]: this is typically between 0.15 and 0.40. Moreover, reference values for the span ratio b_e/b_h are considered: these are typically between 0.8 and 1.0. Continuing with the design process, the maximum upward and downward elevator deflections are determined according to aerodynamic requirements. A maximum elevator deflection of 25^o should not be exceeded as flow

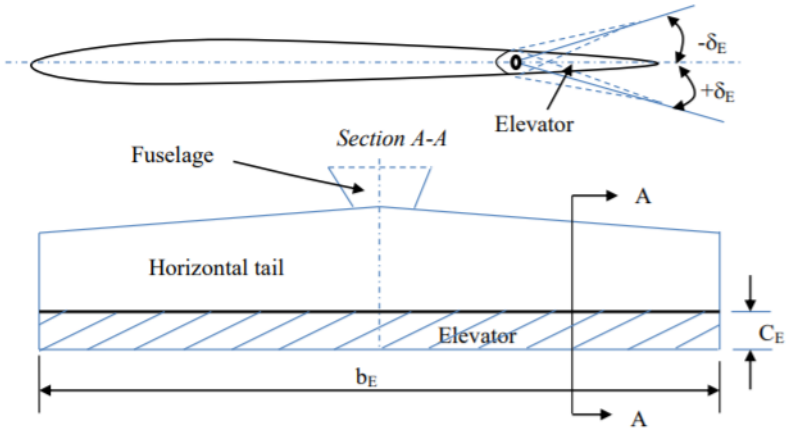

Figure 9.6: Elevator geometric parameters [52]

separation over the tail tends to occur beyond this limit, decreasing the elevator effectiveness.

The horizontal tail lift has to be calculated: this is done by applying Equation 9.2. Here, $\ddot{\theta}$ corresponds to the previously calculated angular acceleration.

$$L_h = \frac{M_L + M_{ac_{wf}} + M_w + M_D + M_T - I_{yy} \cdot \ddot{\theta}}{x_{ac_h} - x_{mg}} \tag{9.2}$$

Equation 9.2 corresponds to the longitudinal moment equilibrium equation. The magnitude of each moment arm is calculated according to the designed pod geometry, whereas the magnitude of each force is found by applying the standard lift, drag and weight equations at cruise level.

Once the tail lift coefficient is estimated with Equation 9.6, it should be checked whether this complies with the elevator requirements by calculating the required angle of attack effectiveness of the elevator: this should be lower than 1 for the elevator to be effective. The angle of attack effectiveness of the elevator is computed by applying Equation 9.3. It should be noted that the maximum elevator deflection is included in the calculation as it provides the most critical condition.

$$\tau_e = \frac{\alpha_h + \left(\frac{C_{L_h}}{C_{L_{\alpha_h}}}\right)}{\delta_{e_{max}}} \tag{9.3}$$

Here, $C_{L_{\alpha_h}}$ is found by assuming that the airfoil chosen for the wing is also suitable for the horizontal tail. The correspondent lift-curve slope is then computed by approximating the airfoil $C_{l_{\alpha_h}}$ for the finite wing $C_{L_{\alpha_h}}$. Moreover, α_h is calculated by applying Equation 9.4.

$$\alpha_h = \alpha + i_h - \epsilon \tag{9.4}$$

Here, the cruise angle of attack α is computed according to the specified $C_{L_{\alpha_h}}$ and the previously selected C_{L_h}. The downwash angle ϵ is computed as follows:

$$\epsilon = \epsilon_0 + \frac{d\epsilon}{d\alpha} = \frac{2C_{L_h}}{\pi \cdot AR} + \frac{2C_{L_{\alpha_h}}}{\pi \cdot AR} \tag{9.5}$$

The current tail lift coefficient is then computed by applying Equation 9.6.

$$C_{L_h} = \frac{2L_h}{\rho V^2 S_h} \tag{9.6}$$

According to the elevator surface area that was previously estimated, an elevator-chord to tail-chord ratio can be selected with Figure 9.7. If this value is higher than 0.5, a fully movable tail should be used.

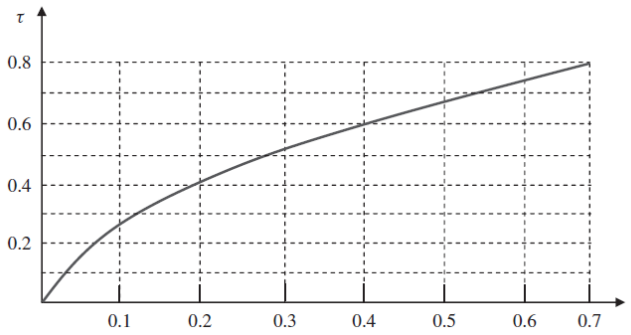

Figure 9.7: Control surface-to-lifting surface chord ratio.

It is now possible to compute the amount of lift that is actually produced by the tail when the elevator is fully deflected. If this does not match the required lift needed for a longitudinal moment equilibrium, the values estimated for the surface area, chord and span must be iterated.

In this case, the final selected geometry leads to a C_{L_h} of 0.45, which produces enough lift over the horizontal stabiliser to balance the longitudinal moments. After the iteration, the parameters listed in Table 9.1 are collected.

Table 9.1: Elevator parameters

Parameter	Value
S_e	0.29 m^2
b_e	0.9 m
c_e	0.32 m
τ_e	0.30

The parameters collected in Table 9.1 still fall within the reference parameters found from statistics [52]. This confirms the validity of the method. It should be noted that the surface area presented in Table 9.1 is split into the two horizontal surfaces.

Once the final lift coefficient of the elevator is found, it is necessary to compute the lift produced by the elevator: this will be used in the next section to evaluate the power required to activate the elevator. In this case, the lift produced by the elevator is the following:

$$L_e = 1.162 \text{ kN}$$

Verification and Validation The approach to check whether the design procedure is reliable is based on a reversed calculation of the longitudinal moment equilibrium.

Figure 8.7 is taken into consideration and it is assumed that the lift generated by the tail is unknown. Then, the moment equilibrium equation is formulated and the required tail lift force is evaluated. This lift is directed upwards, as the centre of gravity of the vehicle is located behind the aerodynamic centre of the wing where the lift is assumed to be applied.

It is also important to check whether the necessary lift can be provided by the combination of the selected tail and elevator surfaces. The increment in lift that the elevator must provide is therefore calculated as the difference between the lift required for moment equilibrium and the lift generated by the wing when the elevator is not deflected. Then the required surface area is computed by dividing the result by the relative parameter according to the standard lift formula. Its magnitude is then compared to the one estimated in the previous subsection, in Table 9.2.

Table 9.2: Results of verification for elevator design

Parameter	From verification procedure	From regular calculations	Discrepancy
Surface area	0.32 m^2	0.29 m^2	9.4%

There is a clear difference between these results. However, it should be noted that the verification procedure relies heavily on approximations made with respect to two aspects: the calculation of the required lift, due to the non-precise weights taken into account in the evaluation of the longitudinal moment, and the calculation of the lift generated by the wing with the non-deflected elevator.

9.3.2. Aileron Design

Ailerons are control surfaces that are usually located at the outboard section of the trailing edge of each of the wings, with the primary function of providing roll control. The working principle of the ailerons is explained using Figure 9.8 [52]. On one the wings, the aileron deflects downward, causing an incremental increase in lift. On the other wing, the aileron deflects upwards, causing a incremental decrease in lift on this wing. This will therefore induce a rolling moment, with the wing experiencing a higher lift force tending to go upward. However, deflecting the ailerons also results in incremental changes in the tangential forces seen by the wings. For this reason, the downward wing tends to go forward, inducing a yawing moment.

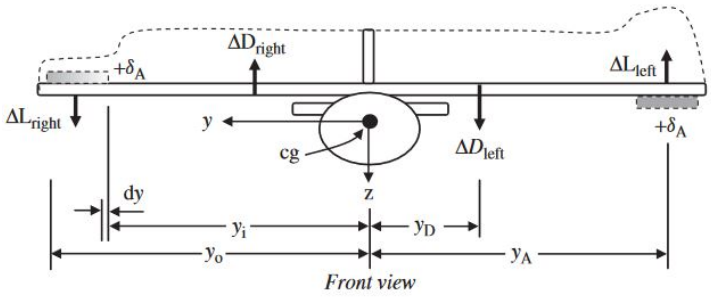

Figure 9.8: Working principle of ailerons

Aileron design is mainly based on requirements on the rolling manoeuvres that an aircraft needs to be able to perform. However, since deflecting the ailerons also causes a yawing moment, measures should be taken to iterate the design of the ailerons if this yawing moment is unwanted.

The first step in the design of the ailerons is selecting the critical flight phase for the operation of the ailerons. This critical flight phase is different for different classes of aircraft. From [52], it was found that aircraft with a maximum take-off mass below 6,500 kg belong to Class I aircraft. For this aircraft class, the critical flight phase is usually during low speeds operations in the order of $1.3V_s$. For this flight phase, the rolling manoeuvre requirement is that a change in bank angle of 30° should be achieved within 1.3 seconds starting from the steady initial bank angle.

Sizing the ailerons to meet this requirement is an iterative process. First, initial values for the geometry are chosen tentatively. With this geometry it is checked whether the rolling manoeuvre requirement is met. If not, the geometry parameters are changed through trial and error until a suitable combination of parameters is found.

When the initial geometry is chosen, the rolling moment coefficient can be calculated using Equation 9.7. In this equation, y_i and y_o represent the inboard and outboard locations of the ailerons, respectively. How they are defined can be observed in Figure 9.8. The aileron effectiveness factor τ_a is obtained from the aileron chord to wing chord ratio C_a/C using Figure 9.7. The maximum chord of the aileron is constrained to 25 % of the wing chord, as there is a spar located at 75 % of the wing chord.

$$C_{l_{\delta_A}} = \frac{2C_{L_{\alpha_W}}\tau_a C_r}{Sb}\left[\frac{y^2}{2} + \frac{2}{3}\left(\frac{\lambda-1}{b}\right)y^3\right]_{y_i}^{y_o} \tag{9.7}$$

When a value for $C_{l_{\delta_A}}$ is found, the maximum value for the rolling coefficient C_l should be determined. This is calculated using Equation 9.8 and depends on the maximum allowable deflection for the aileron δ_A before stall occurs. This value is usually around 25° [52]. Subsequently, the rolling moment L_A in this situation is calculated using Equation 9.9.

$$C_{l_{max}} = C_{l_{\delta_A}}\delta_{A_{max}} \tag{9.8}$$

$$L_A = \frac{1}{2}C_l qSb \tag{9.9}$$

With the rolling moment now known, it should be checked whether this moment is enough to fulfil the rolling manoeuvre requirement. For this, first the steady state roll rate P_{ss} and the steady state bank angle Φ_1 should be calculated using Equation 9.10 and Equation 9.11. S

$$P_{ss} = \sqrt{\frac{2L_A}{\rho\left(S_w + S_h + S_v\right)C_{D_R}y_D^3}} \tag{9.10}$$

$$\Phi_1 = \frac{I_{xx}}{\rho\left(S_w + S_h + S_v\right)C_{D_R}y_D^3}ln(P_{ss}^2) \tag{9.11}$$

Subsequently, the roll rate of the aircraft during this motion is determined using Equation 9.12. Finally, using this value, the time that it takes to reach a certain bank angle can be calculated using Equation 9.13. This time is compared to the required time. If the requirement is not met, the geometry should be altered until it is met. Also, if the time duration of the manoeuvre is much lower than required, the geometry should be iterated.

$$\dot{P} = \frac{P_{ss}^2}{2\Phi_1} \tag{9.12}$$

$$t = \sqrt{\frac{2\Phi_{req}}{\dot{P}}} \tag{9.13}$$

After iterations, the final values for the ailerons can be found in Table 9.3.

Table 9.3: Final values for the aileron design

Parameter	Value
y_i	1.95 m
y_o	3.04 m
C_a	0.21 m
b_a	1.09 m
S_a	0.23 m^2

9.3.3. Rudder Design

The rudders are attached to the vertical tails at the back of the pod. A rudder deflection creates a yawing moment, which can be used to change the heading of the aircraft, as depicted in Figure 9.9. Designing these control surfaces is done by looking at the situation in which a landing is performed with a 90° crosswind of $0.2 \cdot V_s$. This is the most critical load case [52] for which the aircraft has to be designed according to regulations [6]. The steps taken to size the rudder are discussed here.

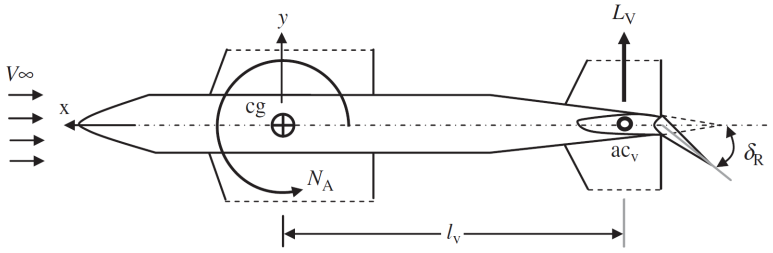

Figure 9.9: Working principle of rudders

Designing the rudder is done by assuming a certain geometry. Then the required deflection is found. If this deflection is smaller than 30°, it can be assumed that no flow separation occurs and the rudder can be used for flight. This is the leading principle throughout the design of the rudder.

The deflection of the rudder can be found by solving Equation 9.14 and Equation 9.15 simultaneously.

$$\frac{1}{2}\rho V_t^2 Sb(C_{n\beta}(\beta-\sigma) + C_{n\delta R}\delta_R) + F_w \cdot d_c cos\sigma = 0 \tag{9.14}$$

$$\frac{1}{2}\rho V_w^2 S_s C_{Dy} = \frac{1}{2}\rho V_t^2 S(C_{y\beta}(\beta-\sigma) + C_{y\delta R}\delta_R) \tag{9.15}$$

The force exerted on the fuselage of the aircraft can be calculated with Equation 9.16.

$$F_w = \frac{1}{2} \cdot \rho V_w^2 S_s C_{Dy} \tag{9.16}$$

The different velocities in these equations can all be related to the stall speed. According to CS23 regulations, V_w is

$$V_w = 0.2 \cdot V_s$$

And V_t is

$$V_t = \sqrt{(1.3 \cdot V_s)^2 + V_w^2}$$

The stability derivatives have to be found to remain with two unknowns and two equations (σ and δ_R). They are found through the use of Equation 9.17, Equation 9.18, Equation 9.19 and Equation 9.20. In these stability derivatives, the contribution of the fuselage , dynamic pressure efficiency and sidewash gradient are found in literature [52]. The other values are calculated or follow from design choices. For example, τ_r follows from a chosen C_v/C_r in Figure 9.7. $C_{L\alpha V}$ is the lift coefficient of the chosen airfoil. A NACA 0030 airfoil was chosen in chapter 8 to house the landing gear.

$$C_{n\beta} = K_{f1} C_{L\alpha V} (1 - \frac{d\sigma}{d\beta}) \eta_v V_v \tag{9.17}$$

$$C_{y\beta} = -K_{f2} C_{L\alpha V} (1 - \frac{d\sigma}{d\beta}) \eta_v \frac{S_v}{S} \tag{9.18}$$

$$C_{L\alpha V} \eta_v \tau_r \frac{b_r}{b_v} \frac{S_v}{S} \tag{9.19}$$

$$- C_{L\alpha V} V_v \eta_v \tau_r \frac{b_r}{b_v} \tag{9.20}$$

These equations are inputs to the system of two equations (Equation 9.14 and Equation 9.15). After iterating the geometry to obtain the required maximum deflection angle, the final values are found. These are shown in Table 9.4

Table 9.4: Final Rudder Dimensions

Parameter	Value
C_r	0.2 m
C_v	0.66 m
b_r	1 m
V_s	31 m/s
δ_{R_max}	23 deg

Verification and Validation For verification, the required moment created by the rudder to counteract the crosswind is calculated in a different way. The force that is exerted on the side of the aircraft body is determined using Equation 9.16. The moment this creates is found to be $F_w \cdot d_c$ =2,845 Nm. The yawing moment the rudder creates when fully deflected is found by using $L \cdot l_v$. The variable L in this equation can be found with Equation 9.21:

$$L = C_{L_{def}} \cdot \frac{1}{2} \rho V_{app}^2 S \tag{9.21}$$

This yields a rudder yawing moment of 6,423 Nm, which is in the same order of magnitude as the crosswind yawing moment. Possible differences lie in the fact that the fuselage contribution was not taken into account in this verification process.

9.4. Actuator Selection and Design

Every mechanical component of the control system of the vehicle must be activated. In this section of the report, the general actuator system is discussed and the characteristics of the individual actuators are specified.

9.4.1. Actuator System Type

Different energy sources can make the actuator move. These options include hydraulic fluid, pneumatic pressure and electric current. When a control signal is received by the actuator, it will use one of these energy sources to perform the action. An example of such a system is depicted in Figure 9.10[40]. The energy source (e.g. hydraulic power) is one input for the servo valves and the signal is another. An output signal is generated by the actuator to update the flight computer on the current status [40].

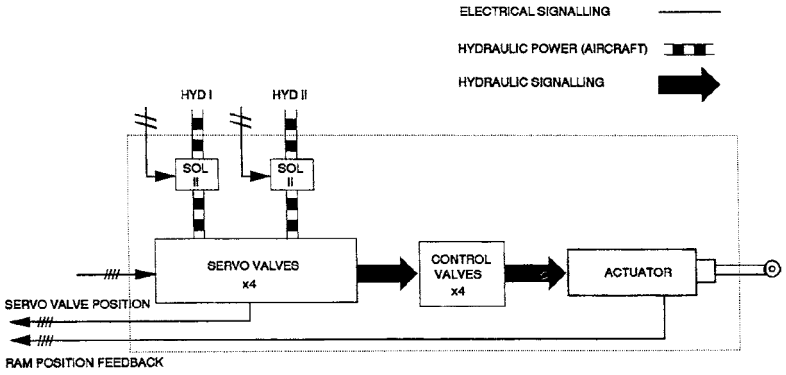

Figure 9.10: Example of an actuator system where the input signal regulates the hydraulic pressure in the actuator

The described energy sources all have their own advantages and disadvantages. Based on this comparison, the right type will be selected for the pod.

- *Hydraulic systems* make use of liquids. The advantage is that in a conventional aircraft, the pilot has to exert a lower force than the force that is applied to the actuator. Also, the actuators can be manoeuvred very accurately in this way. A disadvantage of this system is that it is very costly, maintenance intensive and vulnerable to leaks [1]. Specifically in the design of this pod, a hydraulic system would make the wing-folding mechanism more complex. The pipes would have to fold twice every flight, which causes a significant increase in the risk of failure.

- *Pneumatic systems* are the gaseous representation of the hydraulic systems. This type of system has the benefit of being cost-effective due to the low manufacturing cost. Furthermore, the systems are safer compared to the use of liquids because of air being non-flammable. Disadvantages of this system include slow operations, loudness and sensitivity to vibrations. As the actuators will need to move fast and are subject to vibrations, pneumatics are discarded as a feasible option. [2]

- *Electric current* implies the use of electric motors at the hinge locations. A light-weight actuator design can be achieved, since servos are generally between 0.5 kg and 1 kg in weight [3]. Another advantage is the simplicity of the system compared to the complexity of the hydraulic and pneumatic system. Only connections between the power supply and the actuator are required. Furthermore, the reliability and maintenance of the electrically powered systems are better compared to the other options [26]. A possible drawback is that the required torque of a servo might exceed the available torque.

Taking everything into consideration, the use of electric motors is most favourable. The main reasoning for this is that the required torque for the pod will be small compared to conventional aircraft due to its size and cruise speed.

9.4.2. Actuator Design

Actuators are components that are responsible for moving mechanisms or parts. In this section of the report, actuators are designed for the deflection of control surfaces and for the tilting mechanism.

Control Surfaces Actuator Design

The design of the servos that actuate the control surfaces is based on the hinge moment experienced by each of the control surfaces. The hinge moment can be calculated using Equation 9.22. [4] In this equation, K is a constant that depends on the airfoil camber and flap deflection. The control surface chord and area are represented by C_f and S_f respectively. The torque experienced by the servo τ_S can be calculated using Equation 9.23 [45], in which l_g is the effective lever arm of the servo mechanism. A first estimate for l_g is assumed to be 4/3 [45].

$$H = K \cdot L \cdot C_f \frac{S_f}{S_w} \cdot \frac{1}{C_L} \tag{9.22}$$

$$\tau_s = \frac{H}{l_g} \tag{9.23}$$

A suitable servo can be selected with the torque values that were found. For each of the control surfaces, there are two servo actuators that can provide the full torque necessary to rotate the control surface. This is done for redundancy and safety reasons. The servo is likely to operate at different rotational speeds than desired for the control surface. Therefore, a gear will be required to adjust these speeds. The relationship between the rotations per second n and the desired rotational speed for the control surface $\dot{\delta}$ is found in Equation 9.24, in which i_{gear} is the gear ratio.

$$\dot{\delta} = \frac{2\pi n}{i_{gear}} \tag{9.24}$$

The selected servos for each control surface are listed in Table 9.5, as well as the operational speed of each servo and the desired maximum rotational speed for the control surfaces, which are obtained from [33]. Based on these, the required gear ratio are also found and listed.

[1] Charles Pearson, `https://sciencing.com/list-7425341-hydraulic-system-disadvantages.html`
[2] Kunkhe Controls, `http://www.ekci.com/benefits-and-disadvantages-of-pneumatics.html`
[3] All Servos, `https://servodatabase.com/servos/all?sort=torque&page=95`
[4] `http://www.basicairdata.eu/knowledge-center/design/elevator-hinge-moment/`

Table 9.5: Selected Servo for Control Surface

Control Surface	$\tau_s[Nm]$	**Selected Servo**	**Required Number of Servos**	**Rotational Speed Servo [rps]**	**Rotational Speed Control Surface [rad/s]**	**Required Gear Ratio [-]**
Elevator	5.4	XQ-Power XQ-S5650D	4	0.9	$\pi/3$	5.6
Aileron	3.4	Hitec HS-8380TH	2	1.2	$\pi/4$	9.6
Rudder	2.7	Hitec HSR-5995TG	4	1.4	$\pi/4$	10.8

Wing Actuator Design

The torque required to fulfil the deployment of the wing has to be evaluated and a suitable servo has to be found that is able to provide this torque without exceeding the weight and costs limits imposed by the requirements.

The moment of inertia is calculated to design this actuating mechanism. This is done by assuming that the wing behaves as a flat plate rotating around an axis located in the middle of one of its short ends. Moreover, the moment of inertia of the motor is included. Therefore, the following holds:

$$I_{zz_{wing}} = \frac{1}{12} m\left(4(\frac{b}{2})^2 + c^2\right) \qquad I_{motor} = \frac{m}{8} D^2 + m \cdot (\frac{b}{2})^2 \qquad I = I_{zz_{wing}} + I_{motor}$$

Furthermore, it is assumed that the full rotation of the wing occurs in twenty seconds: during the first ten seconds, the wing is accelerated and completes a rotation of 45^o. After this point, it starts decelerating until it is fully deployed. The torque is thus calculated as the product of the moment of inertia and the required angular acceleration:

$$T = I \cdot \alpha$$

.

With this torque, a suitable servo motor is selected: this is the XQ-S5650D. This servo motor is made of titanium, which weighs only 177.5 g. Its price is approximately €100.

Furthermore, the gear has to be designed for the connection between the servo and the wing, as the rotating speed of the rotor is much larger than the required rotating speed of the wing. The design procedure of the gear follows the one presented in subsection 9.4.2. Specifically, in this case, the desired rotational speed of the wing is $\pi/4$, the rotational speed per gear of the selected servo is 1.1 rps and $i_{gear} = 8.8$.

9.5. Flight Control System

Once all the control devices have been designed, it is important to study how the communication flows between the different components. For this reason, the actuator control system is designed, as well as the set of measurement devices that allow the computation of all relevant calculations on board of the vehicle.

9.5.1. Actuator Control

Since the pod must be completely autonomous, it is necessary to design a control system that is able to actuate itself when needed. This is controlled by a central flight control computer that does not only collect measurements from several sensors placed on the pod, but also sends the inputs to the respective actuators. The communication diagram that depicts the signals from the central system to the actuators is represented in Figure 9.11.

It should be noted that in Figure 9.11, the numbers in parentheses refer to the number of actuators installed at each location. The actuators system has to be redundant. In fact, the hydraulics installed on conventional aircraft are usually tripled to guarantee the effectiveness of the pumps. Here, the option of installing hydraulics is discarded as explained in subsection 9.4.1. Servos are not expected to fail easily, as no mechanical movements are involved. However, the redundancy philosophy should still be applied by installing two servos for every critical mechanism that can cause critical failures to the mission. For this reason, a set of two servos will be placed in correspondence to the control surfaces. However, to reduce the weight of the structure, other critical locations will only be provided with one service, as the failure of the actuator would be detrimental to the mission, but not catastrophic. This is the case for the unfolding mechanism of the wing, for example. In fact, in case failures occurred, the pod would still be able to drive.

9.5.2. Sensors

The external inputs to the flight control computer can be divided into two different categories: flight sensors and communicated inputs. In this section, the sensors of the pod are described. Also, an elaboration is given on how the avionics

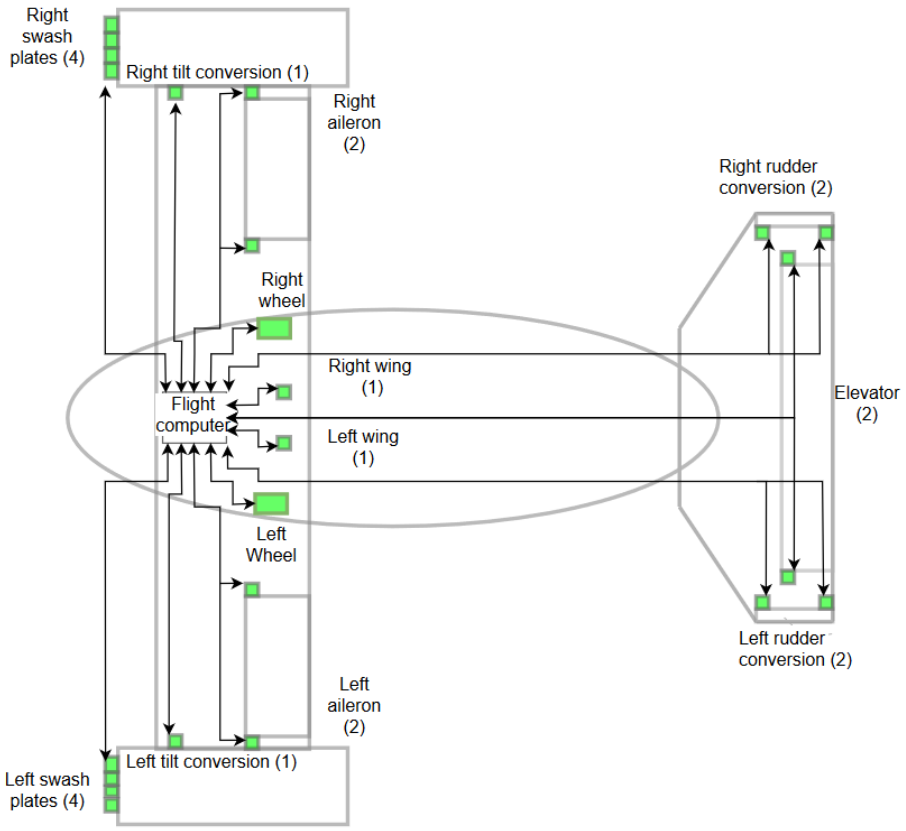

Figure 9.11: Electrical signals to actuators

will process and communicate this data to the flight computer. In Figure 9.12, the flight sensors are depicted. In this figure, *surroundings* is a collective term for a number of lower level systems.

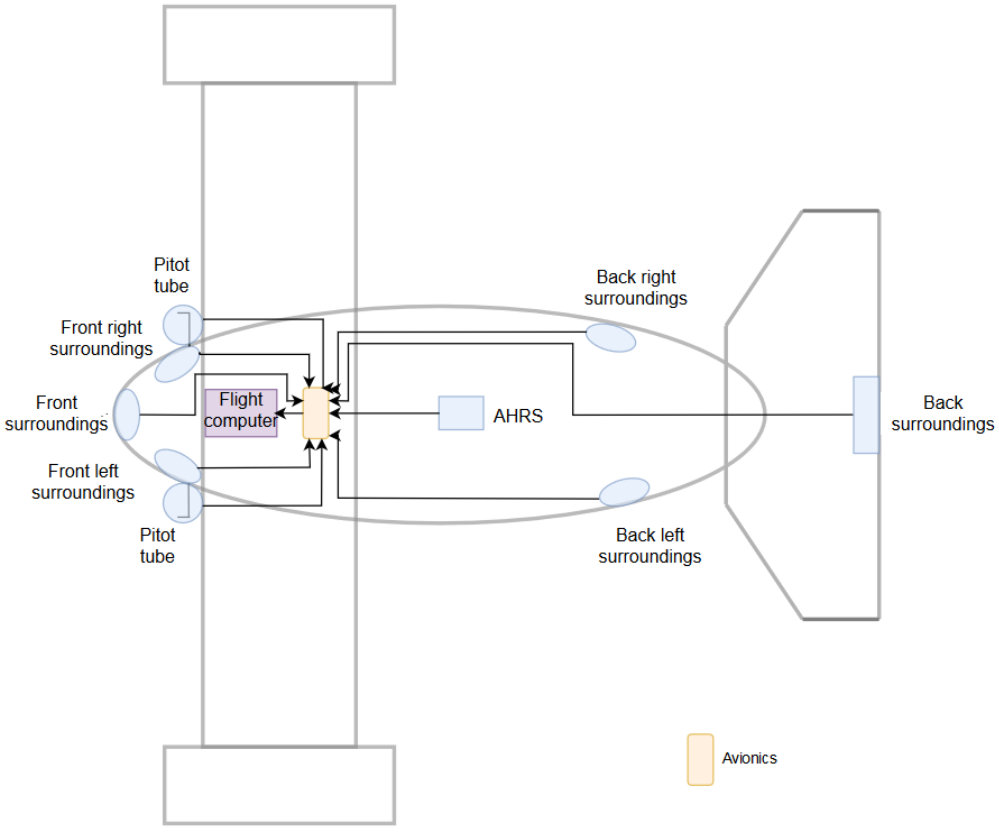

Figure 9.12: Sensors of the pod

A more detailed description of the necessity of the sensors is required to fully understand their selection.

Air Data and Surrounding Sensors

The *surrounding sensors* perform all the measurements directly around the aircraft and can be considered the 'eyes and ears' of the pod. An example can be found in Figure 9.13.

- **Static Pressure** is measured by the static vent. It is an input for the avionics, where the static pressure is used to determine the altitude and velocity of the aircraft
- **Dynamic Pressure** is measured by the Pitot tubes on the sides of the aircraft. It also serves as input for the avionics, where it is used to determine the altitude and velocity of the aircraft together with the static pressure data.
- **GPS Data** is received by a GPS receiver. It is an input for the avionics where the data is used to determine the position, heading and velocity of the aircraft.
- **Cameras** on every side of the pod ensure a 360^o image of the surroundings around the pod at any time. It serves as input for the avionics to ensure that no collisions occur.
- **Heat Cameras** are used for the same reasons as the conventional cameras. The main advantage of using heat cameras is that it allows the pod to have 'vision' when it flies at night.
- **LIDAR** measures the distance from the pod to an object by illuminating the latter with pulsed laser light and measuring the reflected light wave. It is used for a better understanding of the surroundings of autonomous vehicles.
- The **Radar** determines the location of the aircraft with respect to other objects. It is an input for the avionics system for the same reasons as the cameras.

AHRS

The AHRS is the Altitude Heading Reference System, or the on-board reference system. No GPS data is required for it to function. The main difference with an Internal Measurement Unit (IMU), is the addition of a processor unit to output the heading and altitude [35]. In conventional aircraft, the AHRS output and the GPS data are combined with a *Kalman filter* to verify the internal calculations. The system consists of:

- **Gyroscope**, which can be used to determine the heading, attitude and bank angle. A conventional compass is not sufficient, as the electromagnetic waves with which a compass determines the magnetic north deviate around the globe. The gyro in an AHRS system is micro-electro-mechanical (MEMS).
- **Accelerometers** are used to determine the acceleration of the pod. This data can be used for navigational purposes. There should be accelerometers in all three axes of motion.
- **Flux-Gate Magnetometers**, these determine the amount of flux through specific gates located in a certain order. Analysing the voltage output through the gates, the heading of the aircraft can be found.

Avionics

All sensor data first enters the avionics, where the data is processed before it is sent to the flight computer. The flight computer then distributes the right commands to for example the actuators, which is also depicted in Figure 9.12. The data flow will be discussed further in chapter 11. The avionics contain:

- **Positioning System**, which calculates the current position (3D) and heading of the pod. This is done by verifying the GPS data with that of the AHRS system. Also, the data from the static vent and Pitot tube is combined to find the altitude and velocity, which can also be used as a reference [35].
- **Collision Avoidance System** is a system that processes all data coming from the surrounding sensor. It uses this data to locate both stationary and moving objects around the pod using a transponder. In case of an impending collision, the TCAS can output commands to the flight computer to change its direction or brake to avoid a collision.

Redundancy

The aforementioned systems are all of critical importance to the basic functioning of the pod. Therefore, they are selected with great care. Also, redundant systems have to be in place to ensure a fail safe design.

As found in Figure 9.12, the surrounding sensors are located around the aircraft to achieve this redundancy. When one of the Pitot tubes fails for some reason, the other ones will still work. The same principle holds for the avionics and the AHRS. Two identical systems will be installed in every pod. In the event of a sensor failure, this will be communicated to the operational control centre.

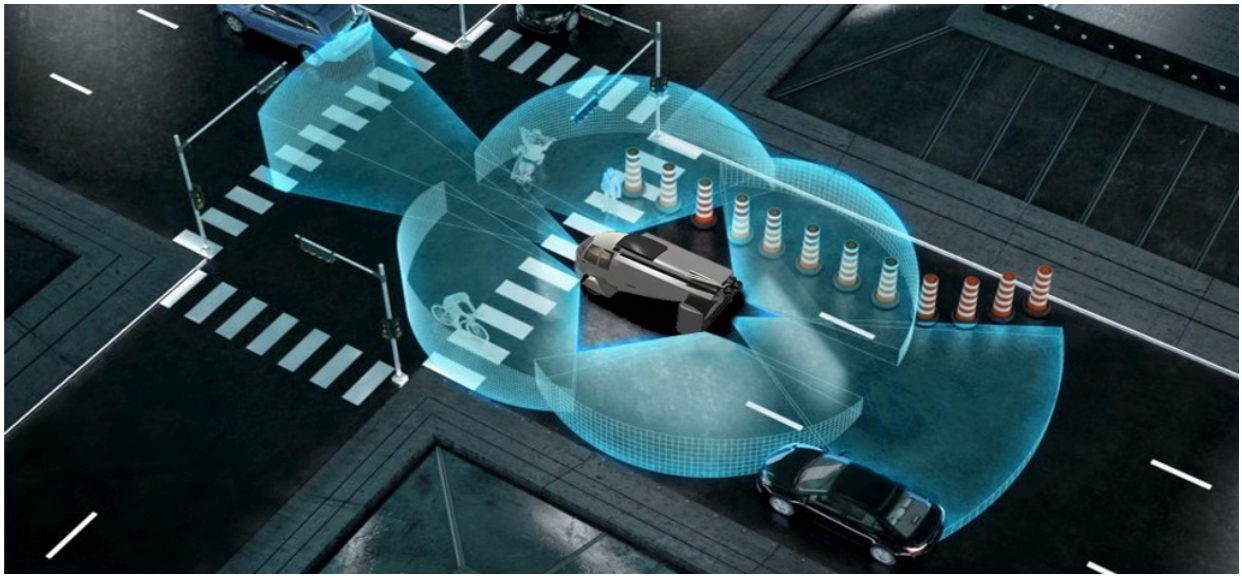

Figure 9.13: Sensors scanning the surrounding during driving

Weight and Cost Estimation

The weight and cost of the sensors is found by carefully selecting off-the-shelf products. One of the selection criteria is that the instruments are certified for use in aircraft. Table 9.6 gives a clear overview of the selection, including their weight and cost.

Table 9.6: Selected components weight estimation

Selected Component	Weight [kg]	Cost [€]
Surrounding Sensors		
Cameras [5]	7.80	750
Radar [6]	1.00	1,050
LIDAR	4.98	2,100
AHRS [7]	0.23	4,000
Avionics		
Positioning System [8]	0.22	543
Communication [9]	2.64	5,990
Total	16.87	14,443

10 Internal Systems

10.1. Requirements and Constraints for Internal Systems

The following requirements that were previously determined relate to the design of the internal systems of the pod.

- POD-SYS-OPP-4: It shall be possible to modify the pods for air freight.
- POD-SYS-PPI-2: The pod shall be able to verify the identity of passengers.
- POD-SYS-PPI-3: The pod shall not be able to take-off if the MTOW is exceeded.
- POD-SYS-PPI-4: The pod shall be able to weigh individual pieces of luggage.
- POD-SYS-PPI-5: The pod shall be able to weigh individual persons.
- POD-SYS-PPI-6: The pod shall be able to communicate with passengers inside the pod.
- POD-SYS-PPI-7: The pod shall be able to keep cabin temperature within the range of 17-23 ^{o} centigrade.
- POD-SYS-PPI-8: The pod shall be able to keep cabin pressure at a minimum level of 0.7 atm at all times.
- POD-SYS-PPI-9: The pod shall not store any personal data of the passenger during flight.

10.2. Cockpit Lay-Out

The cockpit lay-out has to serve the passenger needs in terms of comfort and safety. Passengers will be mainly business travellers and therefore a similar service and comfort level as provided by the short-haul airline business class will be set as a minimum standard. Several components are incorporated in the design to fulfil these needs. These will be explained in more detail in the next sections.

10.2.1. General Lay-out

A general lay-out of the cockpit compartment can be found in Figure 10.1. A maximum of two passengers can be seated in one pod. During their journey, information and entertainment is provided via a large display in front of the passengers. Furthermore, they are able to communicate with the system via the user interface. Some other elements are incorporated in the design, such as WiFi and a drink dispenser to ensure a comfortable and relaxing journey.

10.2.2. Components

The most important items in the cockpit will be further elaborated in the next subsections. Specifications of the components can be found in Table 10.1.

Seats

Economy class type seats have been selected for the design. These seats are recliner seats and deliver sufficient comfort to the passengers during the relatively short trips. The seats are installed at 0.40 m from the back of the compartment to allow the chairs to recline. This will allow the seats to recline 24°. ISO standards for ergonomics are taken into consideration in the design of the seats. This will prevent unnatural seating position and injuries. Seats like the B/E Aerospace 87970 from the company Rockwell Collins are suitable for such a pod configuration.[1]

Dimmable Windows

The windows of the pod should be able to dim to such a level that passengers can sleep during the operation. Dimmable windows from Gentex Corporation can be used, which use electrochromic technology to change the light transmission of the window and are also used on the Boeing 787 Dreamliner. The window will be dimmable in multiple stages and needs to be designed such that the system can also be used to block sun radiation. Furthermore, the windows are designed to reduce UV and infrared radiation significantly.

[1] CabinAir Services, Seats for sale, date accessed: 08-06-2018, http://www.cabinairservices.com/products

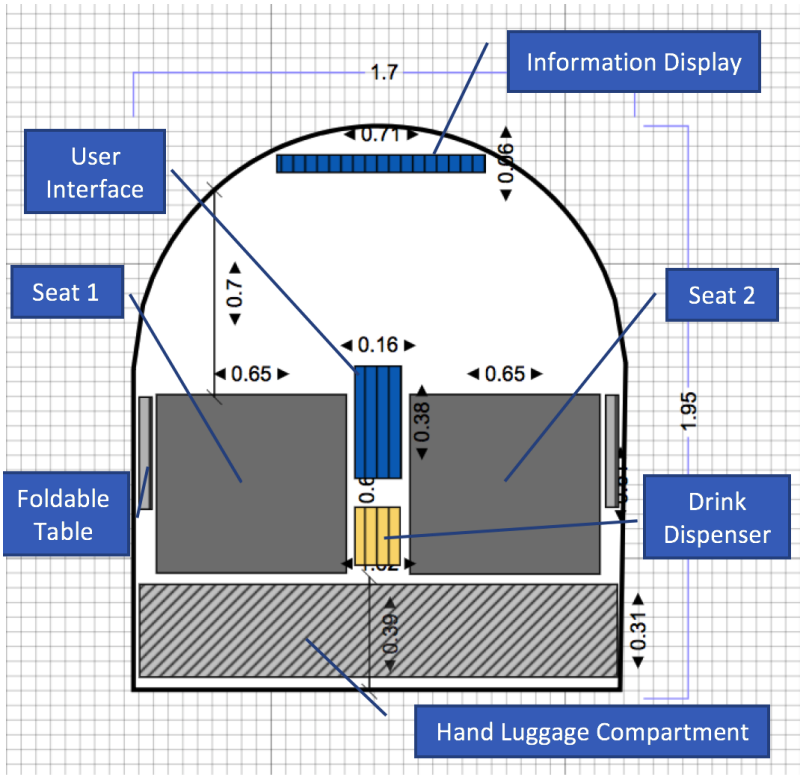

Figure 10.1: Top view cockpit lay-out

Hand Luggage Compartment

The seats are installed at 0.40 m from the back panel of the compartment to allow the seats to sufficiently recline. In between the seats, the back panel and the floor panel, some space is left which will be used as a hand luggage compartment. This way, the passengers can still access the luggage when needed during operations and the space in the cabin is used more efficiently.

Foldable Table

Two foldable tables will be installed in the arm rests, one for each passenger seat. When unfolded, both tables will provide a large workspace for the travellers so that they can comfortably work on the tables and/or have a meeting on board of the pod. The SmartTray X4 premium table has been selected because of its lightweight design. It also provides a solution to hold personal mobile devices. The X4 model has been specifically designed for first class cabins and ensures a higher productivity for business travellers.[2]

Power Plugs

One standard power plug and one USB power port will be installed next to every seat. This allows the passengers to recharge their mobile devices when travelling, so that business travellers can always continue to work on their devices.

Information Display

A large information display will be installed in the front of the pod. This information display shows relevant information about the status of the vehicle and journey such as speed, altitude, route and ETA, among others. Before the flight and in case of an emergency, this display shows the emergency instructions and rules for the passengers. Furthermore, the display will function as a basic entertainment display to show movies, information, etc. This can be controlled using the user interface, explained in the next section of this report. Furthermore, the option to share the screen from your own mobile device is incorporated in the design. A graphical representation of the display is provided in Figure 16.3. Important information and safety messages will always overrule the streaming and will interrupt the entertainment. The Rosen Aviation 32" HD display has been selected for the design. This display is specifically developed for aviation applications and provides high-quality resolutions. An overview of the specifications can be found in Table 10.1. [3]

User Interface

The user interface is located between the passenger seats. This user interface will be used for the communication between the passengers and the system. It consists of a large touchscreen to provide information and inputs to the system. For example, the entertainment system can be controlled via this user interface or environmental settings can be

[2] SmartTray X4. 2018, date accessed: 08-06-2018, http://www.thesmarttray.com/100/X4.html

[3] Rosen Aviation 32" HD display. 2018, date accessed: 08-06-2018, http://www.rosenaviation.com/products/displays/32-hd-remote-electronics-bulkhead-display/

adjusted, such as lighting and temperature. An emergency button is always present on this display. In case of an emergency, this can be communicated via this interface and adequate action can be taken by the system. The Garmin G3X has been selected as the user interface system of choice. This system consists of a 10.6" touch screen, specifically designed for aviation and is widely used all over the world. Specifications can be found in Table 10.1. [4]

ID Verification System

A passport or ID verification system will be installed on the pod. This is installed on the outside of the pod to check the identity of the passengers before entering the pod. This system, combined with the user interface and a smart camera system, is able to check the passengers' identity. Two cameras will be installed in the pod, one in front of the pod and one on the right. Combined with facial recognition software, this system will be able to detect the passengers and perform basic checks. A system capable of these requirements is the PatronScan ID Scanner, the specifications of which can be found in Table 10.1. [5]

WiFi

On-board internet is very important for business travellers to continue their work. Two systems will be available for the pod, dependent on the region of operations and altitude. In highly populated areas and low altitudes, on-board internet is made possible via ground-based mobile broadband towers that send signals up to the antenna of the pod. As the pod travels into different sections of the airspace, it automatically connects to signals from the nearest tower, so there is no interruption of connectivity. If the pod is operated in more remote areas or at higher altitudes, connectivity can be an issue. For this case, another aviation system will be provided as an option for the system. The system consists of a Honeywell Aerowave 100 which uses satellite communication to ensure high-speed connectivity at all times. It has to be noted that this system is expensive and therefore available as an option, details can be found in Table 10.1. [6]

Drink Dispenser

A drink dispenser is installed between the passenger seats to increase the comfort of the passengers during their journey. This drink dispenser consists of a basic water dispenser and an espresso machine designed for aviation applications. The machine can be controlled via the user interface. As for regular business class, these drinks are free of charge for the passengers. A bin will also be installed in between the passengers to collect all the waste. The drink dispenser Aerolux AL-CB28-101 is in line with these requirements, which is also designed to be stable and operative at flying altitudes. [7]

Audio System

A basic audio system is installed in the cabin of the pod. This serves multiple functions, for example safety instructions, entertainment and communication with the control centre if necessary. Two speakers of 180 W are installed in the cabin, which ensure that the passengers can understand safety instruction during noisy conditions e.g. hail.
An overview of all the specifications of the fuel system components is displayed in Table 10.1.

Table 10.1: Specifications of Subsystem Component

Component	No.	Weight [kg]	Cost [EUR]	Dimensions [mm]	Type and Model
Seats	2	20.0	1450	600 x 650 x 1016	B/E Aerospace 87970
Foldable Table	2	2.3	230	500 x 400 x 15	SmartRay X4
Information Display	1	8.5	6800	740 x 438 x 31	Rosen Aviation 32" HD Display
User Interface	1	1.35	3300	203 x 150 x 93	Garmin G3X Touch Flight Display
ID Verification System	1	6.0	2000	376 x 212 x 30	PatronScan ID Scanner
WiFi	1	4.0	16900	378 x 62 x 198	Honeywell Aerowave 100
Drink Dispenser	1	4.5	400	160 x 248 x 330	Aerolux AL-CB28-101
Audio System	1	0.5	80	101 x 203	Pioneer TS-M800PRO
Total Cockpit Systems		**69.45**	**32840**		

10.3. Environmental Control

Environmental Control in the passenger compartment of the pod is very important when it comes to the comfort of the passengers, especially because the target customers are business people, who generally value comfort over the money. A graphical representation of the entire system and its components can be found in Figure 10.2.

[4] Garmin G3X Touch Screen Flight Display. 2018, date accessed: 08-06-2018, `https://buy.garmin.com/en-US/US/p/166058/pn/010-01057-00#`
[5] PatronScan ID Scanner features. 2018, date accessed: 08-06-2018, https://www.patronscan.com/
[6] Honeywell Aerowave 100. 2018, date accessed: 08-06-2018, https://aerospace.honeywell.com/en/ /media/aerospace/files/brochures/a60-1335-001-216-inflightconnectivityaffordableprice-bro.pdf
[7] Aerolux AL-CB28-101, date accessed: 08-06-2018, http://www.aerolux.co.uk/AL-CB28-101-series.html

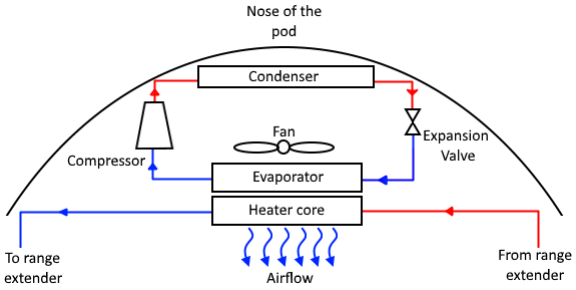

Figure 10.2: Environmental control lay-out

It can be seen from this picture that the heating part of the system will come from the range extender in the back. Since a large amount of heat is produced when the range extender is in use, part of this heat can be used to heat the cockpit. This minimises waste heat and make the overall design more sustainable. Moreover, it can be seen that the condenser is situated at the nose of the pod, which is done to increase the convection in the heat exchanger, making it more efficient. Finally, the evaporator includes a fan, which can be controlled by the user similarly to a fan in the car.

The maximum cooling load needs to be determined before designing this system. To do so, the method described by Fayazbaksh et al. [34] is used. This model is developed to estimate the cooling loads in cars. Since the system will be similar to a regular HVAC (Heating, Ventilation and Air Conditioning) system in a car, the method is assumed to be a good estimate for the required cooling load in the pod when some alterations are done, which will be described later on.

The basic procedure is the following: firstly, the maximum radiation load is determined by selecting a place in the US and following the procedure described by Fayazbask et al. [34]. The place selected is Houston, Texas, which is at (29.8,-95.7). The reason for selecting a place in the US as opposed to a place in Europe is the availability of data. Data for the US is readily available, mainly due to the comprehensive ASHREA ventilation book [8]. Therefore, it is assumed that similar maximum cooling conditions apply in the European environment. The time of day and time of year is varied and the maximum radiation load during the year is found and used in further calculations. Since the pod will mainly be flying, the cooling load due to ground radiation is neglected. Other neglected loads are the loads due to the engines and the load from the exhaust. Aside from this, the radiation load is assumed to be constant at its maximum value to simulate the most critical conditions.

The cabin geometry of the pod is simplified and can be seen in Figure 10.3. The material of the surfaces denoted in this picture can be seen in Table 10.2. The definition of the dimensions can also be seen in the picture.

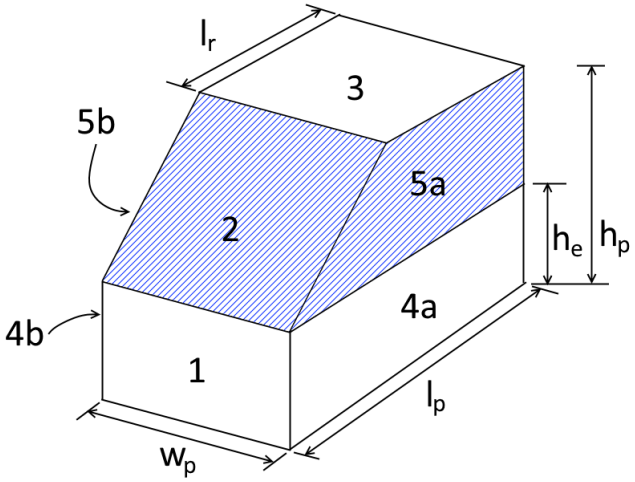

Figure 10.3: Environmental control lay-out

Table 10.2: Materials used in the simplified representation of the passenger compartment of the pod as seen in Figure 10.3.

Surface	1	2	3	4a	4b	5a	5b
Material	Polypropylene	Glass	Polypropylene	Polypropylene	Polypropylene	Glass	Glass

The other loads calculated are: the metabolism load, the ventilation load and the direct heating load. The air conditioning load is then calculated similar to how it is done in the paper [34]. A simulation is set up to calculate the temperature

of the surfaces and the passenger compartment as a function of time, from which the cooling load is calculated as a function of time. The initial conditions can be found in Table 10.3. The results can be found in Figure 10.4 and Figure 10.5. The pull down time is varied such that the peak cooling load is not much more than that of the load to keep the temperature constant. The reason for this is that this leads to a smaller, lighter and more sustainable HVAC system, since it is easier to operate around its maximum efficiency. Other than this, it does not interfere with the comfort of the passengers, since the cooling system can switch on some time before arriving at the passengers' location such that the temperature is lowered before the pod arrives to pick up the passenger.

Table 10.3: Some parameters and the initial conditions used in the simulation of the load calculations.

Parameter	Value
h_e [m]	0.5
h_p [m]	1.24
w_p [m]	1.38
l_c [m]	1.9
l_r [m]	0.9
t_{wall} [m]	0.005

Parameter cont.	Value
t_{glass} [m]	0.003
$T_{external}$ [°C]	30
$T_{internal,0}$ [°C]	50
$T_{surface,0}$ [°C]	50
T_{target} [°C]	23
t_p [s]	310

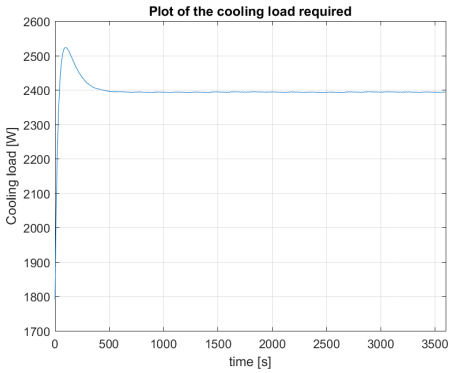

Figure 10.4: Results of the simulation of the power required from the evaporator.

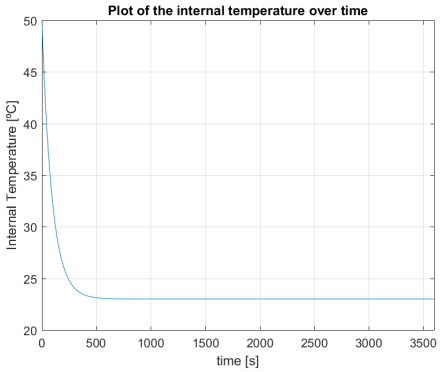

Figure 10.5: Results of the simulation of the internal temperature.

From the plot, it can be seen that the maximum cooling load is 2.5 kW. This is the load that the evaporator needs to provide. The power required from the compressor is found by assuming a COP (Coefficient Of Performance). The COP is defined as the cooling load from the evaporator, divided by the power input of the compressor. In other words, the COP is the useful power divided by the provided power. It is the air conditioning equivalent of efficiency. The power provided from the condenser to the system is not included in the COP, since this power comes from the environment. Therefore, it is possible for a COP to be higher than 1. In fact a COP of 2.5 is assumed here. The compressor power can be found by dividing the evaporator power by this coefficient, which leads to a compressor power of 1.0 kW.

The compressor and other components can now be selected and can be found in Table 10.4 with the associated cost and mass. The final cost is multiplied by a factor of 1.2 to account for the assembly of the HVAC system. The condenser and controller are taken from.[8]

Table 10.4: Components of the HVAC system with the associated mass and price. Note that the price of the controller is set to zero since it comes with the compressor and only a total price of the two combined was mentioned, therefore the price of the controller is included in the price of the compressor. Finally, the price is multiplied with 1.2 to account for the assembly.

Part	Part name	Price [EUR]	Mass [kg]
Compressor	DC Air Conditioner Compressor	738	12
Controller	DC Air Conditioner Controller	0	2
Condenser	Van Wezel 53005708	109	5.18
Evaporator	Four Seasons 54597	43.5	2.6
Expansion Valve	UAC EX 10221C	13.0	0.18
Heater Core	MAC Auto Parts 49-49600	104.3	1.8
Fan	Diederiechs 8654109	74.3	3.2
	Total	1299 EUR	26.96 kg

[8] DC Air Conditioner Compressor and Controller, *date accesed: 07-06-2018*, `https://www.electriccarpartscompany.com/12-610VDC-3412-10236-BTU-DC-Air-Conditioner-Compressor-and-Controller`

These components are regular, off the shelve components that might not be the most efficient when working together. Since a detailed design of the HVAC system is not the objective of this report, so they are not optimal. Therefore, it is recommended to design and optimise this system in more detail in further design phases.

Verification and Validation
The example treated in the paper is used and the results are compared to verify the tool developed. The result can be found in Table 10.5.

Table 10.5: Verification of the AC load model.

Max $\dot{Q}_{AC}$ [kW]	Reference $\dot{Q}_{AC}$[kW]	Difference [%]
2.48	2.85	13

It can be seen that the difference is 13%. This relatively high difference is attributed to the more complex geometric representation of the car used in Fayazbakhsh et al. [34] as well as the previously mentioned loads that have been neglected due to the different situation. Since this is also the preliminary design of the HVAC system, it is assumed that this tool is accurate enough to predict the cooling loads required.

Sustainability
It is generally known that air conditioning systems require quite a lot of power. Therefore an air conditioning system is not the most sustainable of systems. However, since it is a must-have to comply with the requirements, as well as attracting the target customers, it is a necessary evil. That does not mean that no sustainability is taken into account. In fact, it is mentioned several times. First of all, the heat of the heater comes from the range extender in the back, which means that less heat is wasted if heating is required. Aside from this, the pull down time is also relatively long, so that the HVAC system can operate at around its maximum efficiency in all situations.

10.4. Luggage Compartment

The luggage compartment is located right behind the cockpit, separated by a wall. The maximum dimensions for a suitcase are considered to size this compartment. In general, airliners do not have maximum dimensions for suitcases, however, British Airways uses 900 x 750 x 430 mm as their reference dimensions.[9] The compartment is designed such that the suitcases would fit but cannot move a lot in flight.
This results in a very simple luggage compartment geometry, which is only delimited by two walls. One wall separates the luggage compartment from the passenger cabin and the second is located 800 mm behind the cabin. Perpendicular to these two walls, there is a wall on the centre line of the pod. This wall is used there to prevent the luggage from moving when only one suitcase is taken on board. Both sides of the luggage compartment have a door to allow the luggage to be reached from both sides.

Furthermore, the check-in luggage weight will be checked by measuring the difference in tyre pressure. The luggage flow can be seen in Figure 10.6. After the check-in luggage compartment is closed, the passengers will not be able to access the luggage until arriving at the airport.

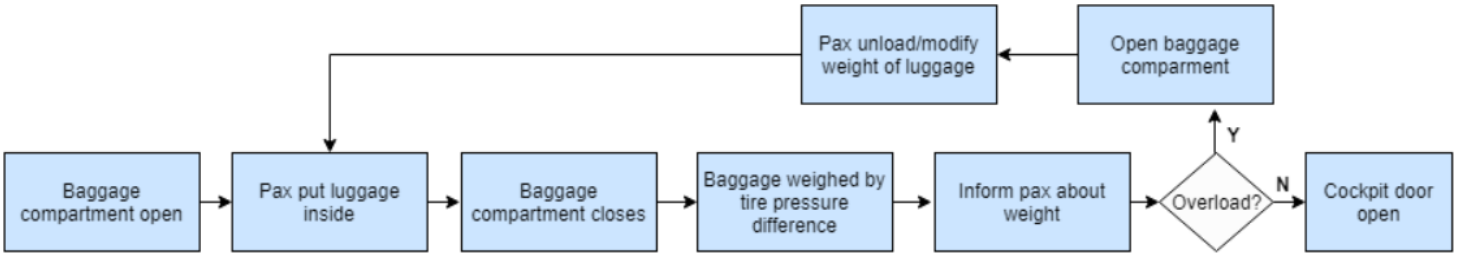

Figure 10.6: Check-in luggage flow

The walls will be made of polyethylene and will be around 3 mm thick. The doors will have an extra structure for stiffness. This gives a weight estimation of the luggage compartment as seen in Table 10.6.
It should be noted that the costs of Table 10.6 already include the manufacturing and installation cost of the component.

10.5. Battery Compartment

The batteries are charged by the range extender and power all the systems on the pod. The size of the battery compartment is determined mainly by three factors:

[9] Airline baggage, *date accessed: 11-06-2018*, `https://wikitravel.org/en/Airline_baggage`

Table 10.6: Luggage compartment weight and cost estimation

Component	Weight [kg]	Cost [EUR]
Walls	4	30
Door	8	400

- **Battery weight**: this is determined by the Class II weight estimation, which sets the battery weight at 109.64 kg with an energy density of 400 Wh/kg. The battery should therefore provide a total of 42,720 Wh.
- **Pod size**: the battery should fit inside the pod, preferably in a location that does not interfere with pod operations. The most convenient location is underneath the passenger/luggage compartments.
- **Interchangeability**: pod availability can be optimised by allowing depleted batteries to be exchanged quickly and automatically for fully charged batteries. This requires the batteries to be clustered together, preferably combined into one large battery pack.

The energy density of 400 Wh/kg is based on new technology involving Lithium-Sulphur cells instead of the widely-used Lithium-Ion cells. The British firm OXIS Energy has already developed lithium-sulphur battery cells for commercial applications. One such cell is the ultra-light POA0323.[10]. It is predicted that the performance of these cells will increase drastically over the next few years, but the current level of technology will be assumed to stay on the safe side.

10.5.1. Size

These cells weigh 0.101 kg each, which means a total of 1,086 cells are required for the battery pack. The cells have a size of 145 mm x 80 mm x 11 mm. The total volume of the battery pack will therefore be at least 0.138 m^3.

10.5.2. Interlocking mechanism

The battery pack must be replaceable. This means that quite a large section of the structure will be missing from the bottom of the luggage compartment. The frame of the battery will therefore have to lock into the structure and be strong enough to act as structural support during operations. Once the pod is empty and the battery has to be removed, the locks are released and the battery is taken out from the bottom by an automated system.

10.5.3. Cost

Since commercial applications are only limited to battery cells at the moment and battery packs are still being developed, the cost estimation is based on projections by OXIS Energy, which aims to provide lithium-sulphur batteries at a cost of 250$/kWh in 2020 once mass production commences. This would result in a total cost of $10,964, or €9,461, which is purely for the battery cells. This excludes the costs of the frame of the battery pack and the interlocking mechanism.

10.6. Fuel Systems

This section will discuss the design of the fuel tank other components of the fuel system.

10.6.1. Fuel Tank

From the Class II weight estimation a fuel weight of 25.4 kg is obtained. With the density of gasoline[11] of 750 kg/m^3, the required tank volume should be 33.4 L. However, allowing for reserve fuel, the tank is designed to hold 40 L of fuel. It is decided to place the fuel tank in the tail of the pod. The tank is given a conical frustum shape to match the shape of the tail. Not the entire cross-section is used for the fuel tank, as this will block the access to the rest of the tail. Taking this into account, the dimensions of the fuel tank are the following:

- Front radius: r_{front} = 267.5 mm
- Aft radius: r_{back} = 155.2 mm
- Length: l_{tank} = 450 mm

The c.g. of the fuel tank is placed at 3.66 m from the nose of the pod. For the material coat, high-density polyethylene is selected, which is commonly used for fuel tanks of cars and other vehicles [29]. The advantage of high-density polyethylene is that it is lightweight, cheap and easily recyclable.

[10] Ultralight Lithium Sulfur Pouch Cell, *date accessed: 18-06-2018,* https://45uevg34gwlltnbsf2plyua1-wpengine.netdna-ssl.com/wp-content/uploads/2018/05/OXIS-Li-S-Ultra-Light-Cell-v4.05.pdf

[11] Fuels - Density and Specific Volume, *date accessed: 05-06-2018* https://www.engineeringtoolbox.com/fuels-densities-specific-volumes-d_166.html

10.6.2. Other Components

The fuel system does not only include the fuel tank itself, but also other components such as fuel pumps, valves and fuel level indicators. The transfer of the fuel is performed by a vane-type fuel pump: these pumps can deliver a constant fuel volume to the engine.[12] Furthermore, various valves [40] are included in the fuel system. First of all, shut-off valves block the fuel flow entirely when necessary. Refuel valves are installed to block the fuel flow when the maximum fuel load is acquired during refuelling. Also, during refuelling, vent valves are used to release air from the tank. Defuelling valves are used to reach the desired level of fuel. If an emergency occurs and fuel has to be dumped, fuel dump valves will be available to make this possible. Finally, non-return valves are added to assure the correct direction of the fuel flow. The last component is the fuel level sensor. Measuring the fuel level is performed by ultrasonic fuel level sensors. These sensors are relatively small, but still have a high accuracy.[13]

An overview of all the specifications of the fuel system components is displayed in Table 10.7.

Table 10.7: Specifications of the fuel system components

Component	No.	Weight [kg]	Cost [EUR]	Dimensions [mm]	Type and Model
Fuel Tank	1	5	50	450 x 535 x 535	N/A
Fuel Pump	1	2	85	97 x 117 x 200	Carter Universal Electric Fuel Pump
Shut-Off Valve	1	0.5	150	119 x 34 x 72	Eaton Shut-Off Valve FRH150010D
Drain Valve	1	0.05	110	15 x 15 x 20	Curtis CCB-38000
Non Return Valve	1	0.23	100	120 x 93 x 93	Eaton Non Return Value 21M0018
Refuel Valve	1	0.225	60	45 x 45 x 50	SPRL V2 ON/OFF VALVE
Vent Valve	1	0.02	205	32 x 41 x 41	Eaton Vent Drain Valve 28-0004
Defuel Valve	1	0.4	20	150 x 80 x 80	Carter Aircraft Defuel Valve P/N 600213-5
Fuel Level Sensor	1	0.25	20	68 x 68 x 80	Holykell Ultrasonic Level Sensor UE3003
Total Fuel Systems		**8.675**	**800**		

Verification & Validation

As the fuel system is treated on quite a high system level and no specific formulas are used, extensive verification and validation is not performed on this subsystem. However, it was verified that the fuel tank and the other components will fit in the assigned section of the pod by combining the geometries in the 3D model. Furthermore, it was verified that the pump could provide the necessary fuel flow to the range extender. In this sense, the fuel system is still verified.

Sustainability

The sustainability approach is applied to the fuel systems by means of the material selection of the fuel tank. The decision for high-density polyethylene is also based on the fact that it is easily recyclable. This way, the fuel system contributes to the requirement that the pod should be recyclable for at least 60 % by weight.

10.7. Pod Adjustments

The service could also be convenient to perform cargo deliveries, so it should be possible to modify the pod to carry air freight. Furthermore, the vehicle is designed to be able to accommodate different categories of passengers, including those with reduced mobility. The adjustments of the pod for these two cases are described throughout this section of the report.

10.7.1. Cargo

One of the requirements of the pod is that it shall be adjustable to transfer freight cargo. For this, the cockpit equipment and luggage compartment walls would be removed from the pod. Replacing the mass of the passengers and their luggage would result in a maximum allowed cargo mass as constructed in Table 10.8.

[12] Types of Aircraft Fuel Pumps, *date accessed: 06-06-2018*, http://okigihan.blogspot.com/2017/06/types-of-aircraft-fuel-pumps.html

[13] Capacitive fuel sensors, *date accessed: 07-06-2018*, `http://fuel-level.com/index.php/en/products/capacitive-sensors/66-epsilon-fuel-level-sensor-4`

Table 10.8: Masses that can be removed from original pod and used for cargo

Component	**Weight [kg]**
Cockpit equipment	65
Luggage compartment walls	4
Passenger and luggage	230
Total cargo weight	**299**

Knowing the maximum cargo mass, a system can be selected to store the cargo on the pod. For the luggage compartment, aircraft pallets will be designed according to the size of the compartment. The shape of the pallet matches the pod's fuselage and can be seen in Figure 10.7. The cockpit door limits the size of the pallet that can be used for the freight stored in the cockpit. Therefore, a display pallet will be used for this. The dimensions and the loading capacities of the pallets are displayed in the following list, where the load capacity of the luggage compartment pallet is based on reference pallets used for actual cargo transfer [9]:

- Luggage compartment pallet:
  Dimensions: 1200 x 1100 x 900 mm; Maximum loading capacity: 300 kg.
- Cockpit pallet:
  Dimensions: 800 x 600 x 900 mm; Maximum loading capacity: 250 kg.[14]

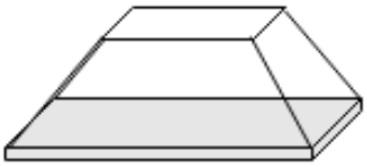

Figure 10.7: Cargo pallet for luggage compartment

More cargo can be taken on board than the maximum allowed cargo. Therefore, it can be concluded that the pod is suitable to carry freight, but it is not optimal for it. Making the pod more suitable for transport can either be done by making the pod more compact or by designing it such that it can take off with a higher maximum take-off weight. Both of these options would require a redesign of the pod.

10.7.2. Reduced Mobility

Disabled people will also be able to make use of the system by request. The passenger has the possibility to choose for a special pod adapted to his special needs when booking the service through the app.

Special needs pods will be able to transport one disabled person, who will be accompanied at every moment with a helper. The helper will arrive at the pick-up location with the pod. There, he will help the passenger to board the pod. Furthermore, he will load the luggage and folded wheelchair into the luggage compartment. The pod configuration remains unchanged, as reducing the passengers to one leaves enough space in the luggage compartment to store the passenger wheelchair.

[14] Displaypallet 60x80cm - 4 weg, *date accessed: 18-06-2018*, https://www.123pallets.nl/pallets/displaypallets-aanbod/product-4-weg-display-pallet-nieuw

11
Electric Systems

In this chapter the electric systems are discussed. Firstly, the lighting system is determined. This is followed by presenting the communication flow diagram in section 11.2. Furthermore, the data handling block diagram and electric block diagram are presented in section 11.3 and section 11.4 respectively. Lastly, the hardware and software block diagrams are given in the final section of this chapter.

11.1. Lighting System

The lighting system should ensure safe operations during night time and increase the visibility of the pod for other persons and vehicles. The lighting system is divided in external and internal lighting. The external lighting has been further divided in lighting for the driving and flying part, due to the different requirements for both modes of operations.

11.1.1. External Lighting

The external lighting consists of all the lights mounted on the outside of the pod. The driving and flying mode require different lighting and are therefore ivided in two separate systems.

Driving Lighting

To save resources at this stage of the project, off-the-shelf lights are selected for the design. When mass production of the pod starts, custom-made lights become a more feasible solution, but for limited series, this is still too expensive. For the driving mode, two types of lights are selected, namely for the front and for the back of the pod, as both have different functions.

Headlights

In the driving mode, the head lights should at least perform the following functions:

- Main beam light
- Dipped beam light
- Fog light
- Direction indicator

The Osram LEDriving XENARC headlights are selected as the most suitable lights available for the design. These LED lights provide up to 70 % more light compared to standard halogen lamps and have a 20 m longer light cone, which improves the visibility. Furthermore, these LED lights are very energy efficient, making these lights more sustainable than conventional lights. [1] These headlights are also used on the Volkswagen Golf VI and are therefore widely used and easily available. The specifications of the lights can be found in Table 11.1.

Taillights

The tail lights should perform the following functions:

- Braking light
- Reversing light
- Fog light
- Direction indicator
- Emergency Stop Signal

Also, for the tail lights, energy efficient LED lights are selected for the pod. To decrease complexity of the system, corresponding taillights are selected in combination with the headlights. Therefore, the off-the-shelf Golf VI LED tail lights are selected. These lights are readily available, perform all the required functions and are energy efficient. [2]. The details of the tail lights can be found in Table 11.1.

[1] Osram. 2018, date accessed: 08-06-2018, https://www.osram.com/am/ecat/LEDriving20XENARC20BLACK20Edition20Golf20VI-LED20headlights-Cars-Aut
com/en/GPS01_2903369/PP_EUROPE_Europe_eCat/ZMP_4055174/

[2] Golf VI Tail Light. 2018, date accessed: 08-06-2018, https://www.nighteyeled.com/products/nighteye-car-styling-for-vw-golf-6-tail-lights-2009-

Flying Lighting

Compared to the lights for the driving mode, it is not possible to select off-the-shelf solutions that can perform all the functions at once. Therefore, different types of lights are selected to perform the individual functions.
The flying lights should perform the following functions:

- Navigation/positioning lights
- Landing lights
- Anti-collision lights

An overview of the lighting installation and specifications can be found in Figure 11.1 and Table 11.1. Figure 11.1 provides the overview of the different lights installed with their respective colours and angles. AvioLight is the preferred partner for the flying lighting. AvioLights produces highly efficient LED lights, which are small and lightweight compared to competitors and other conventional lights. Also, the lights are produced at a competitive price, which makes them widely used in aviation. One Navigator Ultra 360 light is installed at each wing tip, this light combines several functions such as anti-collision (strobe) and positioning. Furthermore, a Red Eye is mounted at the belly of the pod and a Tail Star at the tail, both function as anti-collision lights and/or positioning lights. [3].

Regarding the VTOL requirement, a specific light is required that can illuminate the landing area of the pod, located immediately below the pod. Therefore an additional landing light is installed in the belly of the pod to illuminate this spot during landing. The highly efficient 90361 LED landing light is selected from Whelen company, which is efficient and lightweight as well[4]. The specifications can be found in Table 11.1.

(a) Wing tip lights (b) Belly light (c) Tail light

Figure 11.1: Flying lighting

Table 11.1: Specifications lighting system

	Function	No.	Position	Weight [g]	Cost [EUR]	Dimensions	Power [W]	Type and Model
Driving	Head lights	2	Nose	446 (each)	889 (pair)	630x310x580	25	Osram LED driving XENARC (Golf VI)
	Tail lights	2	Tail	450 (each)	646 (pair)	220x500x700	20	Golf VI Led Tail lights
Flying	Nav./Pos./Strobe	2	Wing tips	190 (pair)	300 (pair)	95x50x27	6/29 (Pos/Stb)	AvioLights Navigator Ultra 360
	Pos./Strobe	1	Tail	50	170	35x37x26	5/40 (Pos/Stb)	AvioLights Tail Star
	Beacon/Anti-coll.	1	Belly	50	170	37x46x26	40	AvioLights Red Eye
	Landing	1	Wing	590	1015	119x73	42	Whelen 90361
Internal	Ambient lighting	2	Cabin	410 (each)	300	457x31x27	15	SCHOTT HelioJet Spectrum Type I
Total				**4.22kg**	**3790**		**254**	

11.1.2. Internal lighting

Internal lighting is very important to the passenger comfort and travel experience. By changing the lights depending on the time of the day or the needs of the passengers, the human perception of the environment can change drastically.

[3] AvioLights Specifications. 2018, date accessed: 08-06-2018, `http://aviolights.com/products`
[4] AvioLights Specifications. 2018, date accessed: 08-06-2018, `http://www.whelen.com/aviation/product.php?headid=13&prod_id=112`

By using appropriate colour schemes, passengers will feel more relaxed and comfortable during their journey, which is particularly important for frequent flyers. The lights have a standard program based on the outside light conditions and can be adjusted to the passenger needs via the user interface. Different lighting modes can be selected, for example a functional white light to work, or a more ambient light scenarios to relax during the journey. The Schott HelioJet Spectrum LED light strips are selected as the internal lighting system for the cabin. This system provides both functional and ambient lighting by using energy-efficient LED technology. Compared to other conventional LED technology, this design uses active LED management, which permanently monitors and controls each LED. This way, Schott provides a higher colour stability and a more homogeneous light distribution compared to competitors. The LED strips can produce over 16 million colours, which makes fully customised lighting patterns possible for customers. Furthermore, the HelioJet system uses fewer LEDs leading to lower costs and lower energy consumption. [5] Two HelioJet strips will be installed on both the sides of the cabin and specifications can be found in Table 11.1.

11.2. Communication Flow Diagram

A communication flow diagram is developed for the final design. This diagram shows the flow of data between the subsystems of the pod and the environment around it. Since the system needs to be able to operate almost fully autonomously, it is essential to have a good overview of how the data streams flow within the system. The diagram can be seen in Figure 11.2. This diagram only shows the data flow between the subsystems. It does not include any other connections between the subsystems. For instance, the Electrical Power Distribution System provides power to all subsystems. However, it only sends and receives data from the Central Processing Unit (CPU) that handles all the data in the pod.

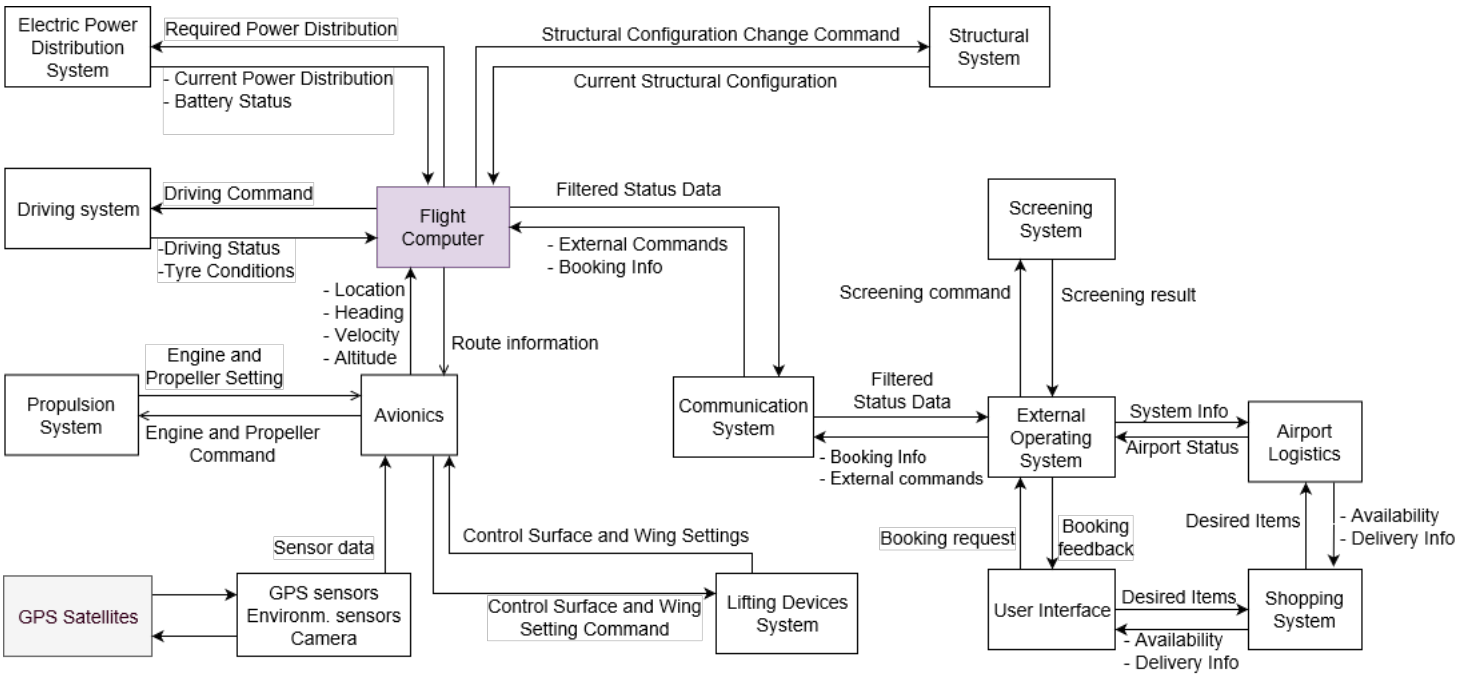

Figure 11.2: The communication flow diagram of the system

11.3. Data Handling Block Diagram

The data handling diagram of the pod is shown in Figure 11.3 with estimation of the data rates within the subsystems. Inside the green box, equipment units are grouped together. These are needed to control the internal instrumentation of the pod, such as cameras and AHRS. The blue box consist of passenger-related hardware such as the user interface, located inside the pod. The orange coloured box depicts the on-board computer. Inside this computer, there are elements such as the watchdog unit. This element is used to ensure that the computer does not remain stuck at a particular stage of the processing it performs. This is a protection usually intended to restart the system when a defined action is not executed within a given time.

It can be seen that, in the pod internal avionics, the three components that contribute the most to the data rate are included explicitly in the figure. These are the camera, Lidar and Radar. The data rates are estimated by using references with a safety margin of 20 %. Moreover, other components of the avionics contribute negligibly to the data rate between

[5] Schott HelioJet Spectrum Specifications. 2018, date accessed: 11-06-2018, https://www.schott.com/aviation/english/products/heliojetspectrumcc.html#block362356

the on-board flight computer and the avionics.[6] [7] It has to be noted that these data rates are only an assumption. For future development, the data rates within the pod system should be examined and the handling block diagram should be expanded.

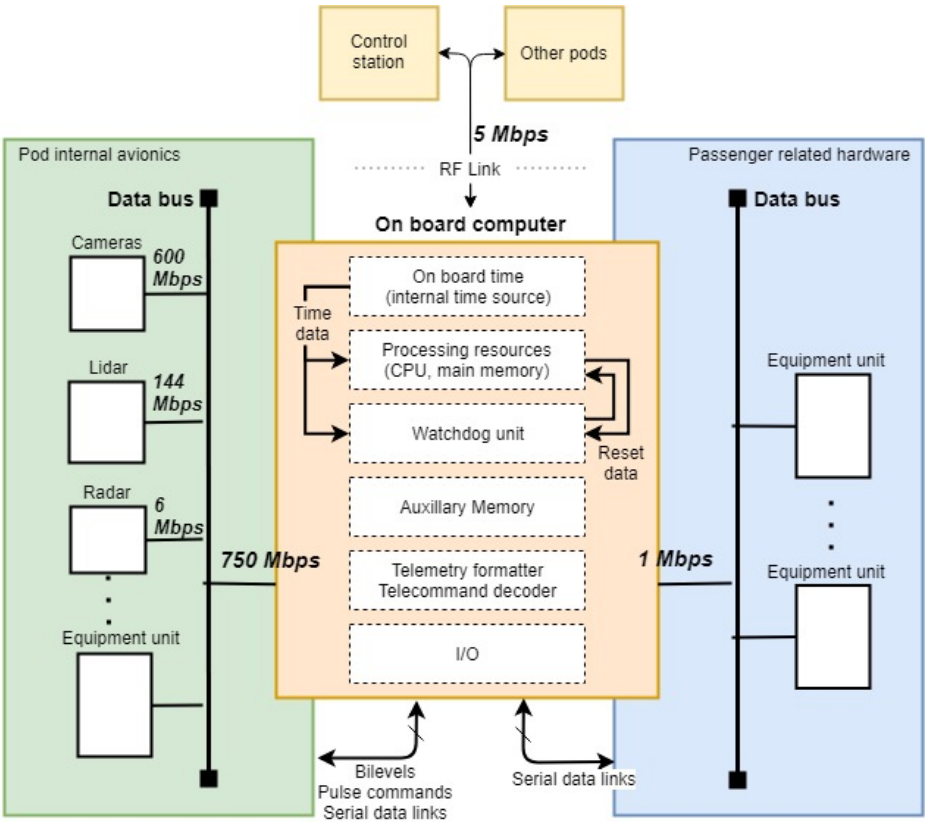

Figure 11.3: The data handling block diagram of the system. The green box consists of equipment units that are needed to control the pod internally. The blue box consists of passenger-related hardware and the orange box depicts the on-board computer.

11.4. Electrical Block Diagram

The electric block diagram of the pod is shown in Figure 11.4. It is a simplified representation of the electric system of the pod. It shows that that the battery can be charged by an internal combustion engine or by an external charging system. A voltage regulator is used to regulate the voltage over the different components. The following subsystem division holds: the red boxes represent the subsystem that are only in operation during flight, whereas the components in the green boxes represent the subsystems that are only in operation during driving. The cabin systems that require power during driving and flight are displayed in the blue boxes. Finally, the CPU, communication, systems, doors and actuators are represented by the grey boxes. For every component, it is indicated whether the electric connection requires a variable resistor or a switch. The latter is chosen between the battery and the corresponding components if it requires a continuous power when it is active. An example is turning the lights on and off. The variable resistor is used to control the current that flows to the components and thus controls the power provided to the concerning component. This is used if the component requires variable power during operation. An example is the electric motors that provide mechanical power to the rotors.

[6] Just one autonomous car will use 4,000 GB of data/day, *date accessed: 22-06-2018*, `https://www.networkworld.com/article/3147892/internet/one-autonomous-car-will-use-4000-gb-of-dataday.html`

[7] Autonomous cars will generate more than 300 TB of data per year, *date accessed: 22-06-2018*, `https://www.tuxera.com/blog/autonomous-cars-300-tb-of-data-per-year/`

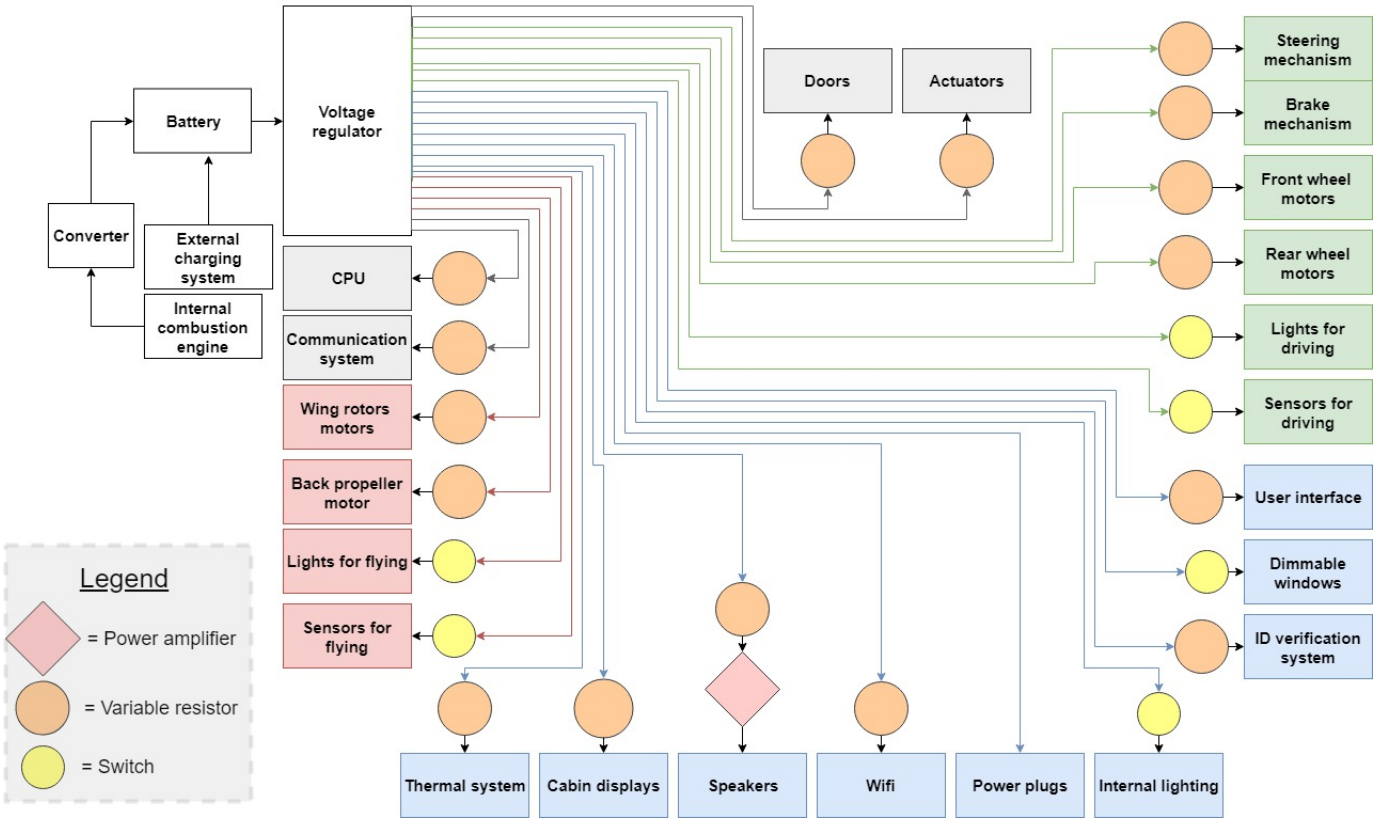

Figure 11.4: Electrical block diagram

It should be noted that in Figure 11.4, the actuators correspond to the actuators defined in subsection 9.5.1. Additionally, the sensors correspond to the sensors defined in subsection 9.5.2. Moreover, the lights correspond to the lights represented in section 11.1. Regarding the electric motors, the required AC/DC inverters are implemented in the electric motors themselves.

11.5. Hardware and Software Block Diagram

In this section, the hardware and software block diagrams are presented. This is done to illustrate the system components with their interactions and relation. They contain blocks connected by arrows; the blocks contain the name of the system component and the lines contain a description of the interaction or physical resource flowing though it. The hardware block diagram is shown in Figure 11.5.

The software of the pod operation is presented in software block diagrams as shown in Figure 11.6 and in Appendix D in more detail. Firstly, the software block diagram regarding the main software is represented in Figure 11.6. It shows that the CPU software is connected to the central control rooms during the entire operation. Furthermore, it can be seen that the CPU determines the required software at every moment with the feedback from the central control room. The software includes the autonomous flying mode, autonomous driving mode, pod take-off mode and pod mode conversion. The software block diagram for flying mode, driving mode, take-off, pod mode conversion and cabin systems can be found in Appendix D.

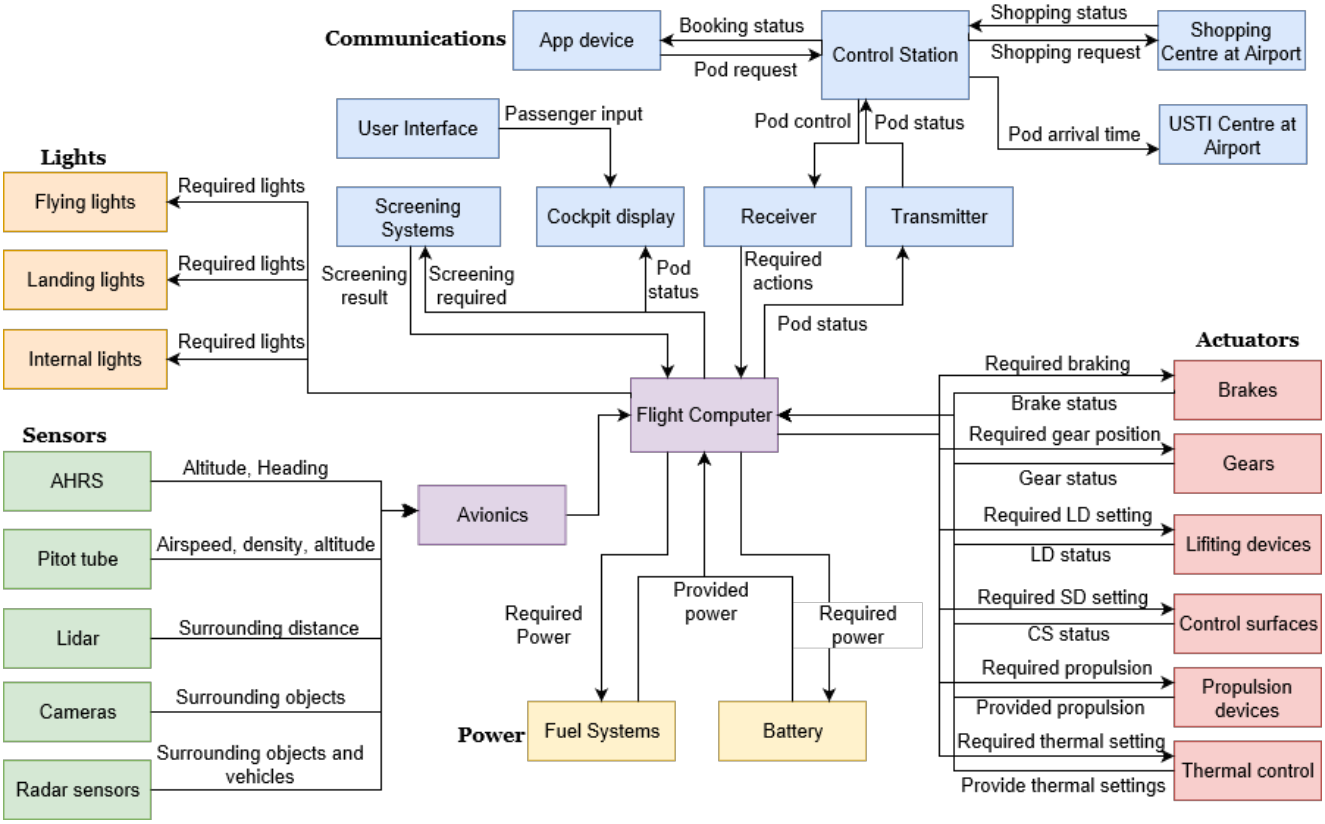

Figure 11.5: Hardware diagram of the system. The sensors are grouped together in green. Lights in orange. Communications in blue and actuators in red

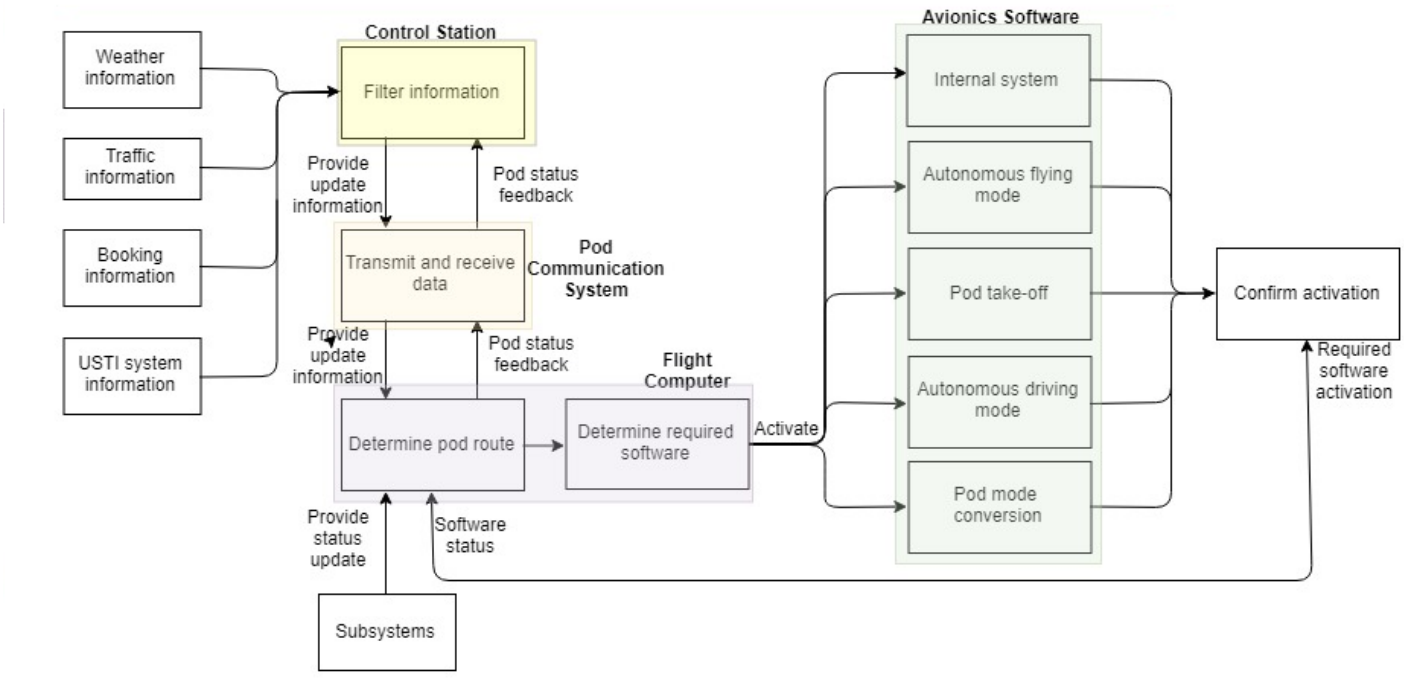

Figure 11.6: Software block diagram for the main software

12
Emergency Systems

Throughout this chapter, the systems that come into play when an emergency situation occurs are described. Several preventive measures are also presented. In previous stages of the design process [3], a preliminary risks analysis was performed. Here, the most frequent failures with the worst consequences are listed. From this analysis, the most critical situations relate to CPU, wing, battery and control failures. These risks have catastrophic consequences, in some cases leading to critical situations such as a crash or fire outbreaks for which an emergency procedure needs to be followed.

12.1. Requirements and Constraints for the Emergency System

The following requirements relate to the emergency systems:

- POD-SYS-OPP-8 The pod shall not have any single point of failure during operations.
- POD-SYS-F-10 The pod shall be able to perform an emergency landing within one minute after emergency landing is requested.
- POD-SYS-F12 The pod shall be able to perform and emergency landing on water
- POD-SYS-D-14 The pod shall have a crash worthiness that would guarantee a five star rating from the EURO NCAP test.

12.2. System Failure Emergency Procedure

The pod is autonomous and redundancy measures are applied in the design procedure to ensure the safety of the system and to reduce the risk of failure. However, in case a system failure still occurs, detection and warning systems must be implemented. Similarly to modern aviation, sensors are placed on the pod to identify complications and send signals to the control warning panel placed in the control operator room. A warning message is also displayed on the screen in the passenger cabin. Operators will then receive updated information of what the system failure is and which safety/emergency measures are taken to recover to a safe condition. The operator may decide to overrule the autonomous system if necessary at any moment. In the meanwhile, the cockpit display panel shows instructions informing the passenger about the emergency situation to direct the user during the emergency procedures. The sound of an alarm keeps the passenger on alert at all times.

Before the pod picks up a passenger, it analyses the route and distinguishes the possible pre-defined landing locations on the route in case an emergency landing is needed. Furthermore, the pod is equipped with an automated emergency landing system in case the failure is too critical to arrive at the destination safely. An emergency landing, in any case, is ensured to start within one minute after the failure is detected. If the pod is unable to continue operating in flying mode, but the driving mode is still operative, the pod needs to drive to the airport. This way, it is not necessary to rescue the vehicle along the route and the passenger is still able to reach the airport. Furthermore, life vests are carried underneath the passenger seats in case the pod performs an emergency landing on water.

When a critical failure occurs, its consequences result in extreme situations such as a fire or crash, in which the emergency procedures present slight differences from the general procedure. These situations are analysed below:

Fire Emergency Procedure

Fire initiation on the pod is a particularly serious event, since the structure is not likely to remain intact in the continued presence of fire or hot gases. The most probable place for a fire to ignite is the propulsion compartment. Fires may start as a result of mechanical damage leading to the compartment breaking up or overheating. The escape of hot gases may affect the structure. The same can be stated for escaping fuel coming into contact with hot surfaces. As a matter of fact, the risk is rather high as all the required elements for starting a fire are present: large amount of fuel, plenty of air and hot surfaces.

The pod is equipped with two fire detection systems, one located in the bay where the power plant of the system is located and one placed in the passenger compartment. The fire detectors are provided with temperature sensors and

connected both with the passenger display panel and the control room.

After a fire detection, an inertial switch is triggered that shuts down the motors. The fuel system is isolated by closing a valve that stops the fuel flow in the pumps. Furthermore, the aircraft battery is disconnected from the busbar and extinguishing fluids are discharged into the engine bay. If this series of events occurs, the pod is required to perform an emergency landing as soon as possible.

Crash Emergency Procedure
Crashes can occur during flying or driving, either as a consequence of internal failure or due to impact from outside. Depending on the intensity of the impact, different emergency procedures are applied. If the pod can continue flying after the collision, then it is repaired at the airport upon arrival. However if the crash is critical for its flying performance, the pod must perform emergency landing.

The performance of the pod structure in road crashes is described in subsection 8.3.2, where the compliance with the EURO NCAP test is proved. In case of a crash while driving, the main safety feature is the installation of an airbag system. This reduces the damage caused by the crash. Furthermore, the inertial switch is automatically triggered when a crash is detected, isolating the fuel system and shutting down the motors. Finally, an e-call system is also implemented in the system. As the position of the pod is known and recorded at every moment by GPS, the e-call system automatically calls the police informing them about the emergency location. A notification is also sent to the control room and the maintenance operators.

12.3. Prevention and Documentation

Some parts of the pod, such as the fuel tank, can be considered an explosion hazard. In the past, fuel tank explosions have occurred in commercial aircraft mainly due to lightning strikes and external fires. For this reason, the FAA sets limits on energy (in microJoules) and current (in mA) that can be dissipated in these components. Also, the level of oxygen of these components should not exceed 12%. In addition to that, these spaces should be filled with reticulated foam or with nitrogen gas, which will prevent a large scale explosion [40].

The pod does not have a cockpit voice recorder (CVR) or a flight data recorder (FDR), also referred to as black boxes in the press. The former is not applicable as there is no pilot in the pod. The latter is also not applicable as it is not required by the regulations.[1] These regulations apply to airplanes and rotorcrafts that have more than five passengers or fly at an altitude higher than 25,000 feet (~7.6 km). Therefore, it is decided to omit them to reduce the weight and costs of the pod.

12.4. Sustainability

In case the emergency situation is so critical that an emergency landing is not possible, having a parachute on board would be a good solution to increase the passenger survivability. Having a parachute for the pod contributes to a more sustainable system in two ways. First, having a parachute reduces the impact with the ground, making it possible to reuse parts of the pod that are not heavily damaged. Secondly, it creates an opportunity for the investigation crew to examine the broken parts and learn from previous design mistakes. In the industry, this is known as an increase in product knowledge.

However, a parachute system will not be implemented. This decision is based on the weight and cost. The cost of this kind of system is approximately 15,000 $. Furthermore, a 23.3 m diameter parachute is required to carry the USTI maximum take-off weight [13]. This would increase the weight of the pod and reduce performance. Furthermore, the case in which the parachute system would be needed is very extreme and not very likely, as the aircraft can perform an emergency landing by gliding.

[1] Which aircraft are required to have a black box? Aviation.com *date accessed: 30-05-2018*, `https://aviation.stackexchange.com/questions/1684/which-aircraft-are-required-to-have-a-black-box`

III

Operations Design

13

Functional Overview

This chapter gives an overview of the various functions that the system has to perform. In section 13.1, the functional flow diagram for the system is discussed and section 13.2 will elaborate further on these functions by means of the functional breakdown structure.

13.1. Functional Flow

The Functional Flow Diagram is generated to provide a better understanding of the functionality that the system has to fulfil. Three levels of detail are presented. The first level is displayed in Figure 13.1. The second level is presented in Figure 13.2, Figure 13.3 and Figure 13.4. The third level is presented in Appendix B.

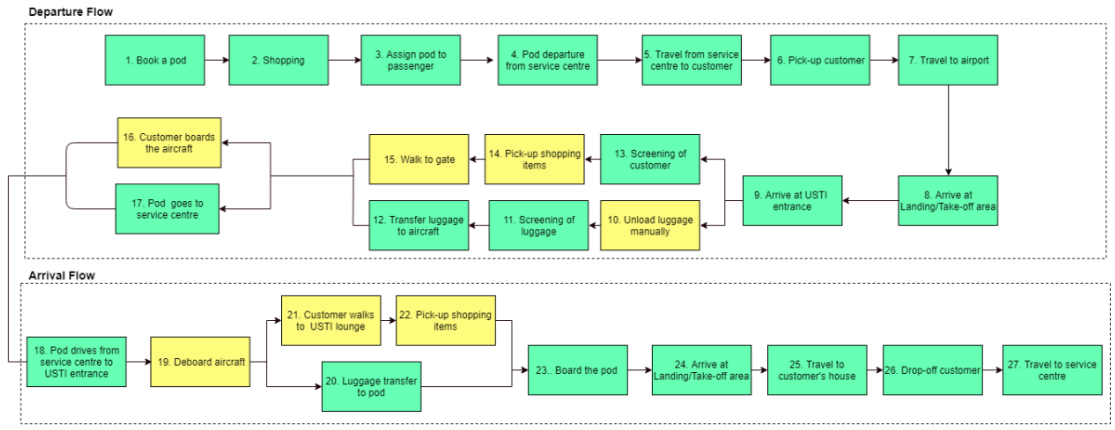

Figure 13.1: First level Functional Flow Diagram

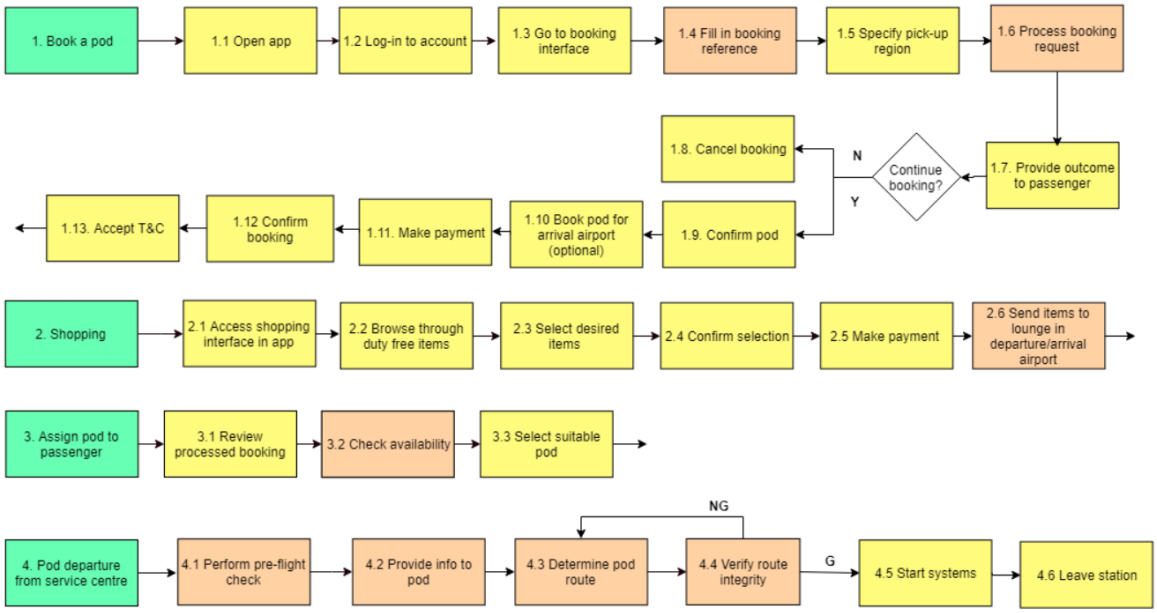

Figure 13.2: Second level Functional Flow Diagram (Part 1)

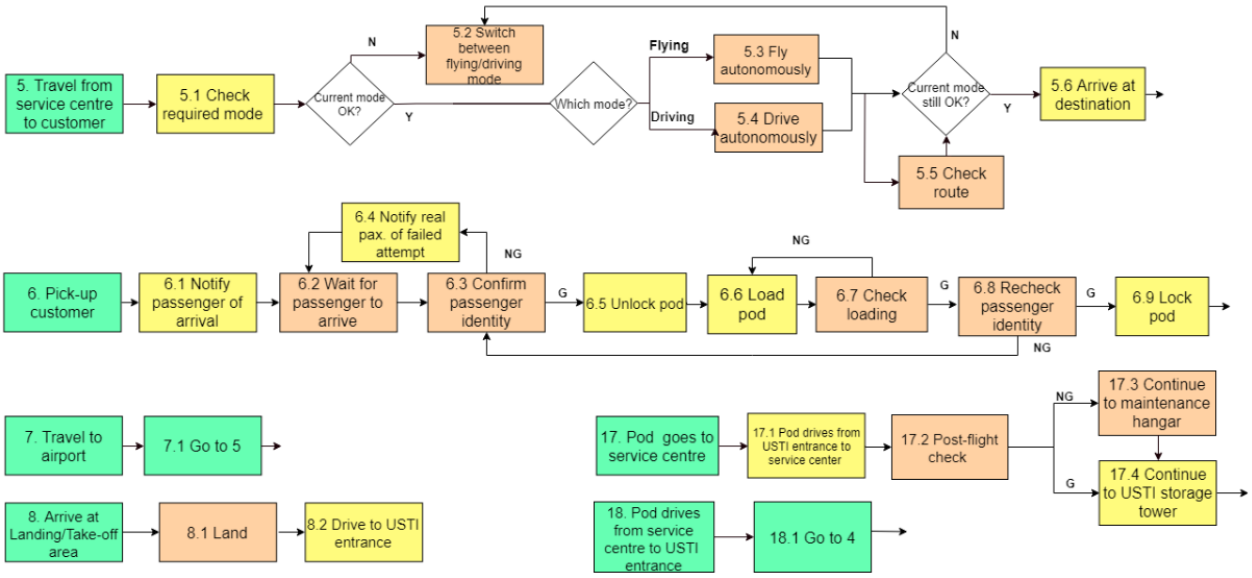

Figure 13.3: Second level Functional Flow Diagram (Part 2)

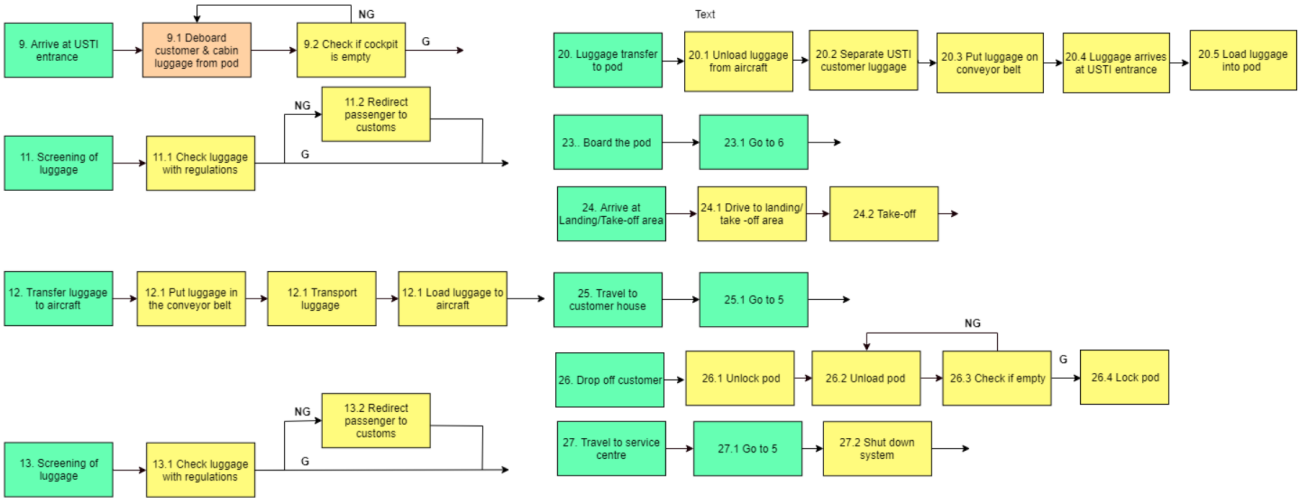

Figure 13.4: Second level Functional Flow Diagram (Part 3)

13.2. Functional Breakdown

A follow up of the functional flow diagram described in section 13.1 is the functional breakdown structure. The functional breakdown contains the same functions as the functional flow. However, for some functions, an extra level of detail is added. The functional breakdown structure can be seen in Appendix B.

14
Control of Operations

The operations of the system surrounding USTI are a major part of the project. This chapter will focus on these operations that allow the USTI system to function properly.

14.1. Requirements and Constraints for Control of Operations

The following requirements relate to the operational control of the pods:

- POD-SYS-SC-1: The pods shall be able to communicate with an external system at all times.
- POD-SYS-SC-2: The control system shall be able to be monitored by at least one person at all times.
- POD-SYS-SC-3: The pod shall have the possibility to be externally controlled.
- POD-SYS-SC-4: The system shall be able to assign pods to customers without human interaction.
- POD-SYS-SC-5: The system shall be able to generate the quickest route to get to final destination.
- POD-SYS-SC-6: The system control shall be able to analyse the current schedule of all pods.
- POD-SYS-SC-7: The system shall be able to adapt pod schedule if a more efficient schedule is possible.
- POD-SYS-SC-8: The system shall be able to analyse road integrity.
- POD-SYS-SC-9: The system shall be able to adapt the route of a pod.
- POD-SYS-SC-12: The passengers in the pod shall not perceive any waiting time in case the route is redetermined.
- POD-SYS-SC-13: The system shall assign a pod for the passenger within 10 seconds after a request is made.
- POD-SYS-MT-1:The pods shall be inspected internally and externally after arrival at the airport.
- POD-SYS-MT-2: The pods shall be cleaned after arriving at the airport.
- POD-SYS-MT-3: The pods shall be inspected thoroughly every 50 flights.
- POD-SYS-MT-4: The maintenance operations shall not result in unavailability of pods.
- POD-SYS-MT-6:The pods shall be able to scan the functioning of its own subsystems.
- POD-SYS-MT-7: The pods shall communicate necessary maintenance operations to the responsible team.

14.2. Control Station

This section describes the level of authority the control station has and the amount of people that the so-called 'controllers' have. The control station refers to the facility from which all the pods are controlled. The integration of the control station in the infrastructure will be described in chapter 15.

14.2.1. Level of Authority

The level of authority the controllers have is an important aspect for the pod control. The more authority the controllers have, the more prone the system is to hacking. On the other hand, in an emergency situation, full authority (e.g. fully externally controllable) could be beneficial for achieving a safe landing and makes it easier to certify the aircraft.

Taking these reasons into account, the design team selected a restricted level of authority. The pod will be fully controllable by a bunk pilot during initial testing. After a number of tests have been carried out successfully, the pod will move towards more autonomy, converging towards a design in which the controller can only adjust the route, velocity and the no-go zones.
When the pod is in an emergency situation, its route can be diverted to a location that the controller finds suitable. Furthermore, it should be possible for the controller to change the velocity of the pod, for example when there is a lot

of traffic at the destination. Instead of waiting at the airport, the perceived waiting time is minimised by reducing the velocity of the pod. Furthermore, the controller should have the possibility to alter the no-go zones for pods. Certain parts of airspace have to be restricted, as will be described in chapter 15. How exactly overruling the system works is discussed later in this section.

14.2.2. Controller Training and Allocation

The controllers at the control station oversee the safety of the pod and act when necessary. An individual should undergo extensive training to become an authorised controller. For the sake of simplicity, the controllers will have the same license as the air-traffic controllers guiding conventional aircraft. This has multiple benefits: firstly, training is at the airport control facility, which makes a new training program unnecessary[5]. And secondly, the controllers will have insights regarding the routes to take and will know how to closely communicate with the airport ATC. Controller training should be reconsidered after the project is successfully operative for many years.
The controller arrangement is determined as following to ensure a sufficient level of safety and to optimise the amount of controllers in the area:

- One controller always oversees the hub. As the airport is a critical location in terms of traffic, this controller plays a major role. If there are less than thirty pods in the controlled area, then this is the only controller operative.
- When more than thirty pods are in the controlled area, a second controller is added to ensure that the system remains clear and controllable. The number of controllers required can be found by solving: ceiling(#pods / 30).
- The control area is divided over the controllers.

Also multiple redundant controllers should be available. This is a safety measure to ensure the controllers will never be understaffed. Furthermore, the controllers will not be allowed to work for more than ninety minutes, optimising their focus while they are working.

14.2.3. Controller Interface

The control station can always monitor and follow the system via screens. An example of such a screen is presented in Figure 14.1. As can be seen in the figure, the control station has access to information about the pods and its passengers. Failure in a component of the pod is shown immediately. When the route or velocity of the pod is to be changed, this can be done through a separate touchscreen that has an enlarged radar image that includes the current route. For safety reasons, the flight parameters cannot be changed with one touch. A second confirmation is required.

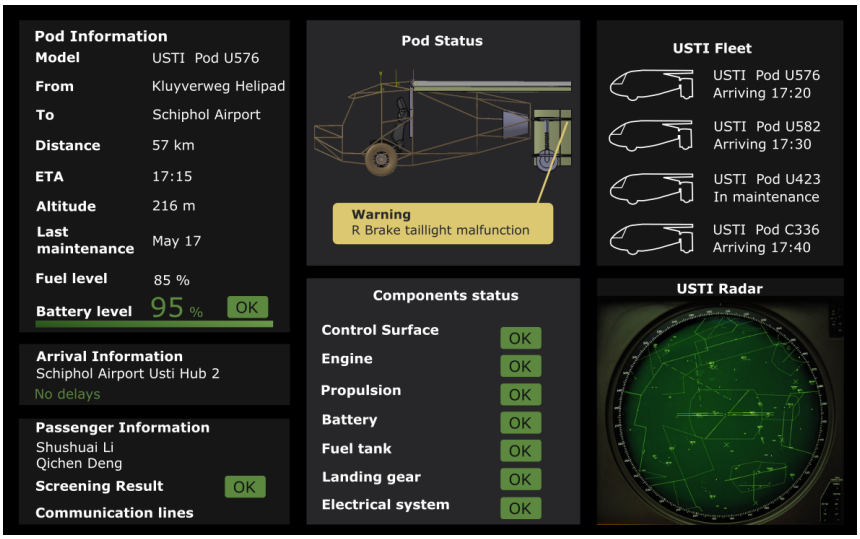

Figure 14.1: A display screen of the control station

14.2.4. Hacking Prevention

Hacking is a serious issue that the drone-industry has faced for many years [58]. Especially unmanned aerial vehicles designed for military purpose require a high level of security. Two types of attack are possible: *hardware attacks* and *remote attacks* [57].

One speaks of a hardware attack when the hardware of the pod is attacked and/or altered. When an attack is successful, the consequence can be severe. For hackers, it is not easy to perform such an attack as the hacker has to be physically present. To prevent this type of hacking, the pod is designed to ensure that sensitive components such as the avionics

and flight computer are located in inaccessible locations. The pod will signal the control station when someone tries to access it.
The remote attacks consider the links between the external interfaces and the pod (e.g. GPS or control station). When this type of hacking is successful, the effects might remain invisible for a longer period of time. The following measures can be taken to prevent a breach [21]:

- Have the highest and newest security standards
- Solely partner with trusted vendors
- Strong quality assurance standards
- Strong encryption of data
- Redundant subsystems to be able to verify data
- Receiver Autonomous Integrity Monitoring (RAIM) on board.

14.3. Maintenance Station

Regulations and guidelines for maintenance have been established by EASA. In this section, an overview will be given on the frequency of maintenance. In addition to that, high-level contents of the maintenance program will be discussed. Maintenance is carried out by employees who have a part-66 certification.[1] The pre-flight and post-flight checks can also be carried out by people with basic knowledge of the pod.

14.3.1. Maintenance Frequency

The frequency in which the aircraft is inspected is described in the maintenance program. However, regulations dictate the minimum required maintenance. For USTI, different types of checks with their own respective frequencies can be distinguished:

- A *pre-flight check*. This is a quick check to see whether the pod is ready to fly. Primary flight controls are among the tested systems. Furthermore, the pod is prepared for the flight. Charged batteries are put into the pod, while the fuel tank is filled. A dedicated location for this check and preparation will be discussed in chapter 15.
- A *post-flight check*. This checks whether the pod has been damaged during the journey. This inspection is performed internally and externally on the most critical flight components. At the same time, the pod is cleaned internally and externally and the batteries are taken out for charging. Including everything, this process takes approximately fifteen minutes.
- A 100h check [5]. This is a check on a deeper level. Critical components such as the transponder and altimeter are checked. It should be noted that the 100h limit may be exceeded by 10h.
- An annual check. This can be compared to the "B" check in conventional aircraft maintenance. Less critical components are inspected during this inspection. However, the aircraft is not disassembled in any way. This type of overhaul takes approximately one day.
- "C" check. The frequency of occurrence of this overhaul is determined by the aircraft manufacturer. Usually, the check is done once every 26 months [5]. It entails the most thorough inspection of the pod, including the disassembly of certain parts. These include the engines/motors, interior, landing gear and empennage. The duration of this overhaul takes between two and six weeks.

These are hard constraints for the pod maintenance to ensure a minimum lifetime of ten years. The margins described are in place to ensure that the pod availability does not fall below the minimum set by demand. As pods are booked at least six hours in advance, the demand can be taken into account. While planning maintenance, an attempt shall be made to schedule as many events during the minimum demand times. These moments include nighttime.
For the future, the possibility of automated maintenance is becoming increasingly attractive. The use of a robot decreases the cost, while increasing the accuracy and thus safety [43]. A human needs to go over for the final maintenance check to minimise maintenance errors.

14.3.2. Maintenance Program

The maintenance program is a document describing all checks involved with maintaining the pod in both the 100h checks and the annual checks. Additionally, it elaborates on the required qualification of employees and the frequency of maintenance. The document is created by the manufacturer, after which it is certified by the responsible authorities (EASA).

More specifically, the document describes the tasks of the inspection in detail. Only after a successful completion of the actions, the airworthiness can be considered verified. The total and throughput time of the maintenance are included

[1] How to get an EASA Part-66 Licence? EASA, date accessed: 30-05-2018, `https://www.easa.europa.eu/faq/21067`

in the document, too. The program has to be revised and verified annually by the airworthiness authority (EASA) [5].

For this specific project, the maintenance program will document the frequency of overhauls described before. Also, the inclusion of tilting wings enforce more frequent inspections on the attachment location of the wing to the main body of the pod.

The tasks seen in the figure above will be done according to a general step-wise approach. This approach was taken from A. Kara et al. [31]. and can be found in Figure 14.2.

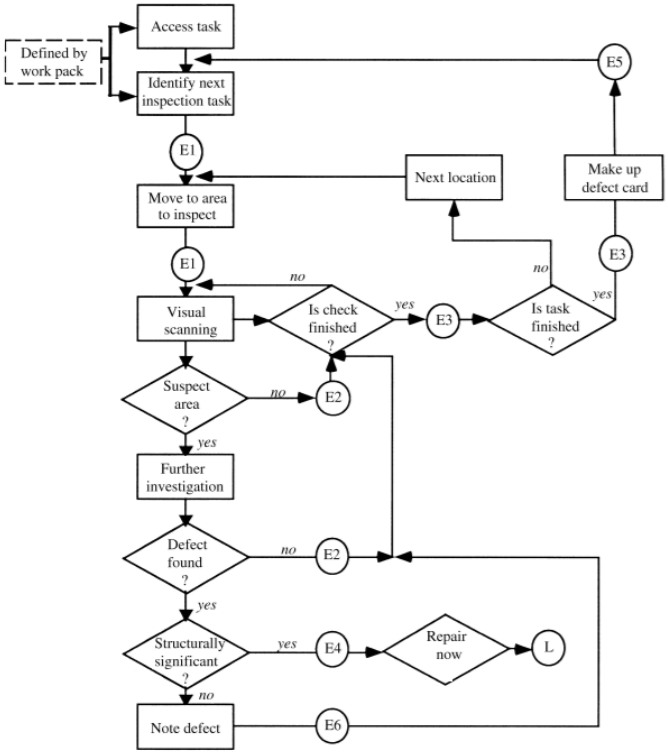

Figure 14.2: General maintenance procedure taken from A. Kara et al. [31]

Sustainability
The maintenance and control program impacts both the environment and the amount of local employees working. With the planned maintenance and control plan, the welfare of the local community can increase. Also, the USTI controllers will be trained to reduce levels of noise and emissions. The maintainers are schooled to efficiently separate waste flows, ensuring no harm is done to the environment.

14.4. Algorithm for Pod Allocation

An algorithm is developed that optimises the distribution of the pod in terms of time, distance covered and consumption. These three aspects can be directly related as follows:

- **Maximum time efficiency**: the fastest route has to be selected to allow each passenger to reach its destination as quickly as possible. This implies a combination of driving and flying manoeuvres. Moreover, the journey of each pod must be optimised such that its availability during the day is at a maximum.
- **Maximum range efficiency**: as the range that each pod can travel is limited, it is important to guarantee that each journey is no longer than 300 km. However, the distance should be maximised within this range to make each journey more fuel efficient. For example, it might be convenient to perform one single journey to drop off one passenger and pick up another one, as long as the distance covered is shorter than 300 km and the requested flight times of the two passengers are compatible.
- **Minimum Fuel Consumption**: each pod is designed to be able to perform 30 % of the journey with its electric motor, and 70 % of the journey with its thermal engine. For this reason, it might be better at times to take shorter journeys and allow the pods to operate only with the electric motor to reduce fuel consumption and emissions.

The algorithm that performs such optimisations can be visualised in Figure 14.3. The inputs of the algorithm are provided by the user. These are the location of pick-up/drop-off, the time of departure or arrival. Moreover, a map must be

imported from an online database. The algorithm outputs the list of most convenient routes.

Verification and Validation
The algorithm is partly verified by manually programming a tool on *MATLAB* that is able to perform the following steps:

1. Generate a map divided into several different areas, according to the selected mesh size.
2. Generate a list of random passengers requesting a pick-up or a drop-off service at a specific location within the mesh and at a specific time of day.
3. Calculate all possible combinations of routes that allow the pod to depart from the airport, drop off the first passenger, travel to the pick-up location of the second passenger and travel back to the airport.
4. Get rid of all infeasible combinations, due to a range longer than 300 km.
5. Get rid of all infeasible combinations, due to incompatible requested times.
6. Finds the most convenient combinations in terms of time efficiency.

Every further validation method should be implemented at later stages of the design procedure, once the system becomes operative. This includes the optimisation of fuel consumption.

Sustainability
The algorithm is designed to minimise fuel consumption, pushing the whole design towards a more sustainable product. In fact, by reducing the fuel consumption, not only the operating costs of the service decrease, but also the emissions.

Another aspect that should be taken into account is the fact that by maximising the travelled range to the 300 km limit, the overall distance covered by the entire service is lower, resulting, once again, in a reduction in fuel consumption.

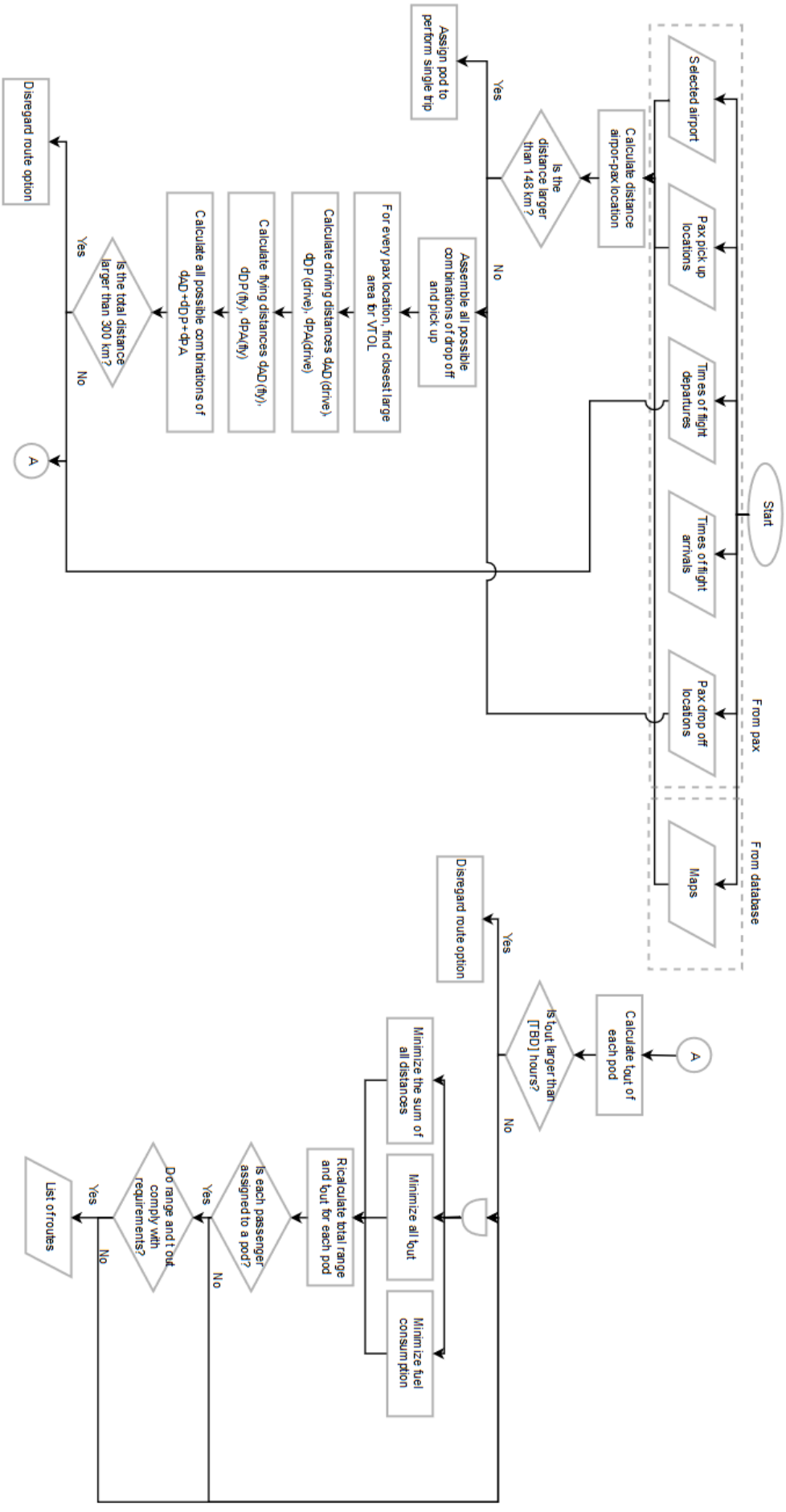

Figure 14.3: Algorithm for pod allocation

15
Infrastructure Design

The design of infrastructure is described in this chapter. Amsterdam Airport Schiphol is used as an example. Firstly, the pod routes around Schiphol are examined in section 15.2. This is followed by the description of the arrival and departure operations at the airport in section 15.3 subsection 15.3.1. Additionally, the maintenance, storage and control facilities are discussed. The chapter finishes with a long-term vision regarding the airport design and operations.

15.1. Requirements and Constraints on Infrastructure Design

For the infrastructure, the following requirements need to be adhered to:

- POD-MIS-7: The pod shall be able to operate with the already-existing urban infrastructures.
- POD-SYS-F-4: The pod shall not interfere with current air traffic;
- POD-SYS-MT-5: Maintenance of the pods shall not require a change in the infrastructure of the airport.
- POD-SYS-ST-1: The pods shall be able to be stored within current airport infrastructure.
- POD-SYS-ST-2: The pods shall be able to leave the storage facility autonomously

15.2. Arrival and Departure Routes around Schiphol

The arrival and departure operations at the airport are designed in line with the project objective of minimising the waiting time. To analyse whether a pod can approach Schiphol airport without significant interference of air traffic, the three most common situations are analysed, as can be seen in Figure 15.1, Figure 15.2 and Figure 15.3. The departure and approach routes are similar to each other. Yellow areas are avoided because of air traffic. Additionally, the high density populated areas is avoided to ensure the environment is minimally affected in terms of noise. For Figure 15.2 and Figure 15.3, it can be seen that there are two options for approaching from the east and south of Schiphol. The first option corresponds to flying above a runway, which is only possible if no aircraft is landing at that moment.

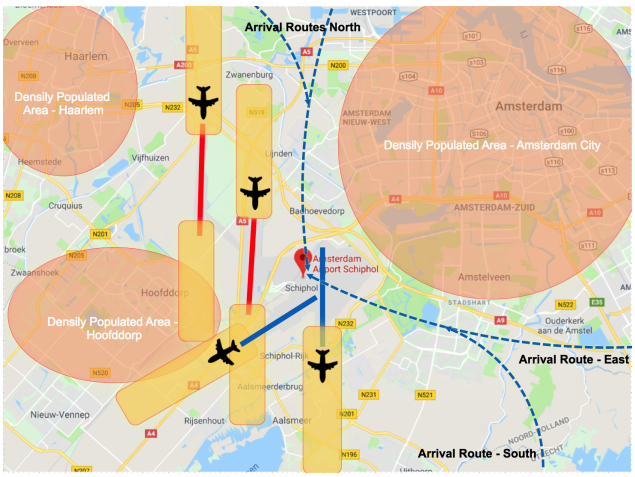

Figure 15.1: Schiphol arrival approach situation 1

Figure 15.2: Schiphol arrival approach situation 2

15.3. Arrival and Departure Operations

The closer the pod lands to the final destination, the more time-efficient the system is. The top floor of one of the parking garages at the airport shall be dedicated to these landings. This gives the pod the ability to drive between the airport departure area and the landing site with ease. The pod brings the passenger up to a dedicated entrance at the departure area. The example of arrival of the pod at Schiphol is displayed in Figure 15.4. For Schiphol, the parking garage P2 could be used for landing, as indicated in Figure 15.5. The pod users have the ability to enter an USTI dedicated

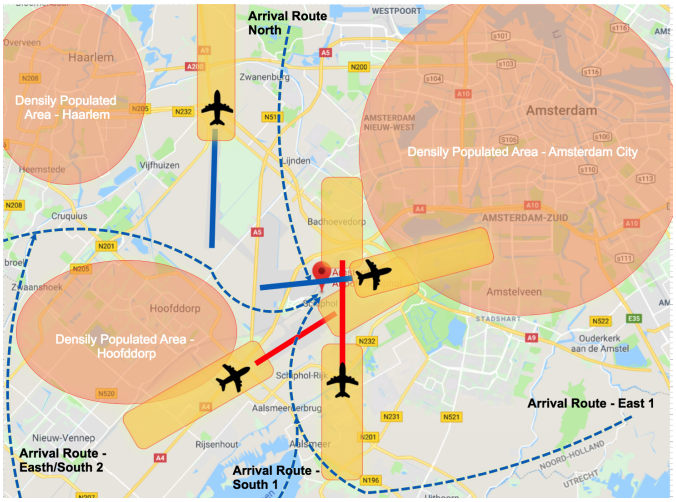

Figure 15.3: Schiphol arrival approach situation 3

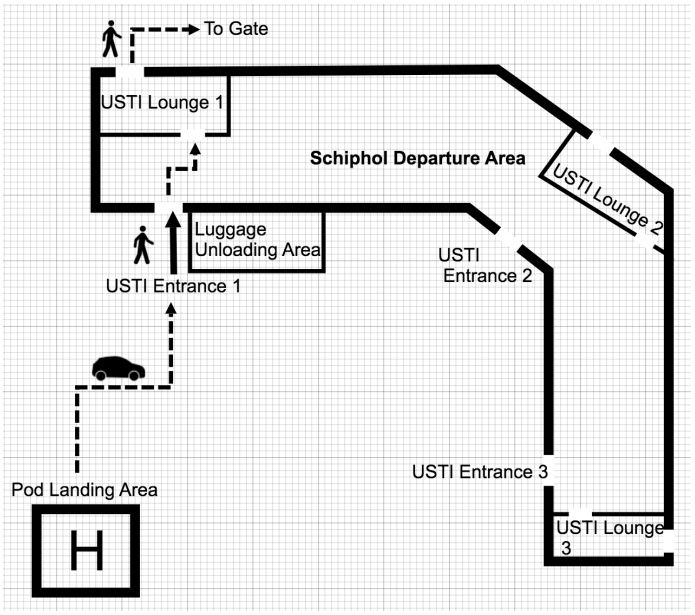

Figure 15.4: Schiphol arrival by pod

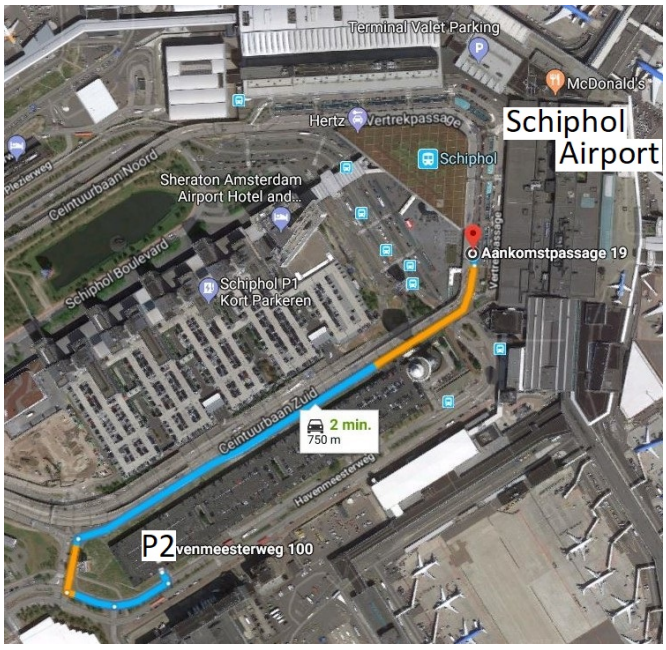

Figure 15.5: Landing and take-off location for USTI pods with route to departure terminal example at Schiphol airport

lounge, where the pod users and their hand luggage are screened. However, taking into account that Schiphol is one of the biggest airports in Europe, it would be time efficient to place multiple screening lounges at multiple locations at the airport. This will reduce the distance from the screening lounges to the different gates and consequently a more time efficient process is created. For Schiphol, this will result in three lounges evenly distributed over the departure terminals.

When arriving at the airport for a flight, the unloading of the hold luggage is performed at the departure terminal entrance, as can be seen in Figure 15.4. The hold luggage is manually unloaded from the pod and placed on a conveyor belt, which brings the hold luggage into the screening system. This is done prior to travelling to the lounge, as the luggage needs to be transferred to the right aircraft in time. This will contribute positively to optimising the waiting time.

15.3.1. USTI Lounge

The hub layout corresponds to a lounge where the passengers are screened. The hub provides comfort but also ensures that the pod service can be implemented easily at the airports in Europe. A possible hub lay-out is depicted in Figure 15.6. A 3D view can be seen in Figure 15.7. For example, a higher passenger flow will require larger screening capacity. Besides private screening, the hub consists of a lounge area with food and beverages for the pod passengers. This will allow the users to relax if their flight is delayed or if the passengers have sufficient time left before boarding their flight. The hub for departure is the same hub for arrival. Thus, arriving passengers can use the meeting room or relax area if they do not have the urge to leave the airport right away. The hub will also provide a shopping pick-up point after the screening. This gives the users the ability to order a product in advance and thus make the journey more time efficient, without

reducing revenue.

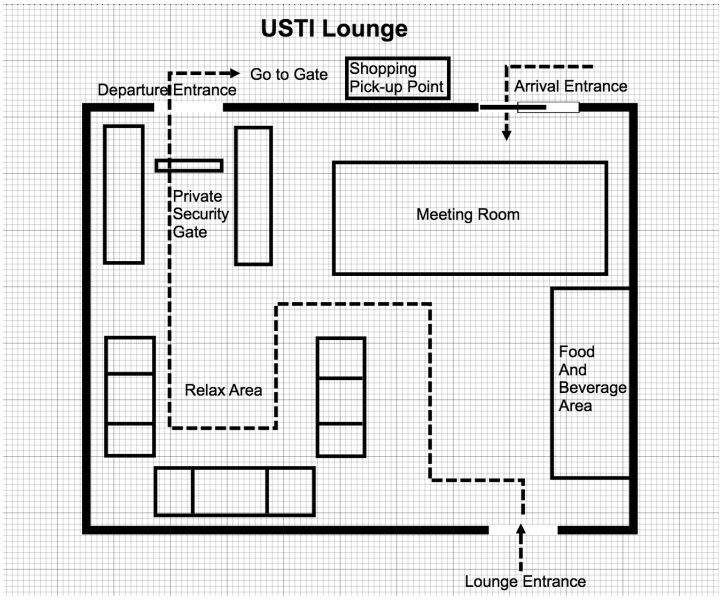

Figure 15.6: Top view airport USTI lounge layout

Figure 15.7: 3D view airport USTI lounge layout

15.3.2. Luggage Flow

When arriving at the airport by pod, the luggage is placed on a conveyor belt. Moreover, when arriving at the airport by aircraft, the luggage is transported to the pod take-off site, where it is placed in the pod. New conveyor belt infrastructure is required. The hold luggage will be labelled with an identification number, before directly being transferred to the screening system of the airport. For Schiphol, this is the handling area below Departure Lounge 3 for USTI entrance 1, as indicated in Figure 15.4. For USTI entrance 2 it will go to the handling area below Pier E and for entrance 3 it will go to the handling area below Pier D. These are the handling areas currently in use at Schiphol[50]. From the handling areas, it will be distributed to the right airplane with the current system.
Regarding the transportation of the luggage from the aircraft to the pod take-off site, a combination of conveyor belts and manual transportation is used.

15.3.3. Time Breakdown

For the operations described in the previous sections of this chapter, the estimated time breakdown is shown in Figure 15.8 and Figure 15.9. Figure 15.8 presents the estimated time breakdown for arriving at the airport, whereas Figure 15.9 presents the time breakdown for leaving the airport. It can be seen that regarding the former, a minimum time of thirty minutes between arrival at the airport and boarding the airplane can be achieved with the previously described process. For the long-term vision described in section 15.5, this time span can be minimised to fifteen minutes. When leaving the airport, a minimum time span of 25 minutes can be achieved as is shown in Figure 15.9.

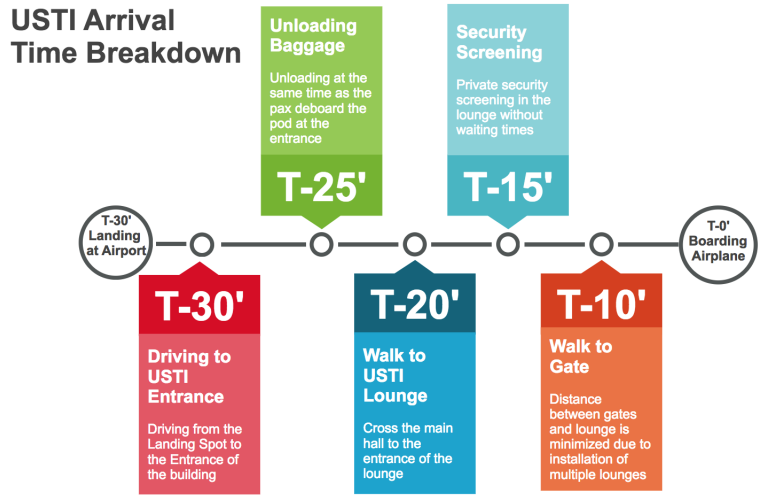

Figure 15.8: Arrival time breakdown

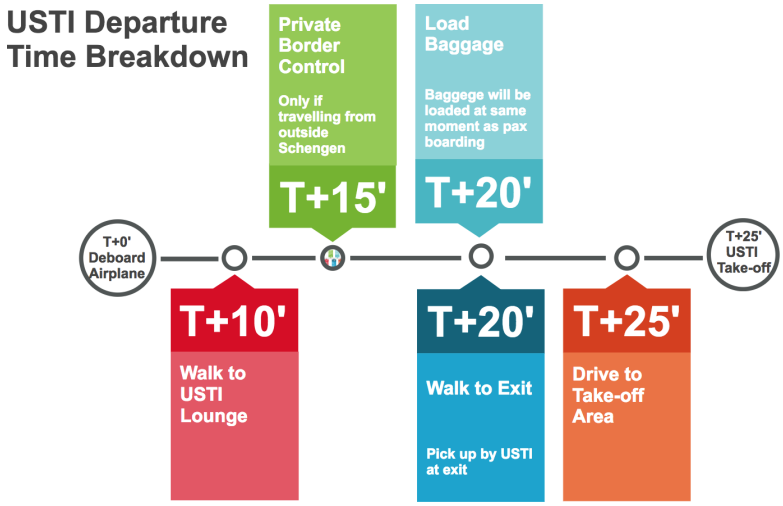

Figure 15.9: Departure time breakdown

15.3.4. Screening

The screening is optimised to reduce the waiting time for the passengers. This is done in multiple ways:

- Screening in a special lounge
- Use of CT scanners
- Use of automated screening lanes

Because screening is performed in the USTI lounge, the passengers will not interfere with other travellers and therefore do not have to stand in line with them to be screened. The CT scanners speed up the process because contrary to X-ray systems, bags do not have to be unpacked for screening[1]. The automated screening lines help to save time because of continuous use possibilities. The checked baggage is separated from the passenger as soon as the pod arrives at the USTI entrance and is also scanned by a CT scanner.
A precise estimate of the amount of the inflow of passengers can be obtained, since passengers book the pods up to six hours before the flight departure. For a Schiphol sized airport, this estimate is set to be one pod every three minutes. From subsection 15.3.3, the time spent at the airport is estimated to be thirty minutes, the amount of pod users will therefore be around twenty. Two screening lanes in every lounge of the airport are necessary to optimise passenger flows. The required personnel to perform the screening on these passengers is given in Table 15.1.
The amount of personnel for the individual frisking of passengers is set to two, because both a man and a woman should be present to prevent people from getting uncomfortable when being searched. As all the pod arrivals are monitored,

[1] New technologies and strategies strive to increase airport security and passenger experience, *date accessed: 15-06-2018*, http://www.futuretravelexperience.com/2016/08/new-technologies-strive-to-enhance-airport-security/

Table 15.1: Required personnel for screening

Task	Number of personnel
Searching passengers in case of failed screening	2 per lane
Over look automated CT screening lanes	1 per lounge
Unloading checked luggage from pod	1 per USTI entrance

an accurate prediction of the number of passengers arriving in each lounge can be made. Therefore, the amount of personnel required in each lounge can be estimated up front. Thus, no excessive personnel is present in the lounges, or, if necessary, additional personnel can be sent to a lounge in time.

15.4. Maintenance, Storage and Control Facilities

This section describes the location and lay-out of the maintenance, storage and control facilities. The flow at these locations will also be discussed. For the sake of simplicity, these facilities are combined at one location. This way, the entire team operates closely together.

15.4.1. Location

The location of the facilities is chosen to be close to the airport, but not at the airport itself. This is due to the fact that conventional airport facilities do not allow for new infrastructure. A cheap and spacious location, preferably close to the airport is selected. This location differs per airport.

In case of Schiphol, the surrounding area consists mainly of meadows that are accessible within minutes from the terminals of the airport. As an example, the *Sloterweg*, north of the airport, is chosen. This location would be suitable as it only requires a ten minute drive from the airport. After dropping off a passenger at the gate, the pod autonomously drives towards the facility hub to be cleaned, inspected and stored until further use. The location is shown in Figure 15.10

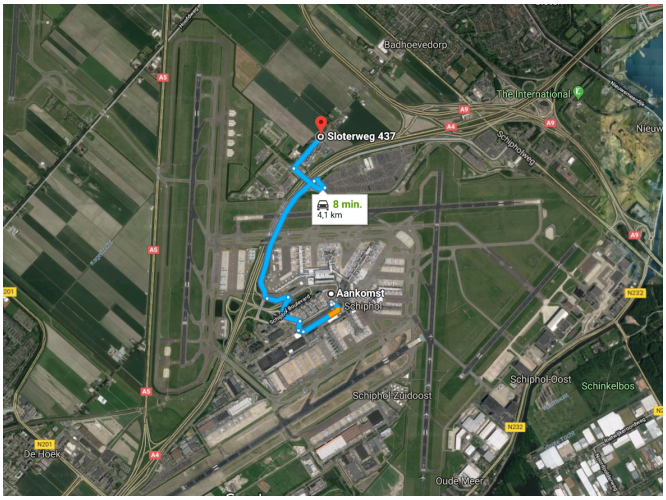

Figure 15.10: Maintenance and storage facility location example Schiphol airport.

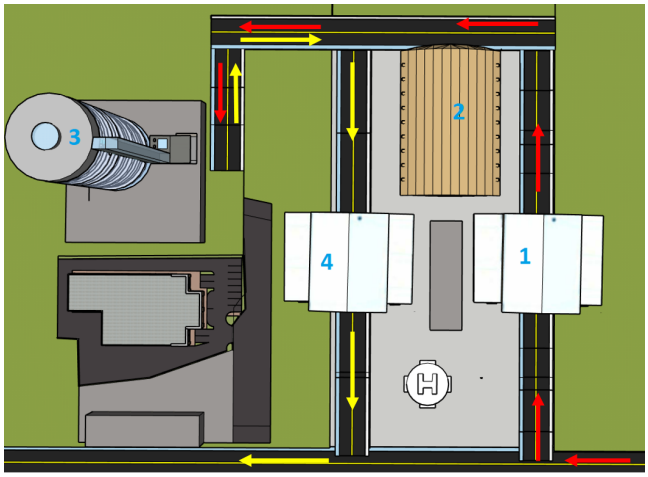

Figure 15.11: Maintenance and storage facility lay-out and flow example.

15.4.2. Lay-out

The lay-out is depicted in Figure 15.11. The pod drives (after drop-off at the airport) or flies (after drop-off at final destination) to the facility hub, where it enters a hangar (number 1 in the figure). In this hangar, the post-flight inspection takes place, the batteries are removed for charging and the pod is cleaned. If a problem is found during inspection or a more in-depth check is required, the pod moves to the bigger hangar where it is further inspected and repaired (number 2). Then the storage of the pods occurs in the tower indicated with a 3. This type of tower is chosen, because the area around airports usually already have a purpose, so these towers are produced over big parking areas. Furthermore, they are covered with UV-protected glass, such that the pod skin does not degrade. In these towers, an automated system stores and takes out the pods. When pods start a new mission, they first are taken through a smaller hangar (number 4) where they are loaded with fuel and the charged batteries. The pre-flight check is also carried out here. Then the pod drives to the take-off site (to pick up a passenger at home) or drives to the airport (to pick up a passenger at the airport). The flow of the pods is indicated with the red (arriving) and yellow (departing) arrows.

On the terrain located between the two small hangars, there is a smaller building dedicated to charging of the batteries. These are automatically distributed and retrieved from the hangars. The building on which the storage tower is built is

the control station. This is the beating heart of the entire system. The pods drive up the building using a ramp. The other two buildings are used as front office and meeting rooms.

15.5. Long-Term Vision

The system designed in the previous section is made to ensure easy implementation for various, currently existing airports. Nevertheless, a long-term vision is developed that includes the creation of more infrastructure to make the system more time efficient and more comfortable. The most optimal system provides the ability of landing or take-off by the pod on the roof of the airport. The roof of the airport would be directly connected to the lounge by an elevator. Alternatively, the pod could be directed to an underground drop-off location. From there, the passengers can easily enter the airport by taking an elevator that goes straight to the lounge. This futuristic long-term situation is schematically visualised in Figure 15.12. Here, the facade of the International Airport of Denver is used as reference.

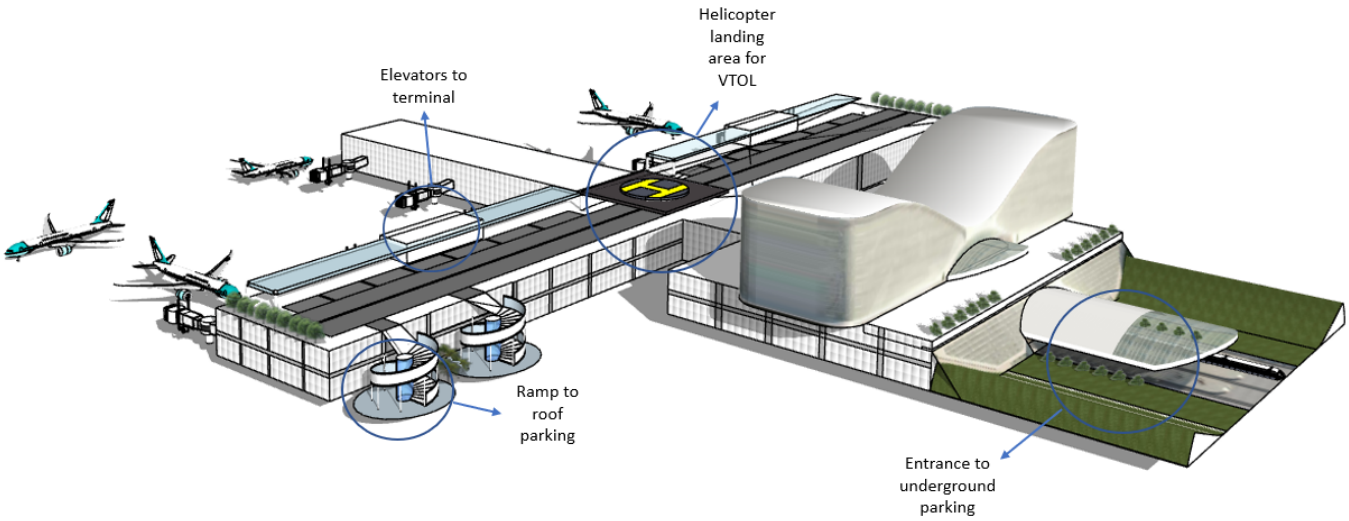

Figure 15.12: Futuristic vision of airport with integrated parking facilities for USTI pods

Moreover, screening of both the passengers and their luggage can be performed at the parking location where the passenger is dropped off by simply installing screening hardware right next to the parking location. This is depicted in Figure 15.13

Figure 15.13: Vision of the future: screening upon arrival

16 User Interface

Passenger comfort and satisfaction is increased by designing a high-end user interface. In this chapter, the application with which bookings can be performed is discussed, after which the user interface in the pod is designed.

16.1. Requirements and Constraints on User Interface

- POD-SYS-SH-1: Shopping shall be possible during the pre-flight and flight phase
- POD-SUB-A-1 The user interface shall be user-friendly.
- POD-SUB-A-2 The customer shall be able to order a return pod while int the pod.
- POD-SUB-A-3 The customer shall be able to report an emergency through the app.

16.2. Mobile App

An initial iteration of the app is developed to show a proof of concept for the booking of a pod. The process of booking a pod can be seen in Figure 16.1. The screen on the left is the screen at start up. After logging in, the user arrives at the second screen, which features a bottom navigation menu with three options: Booking, Manage and Account. The Manage tab is used to manage trips already booked and will be discussed later. The account tab has not been developed, however, it should include the option to receive messages to inform the passenger of delays.

Figure 16.1: Booking process using the app. Screen 1: Start up screen, screen 2: Flight booking information screen, screen 3: Passenger information screen, screen 4: pick-up location screen, screen 5: pick-up information

On the second screen, the passenger fills in their booking information. The passenger also checks if special assistance is required. When the passenger has entered this information, the system will receive the flight information. The passenger fills in their name and, if applicable, the name of the second passenger at the third screen. Then the passenger has the choice between only booking a pod to go to the airport, only a pod to take them to the destination, or using both options (so fully door-to-door). At the next screen, the passenger selects the pick-up location (or drop-off, depending on what the earlier choice was) and the system shows the route taken. If the passenger accepts this journey, the final screen in the picture shows flight information and at what time the passenger is expected at the pick-up location. The passenger will be able to book a pod until six hours in advance of the flight.

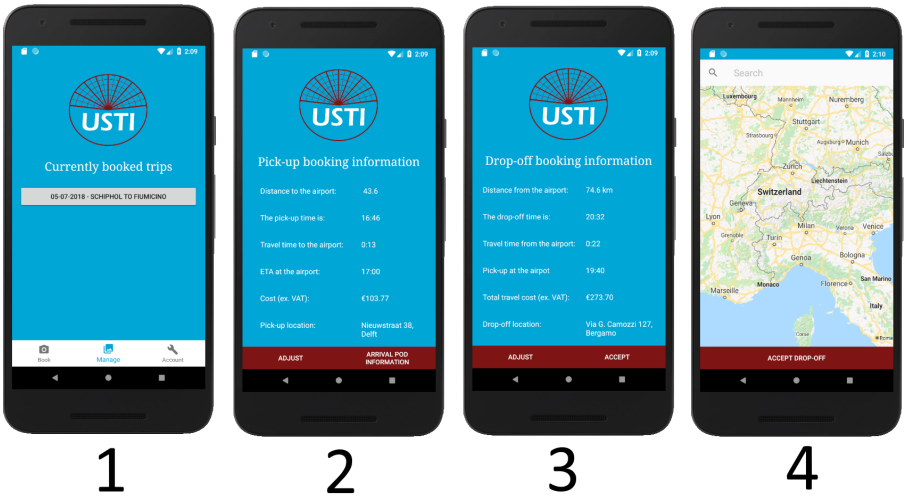

Figure 16.2: Editing a booked trip. Screen 1: overview of booked trips, screen 2: booking information of pick-up, screen 3: booking information of drop-off, screen 4: editing booked drop-off location

In Figure 16.2, the process of changing the drop-off location is shown. First, a list of currently booked travels is shown. The users selects the trip to be edited and then selects the new drop-off location. The user is able to change the exact pick-up location until one hour before the flight. At this screen, there should be the option to go to the shopping, however, since this is just a proof of concept, the shopping is left out for now. Finally, the passenger should also be able to notify the operator that there is something wrong with the pod through the app if the screen inside the pod is non-responsive. This will be another entry in this screen that will show up when the passenger enters the pod.

Note again that the app is relatively preliminary and some important characteristics are missing, like shopping, emergency options and account support. This is because of the time constraint on the project. However, in later design phases, this app should be developed in more detail.

16.3. Pod Display Screen

After entering the pod, the passengers can track the process via a screen located in front of the seats. This screen shows information about the pod such as the pod status, environmental settings, emergency messages and the airplane flight status, among others. On the upper side of the display, a menu line fades in when activated. In Figure 16.3, the menu option "Route" is selected, displaying the current trip details.

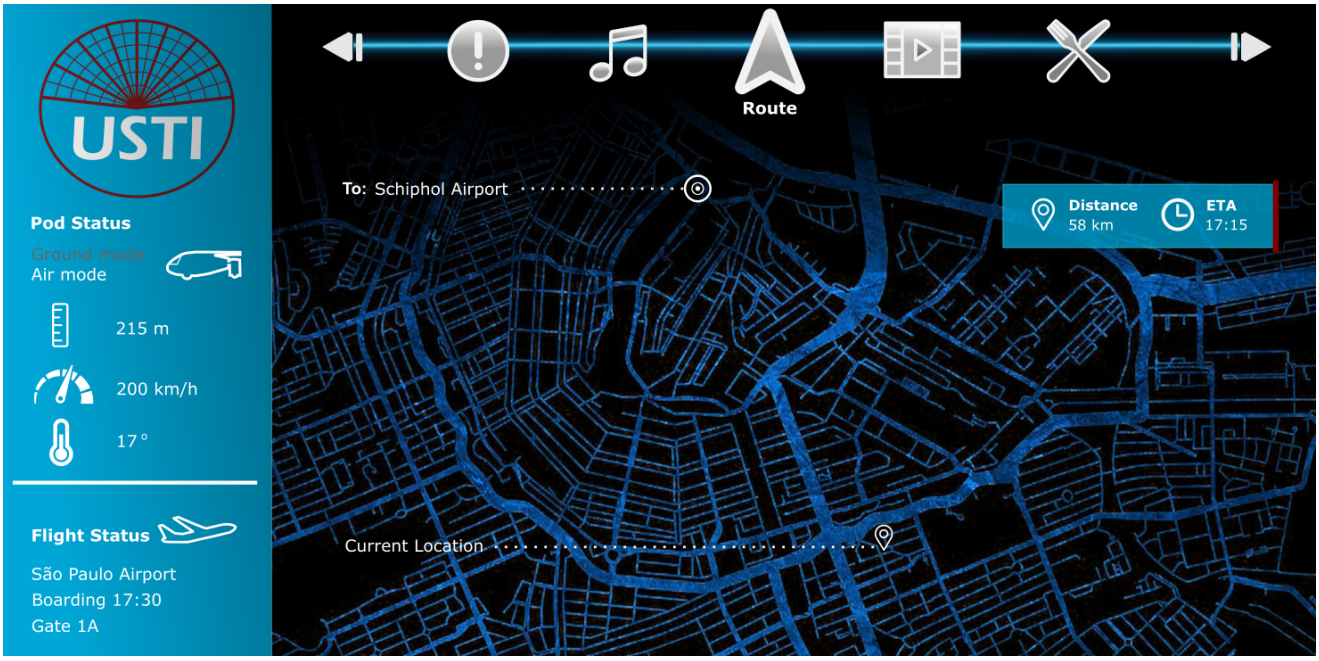

Figure 16.3: The display screen for passengers inside the pod

17
Regulations

This chapter covers the different regulations the designed system has to adhere to. It will start with the air traffic control regulations and after that the vehicle certification is discussed. Finally, based on these regulations, the cruise altitude is determined.

17.1. Air Traffic Control and Regulations Around Cities

Nowadays, urban airspace is reasonably open for business. The current air traffic control (ATC) systems are capable of handling a VTOL service that is scaled to hundreds of pods. For example, in an international city like São Paulo, it is known that hundreds of helicopters fly each day.[30] However, to successfully operate an on-demand system of autonomous flying pods, the frequency and density of vehicles operating over metropolitan areas will increase significantly. New ATC systems are required to handle this increase in complexity. Although the pod does not have to adhere to the visual flight rules (VFR), alterations in VFR are needed for piloted vehicles due to an increase of airspace density by autonomous pods like USTI.

One of the biggest operational barriers to deploy USTI in cities is the absence of sufficient nearby locations to land and take off. Even if USTI was certified to fly today, cities simply do not have the necessary take-off and landing sites to operate optimally, thus driving is an essential part of the journey. Furthermore, some parts of cities have their airspace locked down.

17.2. Vehicle Certification

Legislation in most countries prevents autonomous vehicles from driving on the road, but that trend is positively shifting.[30] Countries like Belgium, France, Italy and the United Kingdom have plans to run transport systems for autonomous vehicles, while in Germany, the Netherlands and Spain, it is possible to do public testing in traffic. Thus, in the near future, the pod is allowed to be fully operative on the ground.

Before USTI can fly in any country, it also needs to comply with regulations of aviation authorities tasked with assuring aviation safety. These regulations impose standards for vehicle design, production, maintenance and operating requirements. The EASA and FAA function as regulators for 30 % and 50 % of the world's aviation activities, respectively, meaning that USTI developers will eventually need to secure their approval to achieve an active system. Collaboration between the FAA and EASA has resulted in mutual arrangements[1] such that an aircraft approved in one jurisdiction can be flown in another.

17.3. Cruise Altitude

The cruise altitude is determined by many different aspects of the system and external factors. Some of these aspects can be conflicting as one requires a higher altitude and the other a lower.

The main aspects are:

- Rules and regulations
- Airspace restrictions
- Performance
- Safety in case of an emergency
- Sustainability: sound, view and emissions

The influence of the aspects on the altitude determination is discussed in the sections below and finally the optimal cruise altitude are determined.

17.3.1. Rules and Regulations

Internationally, all the regulations regarding minimum altitudes are similar. The regulations stipulate the following minimums:

[1] Aviation Safety Agreement Between The United States and The European Community. FAA, 2011, date accessed: 12-06-2018, `https://www.faa.gov/aircraft/repair/media/EASA_EU_roadshows.pdf`

- Over congested areas or cities: a minimum of 1,000 feet above highest obstacle [2]
- Elsewhere: a minimum of 500 feet above highest obstacle [3]

So, when maintaining a minimum altitude of at least 2000 feet it should be sufficient for all locations, assuming buildings higher than 1000 feet can be avoided.

17.3.2. Airspace Restrictions

With regards to airspace, a negotiation will probably be necessary with ATC to devise the procedure and make specific regulations for this system. In current controlled airspace classes, the autonomous system would not be allowed. Furthermore, the pod will have to fly at low altitudes to prevent any conflicts with existing air traffic. At low altitudes, the pod can fly below congested routes and below most of the controlled airspace. It can be seen that a significant part of the controlled airspace starts from 4,500 feet upwards. So, flying below 4,500 feet will avoid most of the controlled airspace.

17.3.3. Performance

The performance of the pod increases slightly with increasing altitude, due to the lower air density. Considering the relatively short range of the pod, flying at very high altitudes will not be feasible due to the high amount of energy required to climb. At lower altitudes, the density decreases are limited, e.g. at 5,000 feet, the air density decreases by 14 % compared to sea level conditions. This decrease in density leads to a decrease in the required power of 3.3 %.

17.3.4. Safety in Case of an Emergency

In the unlikely case of a complete loss of power, the pod will have to make an emergency landing. Therefore, flying at higher altitudes provides more time for the system to either try to solve the problem or to make a safe emergency landing. With the limited glide ratio of 9.2, flying at higher altitudes will increase the range in case of an emergency, increasing the chances of finding an ideal emergency landing spot.

17.3.5. Sustainability

The sustainability factor has multiple aspects such as sound, view and emissions. First of all the sound decreases with the distance squared. Flying at a higher altitude will thus significantly decrease the noise levels for communities and cities. Furthermore, flying at higher altitudes will decrease the disturbance of the view over landscapes. Also, emitting the pollutants at higher altitudes will decrease the direct effects on the people in the neighbourhoods below.

17.3.6. Determination of Cruise Altitude

Considering all aspects above, it can be concluded that the pod has to maintain a minimum altitude of 2,000 feet and maximum of 4,500 feet, mainly based on regulations and airspace restrictions. The cruise altitude can be altered based on the specific trip range. For further calculations, a cruising altitude of 2,000 feet is used, as this is the most critical with regards to performance.

[2] VFR Regulations in the Netherlands, *date accessed: 15-06-2018*, https://www.win.tue.nl/~jldejong/gliding/Voorschriften/AIC-Bs-MALs/AIC-B2003-0320VFR-Flights/VFR-Flights-AICB-03-03.pdf

[3] VFR Regulations in the Netherlands, *date accessed: 15-06-2018*, https://www.win.tue.nl/~jldejong/gliding/Voorschriften/AIC-Bs-MALs/AIC-B2003-0320VFR-Flights/VFR-Flights-AICB-03-03.pdf

IV

Final Analysis

18
Business Plan

Defining a clear business plan is important when designing a product that is not only effective, but also competitive on the market. In this chapter, the project Gantt chart is presented to provide a clear overview of the design process. Furthermore, the project costs are analysed.

As it is assumed that the product is sold to an operating company after manufacturing, the costs can be divided into costs for the designing company and costs for the operating company. The designing company is the company responsible for the design and manufacturing of the pod. This company then sells it to the operating company, which sells the service to the customers.

18.1. Project Gantt Chart

The planning of the project from the start until the operation launch phase is presented in Figure 18.1. Apart from the design operations, it also shows the different production and the marketing phases. The latter is indicated by the diagonal green lines in the chart. Moreover, certification, negotiations with the operators, the facility design and facility production are included. From the chart, it can be seen that the operation launch is in 2028. Figure 18.2 shows the planning of the project from the launch until twelve years of operation. Among other things, this chart takes in to account the business expansion regarding European airports as well as the disposal of the first pods.

18.2. Designing Company

The costs for the design company include all the expenses that occur before the service becomes operative. In this section, the breakdown structure of all costs is provided, followed by a detailed explanation of the cost components. From these costs, the selling price of each pod is determined. Finally, the return on investment is analysed.

18.2.1. Cost Breakdown Structure for Designing Company

The cost breakdown structure for the designing company is presented in Figure 18.3, it includes development costs, manufacturing costs and operational costs. In this subsection, the calculations of the development and production costs are discussed. Operational costs include the renting costs of the company facility, the price of the electricity and other organisational issues. These are not treated in this chapter as they are assumed to be a marginal part of the running costs of the company.

An explanation of the derivation of development and manufacturing costs is provided in the following paragraphs.

Development Costs

The development cost is "the non-recurring effort required to bring an aircraft concept to production" [37]. In this section, this is estimated according to the procedure proposed by the document of Large [44].

Firstly, the engineering hours necessary for the development of the vehicle are estimated. This is done by applying Equation 18.1 to calculate a unit factor indicating the engineering hours required, as derived from statistical data.

$$E = 4.86 \cdot W_{OE_{lb}}^{0.777} \cdot V_{knots}^{0.894} \cdot Q^{0.163} \tag{18.1}$$

This relies on two important inputs: the maximum take-off mass and the velocity at which the vehicle is supposed to fly. The result is then transformed into engineering hours by relating it to statistical data. Furthermore, it is multiplied by the average engineering salary of the Netherlands [1] to obtain the engineering costs necessary for development.

It should be noted that Equation 18.1 implies that statistically, larger aircraft typically require longer development costs. However, in this case, the design process includes the development of an autonomous system and the addition of a hybrid engine and both technologies have not yet been frequently used in flying vehicles. Therefore, it is decided to apply a safety factor of 1.4 in the estimation procedure, as it is expected that the costs will increase drastically.

[1] Average Salary in Amsterdam, date accessed: 15-06-2018, https://www.payscale.com/research/NL/Location=Amsterdam/Hourly-Rate

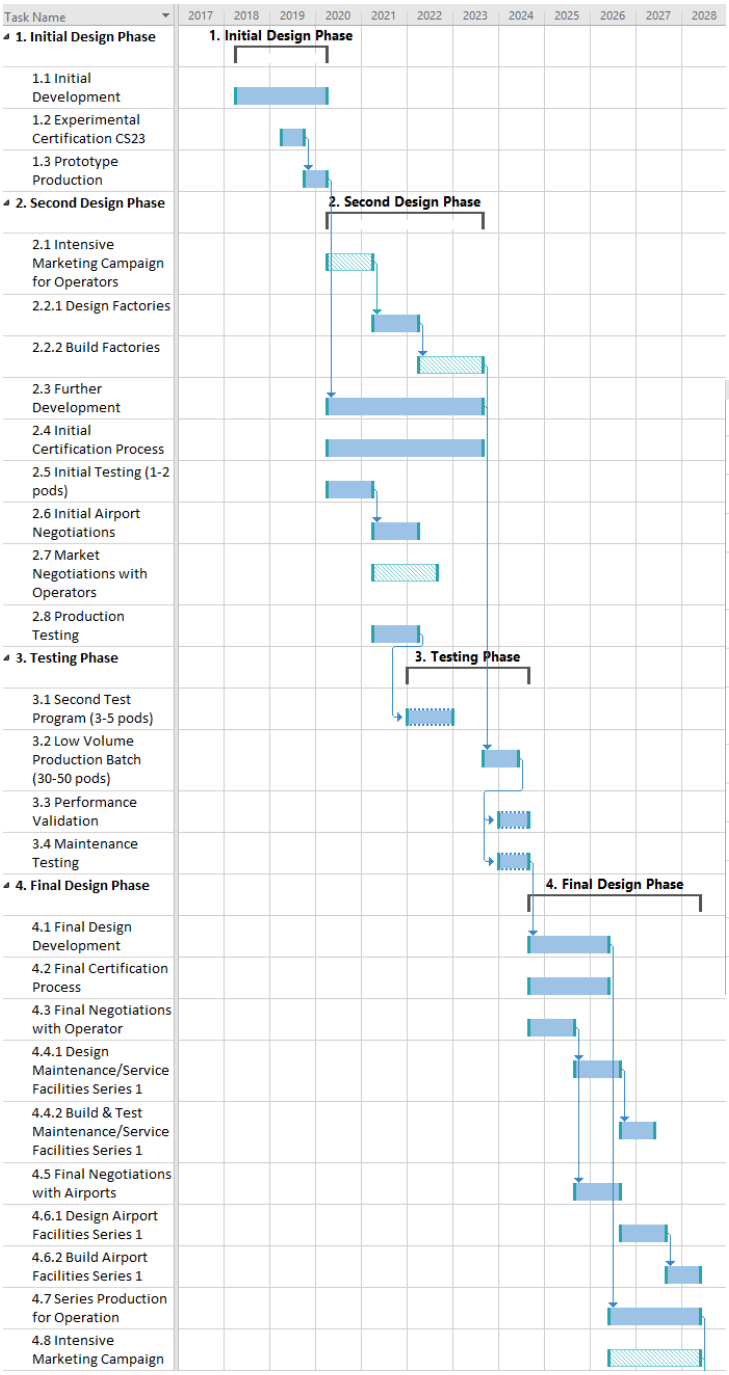

Figure 18.1: Gantt Chart regarding the project timeline of 2018 until 2028

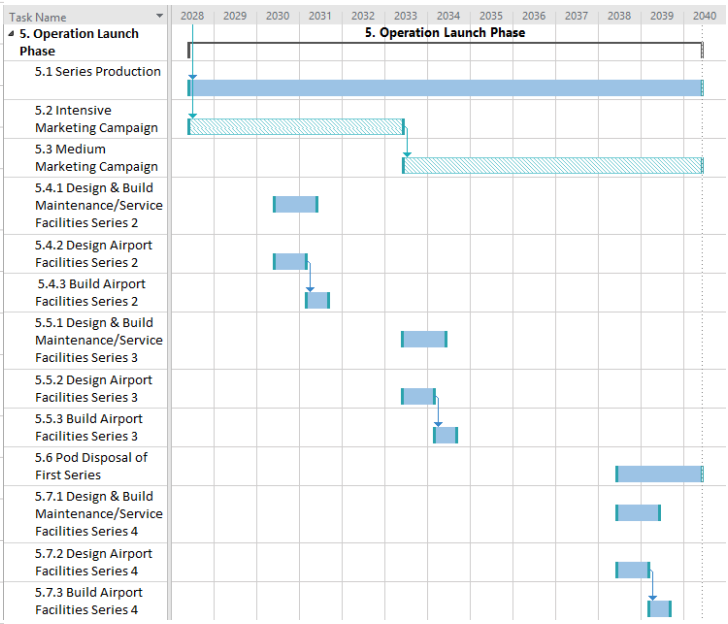

Figure 18.2: Gantt Chart regarding the project timeline of 2028 until 2040

A better understanding of the costs distribution over time is necessary for an accurate business plan formulation. This is based on statistical data of non-recurring costs of aeronautical products [37].

The statistical model estimates the profile of cash flow as a function of time, based on the fact that the average development time for an aircraft project takes around five years, including the first prototyping. The overall development costs as collected from reference aircraft data are plotted with respect to the development time in Figure 18.4, which shows the typical curve of a normal distribution.

Here, it can be seen that the non-recurring time is broken down by separate processes comprising the development effort. These can be summarised as:

- Engineering
- Tool design
- Tool fabrication
- Support

The plot is normalised over time to confirm the general validity of the method. This can be visualised in Figure 18.5. The shape of this curve confirms that at the beginning of the design process, the development costs increase slowly dur-

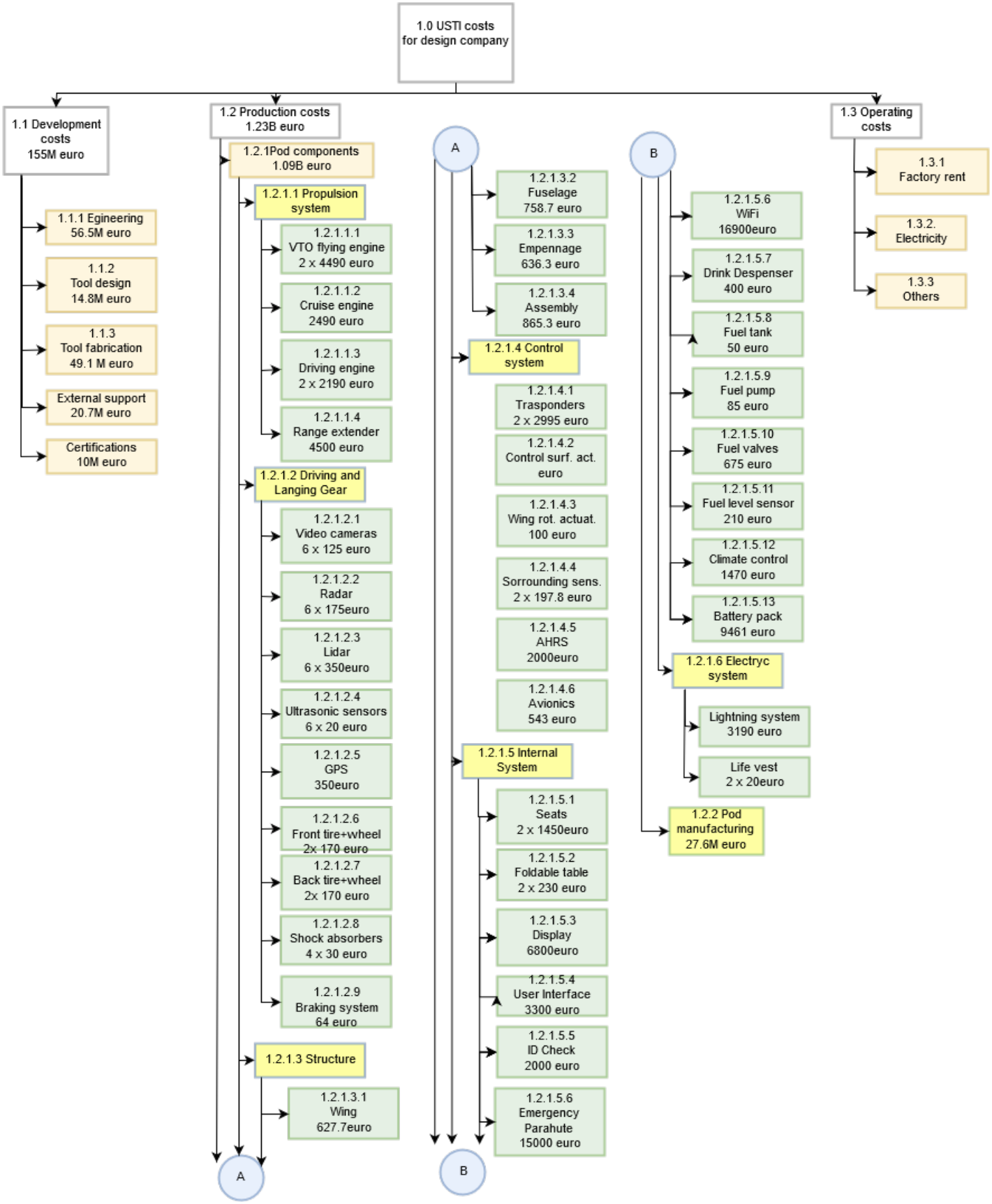

Figure 18.3: Cost breakdown structure of the designing company

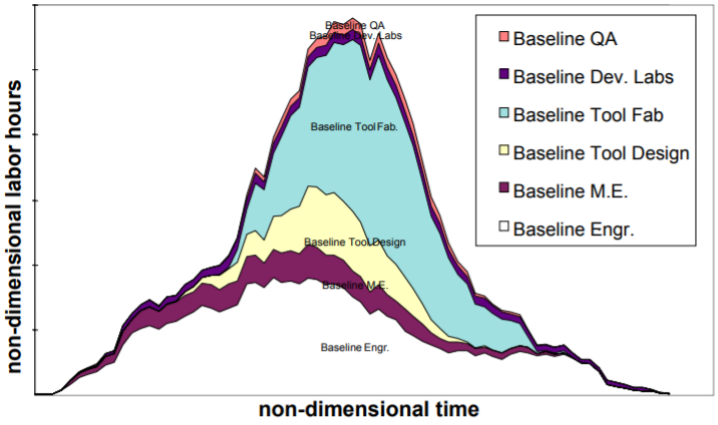

Figure 18.4: Statistical data of development time

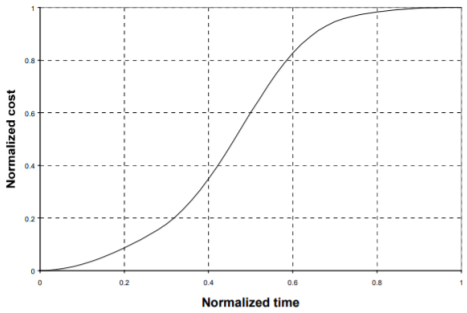

Figure 18.5: Cumulative non-recurring costs over time

ing the conceptual design phase. However, as the detailed design phase is reached, costs increase fast as prototyping is started. Once the product is finalised and only final adjustments are required, the cost rate decreases, until the total development time is reached.

From this statistical study, a reference distribution of the development costs over time is obtained. Furthermore, Table 18.1 indicates what percentage of the development cost is expected to be spent and at which moment throughout the development phase. However, the exact timing was reviewed in the definition of the marketing strategy.

Table 18.1: Distribution of the development costs over time

Process	**Engineering**	**Tool design**	**Tool fabrication**	**Support**
Percentage of development cost [%]	40	10.5	34.8	14.7
Start time [%]	0	22	27	0
Duration [%]	100	45	50	100
Cost per process [€]	56.5 M	14.8 M	49.1 M	20.7 M

Total development cost €145 M

A margin is added to the estimation of certification costs. From the interview with the engineering team of Pal-V, it is discovered that a plausible investment for certification costs should be around €10,000,000.

The development costs appear to be rather low: this is due to the fact that the statistical relation is highly dependent on the operational empty weight of the aircraft which, in this case, is very low. However, this estimation is reliable as the designing team is not planning to produce completely new components (such as, for example, engines) but to install already existing technologies. For this reason, the material and production costs are rather high as can be seen in Table 18.2.1.

Production Costs

Production costs are particularly important for the development of a product, not only because they make the product appealing to the industry, but also because they give a clear indication of what the selling price of the vehicle should be.

The production costs of the vehicle can be divided in:

- **Material costs.** These are estimated throughout the subsystem design phase and have already been mentioned in Part I of this report. Specifically, for each subsystem, the part costs are collected. A detailed list of all components prices is found in Figure 18.3.
- **Manufacturing costs.** These can be subdivided in:
  - **Manufacturing of materials costs.** For the structure of the vehicle, the manufacturing costs have been listed in subsection 8.3.7. It should be noted that, in the cost breakdown structure, they have already been included under the cost of the singular components, as a more detailed explanation can be found in subsection 8.3.7. For example, in the case of the fuselage, the cost indicated in the diagram includes both materials and manufacturing costs. A margin is added to the overall manufacturing costs to find the assembly costs: for the assembly of the structural frame, this has already been estimated in subsection 8.3.7. Figure 18.6 is used to give an estimation of the assembly of all other components[37].
  - **Manufacturing engineering costs.** These can be estimated according to reference aircraft data [47]. Specifically, Equation 18.2 is used to estimate the labour required for manufacturing.

$$M_{hrs} = 7.37 \cdot W_{OE_{lb}}^{0.82} \cdot V_{knots}^{0.484} \cdot Q^{0.641} \cdot (10)^{-3} \tag{18.2}$$

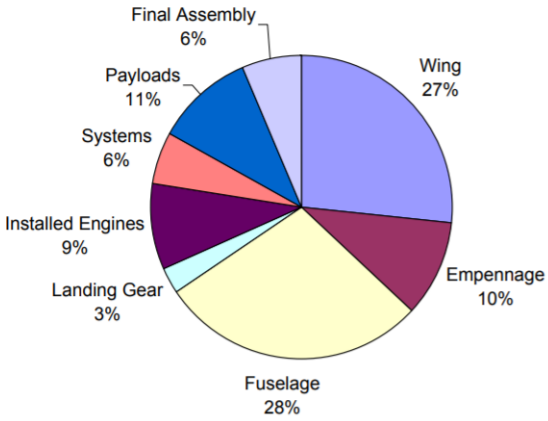

Figure 18.6: Distribution of manufacturing costs

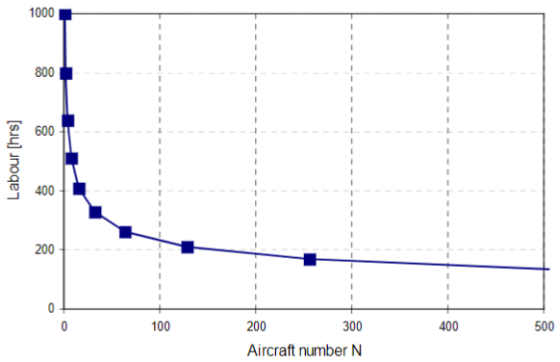

Figure 18.7: Manufacturing learning curve

Initially, Q is set equal to 1 to estimate the manufacturing costs of one vehicle. Then, it is increased to the market volume to evaluate the total costs. The result is then multiplied by a factor obtained from statistical references to convert it to hours. This leads to a labour time of 174 hours per pod. An estimation of the average price per labour hours is then used to compute the final manufacturing costs. The results of these calculation are listed in Table 18.2. Unlike development costs, manufacturing costs are recurring costs and are subjected to a relevant learning curve which leads to a reduction in overall costs over time. The decrease in costs is most noticeable early in the production cycle, it tends to decay later in the process. The general behaviour of the learning curve is shown in Figure 18.7 [54]. As it can be seen, jumps occur when a new production process is initialised. These jumps are ignored in the costs analysis.

In chapter 3, the initial market volume was estimated to require the production of 11,841 pods. By assuming a slope of the logarithmic learning curve of 85 % [37], the conclusions presented in Table 18.2 are drawn. It should be noted that the meaning of the learning curve is that every year, the manufacturing costs of the pod decrease of 15 %.

Table 18.2: Overview of production costs

Production cost per vehicle	
Material costs [€]	**Manufacturing costs [€]**
101,351	10,441

Production cost per market volume		
Material costs [€]	**Manufacturing costs without learning curve [€]**	**Manufacturing costs with learning curve [€]**
1.09 B	49 M	27.6 M

Total production cost per vehicle [€]
111,792

Total production cost per market volume [€]
1.23 B

Price Determination for Designing Company

The marketing strategy for the design company is based on the timeline depicted in Figure 18.8, which shows the expected flow of capital invested and earned. The timeline is derived from the Project Gantt Chart presented in section 18.1. All investments are indicated in green according to their time of occurrence and duration, if applicable.
This timeline includes the major development costs, production costs of the first prototypes, the low volume test batch of pods and the certification costs. Furthermore, the production costs for the pod are depicted. The 85 % learning curve is included for the manufacturing costs. For this analysis, the material costs are assumed to be constant.

Revenues are accounted for in blue and occur upon the delivery of the pod. The revenues are a function of the selling price per pod and is the variable of this analysis. It is assumed that the project needs to break even seven years after the start of operations to find the price of the pod. As operations are planned to start in 2028, the project should break even in 2035.

For the calculations, an average annual interest rate of 3 % is assumed. This seems like a rather low value, but it includes the fact that some investments come from bank loans, whereas other investments come from angel investors who are paid back in terms of company shares or a certain percentage of the profit. With this interest rate, the present time value of all investments and revenues are calculated. This calculation takes into account the effect of recurring investments or investments that are spread out over a certain period of time.

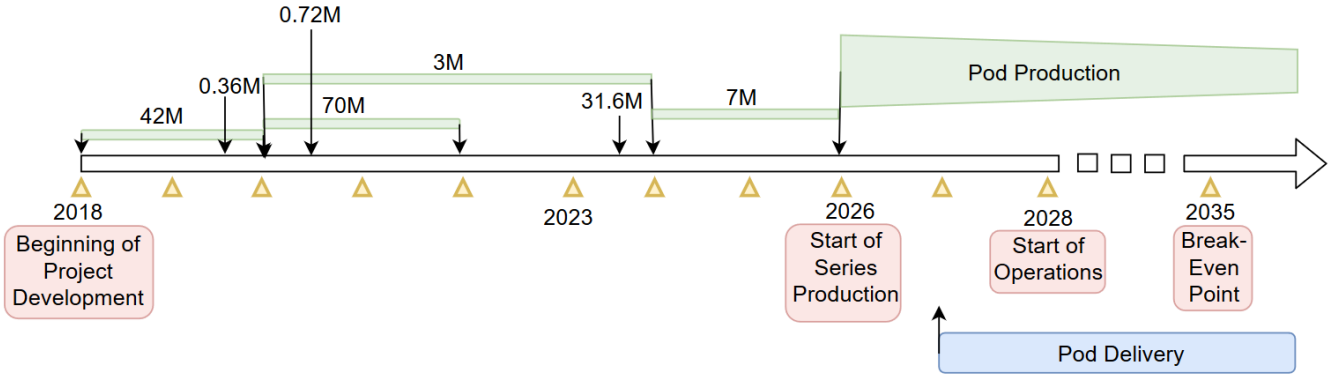

Figure 18.8: Timeline of investments and revenues for the designing company

Using the present values, the Net Present Value is calculated using Equation 18.3. The NPV indicates the expected profitability of a project. An NPV of zero indicates that the project exactly breaks even. Therefore, by setting the the NPV equation to zero, it can be analysed what price should be asked for each pod to break even in 7 years after the start of operations. This price is found to be €197,767 per pod.

$$NPV = PV_{incomes} - PV_{expenses} \tag{18.3}$$

18.2.2. Return on Investment

From the overview of the total costs and revenues presented in Table 18.3, the Return on Investment can be calculated. This is defined as the percentage difference between the total revenues and total costs. A gross Return on Investment of 69.4 % is found. However, this does not yet include the amount of interest and rent to be paid. When this is included, a net return on investment of 15 % is found. If lower interest rates than the currently used 3 % can be negotiated, or a larger deal of private investors can be attracted, the net Return on Investment is likely to increase, and the project would become more profitable.

Table 18.3: Overview of costs and revenues

Total Revenues		**Total Cost**	
Pod Selling	€2300 M	Development Costs	€140 M
		Certification Costs	€10 M
		Production of Prototypes	€4.6 M
		Series Production Cost	€1200 M
		Manufacturing Cost	€72.1 M

18.3. Operating Company

The operating company is the company that buys the pod from the manufacturer and sells the service to the customers. This chapter will provide more information on the financial situation of this company with a cost breakdown and revenue prediction.

18.3.1. Cost Breakdown Structure for Operating Company

The cost breakdown is divided into the operational costs and the depreciation costs. First, the operational costs are examined, followed by the deprecation costs.

Operational Cost

The operating costs are the costs related to the operations of the pod and consist of Direct Operating Costs (DOC) and Indirect Operating Costs (IOC). As these costs are directly related to the amount of operations and the duration of the operations, these costs will largely determine the ticket price of the system. The DOC consists of costs such as maintenance and flight costs. The IOC consists of costs such as cargo handling costs and facility costs. An overview of the operating cost breakdown can be found in Figure 18.3. The top-down method from [60] is used to make a first estimation of the operating costs of the system. This method uses two different methods to determine the operating costs. For the DOC, the method from Roskam is used and for the IOC, the method developed by Maddalon is used. This is because Roskam only provides the IOC as a fraction of the DOC, so there would be no breakdown of the IOC.

The DOC and IOC are calculated using statistical methods with the following input parameters:

- Weights:
  - Fuel
  - Cargo
  - Airframe
- m_{TO}
- Range
- Speed
- Block Time
- Prices:
  - Airframe
  - Propellers
  - Engines
  - Avionics

The formulas for the DOC and IOC found in [60] are based on Roskam and Maddelon. Both DOC and IOC are calculated using different methods and the final values can be found in Table 18.4.

- **DOC:**
  - **Fuel Cost.** The fuel cost consists of the cost of the gasoline for the range extender. The costs for the electricity of the battery are neglected here, because this cost is very small compared to the cost of gasoline.
  - **Maintenance Cost.** The maintenance costs consists of labour costs and material costs required for the maintenance of the engine and airframe.
  - **Cost of Landing Fees, Navigation and Registry Taxes.** The landing fees are a function of the MTOM. The navigation and registry taxes are calculated as a factor of the other DOC components.
- **IOC:**
  - **System Costs.** The system cost is based on the the labour costs for the engines and airframe.
  - **Cost of Facilities.** This is the cost of the local facilities and is a function of the MTOM.
  - **Cost of Contractors.** This is the cost of the contractors, although the system works autonomously, some personnel will be required, for example, for ground operators. It can be expected that this estimation is rather conservative for this project as it is based on data for conventional aircraft.
  - **Cost of Pax Handling.** This cost includes all costs involved in the handling of the passengers, it is mainly dependent on the number of passengers.
  - **General and Administrative Costs.** This includes some costs that are always present for the normal operation of a company, it is based on the values of the other IOC components.

Table 18.4: Operational cost breakdown

	Cost Parameter	**Value**	**Unit**
DOC	Fuel Cost	0.45252	USD/nm
	Maintenance Cost	0.31903	
	Cost of Landing Fees, Navigation and Registry Taxes	0.04892	
	Total DOC	**0.82049**	
IOC	System Costs	0.03336	USD/nm
	Cost of Facilities	0.02002	
	Cost of Contractors	0.15023	
	Cost of Pax Handling	0.08271	
	General and Administrative Costs	0.01411	
	Total IOC	**0.300446**	
	Total Operating Costs	**1.121**	USD/nm
		0.52	€/km

Depreciation Cost

The depreciation cost is defined as the depreciation of the different parts of the pod over time and is based on the original price and depreciation period. The depreciation cost is calculated by the time-value of money theory[2], because this is more specific for this project compared to the statistical method from Roskam.

The calculation uses the following variables:

- **Present Value (PV).** This is defined as the current value at time 0. The PV_{income} is calculated using Equation 18.5 and $PV_{expense}$ is defined as the selling price of the pod and is equal to €197,767, which is calculated in the cost breakdown of the design company.

[2] Brigham Financial Management, *date accessed: 21-05-2018*,http://www.swlearning.com/finance/brigham/ifm8e/web_chapters/webchapter28.pdf

- **Net Present Value (NPV).** This is the difference between the PV of the incomes minus the PV of the expenses, which is set to 0 to determine the PMT and can be found in Equation 18.3.
- **Payment per Month (PMT).** This is the value that determines the cost per month for the depreciation.
- **Interest Rate (i).** The interest rate is set at 5 % for the bank loan and an additional 10 % rate is added for the profit margin of the leasing company, because it is assumed that the operating company will not buy the pods directly from the manufacturer, but through a leasing company instead.
- **Amount of Years before Break-even (n).** This is the amount of years until the break-even point is reached, which is set at seven years, considering the expected lifetime of ten years.

Substituting the values from above in Equation 18.4, Equation 18.5 and Equation 18.6 results in a PMT value of €3,764 per month as can be found in Table 18.5.

$$NPV = PV_{income} - PV_{expense} = 0 \tag{18.4}$$

$$PV_{income} = PMT \cdot \frac{1 - \frac{1}{(1+i)^n}}{i^{(12)}} \tag{18.5}$$

$$12 \cdot PMT \cdot \frac{1 - \frac{1}{(1+i)^n}}{i^{(12)}} - 197,767 = 0 \tag{18.6}$$

This monthly depreciation cost is then converted to a cost per km, assuming the pods will operate on average 3,000h per year. This leads to a final depreciation cost of €0.075/km, as can be seen in Table 18.5.

Table 18.5: Depreciation cost calculation

Parameter	**Value**	**Unit**
PMT per pod	3,764	€/month
Flight Hours per month	250	h/month
Required Revenue per pod	15.06	€/h
Cruise speed	200	km/h
Depreciation Cost per km	**0.0753**	**€/km**

18.3.2. Price Determination for Operating Company

Now that the costs for the operator are calculated in subsection 18.3.1, the price for the customers for a trip in the pod can be determined. Combining the operational cost and depreciation cost from subsection 18.3.1, the total operating cost of the system will be €0.59/km. Considering the following, the price of the service can be determined:

- Guarantee a sufficiently large profit margin to account for empty legs, especially in the beginning phase of the system. This is expected to decrease when more people are using the system.
- The system should be competitive with current taxi transportation, prices vary between €2.00 to €2.85 per km in European cities.[3]
- For most business passengers, the company will pay for the transportation, so price is not the most important aspect.
- Most companies can get a value-added tax (VAT) refund, so this can be neglected for price determination.

Considering the aspects mentioned above, a profit margin of 300 % was set as a reasonable margin. This results in a price of €2.38/km, which is comparable to current taxi fares. This profit margin ensures that the operating company will be able to innovate and improve the service for the customers in the future.

Table 18.6: Price determination for customers

Parameter	**Value**	**Unit**
Operational Cost	0.52	€/km
Depreciation Cost	0.07	€/km
Total Cost	**0.59**	€/km
Profit Margin	300	%
Total Price for Customers	**2.38**	€/km
Total Price for customers incl. VAT	2.52	€/km
Example for a 120 km trip excl. VAT	285.85	€

[3] Telegraph Travel, *date accessed: 19-06-2018*,https://www.telegraph.co.uk/travel/news/the-worlds-cheapest-and-most-expensive-cities-to-take-a

18.3.3. Operational Profit for Operating Company

Based on the values for the revenue and cost from the previous sections, a simulation can be made for a sample operating company. A medium sized operating company with 100 pods is used for the calculation, which results in an operational profit of €93 million, the full details of which can be found in Table 18.7. The calculation are based on the financial results for one year. It is assumed that next to the costs, the company will also save 10 % of its revenue for other investments and provisions.

Table 18.7: Operational profit calculation for the operating company

Parameter	**Value**	**Unit**
Hours per year	3000	h/year
Amount of pods	100	
Cruise speed	200	km/h
Cost per km	0.59	€/km
Revenue per km	2.38	€/km
Total revenue	142,922,590	€
Total expenses	35,730,647	€
Investments and provisions	14,292,259	€
Profit	**92,899,683**	**€**

19
Design Analysis

This chapter analyses whether the design meets the requirements that were set previously. Additionally, it will assess the design regarding sustainability in section 19.2.

19.1. Verification of Requirements

The compliance of the mission, system and subsystem requirements is analysed. For every requirement, there are four options: the requirement is fully met, nearly met, not met, or it is yet unknown whether the requirement is met. A summary for this analysis can be found in the compliance matrix in Appendix A. This section will focus on those requirements that are not yet met and on those requirements of which it is unknown whether they have been met. A rationale of why the requirements are not met is given, as well as recommendations for further design. For those requirements of unknown compliance, the compliance analysis is performed or an outline for the analysis is given.

19.1.1. Travel Duration Requirement Analysis

The first mission requirement states that the system is able to reduce the average door-to-door travel time withing Europe to four hours, including all airport operations, in line with the European long-term vision (POD-MIS-1). Two trips between the four largest business hubs in Europe are simulated: Amsterdam, NL to Barcelona, ES and Paris, FR to London, UK. Travel times are analysed for car/taxi, public transport and USTI.

For this analysis, several assumptions are made:

- Travel times for car/taxi and public transport are calculated using Google Maps Distance Matrix API.
- Travel times for car/taxi and public transport are calculated during peak hours, as for these hours the use of USTI is most beneficial.
- For travel by car/taxi and public transport the estimated time spent at the departure airport is 1:10 hours, to account for baggage drop-off and screening.
- For travel by car/taxi and public transport, boarding is assumed to take 35 minutes.
- For travel by USTI, the estimated time at the departure airport is 30 minutes, as according to subsection 15.3.3.
- For travel by USTI, boarding time is assumed to be 15 minutes because of priority boarding.
- Deboarding the aircraft for all modes of transportation is assumed to last ten minutes.

The travel time breakdown for this trip by taxi, public transport and USTI can be seen in Figure 19.1 and Figure 19.2. As can be seen, most time is saved for travelling to and from the airport. Also, time is saved during airport operations, but not as significant. For these trips, the door-to-door travel time is reduced to below four hours, as the requirement states. However, if the flight times are longer than for these trips, or the passenger has to be picked up at a location further away from the airport, it can not be guaranteed that the door-to-door time is four hours. Therefore, it is concluded that this requirement is nearly met.

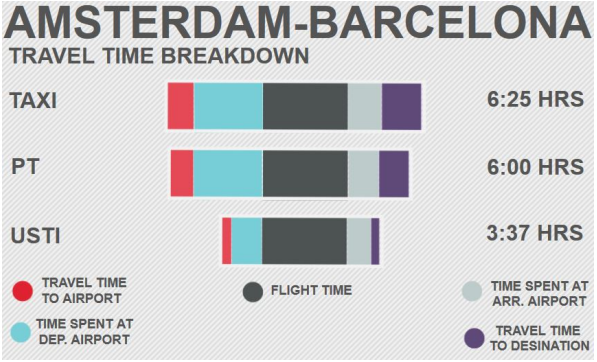

Figure 19.1: Travel time breakdown for a trip from Amsterdam to Barcelona by taxi, public transport and USTI

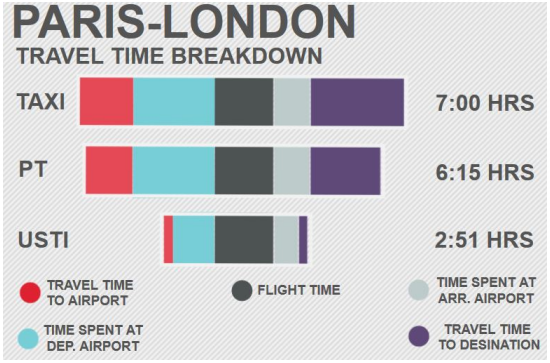

Figure 19.2: Travel time breakdown for a trip from Paris to London by taxi, public transport and USTI

Recommendations to further decrease the door-to-door travel time would be to increase the cruise speed of the pod, or to further optimise the airport operations. This could be done by locating the lounges closer to the existing gates. For new airports to be designed, it can be considered to optimise the new airport for USTI operations. This way, even more time could potentially be saved.

19.1.2. European Coverage Requirement Analysis

Another of the mission requirements is that the range should be sufficient such that 90 % of Europe should be able to use the system to get to an airport (POD-MIS-1). Combined with the requirement that the system shall be able to be implemented in airports with a passenger number greater than 10 million, this requirement is hard to meet. The current coverage of the system can be seen in Figure 19.3.

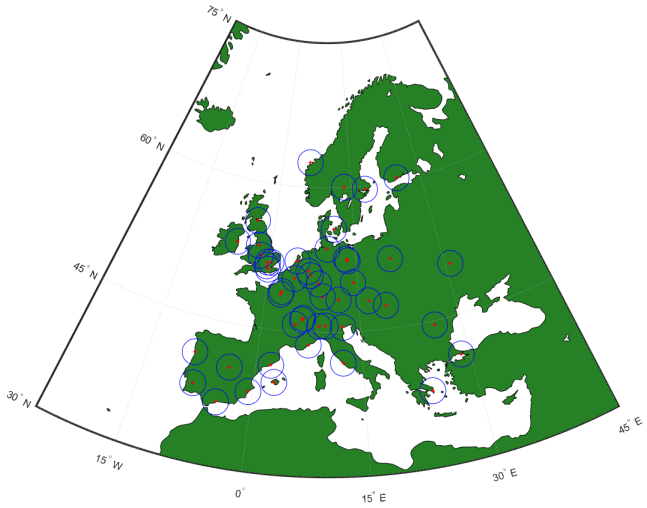

Figure 19.3: European coverage with current USTI implementation

It is safe to assume that this does not cover 90 % of the European population. However, it is reasoned that this requirement is not of high importance when the focus of the system is to transport business travellers. These business travellers mostly live in the urban areas around big cities, which are covered by the system.

19.1.3. Autonomous Operation Requirement Analysis

Another mission requirement was that the system should be able to operate fully autonomously to minimise extra personnel cost (POD-MIS-6). However, the system is designed to operate autonomously in most phases of operation, but the airport operations still involves human operations. Furthermore, the pods are monitored by air traffic controllers in the control centre to externally operate the pods. This is done as regulations do not allow full autonomous operation for flying vehicles.

To further automate the operations, a few options can be considered: automate the luggage unloading and further automate the screening system. Automating the luggage take-out system is hard to implement in current airport infrastructure. However, for the 'airport of the future', a system might be designed such that there is a robot arm at the USTI parking spot, which that automatically transfers the luggage into the conveyer belt system. To further automate the screening, the CT-scanner technology described earlier should be further tested for reliability. Once reliability can be fully assured, there is no need for monitoring people any longer.

19.1.4. Waiting Time Requirement Analysis

One of the system requirements states that the passengers shall not perceive any waiting time (POD-SYS-OPP-9). Whereas in every aspect of the design, effort is put in to minimise the waiting times, there are a few instances where the passenger has to wait: during the conversion from driving to flying mode and during the airport operations in the lounge.

The waiting time during the airport mainly comes from the fact that the passenger still has to walk from the USTI lounge to the gate. In the 'airport of the future' vision, this walking is eliminated or reduced by landing closer to the required gate or distributing the lounges more evenly over the airport.

19.1.5. Recyclability Requirement Analysis

One of the driving requirements of this project is to create a design that is at least 60 % recyclable by its Operational Empty Weight (POD-SYS-OPP-12). In this case, the operational empty weight is assumed to be the sum of the components described in Equation 19.1.

$$m_{OE} = m_{gear} + m_{structure} + m_e \tag{19.1}$$

Note that the propellers and interior are not included in this calculation. However, it can be assumed that seats, for example, can be removed and resold after use. In the pod design phase, the design is extensively driven towards the selection of recyclable materials. This led to the selection of a full aluminium truss structure and tyre rims, which are fully recyclable. Moreover, the skin material of the main body and empennage is selected to be polypropylene, which is also fully recyclable. Additionally, rubber is used for the material of the landing gear tyres. Finally, a study by *university of China* found that on average, 60 % of the engine mass is recyclable [59].

Taking everything into consideration, 78 % of the operational empty weight can be recycled. This is well within the set requirement of at least 60 %. Please note that this is the *potential* weight that can be recycled. The actual recycling of material is dependent on the operator.

19.1.6. Stable Flight Requirement Analysis

During the initial design phase, the requirement was set that the pod should have both statically and dynamically stable flight characteristics (POD-SYS-F-8, POD-SYS-F-9, POD-SUB-FC-1 and POD-SUB-FC-2). These requirements were set as safe flight is only possible when full stability is assured.

Whereas the current design is stable in horizontal flight direction, it is inherently unstable in vertical flight. This is due to the vertical take-off motors being coaxial and their line of action not always being able to correspond with the centre of gravity location. Still, safe vertical flight is assured, as the thrust vector can be rotated by changing the angle of attack of the propeller blades. This way, it can be assured that the thrust vector always goes through the centre of gravity. Therefore, no undesired pitching moments are generated.

19.1.7. Driving Mode Size Requirement Analysis

For the size of the pod in driving mode, the requirement is set within 4.7(l)x1.7(w)x2.0(h) m (POD-SYS-D-13). The final size of the pod in driving mode is 5.10(l)x2.0(w)x1.77(h) m. There are two reasons for not meeting this size requirement: the width of the attachment location of the wing to the fuselage was not correctly accounted for and the attachment of the motors to the wing was not properly accounted for. It is recommended that in further design phases, it should be analysed whether it would be feasible to implement the wing tip motors within the size constraint.

However, even though the exact constraint is not met, the pod will still be allowed to drive on the road. The only reason for trying to meet the size constraint in the future would be to increase manoeuvrability of the pod and to be able to drive in smaller urban areas. Therefore, in this design phase, no iteration is done to more accurately meet this requirement.

19.1.8. Airport Infrastructure Requirements Analysis

Three requirements regarding airport infrastructure are not met. The first requirement states that the passengers should be able to travel from the pod to the aircraft within fifteen minutes (POD-SYS-PL-1). In the current implementation of USTI within Schiphol Airport, this time is thirty minutes. The main reason for not meeting the requirement lies within the fact that the current infrastructure of Schiphol Airport is adhered to. Therefore, passengers are dropped off at the taxi drop-off and have to walk through the departure hall to the USTI lounge, which increases the travel time. It is recommended that, if the airport infrastructure allows for it, the passenger drop-off and the USTI lounge are located at nearly the same location. This way, the pod-to-aircraft time can be reduced to meet the requirement.

The second requirement states that the airport infrastructure cannot be changed for the implementation of the USTI system (POD-SYS-PL-2). Within the current infrastructure and layout of Schiphol, it is found that it is not possible to combine this requirement with the previous requirement that short pod-to-aircraft time shall be assured. Therefore, the choice is made to place the USTI lounges at the current airport. This means a change in airport infrastructure.

The last requirement states that storage of the pods shall be stored within airport infrastructure (POD-SYS-ST-1). However, when analysing the possible storage design options, it was reasoned that storing the pods in a separate building close to the airport would be more feasible. Therefore, this requirement was deemed superfluous.

19.2. Sustainability Analysis

After the initial assessment of sustainability in chapter 4, certain aspects are improved upon. These merely include environmental aspects, which are measured through the EcoDesign Strategy Wheel, as introduced in chapter 4. In this

section, the initial design is compared to the final design using this method.

19.2.1. Emissions

The range extender selected in chapter 6 has a very high efficiency of 31 %. With the specific emission of 0.72 $\frac{kg}{L} CO_2$ [46]. With the fuel tank capacity calculated in this section, the amount of CO_2 emitted by the burning of fuel is found to be 21.6 kg/pax. To find the total emissions per passenger, the batteries are included.[1] Using an appropriate safety factor, a total emission of 35 kg/pax of CO_2 is found on a 300 km journey.

Another type of emissions are the NOx emissions. These emissions are estimated using reference values from S. Ibrahim et al.[53]. The paper gives two possible reference values. To verify both methods, the emissions are calculated using both of these values. The first method uses the typical percentages that make up exhaust gases. The paper states that CO_2 and NOx typically make up 6.25 % and 0.212 % of the exhaust gases. Using the previously calculated values from the CO_2 calculations results in a NOx emission of 0.7327 kg/pax. The other method uses the engine emission factor, which is 2.59 g/kWh. Using an energy density of 9.5 kWh/L [2], the previously mentioned fuel tank volume and the same safety factor used in the CO_2 emissions, the total NOx emission is found to be 0.7381 kg/pax, which is only a difference of 6 g compared to the previous calculation.
Other modes of transport perform as following:

- The average new car available on the market produces 40 kg of CO_2 per passenger on a similar journey [39].
- An average ride with public transport causes an emission of 0.023 kg CO_2 per km per passenger. This is equal to 6.8 kg of CO_2 emitted per passenger [39]. The calculations for public transport include not only trains, but also busses, trams and metros.

19.2.2. Environmental Performance

During the detailed design of the pod, the subsystems are designed to form a more sustainable solution compared to the initial design. The progress and impact compared to the initial design can be seen in Figure 19.4.

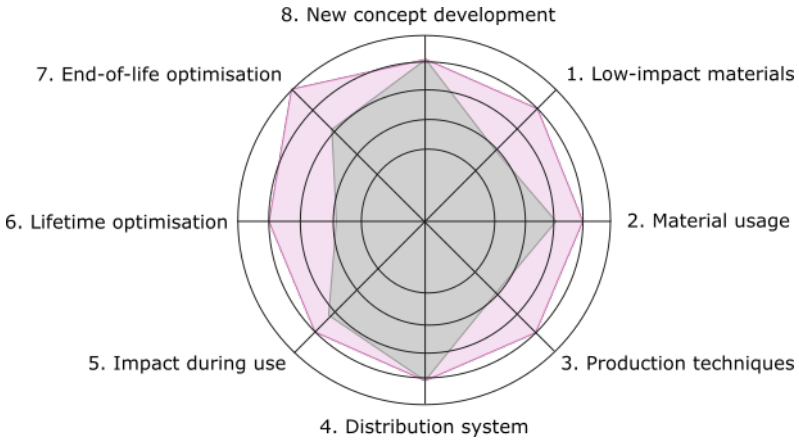

Figure 19.4: Comparison of the initial pod system (grey) and the finalised pod system (pink) using the EcoDesign Strategy Wheel

The reasoning for the scores in the wheel are shortly elaborated below. Please note that a more elaborate clarification is given previously in each chapter.

1. **Selection of low-impact materials.** The pod scored significantly better on this matter by changing to materials that are recyclable and renewable. For example, using materials such as polypropylene for the skin and polyethylene for the fuel tank instead of the initial concept which included carbon fibre.
2. **Reduction of materials usage.** The design has worked towards the selection of the most lightweight design. The selection of a truss structure over a skin-stiffened structure decreases the material weight. Also the density of polypropylene used in the skin is lower than that of carbon fibre.
3. **Optimisation of production techniques.** Aluminium and polypropylene require few steps to manufacture. In the initial design, carbon fibre was one of the used materials, which is generally hard to design.
4. **Optimisation of distribution system.** No significant changes occurred in this area throughout the final design. The logistics aspect remained the same.

[1] Mobiliteit in cijfers. 2013, *date accessed: 23-05-2018*, `https://9292.nl/co2-informatie`
[2] Energy density, *date accessed: 20-06-2018*,`https://en.wikipedia.org/wiki/Energy_density`

5. **Reduction of impact during use.** The overall score increased due to the design having less energy waste now. The range extender selected for the propulsion system has a high efficiency, which led to a decrease of 13 % in CO_2 emissions compared to conventional cars (as calculated in chapter 10. In Figure 19.5, it can be seen that public transport emits significantly less CO_2.

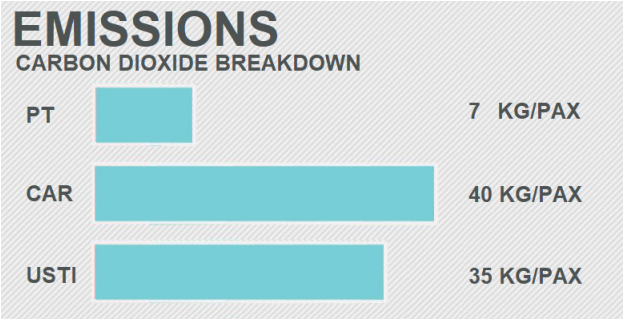

Figure 19.5: Comparison between carbon-dioxide emissions

6. **Optimisation of initial lifetime.** A significantly higher score is assigned to the final designed when compared to the initial design. Especially for maintenance, repair and adapting a more modular design. For example, a clicking mechanism is used to connect the empennage to the fuselage enabling easier maintenance and a lightweight design. Also the repair of materials such as aluminium and polypropylene is generally easier than carbon fibre, which was partially used in the previous design.
7. **Optimisation of end-of-life system.** The pod has an improved recyclability rate by changing to polypropylene. Aluminium also performs well in terms of incineration and reuse.
8. **New concept development.** No significant changes occurred in this area throughout the final design. The system still scores high on this matter as it has a good integration of functions and the shared use capability of the product.

19.2.3. REACH requirements

Only materials adhering to REACH requirements established by the European Chemicals Agency can be used. It should be noted that some substances fall under the so-called CLP regulations of the EU. The purpose of the CLP regulations is to complement the REACH regulations. The compliance of the materials can be found in Table 19.1. There are exemptions for some materials when used in certain ways. For example when certain materials appear in small amount in alloys. [3]

Table 19.1: Substance compatibility with the REACH requirements

Substance	Formula	Classification	REACH / CLP approval
Aluminium	Al	Flammable, but uses are allowed[4]	✓
Copper	Cu	No hazards have been classified[5]	✓
Manganese	Mn	No hazards have been classified[6]	✓
Polyethylene	(C2H4)n	Flammable, but usage is allowed[7]	✓
Polypropylene	(C3H6)n	No hazards have been classified[8]	✓

19.2.4. Social and Economical Performance

Even though the presented tool focuses on the environmental aspect of sustainability, the social and economical impact of USTI are also apparent. This is most notable in the following aspects of the system:

- Design for noise reduction. This is amongst others done by optimisation of the rotors for only horizontal or vertical motion.
- Local employees and manufacturing sites. This creates economical and social welfare in the local community.
- Passenger comfort, which follows from (1) large cockpit design and (2) user-friendly interface in both the pod and on the application.

[3] EU Commission Directive, Official Journal of the European Union. 2017, date accessed: 29-05-2018, https://eur-lex.europa.eu/legal-content/EN/TXT/PDF/?uri=CELEX:32017L2096&from=En

20
Production Plan

When entering the manufacturing phase, a production plan is essential. It is a plan of the production of a product, from start to finish. This is done to leave no room for ambiguity and to make the process repeatable [55]. Another reason is to ensure the correct amount of resources are available. The plan consists of a description of the manufacturing, assembly and integration of the product. The planning includes:

- *A Target Date Chart*, showing the periods reserved for a certain part of the production.
- *A Master Production Schedule*, giving a rate of completion for the manufactured parts
- *A Factory Schedule*, giving a rate of production for parts on which manufacturing operations are performed.
- *A Material Delivery Schedule*, in which the external material and contractor rate is described.
- *Detailed Jig and Tool Availability Schedule*

20.1. Manufacturing Plan

Manufacturing is separated into three parts: main body, empennage and wing. These parts are manufactured in batches before entering a final assembly line, which is described in the next section. The production and manufacturing processes are also discussed.

The main body of the pod is formed by first producing the truss structure, as this is the 'backbone' that carries all the loads. The structure is made by joining extruded parts of aluminium (material selection performed in chapter 8) [20]. The trusses are then welded to each other using machines with great precision. The process of welding is done at very high temperatures and high pressure, which introduces risks for the manufacturing crew [23]. However, this method is the most (risk-) effective production technique compared to its alternatives. Afterwards, the polypropylene skin is attached. Two parts are used that together form the entire skin. Using two parts is necessary, because their division line is where the skin is attached around the truss structure. The polypropylene is formed by heat moulding. Although creating moulds is generally expensive, it is a profitable option. This is because there is a large number of identically shaped pods that will be produced. Two symmetrical skin parts are created to use the same mould twice for the same pod. To mount these parts to the structure, attachment plates are connected to the truss structure to ensure a sufficiently large connection area. The landing gear, lights and interior of the main body are installed afterwards.

The wings are created in a similar manner as those of conventional aircraft. Firstly, the ribs and spars are manufactured out of thin sheets of aluminium by cold forming machines. Holes for riveting and bolting are created and deburred by appropriate machines and checked by workers. Afterwards, these components are riveted together. The wing skin is attached last, by riveting it to the spars and ribs. The motors are mounted to the wing after the wing structure is connected to the rest of the pod. This is done because moving around the entire wing structure with the motors attached to them poses a greater risk than introducing the motors at the assembly line.

The empennage is manufactured by first creating the aluminium ribs and spars through cold forming a metal sheet on a die and punching the required holes into the sheet. They are bolted together and the landing gear is attached to the horizontal tail rib. Afterwards, the polypropylene skin is attached. Unlike the fuselage, the empennage skin is fastened to the inner structure by means of bolting. The production of the empennage surface is done in two symmetrical parts, which is similar to the scenario of the wing.

20.2. Assembly Plan

After the separate parts have been manufactured in batches, the final assembly is done on an assembly line. This is the most efficient type of assembly when considering series production, since one worker performs the same action instead of following the product. The Gannt-chart of both the part manufacturing phase and the assembly phase is shown in Figure 20.1. The estimated throughput time for the assembly of the pod is eight days, as found in chapter 18. Please note that in the weekends the production is paused. Also, this is the estimated time in the most optimised assembly case. Due to the estimated learning curve, the assembly of the first prototype is more likely to be produced in a matter of months. As found in Figure 20.1, the production of the main body is performed in the same time frame as the production of the wings, empennage and landing gear. This indicates two separate teams working on the manufacturing of these parts.

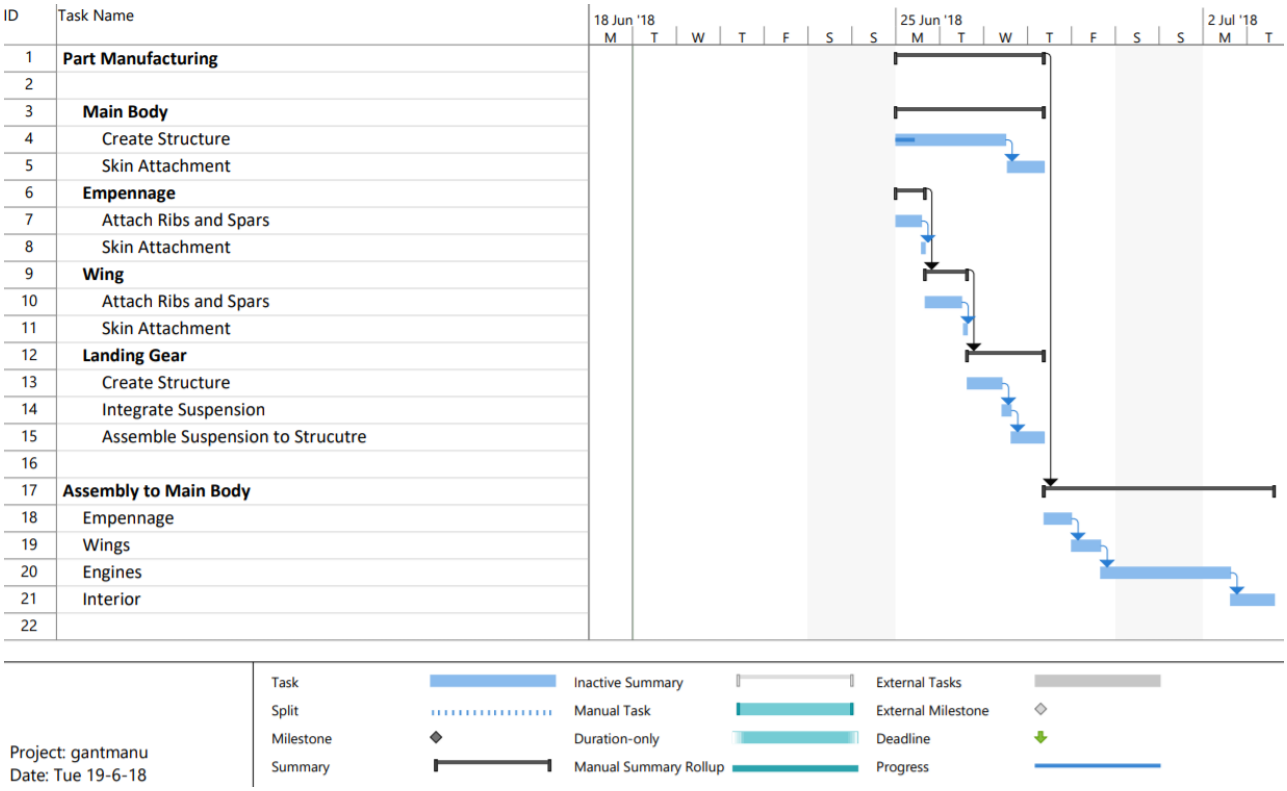

Figure 20.1: Pod manufacturing timeline. Note that the weekends are included. The same time is required at every station in assembly

They create their own batches of parts. The assembly to the main body is depicted in Figure 20.2.

The empennage is attached in step three, after which the wings and rotors are mounted in step four and five respectively. All parts are assembled around the main body of the pod. For this reason, the figure also depicts the part manufacturing of the main body in steps one and two. A more general overview of the batch and line assembly can be seen in Figure 20.3 [54].

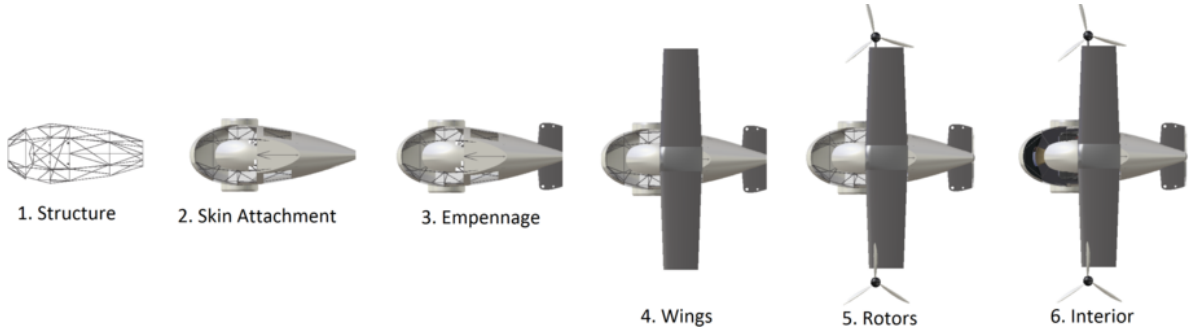

Figure 20.2: High-Level Assembly Flow

As described in chapter 8, the empennage and main body will be connected through a snail cam mechanism. The clicking mechanism is locked after the mechanism is in place to ensure that the parts are not separated during flight. It remains possible to mechanically open these locks for maintenance purposes.

The wings are mounted to the fuselage at the hinge point around which the wing will rotate. The hinge is integrated in the structure of the main body where it is attached to the plate separating the passenger and luggage compartment in the fuselage. It forms the natural connection point between wing and body. Upon connection, the hinge is locked into the wing and then bolted for extra robustness. The manufacturer should act with great care as this is identified to be a critical point in the design. As described in chapter 8, a bracket is attached to the rotors, which makes assembly to the back of the horizontal tail very feasible with of rivets and bolts. The bracket of the wing-mounted motors is attached to a supporting structure. This structure is attached to the wings in the final assembly by bolting to the most forward spars in the wing.

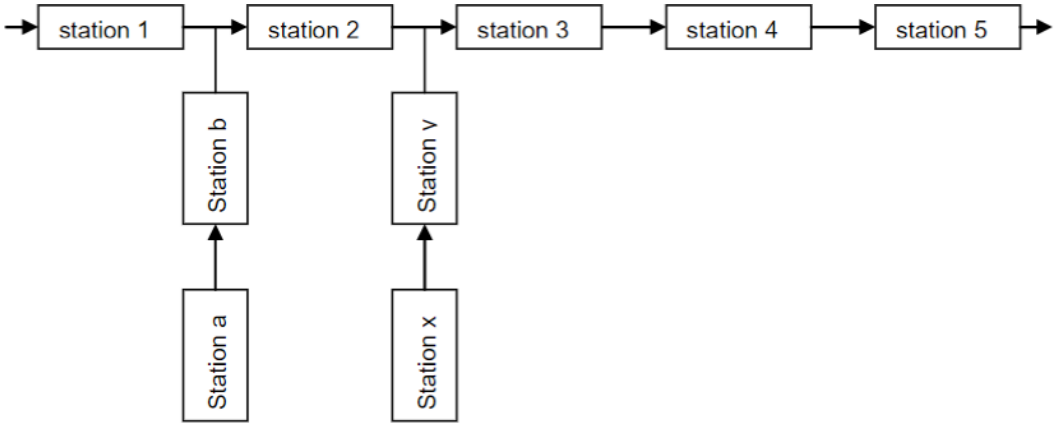

Figure 20.3: Flow of the assembly line (horizontal) with an inflow of separate parts (vertical), created in batches

20.3. Integration Plan

The facility location and lay-out required to meet the manufacturing time of eight days is described in the integration plan. The plan also touches upon the availability of resources and people allocation.

The pods are produced in a factory close to the primary location of operation. For now, the project is assumed to first roll out in the Netherlands. There are multiple reasons that can be linked to this decision:

- A positive effect on the local community because of job opportunities
- Tractability of the used ethics in the factory
- Close communication between the design and manufacturing team

Multiple factors influence the size of the factory, starting with the size of the assembly line. The assembly of the pod is done at four stations. This is a relative small amount, requiring approximately 50 by 20 metres (four stations multiplied by a little over two times the pod length long and wide enough to fit the wing span). Another parameter used to determine the factory size is the batch size that is produced. Buffer parts are created and not used directly after manufacturing, which requires storage space [54]. It should be noted that the work stations where the separate parts are created do not necessarily have to be situated close to each other.

The storage capacity for the buffer is determined by considering the amount of parts manufactured in-house. The structural components are produced in-house, but the internal systems and engines are bought off the shelf. This contributes to a reduction in the size of the factory.

The allocation of employees is different for line assembly and part manufacturing. On the assembly line, the same task is performed by the same people. The time allocated for each of these tasks is fixed and is the same for all stations [54]. In Figure 20.1, this is taken into account. In part manufacturing, employees perform different tasks on one part.

Sustainability

The design contributes to the UN Sustainable Development Goals by taking the following measures:

- Local employees, which has a positive impact on the local community and its wealth.
- Manufacturing methods are optimised to produce the least waste and to expose the employees to the least risk possible.

21

Risk Assessment

During the design and operational phase, the system phases several risks, both technical and operational. In this chapter, a qualitative analysis of these risks is performed. This is graphically represented by the use of a risk map. Moreover a RAMS (reliability, availability, maintainability and safety) analysis of the system is provided.

21.1. Technical Risk Assessment

This section contains the assessment of the technical risks for the different parts of the system. Risks that are not properly managed may lead to unforeseen drawbacks that could negatively affect all other parts of the project. Therefore, for the most prominent risks an assessment of the likelihood and an assessment on the consequence of the risk is made. The likelihood is linked to the maturity of the technology and the state of the technology. The consequence is linked to the severity of the impact.

21.1.1. Risk Assessment

A qualitative approach is applied for the risk assessment. Each risk is assigned a level of likelihood and a level for the consequence. The combination of these factors determines the severity of the risk. For the probability of occurrence of the discussed events, the scale presented in Table 21.1 is used. The scale has five classes, listed with increasing probability of occurrence.

Table 21.1: Levels of measurement for likelihood

Tier	Class	Description
1	Proven model design	Operative existing design
2	Extrapolated from existing model	Based upon existing model from same field but not similar
3	Existing model from different field	Based upon models from other (engineering) fields
4	Working laboratory model	Not operative outside laboratory. Needs V&V
5	Feasible in theory	Idea capable to be done or put into effect

For the consequence of an event, the scaling shown in Table 21.2 is used. It is listed with increasing order of severity of impact.

Table 21.2: Levels of measurement for consequence

Tier	Class	Description
1	Negligible	Inconvenience or non-operational impact
2	Marginal	Degradation of secondary mission or small reduction in technical performance
3	Critical	Mission success is questionable or some reduction in technical performance
4	Catastrophic	Mission failure or significant non-achievement of performance

21.1.2. Risk Map

The summary of the risk analysis can be seen in Table 21.3. Plotting all these values in a risk map leads to Figure 21.1 for the technical part of the system, and Figure 21.2 for the operational side of the system.

Table 21.3: Risk assessment table expressing the risks in terms of likelihood and consequence. The risks are also assessed after mitigation actions.

Technical Risks						**Operational Risks**					
Label	Risk	Before		After		Label	Risk	Before		After	
		L	C	L	C			L	C	L	C
CO-1	Connection loss with airport	1	4	1	2	OP-1	Public opinion after crash	2	3	-	-
CO-2	Connection loss with pod	2	3	1	3	OP-2	Overcrowded USTI lounge	2	1	1	1
PP-1	VTOL propeller damage	1	4	1	2	OP-3	User delayed at pickup point	4	2	2	2
PP-2	Back propeller failure	1	4	1	2	OP-4	Operator unavailability	2	3	1	2
PP-3	Range extender failure	1	3	1	2	OP-5	Unavailability due to bad weather	2	4	1	3
PR-1	Comply with regulations	5	3	4	3	OP-6	Unavailability due to overbooking	3	4	2	2
PR-2	Exceed cost budget	4	4	4	2	OP-7	Maintenance error	3	4	1	4
PR-3	Exceed development time	3	4	3	2	OP-8	Stuck in traffic in driving mode	4	3	2	2
ST-1	Structural failure wing	2	4	1	4	OP-9	Door not opening	1	2	-	-
ST-2	Impact during flying	2	3	1	3	OP-10	Passenger gets lost in airport	3	2	1	2
CT-1	Sensor failure	3	4	1	2	OP-11	No landing space	2	4	1	4
CT-2	Hacking	3	4	-	-	OP-12	Screening system failure	3	2	1	2
CT-3	Pod control computer failure	1	4	1	3						
CT-4	Pod control surfaces failure	1	4	1	2						
DR-1	Autonomous driving failure	1	4	-	-						
DR-2	Lights failure	2	2	-	-						
DR-3	Popped tyre	2	3	2	2						
DR-4	Shock absorber failure	1	2	-	-						
DR-5	Road accident	3	3	1	3						
DR-6	Rear wheels not extending during landing	1	4	1	2						
ES-1	Battery explosion	2	4	2	3						
ES-2	Battery failure to provide power	1	4	1	2						
FS-1	Fuel tank explosion	1	4	1	3						
FS-2	Fuel tank leak	1	3	1	2						
IS-1	Environmental control failure	2	1	-	-						
IS-2	User damage	2	2	-	-						

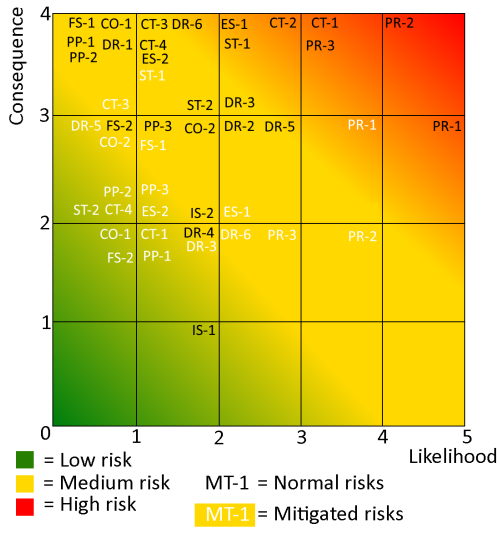

Figure 21.1: Risk map for technical part of the system. Black and white are before and after mitigation, respectively

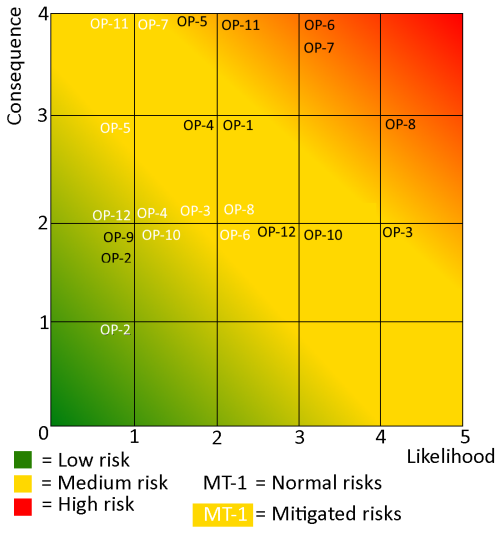

Figure 21.2: Risk map for the operations part of the system. Black and white are before and after mitigation, respectively

21.1.3. Technical Risks

The identified risks are discussed in this section. If applicable, every elaboration includes a possible mitigation for the risk is given.

CO-1: Connection loss with airport. It might be the case that the pod loses connection with the airport or operator due to for example a power outage at the airport. This means that the airport can not tell the pod whether to land or not, as landing at airports is a complex procedure. This risk is mitigated by making the pod autonomous and supplying it with enough sensors to be able to land on its own.

CO-2: Connection loss with pod. It might also be possible that the operator loses connection with the pod due to a failure of the pod communication system. This might lead to catastrophic events, therefore this risk is mitigated by adding a redundant transponders on the pod.

CT-1: Sensor failure. During the operations, the sensors can possibly stop working. This might lead to failure of the system. This risk is mitigated by including redundant sensors as mentioned earlier in chapter 9.

CT-2: Hacking. Due to the full autonomy of the system, hacking poses a risk in this day and age. The mitigation of this risk is left out for now, as designing for optimisation against malware is beyond the scope of this project.

CT-3: Pod control computer failure. It can occur that the flight control computer fails. This can lead to the pod crashing and thus catastrophic failure. This risk is mitigated by selecting a flight computer that has redundancy included.

CT-4: Pod control surfaces failure. The control surfaces of the pod can also get stuck or fail due to other reasons. The pod can switch to VTOL mode or cruise mode depending on what control system has failed to mitigate this risk. For example, if the elevator fails, the pod can switch on the VTOL engines to perform a safe landing.

DR-1: Autonomous driving failure. Autonomously driving vehicles have caused some accidents in the past, some very catastrophic. Therefore, it is important to analyse the risk of failure of the driving system. It is recommended to mitigate this risk with a specialised team as technology for this is rapidly changing over time.

DR-2: Lights failure. Especially during the driving mission, the lights of the pod might fail, causing it to be a danger on the road. This will lead to delays, since another pod needs to come or the lights need to be fixed.

DR-3: Popped tyre. As with all cars, tyres might pop during driving. This can cause a risk, since the pod will not be able to drive to a location where it can take-off. The tyre should be replaced. If circumstances allow it, the pod can still take-off vertically to mitigate this risk.

DR-4: Shock absorber failure. This risk is not critical, the journey might be a bit uncomfortable for the passenger, however the pod is still able to make a landing without damaging the rest of the structure and only needs to go in for maintenance.

DR-5: Road accident. This risk originates from the possibility that the pod will be involved in a road accident which is not the fault of the autonomous driving system. For example, someone else ignoring a red light and hitting the pod. This risk can possibly be catastrophic. However, it is mitigated by designing the structure such that it can take the load of an impact as well as including enough sensors for the driving system to prevent such events.

DR-6: Rear wheels not extending during landing. This might cause some damage in the landing procedure. This is very critical, since a damaged pod can lead to delays as well as costs for the repair of the pod. This risk is mitigated by designing the VTOL motors such that they are able to perform a very soft touchdown to ensure minimal damage.

FS-1: Fuel tank explosion. An explosion can result to mission failure. Mitigation of this risk consists of suppressing by decreasing the oxygen concentration in the relevant compartment and make a casing that limits the dissipated energy.

FS-2: Fuel tank leak. The fuel tank might start leaking, which causes the fuel to deplete rapidly. To mitigate this risk, the pod will be able to fly to a suitable landing position using the batteries installed. This will delay the passenger, however it prevents catastrophic injuries and failures.

ES-1: Battery explosion. Current batteries are not thermally stable. Therefore, there is the risk of a battery exploding and catching fire. This can lead to very dangerous situations. This is mitigated by covering the battery in an explosion resistant housing.

ES-2: Battery failure to provide power. When the batteries fail to provide power, the VTOL capability might be impeded. Therefore, the pod will not be able to land and this will cause catastrophic failure, possibly resulting in injuries.

The pod will be able to land on an airstrip with the back propeller running to mitigate this risk. The back propeller is driven by the range extender in the back. This range extender can directly provide power to the back propeller motor.

PP-1: VTOL propeller damage. The propellers of the VTOL motors might be damaged or stuck in their folded state. This would mean the pod will not be able to land safely. However, similar to ES-2 this is risk is mitigated by the fact that pod can land on an airstrip with the back propeller. A gliding flight is also a possibility.

PP-2: Back propeller failure. This risk will stop the pod from being able to cruise to its destination. Mitigation of this risk is performed by selecting the cruise altitude such that a considerable distance can be glided, as well as the possibility to convert to VTOL to prevent injuries.

PP-3: Range extender failure. This risk can be detrimental for the flying range of the pod. The batteries can provide enough energy for the motors to reach a safe landing location as mitigation of this risk.

PR-1: Comply with certification and regulations. As the autonomous flying and driving pod is a new way of transportation, certifications and regulations are not fully developed yet. At the moment, autonomous driving is only allowed for experimental purposes. However, the trends are developing in favour of autonomous driving.

PR-2: Exceed cost budget. This risk causes project delay and difficulties in feasibility. Mitigation consist of taking larger cost margins and contingencies for the manufacturing costs. For the development costs one can search for more investors and funding.

PR-3: Development time exceeded. This risk delays the start of production and thus the start of the operational phase. This in term causes the cost to increase and thus the profit to decrease. This risk can be mitigated with a good marketing strategy, this attracts enough investors to compensate for the increase in cost.

ST-1: Structural failure wing. Having wings that swing back during the driving part induces higher risk than for conventional aircraft. Nonetheless, safety regulations constrain the wing failure likelihood to be low, since extensive testing needs to be done to be able to certify the aircraft.. Mitigation actions consist of checking more often for metal fatigue and crack propagation.

ST-2: Impact during flying. There is always the risk of flying into birds or other objects that occupy the airspace. Depending on the size of the object, this can catastrophically damage the pod. Enough sensors are included to detect and perform evasive manoeuvres in time to mitigate this risk.

IS-1: Environmental control failure. Just like HVAC systems in current day cars, the HVAC can break down. This causes some slight discomfort for the passenger, however the risk is not critical since the passenger will be on time and the pod is still able to perform the mission. Therefore no mitigation is in place.

IS-2: User damage. Vandalism is always an issue with transporting companies. Aside from this, the user might accidentally damage the pod during operations. This risk is not likely however, since the target customers are not necessarily vandals.

21.1.4. Operational Risks

The risks associated with the operations can be analysed now that the operational aspect is designed. As can be seen from the risk map in Figure 21.2, there is some critical risks associated with the operational part. The consequence of the operational risks are mainly delays at the airport. Every risk will be discussed and the mitigation during the design procedure, if any will be explained as well.

OP-1: Public opinion after crash. This risk is included since it is possible that a pod will crash even if extensive testing is done and adequate measures are in place to prevent this. If this event leads to injuries or even worse to a fatality, this might negatively affect public opinion and thus the number of passengers making use of this system. This will lead to lower revenues and therefore the consequence of such an event is high. The risk can be mitigated by hiring a good marketing team to minimise the potential damage a situation like this.

OP-2: Overcrowded USTI lounge. It might occur that the USTI lounge becomes quite crowded if a lot of passengers arrive at the same time. If too many passengers make use of this system, the USTI lounges will get to crowded and this might cause some delays. This risk is mitigated by developing an efficient algorithm to smoothen the arrival time of the pods as well as setting the price of a trip such that only the target customers are interested in using this system.

OP-3: User delay at pick-up location. This risk comes from the fact that a user might be delayed or forget to go to

the location of pick-up. This can be the result of distraction that cause the user to forget to go to the location of pickup in time. This might cause delays at the airport. This is mitigated with reminder for the passenger some time in advance.

OP-4: Operator unavailability. This risk is based on the fact that some workers in the operation centre might go on strike if the working conditions are not satisfactory or if a big number of employees become sick. This might lead to unsafe conditions if the pods need help from the operator to make a decision, or if a passenger requires assistance in the case of a health issue. Therefore, it might even be so that pods need to stay grounded as a consequence of this. This risk is mitigated by hiring enough people such that substitutes are available in such events as well as including as much automation as possible.

OP-5: Unavailability due to bad weather. This risk is associated with cases of bad weather that the pods are not able to fly. In these situations the operational risks are quite high, since it might cause delays at the airport. This risk is mitigated by only driving in such situations if possible. This means that it takes longer to get to and from the airport. In such events, the pod can leave the station earlier to pick up the passengers.

OP-6: Overbooking. It might be the case that the pods are overbooked. This means that more pods are booked than actually available. This is a risk that can cause big delays in the system overall as well as the possibility of losing customers and trust in the product. This risk is mitigated by having multiple pods available for overflow.

OP-7: Maintenance error. It is always possible that the maintenance might not detect a crack or damage on the pod in any way when inspecting or repairing the vehicle. This risk might lead to the pod crashing in the worst case scenario. This risk is mitigated by incorporating autonomous inspection by a machine as well as inspection by a human afterwards.

OP-8: Stuck in traffic in driving mode. During driving it can occur that the pod encounters heavy traffic. This might cause the pod to be delayed at the take-off side, which causes a delay at the airport. To mitigate this risk, enough landing and take-off sights are selected around busy cities, meaning that the pod spends the minimum amount of time on the road.

OP-9: Door not opening. This risk might occur when the pod is not able to identify the passenger. However, since there are cameras and microphones on the pod, an operator will be able to identify the passenger and open the pod from distance, causing the risk to be non-critical.

OP-10: Passenger gets lost in the airport. Since the passenger needs to enter the terminal of the airport to reach the USTI lounge, it might happen that the passenger will not be able to find the USTI lounge. This risk is mitigated by including enough signs in the airport that guide passengers to where they need to go.

OP-11: No landing space. If the landing spot at the airport has a defect USTI pod or any other obstacle, the landing spot might be occupied, meaning the pod can not land. This can be very risky, since it might be the case that the energy level on the pod is low and the pod is not longer able to fly. This risk is mitigated by including enough landing platforms as well as reserve fuel and battery capacity to make sure the pod will be able to fly to an alternative landing spot.

OP-12: Screening system failure. When a screening gate fails the passengers need to wait, depending on how many screening gates are present in the USTI lounge. This can cause delays and unsatisfied passengers. This risk is mitigated by including enough screening gates in a USTI lounge as well as the possibility of moving incoming passengers to another USTI lounge.

21.2. RAMS Analysis

In this section the RAMS analysis is performed, where the acronym RAMS corresponds to Reliability, Availability, Maintainability and Safety. These four terms are defined in the following subsections.

21.2.1. Reliability and Availability

Reliability is defined as *'the ability of a system to accomplish a required function during a given time interval'*[7]. Constraints on the availability of the system also should be applied to make sure that the system is *'able to operate when the external means are present'* [7]. The reliability of the system can be checked according to four methods. These are ranked in order of priority as follows:

1. Analysis of computed data
2. Simulation with mathematical models
3. Statistical study of large database
4. Expert judging

The wing and tail design procedure can be checked by applying the first method and analysing the performance of ex-

isting vehicles. Where this is not possible, mechanical models such as FEM and NSWC are used, which belong to the second reliability categories. Regarding the propulsion system the third and fourth method can be applied. A statistical analysis of hybrid engines used for cars is performed and accompanied by the expert judging of the team. The first and second are excluded as a hybrid engine to a flying vehicle is relatively new. Furthermore, regarding the electronics components, reliability tools can be used such as FIDES, which belongs to the second category.

A functional analysis of the system is performed to analyse the connections between each system component. This is represented in Figure 21.3, where three main external parties are considered. These are the users, which relate to the system by using the app and the user interface, the manufacturing company, solely responsible of building the pods, and the service operators, which track the service and administrate all airport operations. Within the system, three subcategories are identified: the pod itself, the airport and the app. Connections between these three components mainly happen through the controllers.

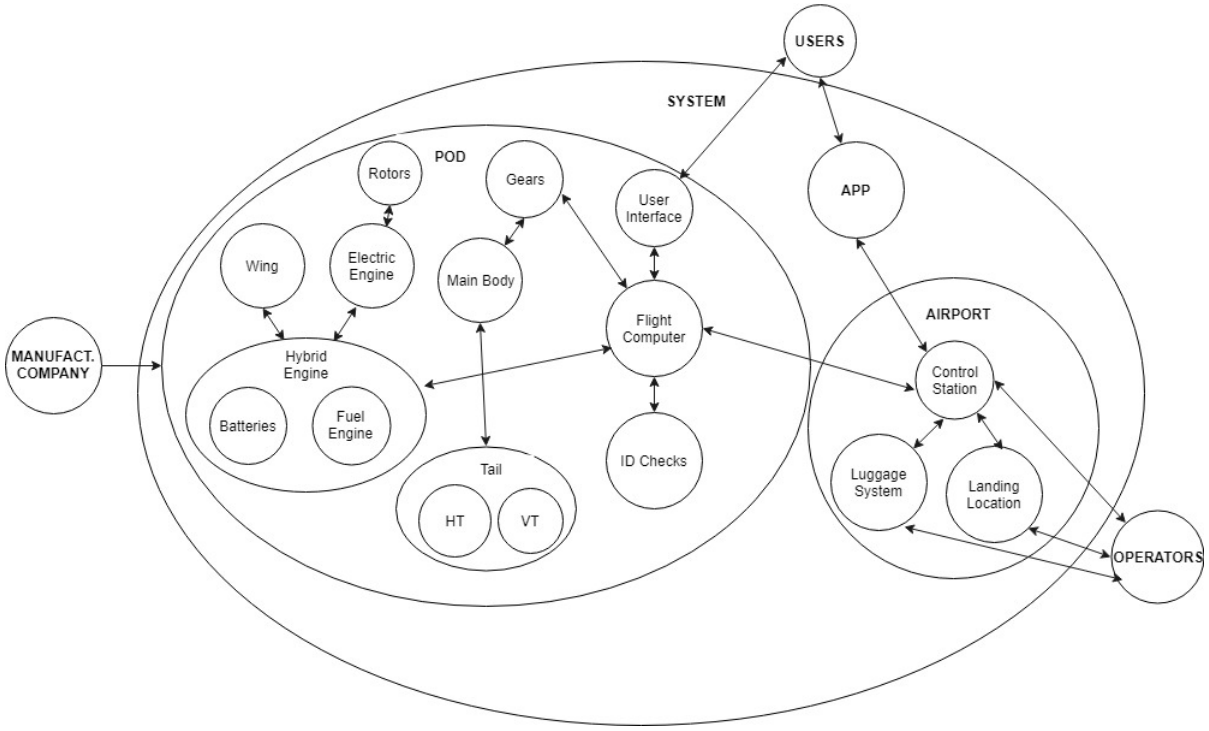

Figure 21.3: Functional analysis diagram

A reliability diagram can be generated to analyse the redundancy of the system: elements can either operate in series or in parallel. When two elements a and b operate in series, the reliability of the system decreases according to Equation 21.1.

$$R_S(t) = R_a(t) \cdot R_b(t) \tag{21.1}$$

On the other hand, when the reliability for elements is indicated in parallel in Figure 21.3, the reliability varies according to Equation 21.2. The elements in parallel correspond to elements that provide redundancy in case of failure due to the other element(s) in parallel.

$$R_S(t) = 1 - [1 - R_a(t)] \cdot [1 - R_b(t)] \tag{21.2}$$

In this case, the reliability diagram is presented in Figure 21.4. The reliability of each element depends on the failure rate and the time period. In general, the most commonly used distribution in the analysis of reliability is the negative exponential distribution. This is represented in Figure 21.5. For this type of distribution, the reliability can be defined as: $R = e^{-\lambda t}$.
The failure rate of each element is estimated according to the complexity and the readiness of the technology. For example, it is assumed that, due to its complexity, the deployable rotors at the wing are more likely to fail than the fixed propeller at the back of the pod. Moreover, the swinging mechanism of the wing is expected to be less reliable than a fixed rotor. The reliability is calculated as $R(t) = 1 - F(t)$. In Table 21.4, the estimated reliability factors are listed. Then, the reliability of each subsystem is calculated by applying Equation 21.2. The final reliability is computed by using Equation 21.1, having a value of $R_s = 0.50$.

This value, which also gives and evaluation of the availability of the system as it proposes alternative approaches, actually considers every failure as critical: in reality, the entire system does not fail if only one subsystem (such as, for example,

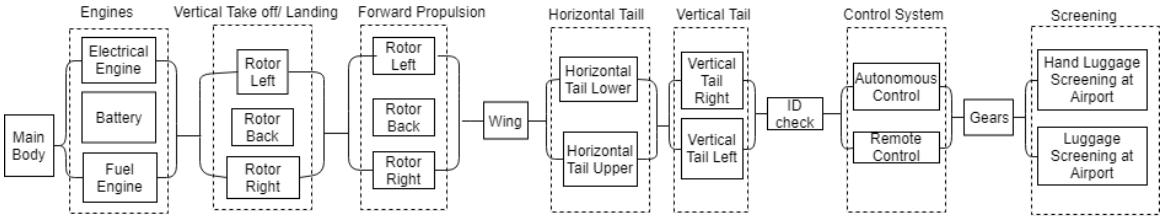

Figure 21.4: Reliability Diagram

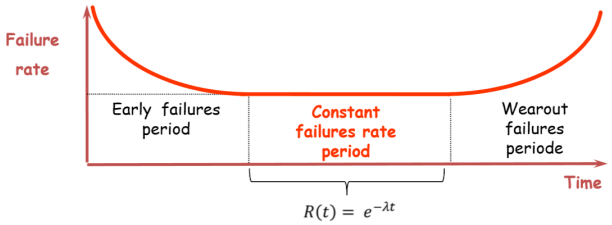

Figure 21.5: Failure Rate vs Time [7]

the screening subsystem) fails.

Table 21.4: Estimated reliability of each element of the pod

Element	Reliability (%)
Rotors at the tips of the wing	80
Propeller at the back of the body	90
Wing	80
Body structure	95
Tail landing gears	95
Fuel engine	95
Battery	90
electric motors	80

Element	Reliability (%)
Vertical tail structure	95
Horizontal tail structure	95
USTI lounge screening	95
Hold luggage screening	95
ID checking mechanism on pod	85
Autonomous control system	65
Remote control system	85
Hold luggage transfer	0.95

For a better understanding of the reliability and availability of the system, two fault trees are constructed: one is for the event that the pod fails and the second one covers the case for which a terror attack occurs. These are the two most dreaded events of the door-to-door service. In the diagram presented in Figure 21.6 and Figure 21.7, and- and or-conditional gates are presented.

21.2.2. Maintainability

Maintainability is defined as *'the ability of a system to be restored in an operating state, during a predetermined time interval'* [7]. First, the Maintenance Significant Items are determined and their respective failure effects. The items which have a large impact on the maintenance program are listed in Table 21.5, as well as the severity of their failure.

Now it is important to list the maintenance tasks along with their effectiveness and the required frequency [1]:

1. Inspections: five types of inspections are included. Firstly, the *annual inspection* is a detailed inspection which occurs after 12 months of operation. The *100-hours inspection* is a high level inspection which occurs every 100 hours of service. The *pre-flight inspection* is a non detailed analysis to check the main functionalities of the system on a daily basis. Similarly, the *post-flight inspection* is a non detailed analysis to detect whether damage has occurred during the pods journey. Lastly, the *C check* is a thorough inspection of the pod with disassemble of necessary parts. This inspection is done every 26 months.

2. Preventive and Progressive Maintenance: whereas preventive maintenance includes the substitution and repair of small parts without involving complex assemblies, in progressive maintenance the main functions of the systems are checked and major changes to the components are performed. These procedures include repairs to the structure, pressurisation of the tyres, substitution of the batteries and alteration of any detected defect.

3. Aircraft Flight Test after Repair or Alteration: this step ensures the validity of the maintenance process and must be performed every time a modification is applied to the system.

[1] The basics of maintenance in general aviation, *date accessed: 22-05-2018*, `https://www.lycoming.com/content/basics-maintenance-general-aviation`

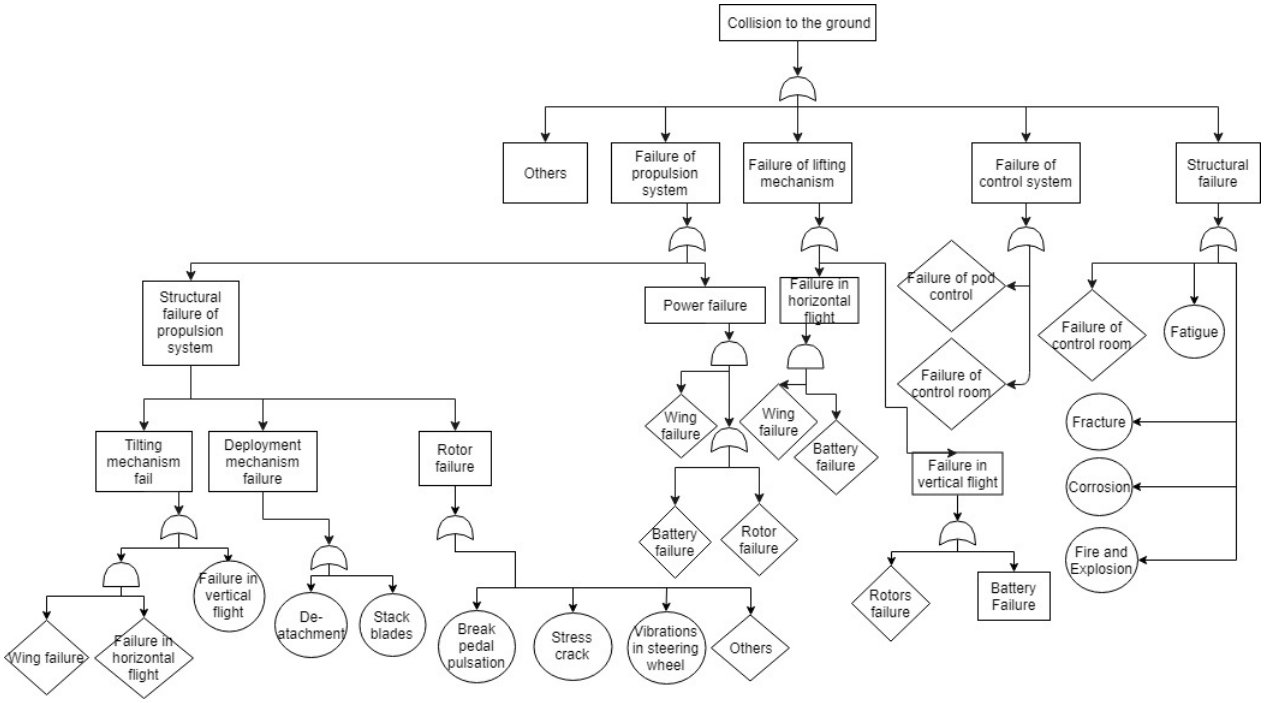

Figure 21.6: Collision to ground fault tree

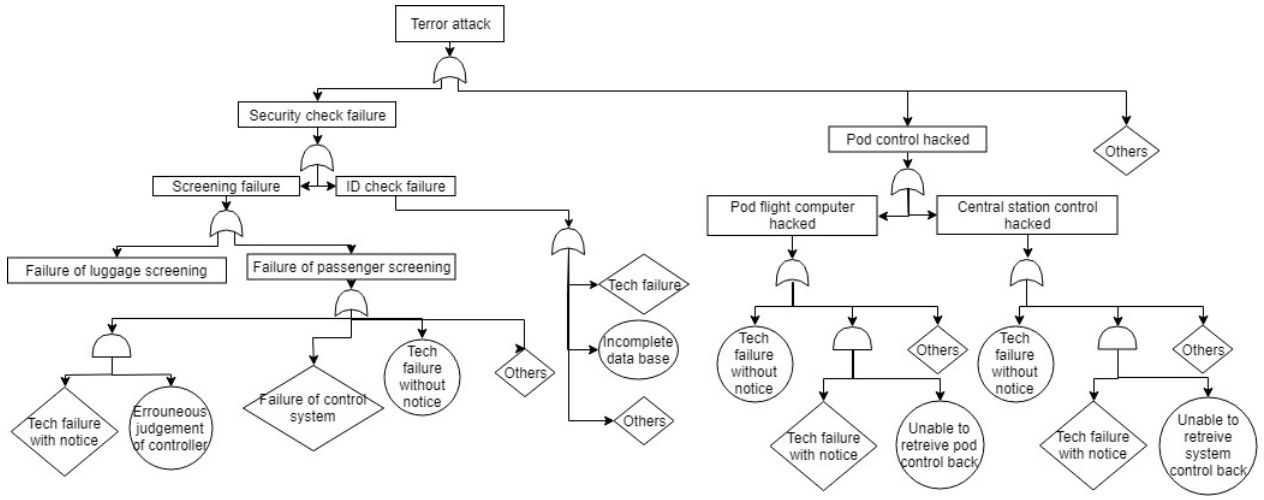

Figure 21.7: Terror attack fault tree

21.2.3. Safety

Safety is defined as the *ability of a system not to generate, in given conditions, critical or catastrophic events* [7]. As explained in Table 21.5, failure of the wing, motors or wheels will be critical for the safety of the system. Therefore, the back up critical safety functions which the system should perform in case of failure is included, as explained in chapter 12.

Some of the previously mentioned critical risks are prevented by designing with safety margins. For example, failure of the wing structure would be extremely deleterious for the system and its damage cannot be mitigated after occurrence. For this reason, the risk of wing failure is avoided by including safety factors throughout the design procedure. In general, the system is designed in such a way that redundancies are included. Since more elements operate at the same time, the system is more reliable as back-up options are available in case of failure.

Furthermore, the screening operations do not alter the safety level of the system, as the same screening machines are used in the USTI lounge as for the screening of the other airport passengers. However, safety is decreased as the passenger are not required to have their items checked before being allowed to depart. This is taken into account by providing the controllers the power to overrule the route of the pod in case of danger.

Table 21.5: Maintenance Significant Items

MSI	Wing	Rotors	Battery	Fuel Engine	Electric motors	Wheels
Safety	Critical (in flight)	Severe (in flight)	Severe (in flight and on ground)	Severe (in flight and on ground)	Critical (in flight)	Critical (on ground)
Detectability	Easily detectable	Easily detectable	Easily detectable	Easily detectable	Difficult to detect	Easily detectable
Operational impact	Critical	Severe	Severe	Severe	Critical	Critical
Economical impact	Very expensive	Expensive	Expensive	Expensive	Expensive	Inexpensive

q

21.3. Sensitivity Analysis

In this section, the design robustness will be tested. This will be done with respect to pod mass, emissions of the pod during operation, pod production costs and pod price.

21.3.1. Mass

A sensitivity analysis is performed to analyse the effect of a change in the most important design parameters on the maximum take-off mass of the pod. This evaluates the robustness of the design estimation. For every considered parameter the value is both increased and decreased by 10%. Subsequently, an analysis on the maximum take-off mass is performed. In this process, all other parameters will remain constant. The results of the sensitivity analysis can be seen in Table 21.6. The table denotes the percentage of change in the maximum take-off mass due to either an increase or decrease in the system parameter value of 10%.

Table 21.6: Sensitivity analysis on the maximum take-off mass

Effect of ... on m_{TO}	**Parameter +10%**	**Parameter -10%**
Payload	+9.9%	-9.9%
Battery Density	-2.3%	+2.9%
Electric/Fuel Ratio	+5.8%	-5.2%
Wing Area	-0.1%	+0.1%
Operational Empty Mass	+3.8%	-3.7%
motor Mass	+1.7%	-1.6%
Wing Span	+1.3%	-1.2%
Vertical Tail Size	+0.2%	-0.1%
Horizontal Tail Size	+0.1%	-0.0%
Range	+3.2%	-3.0%
Cruise Speed	+1.1%	-1.1%

A few effects stand out from this analysis. The most important effect on the maximum take-off mass comes from a change in the required payload that needs to be carried. Changing the amount of payload required greatly influences the necessary Operational Empty Mass, the required power and thus the required amount of batteries that need to be carried. Therefore, it is logical that this has a large effect on the m_{TO}.

The battery density has a significant influence on the m_{TO}, an increase in the battery density will decrease the mass of the batteries and so decrease the m_{TO}. It can be seen that a decrease in the battery density has a larger influence on the m_{TO} than an increase of the density. Furthermore, the changes in electric/fuel ratio affect the m_{TO} significantly. This is because fuel has a much higher specific energy than batteries, therefore when increasing the amount of fuel relative to the amount of electric energy, the m_{TO} decreases.

What also stands out is the effect of the wing area on the m_{TO}. Increasing the wing area happens to decrease the m_{TO} slightly. This might sound counter intuitive at first. The reason for this decrease can be found in the fact that decreasing the wing area increases the aspect ratio if the wing span remains the same. Increasing the aspect ratio has a greater effect on the wing weight than changing the wing area according to the Class II weight estimation performed in section 5.2. This also explains why changing the span has a greater effect on the m_{TO} than changing the wing area.

Another interesting result is that changing the area of both the vertical and horizontal tail barely have any effect on the m_{TO}. This results corresponds with an assumption made in the weight estimation on the final concept. There, the vertical tail and horizontal tail have not been resized from design option 2, and the old values have been used for the new estimation. From this analysis, it is found that this assumption was valid and that it has not influenced the outcome of the weight estimation significantly.

The difference caused by the changes in range are mainly caused by an increase or decrease in fuel and battery weight, which is directly related to the amount of energy required. The cruise speed influences the m_{TO} due to the power re-

quired, which influences the motor design.

A final conclusion on the sensitivity analysis is that for every parameter the percentage effect on the m_{TO} is smaller than the percentage change in of the parameter. This is a desired result. When looking at pure kilograms, the change in m_{TO} might be bigger due to the snowball effect, but the fact that percentage wise the change is smaller, means that the design method is relatively robust and independent.

21.3.2. Sustainability

An important factor in the design is sustainability. Therefore a sensitivity analysis is performed on the emissions. Since the NOx emissions are linearly dependant on the CO_2 emissions in the estimation, this analysis holds for the NOx emissions as well. The results can be found in Table 21.7.

Table 21.7: Sensitivity analysis of both the CO_2 as well as the NOx emissions.

Effect of ... on emissions	Parameter +10%	Parameter -10%
Range extender efficiency	-8.8%	+10.7 %
Range	+10%	-10%
m_{TO}	+9.4%	-8.5%
Cruise speed	+3.9%	-0.07%

The main parameter that stands out is the cruise speed. It can be seen that a decrease in cruise speed does not cause a significant decrease in emissions. When the cruise speeds is increased with 10 %, emissions are increased. This is mainly attributed to the non-linear dependency of drag on velocity.

21.3.3. Production Cost

A sensitivity analysis is also performed to analyse the effect of a change in the operational empty mass on the production cost of the pod. The operational empty mass is both increased and decreased by 10%. The results of this analysis can be seen in Table 21.8. A change of the operational empty mass can be a consequence of changing other design parameters. Such parameters could be the range or cruise speed. The manufacturing cost are estimated as described in subsection 18.2.1. For the material cost an increase or decrease of 10% of the cost of some of the subsystems is estimated. The subsystems included are the propulsion system, structure, driving & landing gear and part of the internal systems. Components that are excluded are for example the cockpit components, the sensors and the lighting.

Table 21.8: Sensitivity analysis on the pod production costs

Effect of ... on pod production cost	Parameter +10%	Parameter -10%
Manufacturing cost	+8.1%	-8.3%
Material cost	+4.1%	-4.1%
Total production cost	+4.1%	-4.1%

This shows that the change of 10% in the operational empty mass results in a lower percentage change for the manufacturing cost. This is a desired result as explained previously. Moreover, the total production cost also shows a percentage change lower than 10%. It shows that the design is relatively robust.

21.3.4. Pod Price

The pod and its service are designed based on a cost requirement. Using the cost analysis, the sensitivity of the price of the pod to several parameters is investigated. Three parameters are varied similar to the other sensitivity analysis performed. The results can be found in Table 21.9.

Effect of ... on pod price	Parameter +10%	Parameter -10%
Percentage of business passengers	-3.6%	+4.4%
Penetration rate	-3.6%	+4.4%
Break-Even Point	+4.0%	-3.3%

Table 21.9: Sensitivity analysis of USTI pod price

It can be seen that if any of the parameters is changed with 10 %, the cost of the pod only increases or decreases with a maximum of 4.4 %. In other words, the market analysis is not necessarily very sensitive to changes. Most notably is the Break-Even Point. If the Break-Even point is decreased, the price increases. The reason for this is that if the Break-Even Point is decreased, the pods need to make more money in a shorter amount of time. This in term means that the price per pod needs to increase.

22 Resource Allocation

Throughout the design process of the system, it is important to take into account several parameters that result from the contribution of different components. An example of this is the operative empty mass of the flying pod. This mass includes many different components. Therefore, it is important to keep track of the value of all these components. This is achieved by setting up a mass budget. Similarly, an energy budget is constructed as well as a cost budget.

22.1. Mass Budget

During the design, the mass of each component is carefully tracked and added to the mass budget. A detailed mass budget of each component can be found in Appendix C. A more general mass budget for all subsystems can be found in Figure 22.1. The exact numbers can be found in Table 22.1.

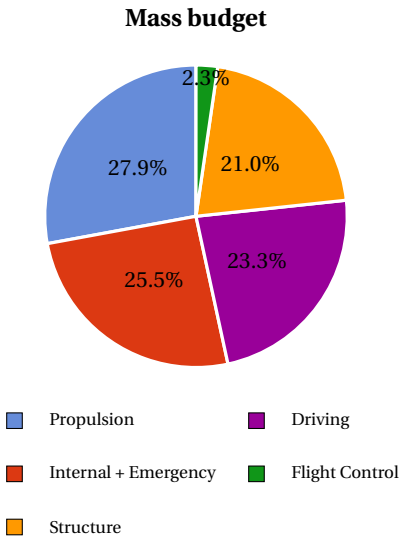

Figure 22.1: Mass budget of the different subsystems

Table 22.1: Exact value of the mass budget for different subsystems

Subsystem	**Mass** $[kg]$	**Percentage** [%]
Structure	100.11	23.3
Driving and LG	90.08	21.0
Flight control	9.85	2.3
Internal systems	108.83	25.3
Propulsion	119.70	27.9
Emergency systems	1.00	0.2

22.2. Energy Budget

To size the propulsion system, the power of each component was tracked and filled in the energy budget. The energy budget for the most critical situation is represented in Figure 22.2 and Table 22.2. The critical situation corresponds to the maximum cruise time possible during flight as the driving is less critical.

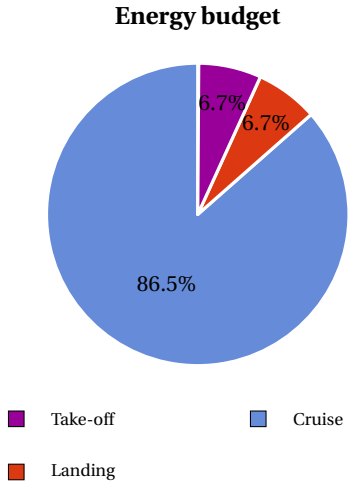

Figure 22.2: Energy budget for the most critical situation

Table 22.2: Energy budget for different subsystems

Subsystem	**Energy** $[MW]$	**Percentage** [%]
Cruise	342.2	86.5
Landing	26.7	6.7
Take-off	26.7	6.7

22.3. Cost Budget

The different costs corresponding to USTI are determined as explained previously in chapter 18. In this section, an overview is given regarding the development cost budget and the operational cost budget. The former corresponds to the phase before the start of the operation phase, excluding the marketing costs and the series production. The operational cost budget corresponds to the budget for the operation of the system.

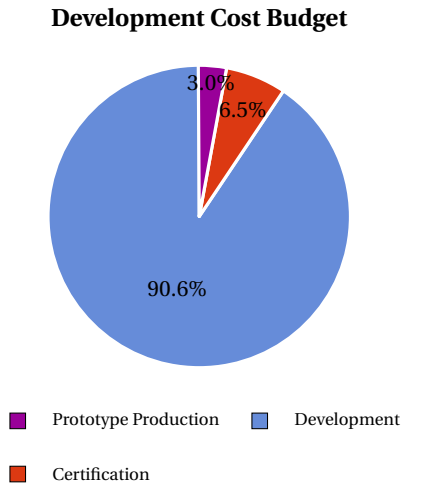

Figure 22.3: Cost budget for the development phase

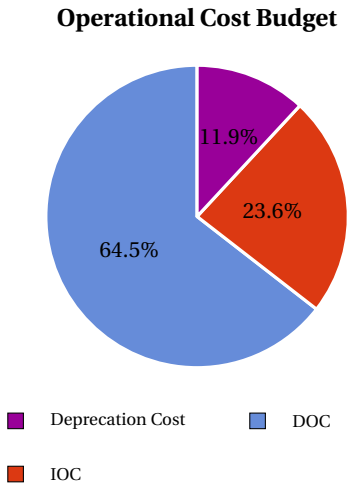

Figure 22.4: Cost budget for operation

23
Conclusion

The purpose of this report is to present the final version of the USTI-system. USTI and its surrounding operations and infrastructure now constitute a coherent, fully functional system that provides door-to-door air transportation to business people travelling by plane, reducing the total travel time to less than four hours within most of the EU.

Central to this system is the USTI-pod, which is designed with the future in mind. In short, a pod can be booked by travellers up to six hours in advance of their flight. The most suitable pod will travel to their location and confirm their identity before allowing access to the pod. USTI will then drive towards an open area where it can take off vertically, after which it will head straight towards the airport at a cruise speed of 200 km/h and at an altitude of 200 m, avoiding both commercial air traffic and recreational drone traffic. Passengers are then dropped off at a dedicated USTI-lounge, where they can get screened and head toward the aircraft immediately. Then they continue on their journey as usual.

On an environmental level, the design surpasses the requirements set at the start with the following results:

- It is now recyclable for 78 % by weight instead of the required 60 %.
- All of USTIs materials adhere to the REACH requirements.
- The inclusion of electric motors lowers the CO_2 output drastically.
- An autonomous system guarantees that pods are assigned as efficiently as possible.

On a societal level, this system has the potential to alleviate the traffic congestions that frequently occur around large airports and business hubs in Europe. Although the pod can operate autonomously, the supporting system at and around the airport still requires operation controllers, security agents and customer service representatives, creating jobs at every airport where the system is implemented. Even more local jobs are created by keeping the development and production of the pod and systems within Europe.

The team has thus achieved the project objective it set out with at the start, negotiating requirements on the way to ensure the feasibility of the designed system. Some examples of such negotiations are:

- The initial cost requirement of €100,000 per pod turned out to be too limiting and a final price of less than €200,000 was agreed upon.
- The pod switched from a 4-seat to a 2-seat configuration after receiving feedback from industry leaders who rightly commented that this system will mostly be used by business travellers who mainly travel alone or in pairs.

These changes allowed the team to design an innovative system and thus designed a system worth investing in it.

A lot of effort has been invested in this design, but there is always room for improvement. For example, a more detailed structural and aerodynamic analysis employing finite element methods could improve upon the overall design of the pod and some requirements could not be verified, because time was a scarce resource and priorities had to be made. These and many other recommendations can be found in the next section.

24
Future Development

Although the design described in this report has been designed successfully to a certain degree, a detailed analysis is required to predict the system behaviour with more accuracy. Moreover, this chapter touches a series of optimised possibilities for future designs.

24.1. Further Analysis

Before USTI is introduced to the market, it is of great importance to perform a more in-depth analysis. Possible actions include:

- Performing a detailed aerodynamic analysis. The use of Computational Fluid Dynamics (CFD) is required to determine the exact aerodynamic properties and effectiveness of the control surfaces. Besides, the exact tip velocity of the rotors can be verified with the use of this tool.
- Analysing the truss structure of the main body more in depth, to find out whether weight can be reduced by structural optimisation.
- Further analysis on possible locations for pod landing close to the airports of application. This is required to show potential customers the feasibility and the convenience of the service.
- In-depth investigation on how the different algorithms of the flight computer work. These include take-off, cruise, landing and pod allocation.
- Detailed examination of the different data rates within the pod itself and between the pod and the control station.
- Studying the contents of the maintenance and production plans in further detail, to ultimately generate the plan such that it will comply to EASA regulations.
- Creating a deeper understanding of the climate control to decrease weight and emissions.
- Design of the control station on a detailed level. The station should be built such that the communication flow between controllers is optimal.
- Assess risk of hacking in more detail and incorporate sufficient intruder prevention mechanisms in the system.

24.2. System Optimisation

Besides recommendations for further analysis, some preliminary recommendations on future system optimisation are identified throughout the project. These incorporate:

- Performing multiple iterative loops. By having a new input weight to the subsystem design, they can be designed for that purpose. Finally, the optimal design is found from the iteration convergence.
- Considering the option of automated maintenance. Implementing machines in maintenance allows for cost-efficient and secure inspections.
- Establishing a new design for cargo-only mode. Whereas the current design is optimised for pod travel, a similar pod can be designed which is efficient for freight.
- Discovering possibilities for other applications of the product. A general in-air taxi service is a feasible application which would create new market perspectives.
- Designing motors, engines and batteries rather than selecting them off-the-shelf. This will increase efficiency.
- Developing the user interface in more detail. This refers in particular to shopping, emergency notifications and account support.
- Learning the process of 3D printing of the Polypropylene skin. This might be more cost effective and ultimately also faster compared to the compression moulding techniques used for the current design.
- Adding solar panels on the wings to decrease the amount of fuel used in aircraft.

Bibliography

[1] *Aviation Maintenance Technician Handbook - Airframe*. Aviation Supplies & Academics, May 2014.

[2] DSE Group 4. *Door-to-door Air Transportation Baseline Report*. Tu Delft, 2018.

[3] DSE Group 4. *Door-to-door Air Transportation Mid-Term Report*. Delft University of Technology, 2018.

[4] Siemens AG. Aerobatic airplane extra 330e, 2016.

[5] European Aviation Safety Agency. *Easy Access Rules for Continuing Airworthiness*. June 2017.

[6] European Aviation Safety Agency. *Certification Specifications for Very Light Aeroplanes CS-VLA Amendment 1*. 5 March 2009.

[7] Apsys Airbus. *RAMS Analysis for Aeronautics*. 2018.

[8] C.H. Bemisderfer. *ASHRAE Fundamentals Handbook 2001*. American Society of Heating, Refrigerating and Air-Conditioning Engineers, 2001.

[9] Boeing. Pallets and containers, March 2012.

[10] H. Brezet and C. van Hemel. Ecodesign: A promising approach to sustainable production and consumption. December 1997.

[11] M. Celli. Personal conversation with aerospace expert consultant, Jun 2018.

[12] R. Wiesner C.N. Keys. Guidelines for reducing helicopter parasite drag. *Journal of the American Helicopter Society*, 20, 1975.

[13] Apogee Components. Properly sizing parachutes for your rockets. October 2005.

[14] S. Coyle. Cyclic & collective. January 2009.

[15] M. Drela. Xfoil: An analysis and design system for low reynolds number airfoils. In Thomas J. Mueller, editor, *Low Reynolds Number Aerodynamics*, pages 1–12, Berlin, Heidelberg, 1989. Springer Berlin Heidelberg. ISBN 978-3-642-84010-4.

[16] P. du Bois and C. Chou. Vehicle crashworthiness and occupant protection, 2004.

[17] European Economic and Social Comittee. Eu standars: regulation (ec). no 443/2009, February 2009.

[18] Emrax. User's manual for advanced axial flux synchronous motors and generators, January 2017.

[19] EPA. Burning fuel and tire pyrolysis, November 1991.

[20] J. Fleischer. Small batch assembly of space-frame-structures with production related deviations of individual components. June 2014.

[21] S. George. Faa unmanned aircraft systems (uas) cyber security initiatives. April 2012.

[22] P. Gijsman, G. Meijers, and G. Vitarelli. Comparison of the uv-degradation chemistry of polypropylene, polyethylene, polyamide 6 and polybutylene terephthalate. *Polymer Degradation and Stability*, 65(3):433 – 441, 1999.

[23] GMFCO. Modern robotic welding technology. April 2013.

[24] J.C. Pascoa J. Morgado, M.A.R. Silvestre. Validation of new formulations for propeller analysis. *Journal of Power and Propulsion*, 2015.

[25] Th. van Holten J.A. Melkert. *Prestaties en vliegeigenschappen van hefschroefvliegtuigen*. Delft University of Technology, July 1994.

[26] R.I. Jones. *The more electric aircraft - Assessing the benefits*. Cranfield University, 2002.

[27] S. Joseph. Design and development of steering and suspension system of a concept car. *KTH Industrial Engineering Master Thesis*, 2013.

[28] Y. Li K. Ang, G. Chong. Pid control system analysis, design, and technology. 13:559 – 576, 08 2005.

[29] N. Harm Z. McGill R. Posey L. Boccacci, J. Erazo. *Polyemer Composite Gasoline Tanks*. University of Oklahoma, 2004.

[30] P. Lannon. *Fast-Forwarding to a Future of On-Demand Urban Air Transportation*. Uber, 2016.

[31] K.A. Latorella and P.V. Prabhu. A review of human error in aviation maintenance and inspection. *International Journal of Industrial Ergonomics*, 26(2):133 – 161, 2000.

[32] R. Lebanc. An introduction to polypropylene recycling. July 2017.

[33] W.S. Levine. *Control System Applications*. Wiley, 2010.

[34] M. Bahrami M.A. Fayazbakhsh. Comprehensive modeling of vehicle air conditioning loads using heat balance method. 08 2013.

[35] Wayback Machine. Ahrs- open pilot project. August 2011.

[36] Mahle. Mahle range extender engine.

[37] J. Markish. Valuation techniques for commercial aircraft program design, Jun 2000.

[38] T.H.G. Megson. *Aircraft structures for engineering students*. Elsevier, 1999.

[39] Vlaamse Milieumaatschappij. Co2 emissions of vehicles. October 2008.

[40] I. Moir. *Aircraft Systems*. Wiley, 2008.

[41] J. Morgado. Development of an open source software tool for propeller design in the maatproject. *University of Beira Interior, PhD Thesis*, 2016.

[42] F. Nicolosi. Advances in composite manufacturing of helicopter parts. *5th CEAS Air & Space conference Challenges in European aerospace*, 2015.
[43] Office of Aviation Research. Automated inspection for aircraft. April 1998.
[44] H.G. Campbell P. Joseph. Parametric equations for estimating aircraft costs.
[45] W.F. Philips. *Mechanics of Flight*. Wiley, 2010.
[46] Mahle Powertrain. Mahle compact range extender engine. April 2016.
[47] D.P. Raymer". *"Aircraft Design: A Conceptual Approach"*. American Institute of Aeronautics & Astronautics, 1992.
[48] J. Roskam. *Airplane Design Part V: Component Weight Estimation*. The University of Kansas, 1985.
[49] J. Roskam. *Airplane Design: Part IV: Layout of landing gear and systems*. Number v. 1 in Airplane Design. DARcorporation, 2000. ISBN 9781884885532.
[50] Corporate Affairs Royal Schiphol Group. Baggage at schiphol. *Schiphol Data*, 2016.
[51] A. Rothwell S. Castagne, R. Curran. A generic tool for cost estimating in aircraft design.
[52] M. Sadraey. *Aircraft Systems Design, A System Engineering Approach*. Wiley, 2012.
[53] I.S. Seddiek and M.M. Elgohary. Eco-friendly selection of ship emissions reduction strategies with emphasis on sox and nox emissions. *International Journal of Naval Architecture and Ocean Engineering*, pages 737 – 748, 2014.
[54] J. Sinke. Production of aerospace materials reader, 2018.
[55] D. Tiranti. Production control: the production plan. June 2001.
[56] W. Toet. Secrets of a formula 1 front wing. March 2016.
[57] A. von Stauffenberg. Cyber security. May 2014.
[58] S. Walters. Drone attack tools. May 2018.
[59] K. Yue. Comparative analysis of scrap car recycling management policies. February 2012.
[60] S.O.L. Zijp. *Development of a life cycle cost model for conventional and unconventional aircraft*. TU Delft, 2014.

Appendix: Compliance Matrix

ID	Requirement	Comply?	Comments
Mission			
POD-MIS-1	The system shall be able to reduce door-to-door travel time within Europe by 4 hours, including all operations.	Nearly	Cannot always be guaranteed, subsection 19.1.1
POD-MIS-2	The system shall be able to be implemented in airports with a passenger number of 10 million per year.	Yes	subsection 15.3.1
POD-MIS-3	The system shall be able to cover the range for which 90% of the European population can access an airport which allows inter-European travelling.	No	But the service has its focus on business passengers, who live in the urban areas, where the +10 m airports also are
POD-MIS-4	The system shall be able to cover a circular area of radius 150 km around the selected European airports. airport	Yes	section 5.2
POD-MIS-5	The system shall always be available for people who booked the service at least one day before departure.	Yes	Up until six hours before departure, section 14.4
POD-MIS-6	The system shall be able to operate autonomously.	Nearly	Full autonomous operation not allowed, section 14.2
POD-MIS-7	The pod shall be able to operate with the already-existing urban infrastructures.	Yes	Near VTOL and STOL capabilities provide this, chapter 6
POD-MIS-8	The cost of the service shall not exceed the cost of a taxi ride which travels along the same route.	Yes	subsection 18.3.2
POD-MIS-9	The system shall have a unit cost of no more than € 100k.	No	Unit cost: €112k euro Table 18.2.1
POD-MIS-10	Total shopping revenues shall not be lower than current shopping revenues.	Yes	Revenues not affected by system, chapter 15
POD-MIS-11	The system shall not negatively impact current safety levels.	Unknown	Not intended, but not known until testing takes place
POD-MIS-12	The system shall be more sustainable than current modes of transportation.	Nearly	subsection 19.2.2
POD-MIS-13	Materials shall only be used according to REACH requirements	Yes	subsection 19.2.2
System			
POD-SYS-OPP-1	The pod shall be able to fit two people and their luggage	Yes	chapter 10
POD-SYS-OPP-2	The pod shall have a minimum lifetime of 10 years	Yes	subsection 14.3.1
POD-SYS-OPP-3	The pod availability shall enable a station to door time of maximum <tbd>	Unknown	Not considered in design of system
POD-SYS-OPP-4	It shall be possible to modify the pods for air freight.	Yes	Possible, but not very convenient section 10.7
POD-SYS-OPP-5	The pod shall be able to convert between different modes of transport.	Yes	Figure 8.3.5

ID	Requirement	Comply?	Comments
POD-SYS-OPP-6	Individual pods shall be possible to be joined into multiple pods.	No	Disregarded due to chosen design option
POD-SYS-OPP-7	The structural performance of the pod shall be based on the European regulations regarding passengers and luggage weight	Yes	Regulations followed for determining max payload weight
POD-SYS-OPP-8	The pod shall not have a single point of failure during operations;	Yes	subsection 21.1.1
POD-SYS-OPP-9	The system shall not cause passengers to perceive any waiting time.	Nearly	subsection 15.3.3
POD-SYS-OPP-11	The pod shall withstand load factors in the range of -1 to +4.5.	Yes	subsection 8.3.2
POD-SYS-OPP-12	The pod shall be recyclable by 60 % of the pod weight.	Yes	subsection 19.1.5
POD-SYS-OPP-13	The pod shall be able to withstand accelerations with a maximum of <tbd> m/s^2	Unknown	Beyond scope of design phase
POD-SYS-OPP-14	The pod shall be able to withstand vibrations with a maximum of <tbd> Hz.	Unknown	subsection 6.4.5
POD-SYS-F-1	The pod shall be able to fly autonomously.	Yes	section 14.2
POD-SYS-F-2	The pod in flying mode shall be able to detect obstacles in all flight directions	Yes	section 9.4
POD-SYS-F-3	The pod in flying mode shall be able to avoid detected obstacles on its route.	Yes	section 9.4
POD-SYS-F-4	The pod shall not interfere with current air traffic	Yes	section 15.2
POD-SYS-F-5	The pod in flying mode shall be able to take-off without a dedicated airstrip.	Yes	Near VTOL capabilities section 9.2
POD-SYS-F-6	The pod in flying mode shall be able to land without a dedicated airstrip.	Yes	Near VTOL capabilities section 9.2
POD-SYS-F-7	The pod shall be able to abort landing if obstacles on desired landing location are detected.	Yes	section 9.4
POD-SYS-F-8	The pod in flying mode shall have statically stable flight characteristics.	No	section 9.2
POD-SYS-F-9	The pod in flying mode shall have dynamically stable flight characteristics.	No	section 9.2
POD-SYS-F-10	The pod shall be able to perform an emergency landing within 1 minute after emergency landing is requested.	Yes	section 12.2
POD-SYS-F-11	The pod shall be able to land in non-urban environments	Yes	
POD-SYS-F-12	The pod shall be able to perform and emergency landing on water.	Yes	section 12.2
POD-SYS-F-13	The pod shall comply with applicable CS regulations on safety;	Yes	subsection 8.3.2
POD-SYS-F-14	The pod have a cruise altitude of no lower than 150 m not to interfere with current recreational drones.	Yes	section 17.3
POD-SYS-F-15	The pod shall be able to fly at cruise speed of 200 km/h	Yes	section 5.2
POD-SYS-F-16	The pod in flying mode shall comply with CS-36 Aircraft Noise regulations	Unknown	subsection 6.4.5
POD-SYS-F-17	The noise level in the pod in flying mode shall not exceed 60 dB at cruise conditions.	Unknown	subsection 6.4.5
POD-SYS-F-18	The pod shall have an efficiency that is competitive with current modes of transport.	Nearly	Competitive with cars, not with public transport subsection 19.2.2
POD-SYS-D-1	The pod shall comply to current traffic regulations	Yes	Not working reference
POD-SYS-D-2	The pod in driving mode shall be able to travel at a maximum speed of 130 km/hrs	Yes	section 7.3
POD-SYS-D-3	The pod shall have a driving range of <tbd> km.	Unknown	subsection 6.3.2
POD-SYS-D-4	The pod shall be able to drive autonomously	Yes	subsection 6.3.2
POD-SYS-D-5	The pod shall be able to analyse traffic conditions	Yes	subsection 9.5.2
POD-SYS-D-6	The pod in driving mode shall be able to detect non-moving obstacles in all driving directions	Yes	subsection 9.5.2
POD-SYS-D-7	The pod shall be able to avoid obstacles without endangering traffic.	Yes	subsection 9.5.2

ID	Requirement	Comply?	Comments
POD-SYS-D-8	The pod shall be able to detect moving obstacle.	Yes	subsection 9.5.2
POD-SYS-D-9	The pod shall be able to avoid collision with moving obstacles.	Yes	subsection 9.5.2
POD-SYS-D-10	The pod in driving mode shall be able to accelerate from 0 to 100 km/h within 10 seconds.	Yes	5.9 s in peak power mode
POD-SYS-D-11	The pod in driving mode shall not exceed the noise level of a current electric car	Yes	subsection 6.4.5
POD-SYS-D-12	The noise inside the pod in driving mode shall not exceed 60 dB.	Unknown	subsection 6.4.5
POD-SYS-D-13	The size of the pod in driving mode shall not exceed 4.7(l) x 1.7(w) x 2.0(h) metres.	No	5.10 (l) x 2.0 (w) x 1.77 (h) metres, subsection 19.1.7
POD-SYS-D-14	The pod shall have a crash worthiness that would guarantee a 5 star rating from the EURO NCAP test	Unknown	Only front and side impact tested, subsection 8.3.2
POD-SYS-SC-1	The pods shall be able to communicate with an external system at all times.	Yes	section 11.2
POD-SYS-SC-2	The control system shall be able to be monitored by at least one person at all times.	Yes	section 14.2
POD-SYS-SC-3	The pod shall have the possibility to be controlled externally.	Yes	section 14.2
POD-SYS-SC-4	The system shall be able to assign pods to customers without human interaction.	Yes	section 14.4
POD-SYS-SC-5	The system shall be able to generate the quickest route to get to final destination.	Yes	section 14.4
POD-SYS-SC-6	The system control shall be able to analyse the current schedule of all pods.	Yes	section 14.4
POD-SYS-SC-7	The system shall be able to adapt pod schedule if a more efficient schedule is possible.	Yes	section 14.4
POD-SYS-SC-8	The system shall be able to analyse road integrity.	Yes	subsection 9.5.2
POD-SYS-SC-9	The system shall be able to adapt the route of a pod.	Yes	section 14.4
POD-SYS-SC-10	The system shall be able to verify if passengers are allowed to fly.	Yes	chapter 10
POD-SYS-SC-11	The pod shall not store personal data of passengers after their flight.	No	Not possible for smooth operation
POD-SYS-SC-12	The passengers in the pod shall not perceive any waiting time in case the route needs to be redetermined.	Unknown	Can only be known once testing of pod takes place
POD-SYS-SC-13	The system shall be able to select a suitable pod for the passenger within 10 seconds after request is made.	Unknown	Can only be known once dispatch algorithm is fully designed.
POD-SYS-PPI-1	The pod shall only be accessible to the customers who actually booked the service;	Yes	chapter 10
POD-SYS-PPI-2	The pod shall be able to verify the identify of passengers.	Yes	chapter 10
POD-SYS-PPI-3	The pod shall not be able to take-off if MTOW is exceeded.	Yes	section 10.4
POD-SYS-PPI-4	The pod shall be able to weigh individual pieces of luggage.	Yes	section 10.4
POD-SYS-PPI-5	The pod shall be able to weigh individual persons.	Yes	section 10.4
POD-SYS-PPI-6	The pod shall be able to communicate with passengers inside the pod.	Yes	chapter 16
POD-SYS-PPI-7	The pod shall be able to keep cabin temperature within the range of 17-23 degrees centigrade.	Yes	section 10.3
POD-SYS-PPI-8	The pod shall be able to keep cabin pressure at a minimum level of 0.7 atm at all times.	Yes	chapter 17
POD-SYS-PPI-9	The pod shall not store any personal data of the passenger during flight.	No	section 14.2
POD-SYS-SH-1	Shopping shall be possible during the pre flight and flight phase	Yes	section 16.2
POD-SYS-SH-2	Shopped items shall be delivered to the customer before flight when purchased during pre-flight phase.	Yes	chapter 15
POD-SYS-SH-3	Shopped items shall be delivered to the customer directly in the pod when purchased during flight phase.	Nearly	Only if WiFi is available on aircraft
POD-SYS-SH-4	Duty free shopping shall be assured for pod passengers.	Yes	Regular shopping experience

ID	Requirement	Comply?	Comments
POD-SYS-SH-5	Shopping delivery shall not add waiting time for the passenger	Yes	chapter 15
POD-SYS-SH-6	Shopping offer variety shall remain constant	Yes	Regular shopping variety
POD-SYS-PL-1	The system shall transport the luggage of pod users from the pod to the aircraft and vice versa shall be less than the time to transport the pod users.	Yes	subsection 15.3.2
POD-SYS-PL-2	The system transport the pod users from the pod to the aircraft and vice versa shall be less than 15 minutes.	No	subsection 15.3.3
POD-SYS-PL-3	The infrastructure of the airport shall not be changed for the transportation of the pod users and their luggage.	No	section 15.3
POD-SYS-MT-1	The pods shall be inspected internally and externally after arrival at the airport.	Yes	section 14.3
POD-SYS-MT-2	The pods shall be cleaned after arriving at the airport.	Yes	section 14.3
POD-SYS-MT-3	The pods shall be inspected thoroughly every 50 flights.	Yes	As according to EASA regulations, section 14.3
POD-SYS-MT-4	The maintenance operations shall not result in unavailability of pods.	Yes	section 14.3
POD-SYS-MT-5	Maintenance of the pods shall not require a change in the infrastructure of the airport.	Yes	section 14.3
POD-SYS-MT-6	The pods shall be able to scan the functioning of its own subsystems.	Yes	section 14.2
POD-SYS-MT-7	The pods shall be able to communicate necessary maintenance operations to the responsible team.	Yes	section 14.2
POD-SYS-MT-8	The cost per pod for maintenance shall be less than 30 % of the total operating cost	Yes	subsection 18.3.1
POD-SYS-ST-1	The pods shall be stored within current airport infrastructure.	No	Better solution found, section 14.3
POD-SYS-ST-2	The pods shall be able to leave the storage facility autonomously	Yes	subsection 15.4.2
Subsystem			
POD-SUB-PROP-1	The propulsion system shall provide a constant vertical rate of climb of 3 m/	Yes	section 6.4
POD-SUB-PROP-2	The propulsion system shall provide total combined flying and driving range of 300 km	Yes	section 5.2
POD-SUB-PROP-3	The propulsion system shall provide Vertical Take-Off and Landing (VTOL) capabilities	Nearly	section 9.2
POD-SUB-PROP-4	The propulsion system shall provide (Extra) Short Take-Off ((E)STOL) and Landing capabili- ties	Yes	section 9.2
POD-SUB-PROP-5	Propeller tip speeds shall not exceed Mach 0.	Yes	section 6.4
POD-SUB-PROP-6	The batteries of the hybrid system shall provide enough energy to cover 30 % of the total range	Yes	section 5.2
POD-SUB-FC-1	The pod shall have stable flight characteristics in horizontal fligh	Yes	section 9.2
POD-SUB-FC-2	The pod shall have stable flight characteristics in vertical flight	No	However, pseudo-stability is assured, section 9.2
POD-SUB-FC-3	The pod shall reach a minimum pitch acceleration of 0.32 rad/s ^{2} in cruise conditions	Yes	chapter 9
POD-SUB-FC-4	The pod shall reach a bank angle of 30 ^{o} within 1.3 seconds from a steady bank angle/	Yes	chapter 9
POD-SUB-FC-5	The pod shall land safely with a 90 ^{o} crosswind of 6.2 m/s.	Yes	chapter 9
POD-SUB-SC-1	The screening shall be monitored by a responsible team	Yes	chapter 15
POD-SUB-SC-2	The screening system shall be able to communicate doubtful objects to the responsible team	Yes	chapter 15
POD-SUB-SC-3	The responsible team shall be able communicate with questionable people within 1 minute	Yes	chapter 15
POD-SUB-SC-4	The screening system shall allow the possibility to recheck items	Yes	chapter 15

Table A.1: Compliance Matrix

B

Appendix:Functional overview

B.1. Third Level Functional Flow Diagram

The third level accuracy functional flow diagram can be observed in Figure B.1, Figure B.2 and Figure B.3.

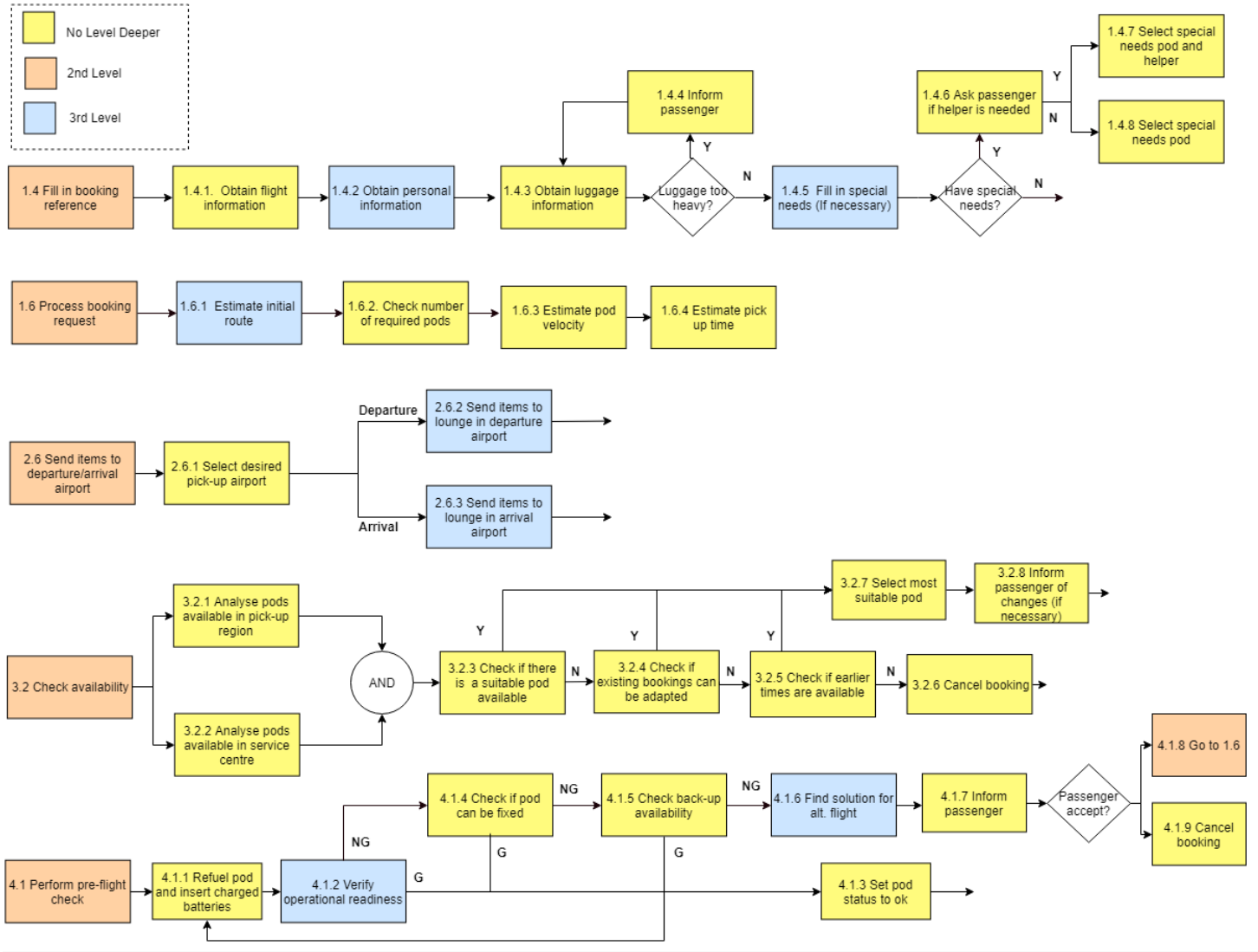

Figure B.1: Third Level Functional Flow Diagram 1

B.2. Functional Breakdown

The functional breakdown structure can be seen from Figure B.4 to Figure B.7.

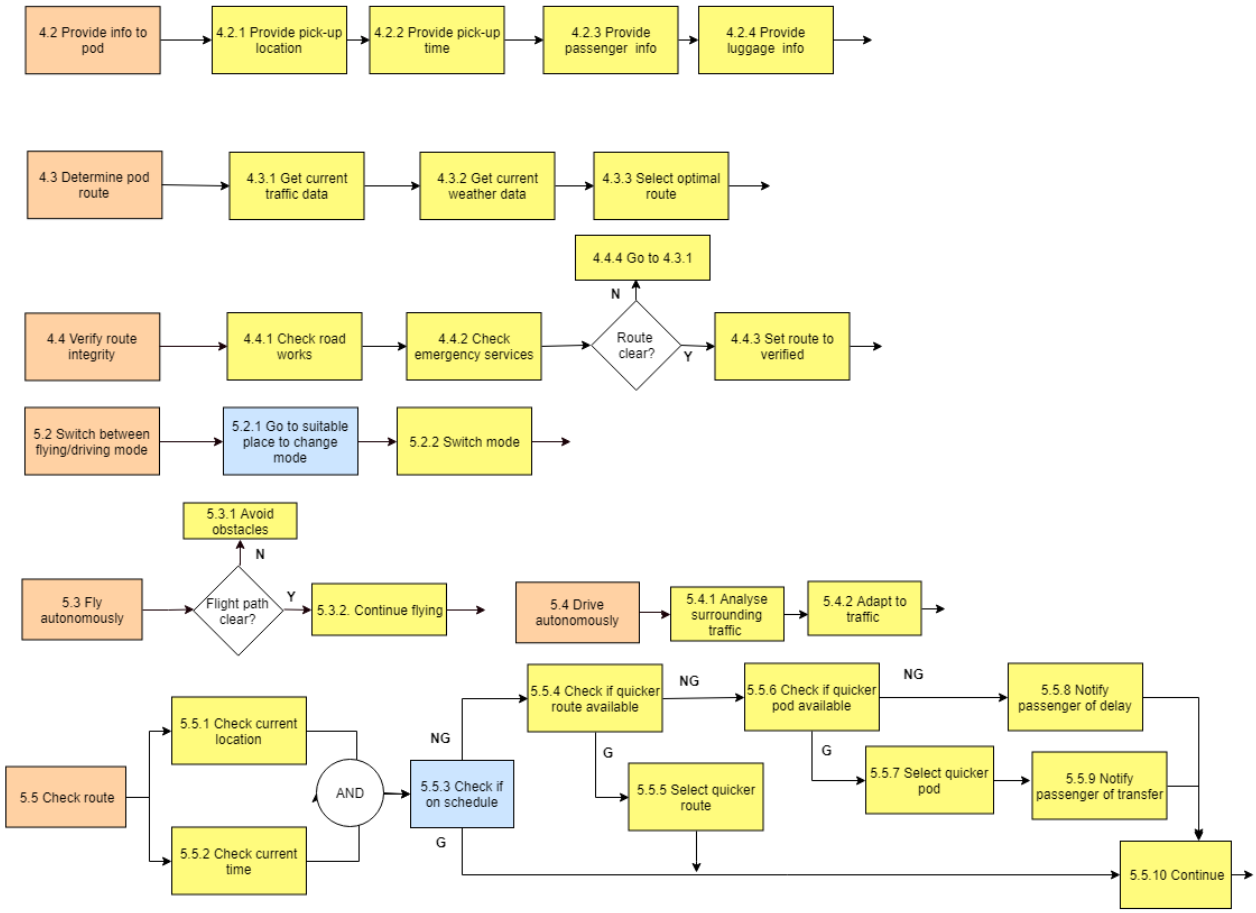

Figure B.2: Third Level Functional Flow Diagram 2

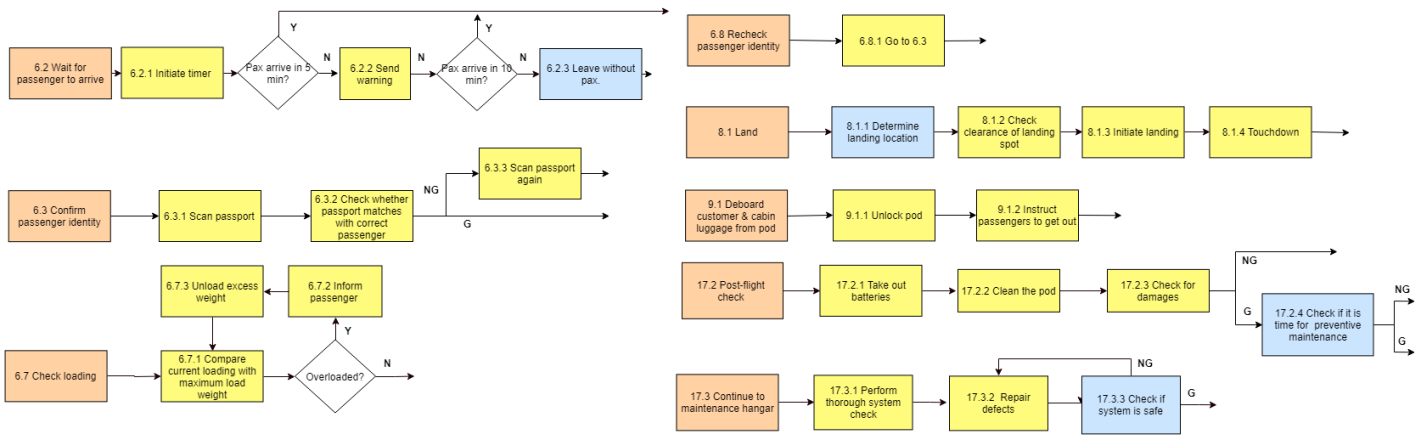

Figure B.3: Third Level Functional Flow Diagram 3

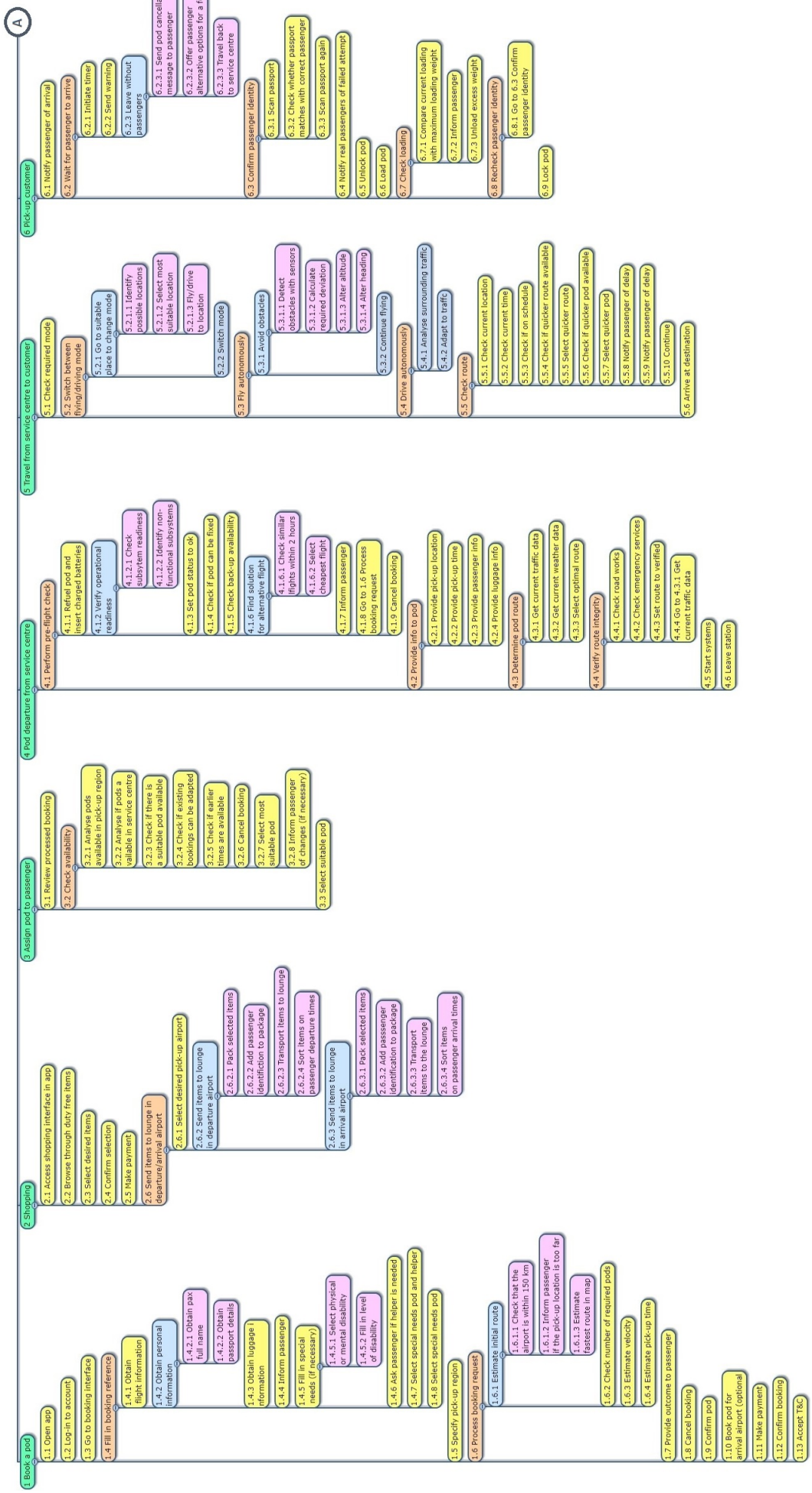

Figure B.4: Functional breakdown structure part 1

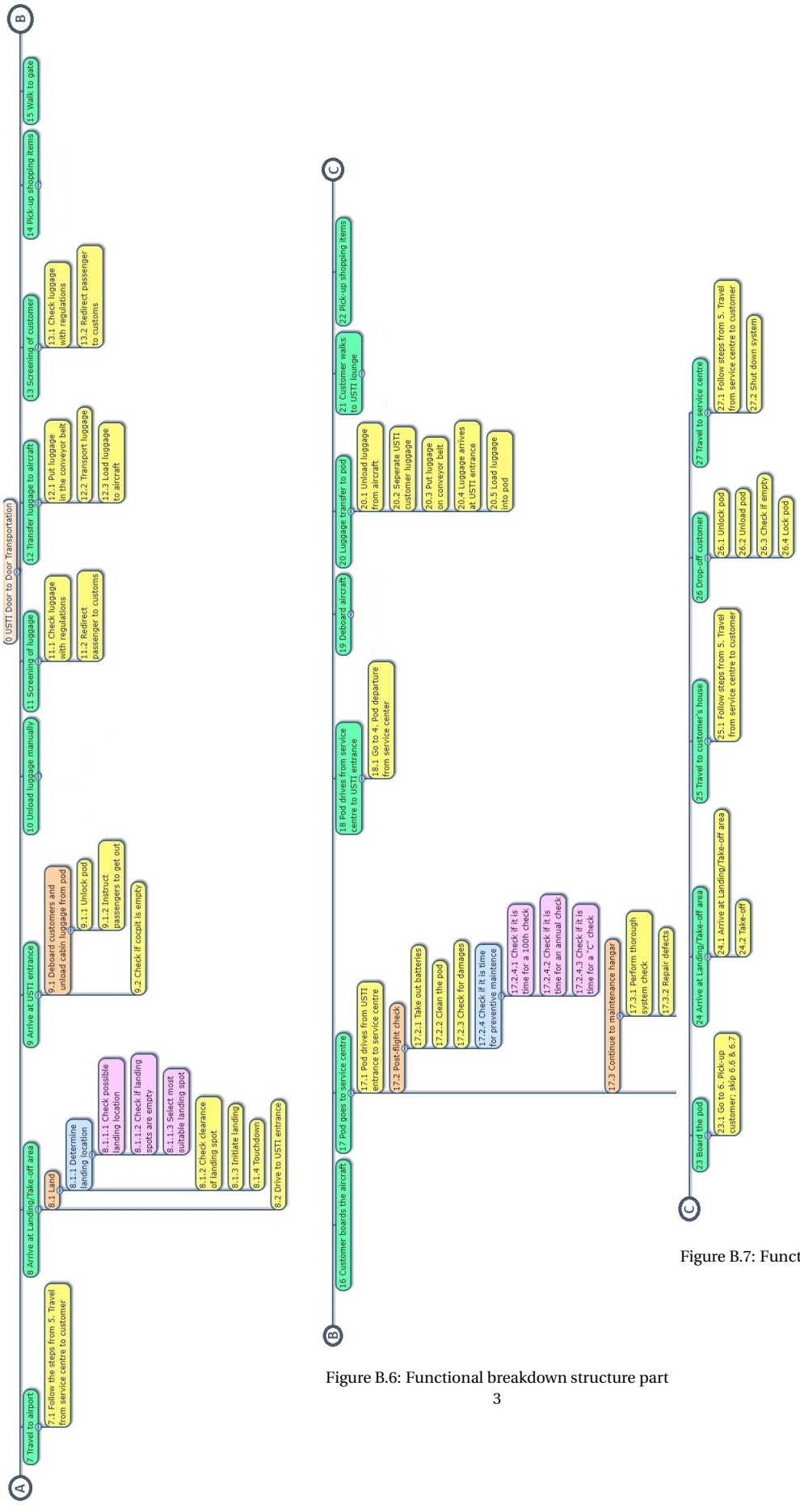

Figure B.5: Functional breakdown structure part 2

Figure B.6: Functional breakdown structure part 3

Figure B.7: Functional breakdown structure part 4

C
Detailed Mass Budget

The detailed mass budget can be found in Table C.1.

Table C.1: Detailed mass budget of the pod.

Subsystem	**Part/Component**	**No. of parts**	**Mass per component** $[kg]$	**Total mass** $[kg]$
Propulsion	VTOL Flying Egine	2	19,90	39,80
Propulsion	Cruise Flying Engine	1	12,30	12,30
Propulsion	Driving Engine	2	6,80	13,60
Propulsion	Range Extender	1	50,00	50,00
Propulsion	Take-off Propeller	2	1,5	3,00
Propulsion	Cruise Propeller	1	1,00	1,00
Driving & Landing Gear	Video Cameras	6	1,30	7,80
Driving & Landing Gear	Radar Sensors	2	0,50	1,00
Driving & Landing Gear	Lidar	6	0,83	4,98
Driving & Landing Gear	Ultrasonic Sensors	1	0,70	0,70
Driving & Landing Gear	Front Wheel + tyre	2	13,70	27,40
Driving & Landing Gear	Back Wheel + tyre	2	10,70	21,40
Driving & Landing Gear	Shock Absorpers Front	2	1,7	3,40
Driving & Landing Gear	Shock Absorpers Back	2	1,70	3,40
Driving & Landing Gear	Breaking system	1	18,00	18,00
Driving & Landing Gear	Steering Control System	1	2,00	2,00
Structure	Main Body (Excluding Skin)	1	16,95	16,95
Structure	Wing (Including Skin)	1	17,18	17,18
Structure	Empenage	1	6,58	6,58
Flight Control	Flight Control Computer	1	5,00	5,00
Flight Control	Transponder	2	1,32	2,64
Flight Control	Control Surfaces Actuators	10	0,07	0,70
Flight Control	Wing Actuator	2	0,18	0,35
Flight Control	Tilting Rotor Actuator	2	0,06	0,13
Flight Control	Air Data Surrounding Sensors	2	0,40	0,80
Flight Control	AHRS/INS	2	0,115	0,23
Internal Systems	Seats	2	20,00	40,00
Internal Systems	Foldable Table	2	2,30	4,60
Internal Systems	Information Display	1	8,50	8,50
Internal Systems	User Interface	1	1,35	1,35
Internal Systems	ID Verification System	1	6,00	6,00
Internal Systems	WiFi	1	4,00	4,00
Internal Systems	Drink Dispenser	1	4,50	4,50
Internal Systems	Fuel Tank	1	5,00	5,00
Internal Systems	Fuel Pump	1	2,00	2,00
Internal Systems	Fuel Valves	1	1,43	1,43
Internal Systems	Fuel level sensor	1	0,25	0,25
Internal Systems	Baggage Compartment	1	3,90	3,90
Emergency Systems	Life vest	2	0,50	1,00
Internal Systems	Climate Control	1	27,30	27,30
Structure	Fuselage Skin	1	9,2	9,20
Structure	Floor	1	10,2	10,20
Structure	Passenger Door	2	12,00	24,00
Structure	Cargo door	2	8,00	16,00
			Total Mass $[kg]$	429.57

D

Appendix: Software Block Diagrams

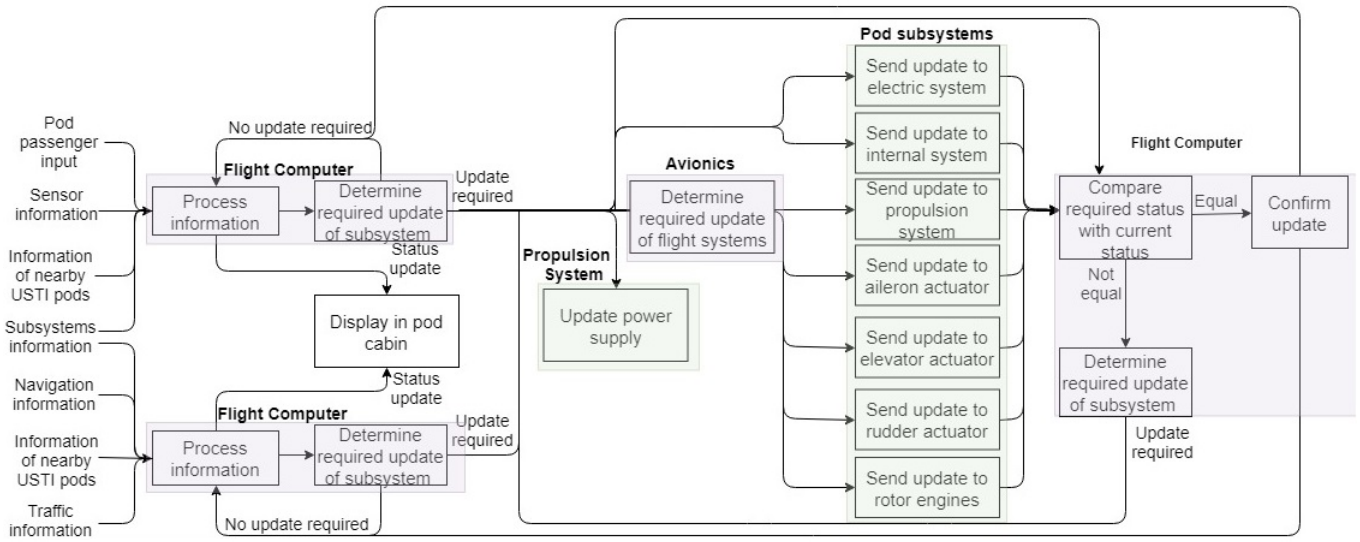

Figure D.1: Software block diagram for flying mode

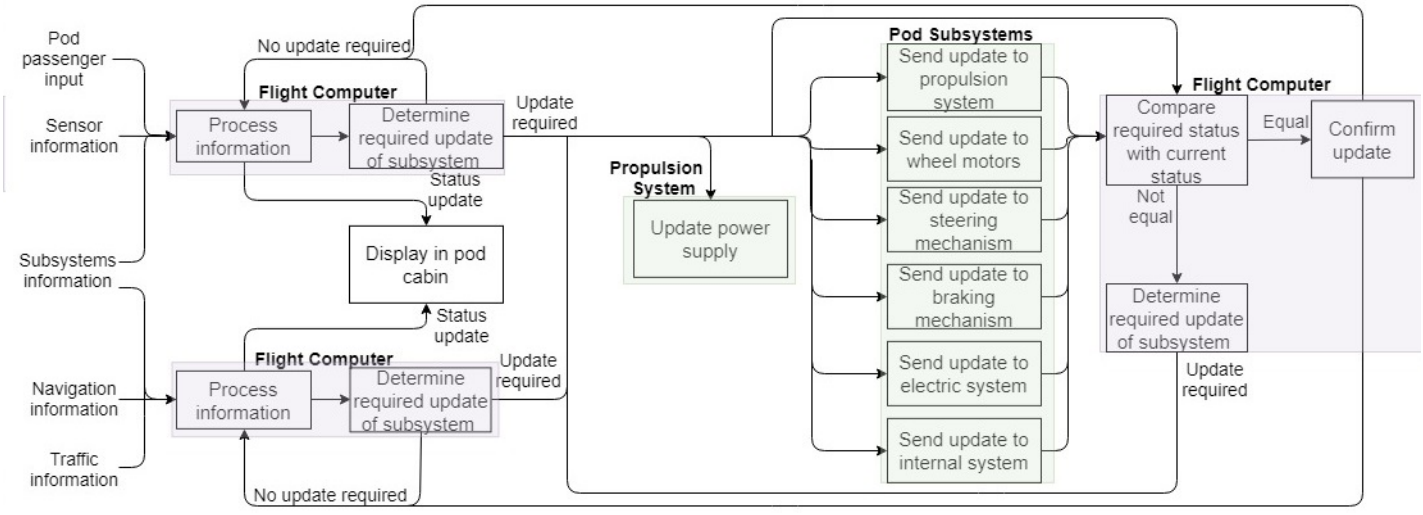

Figure D.2: Software block diagram for driving mode

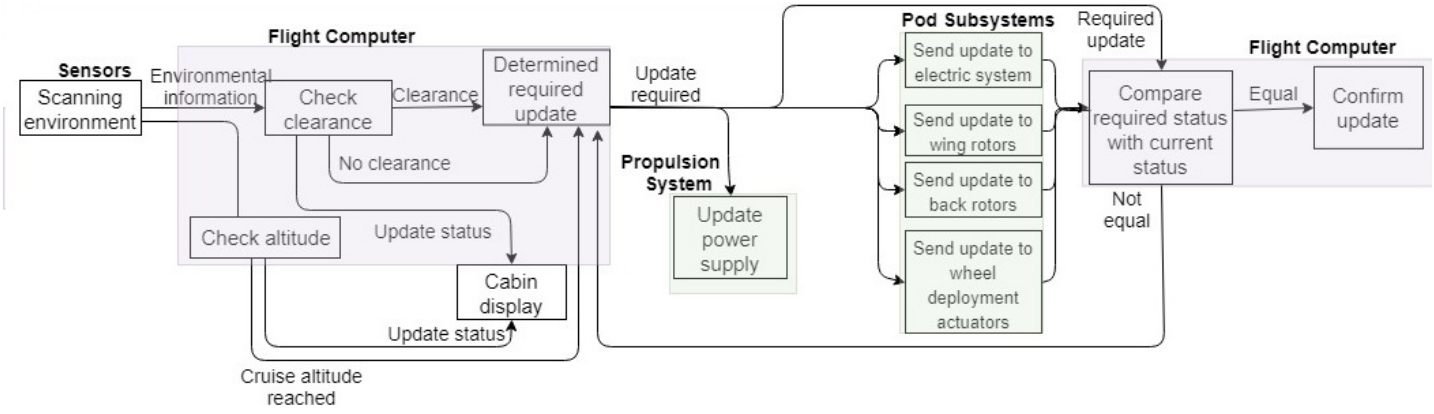

Figure D.3: The software block diagram for take-off

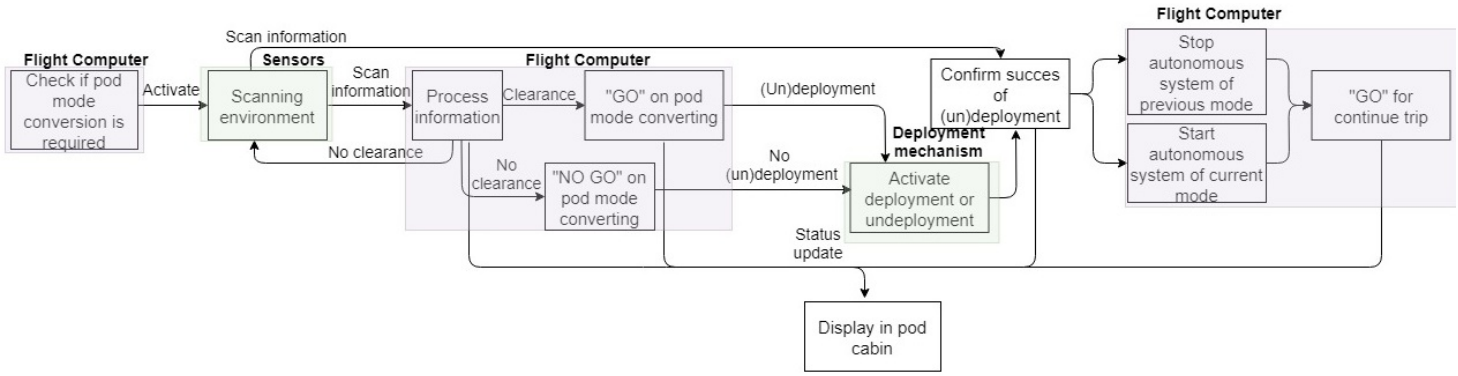

Figure D.4: The software block diagram for the pod mode conversion

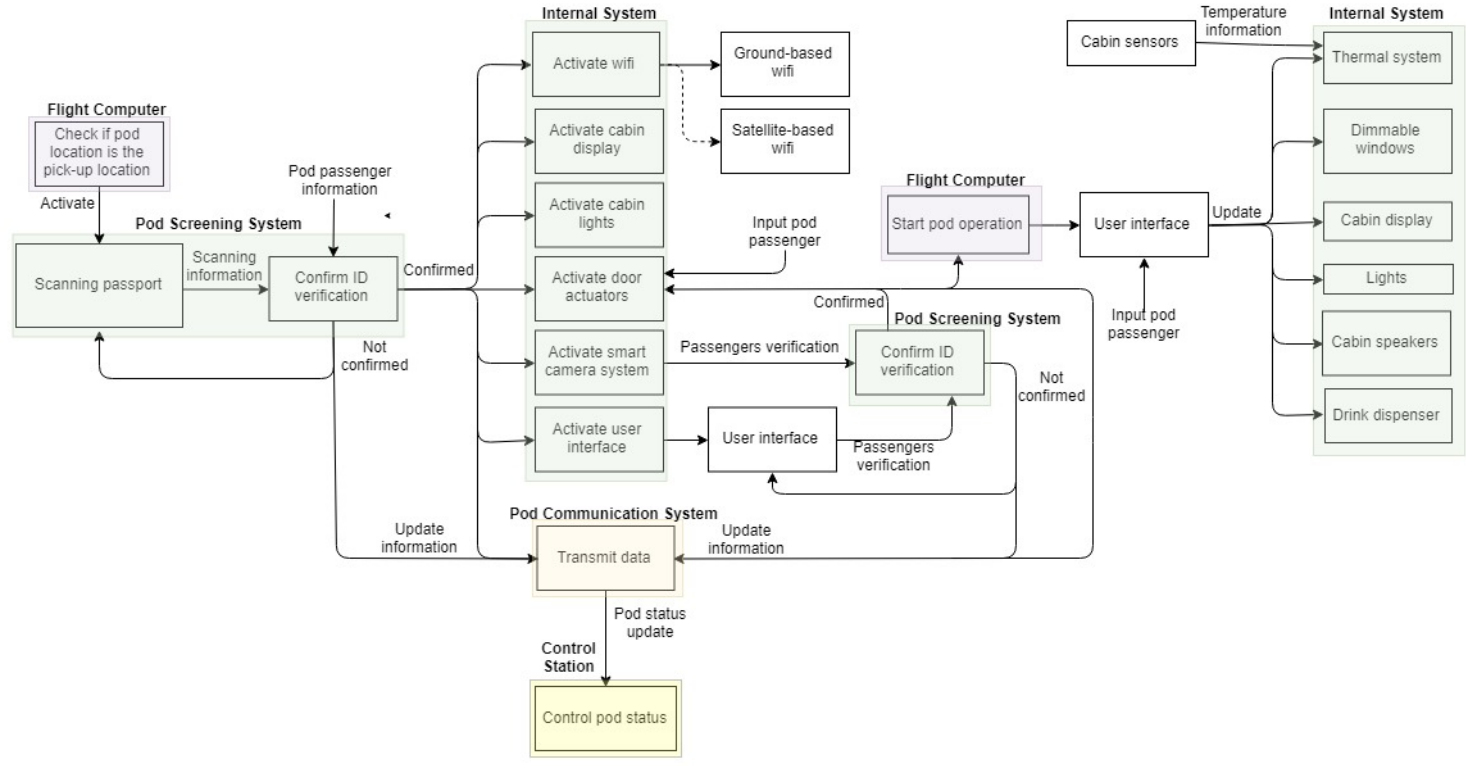

Figure D.5: The software block diagram for the cabin systems